Institut für Wasserbau · Universität Stuttgart

Mitteilungen

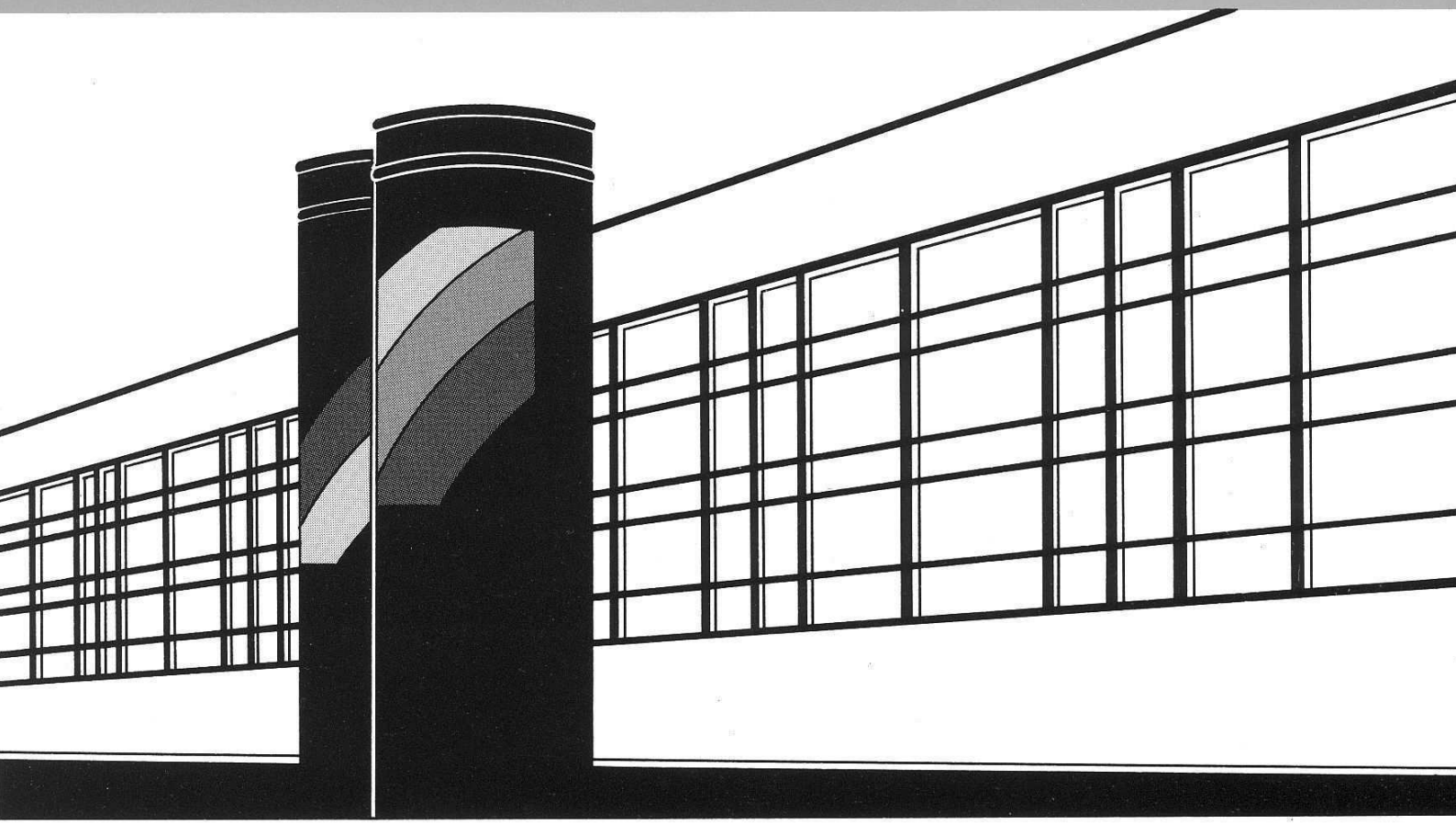

Heft 204

Muhammad Mahboob Alam

Statistical Downscaling of Extremes of Precipitation in Mesoscale Catchments from Different RCMs and Their Effects on Local Hydrology

Statistical Downscaling of Extremes of Precipitation in Mesoscale Catchments from Different RCMs and Their Effects on Local Hydrology

Von der Fakultät Bau- und Umweltingenieurwissenschaften der Universität Stuttgart zur Erlangung der Würde eines Doktor-Ingenieurs (Dr.-Ing.) genehmigte Abhandlung

Vorgelegt von

Muhammad Mahboob Alam

aus Swat, Pakistan.

Hauptberichter:	Prof. Dr. rer. nat. Dr.-Ing. András Bárdossy
Mitberichter:	Prof. Dr. Axel Bronstert

Tag der mündlichen Prüfung: 19. Juli 2011

Institut für Wasserbau der Universität Stuttgart
2011

Heft 204

Statistical Downscaling of Extremes of Precipitation in Mesoscale Catchments from Different RCMs and Their Effects on Local Hydrology

von
Dr.-Ing.
Muhammad Mahboob Alam

Eigenverlag des Instituts für Wasserbau der Universität Stuttgart

D93 Statistical Downscaling of Extremes of Precipitation in Mesoscale Catchments from Different RCMs and Their Effects on Local Hydrology

Bibliografische Information der Deutschen Nationalbibliothek
Die Deutsche Nationalbibliothek verzeichnet diese Publikation in der Deutschen Nationalbibliografie; detaillierte bibliografische Daten sind im Internet über http://www.d-nb.de abrufbar

Alam, Muhammad Mahboob:
Statistical Downscaling of Extremes of Precipitation in Mesoscale Catchments from Different RCMs and Their Effects on Local Hydrology / von Muhammad Mahboob Alam. Institut für Wasserbau, Universität Stuttgart. - Stuttgart: Inst. für Wasserbau, 2011

(Mitteilungen / Institut für Wasserbau, Universität Stuttgart: H. 204)
Zugl.: Stuttgart, Univ., Diss., 2011
ISBN 978-3-942036-08-5
NE: Institut für Wasserbau <Stuttgart>: Mitteilungen

Herausgegeben 2011 vom Eigenverlag des Instituts für Wasserbau
Druck: Document Center S. Kästl, Ostfildern

Contents

Acknowledgements

I can not thank Prof. Bárdossy enough for his support throughout my stay here at the Institute of Hydraulics. I am grateful to him for giving me a chance to work here at IWS. It was only possible through his constant guidance and extreme patience with me that I was able to finish my PhD. I truly believe that the scientific ideas that he cultivated in my mind would help me immensely in my future life.

I would also like to thank here Prof. Axel Bronstert who gave me valuable feedback about my work and guided me whenever it was required. Thanks are also due to Prof. Caspary whose ideas and review of my work motivated me immensely to improve both my PhD. research and our common project ENSEMBLES work. I would thank also Dr. Edwin Ayros of Fichtner GmbH for his kind support whenever it was required and for giving me a chance to work at Fichtner.

Once I leave IWS, the thing I am sure to miss the most would be the great working environment here. I would like to thank Ferdinand, Thomas, Min, Jing, Henning, Christian, Shailesh, Claus and Jan for their great company and help. I wish all of them a bright and successful future and hope that we would be in touch wherever we are in our future lives. I, Min and Jing always considered Helen and Pawan as our role models when we started our PhD almost at the same time and hence I can not forget their help, ideas and support. I would specially like to thank Frau Uhrmann for her support throughout my stay here. Whenever there was a need for fulfilling some bureaucratic formalities she was always there to help. She is soon going to retire and I wish her peaceful and content life. Special thanks are also due to Dr. Jochen Seidel for his support whenever it was required.

I would do great injustice if I do not mention my family here. My stay in Germany since starting my MSc. here was long enough for me to observe some drastic changes in my country in general and in Swat (from where I belong) in particular. Unfortunately those changes were not for the betterment. In spite of all the difficult situations that my immediate and extended family faced, I was always given unconditional and tremendous support. I can not pay back for the support that I received from my parents and my brothers and sister. Last but surely not the least I have to thank my beloved wife Aisha and our daughter Amina. There presence here in Germany really changed my life. After a tiring day in the office, their company always relaxed and refreshed me. I hope now that I am finished with my PhD., I could take some burden of raising our daughter off from my wife and give her a chance to concentrate on her career.

List of Figures

List of Tables

List of Abbreviations

Abbreviation	Meaning
API	Antecedent precipitation index
BMBF	Bundesministerium für Bildung und Forschung
CART	Classification And Regression Trees
CCA	Canonical Correlation Analysis
CRCM	Canadian Regional Climate Model
CP	Circulation Pattern
DWD	Deutscher Wetterdienst
ECMWF	European Centre for Medium-Range Weather Forecasts
EOF	Empirical Orthognal Analysis
EU	European Union
EVT	Extreme Value Theory
FORTRAN	Formula Translator (Programming language)
GCM	Global Circulation Model
GIS	Geographical Information System
HBV	A Swedish rainfall-runoff model
IAHS	International Association of Hydrological Sciences
IPCC	Intergovernmental Panel on Climate Change
IWRM	Integrated Water Resources Management
KNMI	Koninklijk Nederlands Meteorologisch Instituut
m.a.s.l.	Meters Above Sea Level
MF	Moisture Flux
MPI-M	Max-Planck-Institut für Meteorologie
MSLP	Mean Ssea Level Pressure
NCAR	National Center for Atmospheric Research
NCEP	National Center for Environmental Prediction
NOAA	National Oceanic and Atmospheric Administration
OPAQUE	Operationelle Abfluss- und Hochwasservorhersage in Quellgebieten
PDSI	Palmer Drought Severity Index
PHDI	Palmer Hydrological Severity Index
RCM	Regional Climate Model
SMHI	Swedish Meteorological and Hydrological Institute
SRES	Special Report on Emissions Scenarios (by IPCC)

List of symbols

Symbol	Definition
α	Vector of stochastic parameters of statistical downscaling model
β	Model parameter
$\Delta Q(t)$	Discharge increment or decrement
ϵ	Random part of climate that could not be explained by the model formulation
$\Gamma(\alpha)$	Gamma function
$\Gamma_{0i}(t^*)$	Spatial covariance matrix
$\Gamma_{1i}(t^*)$	Spatial covariance matrix for 1 day lag
λ	Parameter of exponential distribution
π	Long run relative frequency of precipitation day
$\mu_0(t^*, u)$	Expectation of precipitation on julian day t^*
$\psi(t)$	Random number of independent normal distribution
$\rho(a, b)$	Parameter describing spatial structure of rainfall occurrence between stations a and b
API	Antecedent precipitation index
b_0, b_1, b_k	Parameters of logistic regression
$C_i(t^*)$	Spatial variability matrix
$C_\Delta(t)$	Ratio of precipitation coverage in neighborhood Δ
$dQ_+(t)$	Positive values of discharge increment/decrement time series
E	Expected value
F_{dQ}	Probability distribution function of discharge increment/decrement
$g(i, t)$	Normalized anomaly vector
$h(a, b)$	Distance between station a and b
$I(u, z)$	Binary indicator variable conditioned upon z
$I_{dQ \approx 0}$	Binary indicator of dry day in discharge increment/decrement time series
K	Total number of stations used in CP classification and downscaling
K_0	Recession coefficient of near surface runoff
K_1	Recession coefficient of interflow
K_2	Recession coefficient of baseflow
K_{perc}	Recession coefficient of percolated flow
$L(\lambda)$	Likelihood function for certain parameter
L_{var}	Large scale variable in statistical downscaling
$O_1..O_6$	Objective functions
p_i and q_i	Parameters dependent upon circulation pattern and time

Symbol	Definition
p_{00}	Probability of occurrence of dry day followed by dry day
p_{01}	Probability of occurrence of wet day followed by dry day
p_{10}	Probability of occurrence of dry day followed by wet day
p_{11}	Probability of occurrence of wet day followed by wet day
p_{dQ_+}	Probability of occurrence of positive values in discharge increment/decrement time series
$Q(t)$	Discharge for time t
Q_0	Near surface runoff
Q_1	Interflow
Q_2	Baseflow
Q_{perc}	Percolated flow from upper reservoir of HBV model to lower reservoir
r_1	One lag autocorrelation
S_{var}	Surface variable in statistical downscaling
t^*	Julian day
u and v	Westerly and southerly wind components
$\mathbf{V}$	Membership function vector
$w_\alpha(x)$	Wetness index of CP α at location x
$W^n(t,u)$	Normally distributed random variable at certain time and location
z	Threshold precipitation amount
Z_{1P} and Z_{2P}	Performance measures of CP classification methodology
$Z_D(x,t)$	Downscaled precipitation amount at certain location and time
$Z_R(x,t)$	Precipitation amount simulated by RCM at certain location and time

Kurzfassung

Globale Klimamodelle sind das einzige Werkzeug, um die Effekte des globalen Klimawandels in Bezug auf quantitative Veränderungen in den unterschiedlichen meteorologischen und hydrologischen Variablen abzuschätzen. Niederschlag und Temperatur sind dabei zwei der wichtigsten Größen, da sie andere meteorologische Variablen, (wie z. B. die Luftfeuchtigkeit oder die Verdunstung), hydrologische Variablen (wie z. B. den Oberflächenabfluss) und ganz direkt die Lebensbedingungen des Menschen (z. B. die Nahrungsmittelproduktion) stark beeinflussen. Unter den weiteren großräumigen und lokalen Bedingungen, die das Auftreten von Niederschlag und die Niederschlagsmenge bestimmen, spielen die geographischen und topographischen Gegebenheiten die wahrscheinlich wichtigste Rolle. Darum müssen diese Größen, für jedes einzelne Zielgebiet einer Klimawandelabschätzung lokal analysiert werden. Unglücklicherweise ist die Skala, auf der die globalen Klimamodelle (engl. "Global Circulation Models" - kurz: "GCM") arbeiten, zu groß für sinnvolle Untersuchungen zukünftiger Niederschlag- und Temperaturverhältnisse auf lokalem Maßstab. Deshalb wurden andere Methoden entwickelt, um die Nützlichkeit und die Auflösung der GCM-Daten auf lokaler Ebene zu erhöhen (sog. "Downscaling").

Als eine grobe Einteilung der Dowscaling-Methoden spricht man von statistischem und dynamischem Downscaling. Beim statistischen Downscaling wird versucht, eine Beziehung zwischen den großskalig simulierten Variablen aus den GCMs (Prädiktoren) und beobachteten lokalen Messwerten (Prädiktanten) zu etablieren. Unter der Annahme, dass diese Beziehung in der Zukunft konstant bleiben wird, kann sie dazu genutzt werden, die zukünftigen lokalen Werte der Prädiktanten aus den simulierten Zukunftszenarien der Prädiktoren vorherzusagen. Der Ansatz des dynamischen Downscaling mittels regionaler Klimamodelle (engl. "Regional Circulation Models" - kurz: "RCM") besteht darin, eine physikalisches Model mit mehr oder weniger der gleichen Komplexität wie das GCM in dieses einzubetten. Das RCM erhält seine Eingabewerte als Randbedingungen aus dem GCM und berechnet die vorliegenden physikalischen Gleichungen erneut auf einer deutlich feineren Skala. Damit können die lokalen Einflussfaktoren berücksichtigt werden. Es angenommen, dass die Ergebnisse somit besser für Untersuchungen im lokalen Maßstab geeignet sind. Beide Downscaling-Methoden werden weltweit vielfältig in Klimawandel-Studien und Klimafolgekosten-Analysen eingesetzt. Die Güte der Ergebnisse ist sehr unterschiedlich und es werden ständig neue Techniken entwickelt, um diese zu verbessern. Beide Methoden haben ihre typischen Vor- und Nachteile. Satistische Downscaling Methoden sind weit weniger rechenintensiv. Allerdings basieren sie auf der Annahme, dass der Zusammenhang zwischen globalen und lokalen Variablen konstant ist, was in manchen Fällen schwer zu rechtfertigen ist. RCMs auf der anderen Seite können zwar die physikalischen Gleichungen auf einem lokalen Maßstab lösen, erben aber über die Randbedingungen die Modelfehler aus dem antreibenden GCMs.

In dieser Arbeit wird eine statistische Downscaling Methode vorgestellt, die versucht, die aus dem GCM geerbten Modellfehler zu korrigieren. Es werden drei RCMs für den deutschen Teil des Reineinzugsgebiets betrachtet. Die Methode basiert auf einer Korrektur der Quantile der Verteilung der Niederschlagswerte (in einigen Untersuchungen auch der Temperatur). Nach der Korrektur werden Szenarios des zukünftigen Niederschlags entwickelt. Darüber hinaus wird eine räumlich detaillierte Version des konzeptionellen hydrologischen Models HBV für den deutschen Teil des Rheineinzugsgebiets kalibriert und mit den rohen sowie den korrigierten Zukunftsdaten beschickt. Damit soll eine sinnvolle Prognose des hydrologischen Regimes dieses wichtigen europäischen Stroms ermöglicht werden.

Die im letzten Abschnitt erwähnte Downscaling-Methode wurde auf zwei verschiedene Weisen implementiert. Im ersten Fall wurde die Methode auf die RCM Daten angewandt, ohne irgendwelche Einschränkungen in der Quantil-Quantil Transformation zwischen den Kontroll- und den Szenarioläufen für die Zukunft zu berücksichtigen. Im zweiten Fall wurde die Quantil-Quantil-Transformation auf das Auftreten bestimmter großräumiger Wetterlagen (engl. "Ciruclation Patterns", kurz: CPs) konditioniert. In einem vorherigen Abschnitt wurde kurz diskutiert, wie Niederschlag in seiner Häufigkeit und Menge von verschiedenen Phänomenen beeinflusst wird. Neben den geographischen und topographischen Verhältnissen am Erhebungsort spielen dabei auch die großskaligen atmosphärischen Strömungsverhältnisse eine Rolle. Es wird somit angenommen, dass die Konditionierung der Downscaling-Methode auf die Wetterlage bessere Ergebnisse bringen könnte.

Um das oben skizzierte Konzept zu verwirklichen, wurde eine Klassifizierung der Wetterlagen durchgeführt. Die Klassifizierung basiert auf einem Fuzzy-Logik Regelsystem. In dieser Arbeit werden zwei neuartige Fuzzy-Logik Klassifizierungsmethoden vorgestellt: Die erste Methode basiert auf den Niedrigwasser-Abflussverhältnissen der Flüsse im Untersuchungsgebiets, die andere auf einem Clustering von Niederschlagsmessstationen. Die neue Klassifizierungsmethode scheint eine bessere Klassifizierung der Wetterlagen zu liefern, gemessen daran, dass der Unterschied zwischen den einzelnen Klassen ausgeprägter ist und Ähnlichkeit der Mitglieder einer Klasse erhöht. Um die Klassifikation zu prüfen, wurde ein Gütemaß namens "Wetness Index" entwickelt. Der Wetness-Index wurde dazu verwendet, besonders kritische Wetterlagen, die also für extrem nasse oder extrem trockene Verhältnisse verantwortlich sind, zu identifizieren. Es konnte gezeigt werden, dass alle extremen Fälle von Hochwasser oder Trockenheit auf die gleichen, kritischen CPs zurückgeführt werden können.

In dieser Arbeit wird darüber hinaus eine weitere statistische Downscaling Methode vorgestellt, die auf einem multivariaten, autoregressiven Model erster Ordnung basiert. Diese Methode verwendet die Informationen der im letzten Abschnitt beschrieben Wetterlagenklassifikation. Die Parameter des autoregressiven Modells werden dabei CP abhängig gewählt. Die Methodik wird auf eine Reihe von Oberstrom-Einzugsgebieten in Süd- und Ostdeutschland angewendet. Oberstrom-Einzugsgebiete haben per Definition eine sehr kurze Reaktionszeit auf signifikante Regenereignisse. Sie tragen

sehr schnell zum Oberflächenabfluss bei und wenn sie Teil des Einzugsgebiets eines großen Flusses sind, können sie auch größere Hochwasserereignisse auslösen. Das Niederschlags-Downscaling für diese Einzugsgebiete wurde mit dem mittleren Luftdruck auf Meereshöhe als Prädiktor und der Niederschlagshöhe an einer lokalen Messstation als Prädiktant durchgeführt. Das Model wurde so aufgesetzt, dass ein Ensemble der täglichen Niederschlagshöhe erzeugt werden kann. Dadurch wird es möglich, die Unsicherheit der Methode mit abzuschätzen.

Letztlich wurde noch eine Untersuchung bezüglich Dürreperioden im deutschen Teil des Rheineinzugsgebietes durchgeführt. Dazu wurde der Palmer Dürre Index verwendet. Es wurde ein FORTRAN-Programm entwickelt, welches verschiedene Dürre Indices wie den Palmer Dürre Index, den hydrologischen Palmer Dürre Index und den monatlichen Feuchteanomalie Index für ein bestimmtes Einzugsgebiet berechnen kann. Das Programm vermag die berechneten Ergebnisse gleichzeitig in einer Karte darzustellen. Die Kartendarstellung ermöglicht es, die Schwere einer Dürre auch für ein größeres Gebiet abzuschätzen. Die Analyse von Dürreperioden wurde für gerasterte Beobachtungsdaten sowie für Daten aus den Kontroll- und A1B-Szenarioläufen dreier RCMs durchgeführt.

1. Introduction

The importance of data for scientific research in any field can not be over emphasized. As in all other fields the advancement in hydrological and meteorological sciences would be halted if representative, relatively accurate and spatially and temporally extensive data were not available. Hydrological sciences particularly requires spatially and temporally extensive data of several physical variables to drive different models (physical or conceptual) to help understand important physical hydrological phenomena. Hydrological models are used to simulate the physical reaction of certain catchment to occurrence of particular short term event or extended absence of certain event. The simulation of hydrological models would only be plausible and reliable if the models are first of all based on hypothesis that are physically and theoretically sound and second of all the developed models are tested (calibrated) on representative data.

Floods and droughts are considered two of the most important hydrological phenomena that affects human life. Be they may loss of life, loss of property or disturbance to eco-system as a whole, the affects of floods and droughts are both short and long term. Modeling of extremes of hydrological phenomena is complicated process. As the extremes events are rare , there may not be enough measured data available to model certain catchment for these extremes. Statistical tests and inference procedures are also hampered by scarcity of data for extreme events. Extreme value theory (EVT) is widely used by hydrologists for flood and drought mitigation. The severity of a hydrological extreme event is expressed as a non-exceedance probability, or equivalently, in terms of return period (Renard and Lang, 2007). Flood frequency analysis are also used for extreme hydrological phenomena simulation while more recently Copulas are used for multivariate extreme value analysis (Chebana and Ouarda, 2008) and (Renard and Lang, 2007). The core of the problem in most of the cases is scarcity of extremes of data and hence different statistical procedures are adopted to cater for this scarcity. The drawback in frequency and return period based analysis was pointed out as early as 1941 in Gumbel (1941) where on page 187 he states:

In order to apply any theory we have to suppose that the data are homogeneous, i.e. that no systematical change of climate and no important change in the basin have occurred within the observation period and that no such changes will take place in the period for which extrapolations are made.

So very early on, it was understood that the climate change is an important phenomenon that needs to be looked into when modeling for important hydrological processes like floods and droughts. Human activities like burning of fossil fuels, changes in land cover and use have impact on concentration of green house gases

which in turn alters the energy balances and tends to warm the atmosphere. The warming of atmosphere results in climate change and alters the usual (observed in past) behavior of hydrological cycle (Some reports indicate that mean annual global surface temperature has increased by about 0.3 °C-0.6 °C since the late 19^{th} century and it is anticipated to further increase by 1 °C-3.5 °C over the next 100 years (Watson et al., 1995). Specification of bounds on flood and drought extremes in changed climate situations for future then becomes questionable. This was also observed by Gumbel (1941) on page 163 where for specific cases of floods he states "*Some authors have tried to introduce upper and lower limits to the discharges, even though it is doubtful that such limits exist*".

Meteorological and hydrological data derived from global and regional climate models are one another possibility for use in modeling for extreme hydrological situations. These models provide extensive data in temporal and spatial resolutions which can be used in hydrological models for simulation in mesoscale catchments. Additionally different scenario considerations in transient run simulations of regional climate models make them useful for climate change assessment. These models are state of the art numerical coupled models that represent different subsystems of earth's climate. Depending upon which global and regional climate model one is considering, they provide different large scale and local scale variables over different characteristic grid sizes over different areas. Although global climate models reliably simulate large scale variables, at finer spatial resolutions, climate models have much smaller skill (Grotch and MacCracken, 1991). It is this limitation of global climate models that downscaling is considered as an important preliminary step in usage of data from global and regional climate models.

This thesis attempts to present statistical downscaling of large scale data from regional climate model using quantile-quantile exchange as a methodology and assesses the results obtained from this methodology by applying the downscaled information to hydrological model on selected catchments of Germany. Circulation patterns (CPs) associated with extremes of hydrological situations are identified both in observational gridded data sets and in regional climate models. CP conditioned downscaling is performed and resulting information is applied to distributed version of conceptual hydrological model HBV for different catchments in Germany to assess the model's response to different scenarios of precipitation.

1.1. Background and Motivations

Global circulation models (GCM) are comprehensive climate models that are based on physical laws represented by mathematical equations that are solved using a three-dimensional grid over the globe. For climate simulation, the major components of the climate system must be represented in sub-models (atmosphere, ocean, land surface, cryosphere and biosphere),along with the processes that go on within and between them (Houghton et al., 2001). All these sub models are working within the whole at a very coarse resolution. Currently, the resolution of the atmospheric part of a typical model is about 250 km in the horizontal and about 1 km in the vertical above

the boundary layer. The resolution of a typical ocean model on the other hand is about 200 to 400 m in the vertical, with a horizontal resolution of about 125 to 250 km.

Given the coarse resolution of GCM, they can not be directly used for hydrological studies on local scale neither are they designed for it. Instead the information from GCM are downscaled to limited-area and finer resolution. This downscaling process is usually called as dynamical downscaling (2.2.1). Regional climate models (RCM) are used to perform dynamical downscaling to make information suitable to be used for regional studies. RCM are driven by coarse resolution GCM models (boundary conditions of RCM coming from GCM), and they provide different variables (hydrological or/and meteorological) at a scale finer than GCM's scale. Unlike the global nature of global circulation models, RCMs cover only a section of the globe, which can be modeled at a finer spatial resolution. RCMs used in this study e.g. have spatial resolution as fine as 25Km x 25Km. Although this resolution may seem to be adequate for regional studies yet to obtain accurate information on the location, quantity and intensity of precipitation and on changes in precipitation characteristics caused by climate change, one may still wish and opt for finer resolution (Bronstert, 2009). Xu (1999) presents the following reasons for insufficient spatial scale and inaccuracies of RCMs.

1. The boundary conditions of the regional model are obtained from the GCM, and therefore frequently contain a systematic error of atmospheric dynamics, which is transferred to the respective region. Errors in the GCM thus directly limit the capacity of the regional climate model.

2. The parameterization of important processes in the RCM, such as the formation of clouds, soil water dynamics, or land-surface interactions, has not yet been resolved in a way that allows for a definition of the natural variability under any weather condition or for the recognition of a possible signal of climate change.

3. The resolution of the RCMs is sufficiently detailed to represent large-scale precipitation patterns. However, these resolutions are not sufficient to cover small scale precipitation, such as convective thunderstorms of local orographic rainfall. Though processes taking place at a smaller scale than represented by the grid box ("subgrid-scale processes") can be parameterized by the subdivision of the grid boxes into a clouded and a cloud-free section, several convective systems cannot be localized within a grid square.

4. Regional climate models have not yet been sufficiently tested with regard to how realistically they represent rainfall-runoff events caused by storm rainfall.

Given these short comings in RCM generated data, a downscaling procedure based upon the quantile-quantile exchange of precipitation quantiles is developed. Observational gridded data set's precipitation amounts are related with RCM control period's precipitation amounts. The relationship is further used for future scenario of precipitation amounts and extreme situations are analyzed. Further, given the importance of extreme hydrological situations,a new methodology for CP classification is introduced and the methodology is applied to smaller head catchments (for floods) and bigger catchments (for droughts) in Germany.

1.2. Organization of thesis

This thesis is organized as follows. After this introduction chapter, a brief over view of different downscaling procedures adopted and used in hydrological and meteorological sciences is presented along with the advantages and disadvantages of each method in chapter 2 called "Downscaling". Chapter 3 "Methodology" then presents the methodology adopted in this thesis for downscaling and circulation pattern classification with that is useful both for extreme wet and dry conditions at the same time. Before the results of application of this methodology are presented in Chapter 5 ("Results-Circulation pattern classification") and Chapter 6 ("Results-Downscaling"), it is felt important to describe the data that is used in this thesis in Chapter 4 called "Catchments and Data". Chapter 7, "Application of PDSI to raw RCM and downscaled RCM data" provides the drought analysis of German part of Rhine basin while Chapter 8 "Application of raw and downscaled RCM information to hydrological model" finally provides the results of possible changes in hydrological regime of river Rhine due to climate change. Discussion and conclusions are then summed up in Chapter 9 ("Conclusions") of this thesis.

2. Downscaling

2.1. Preface

This chapter gives a brief over view of downscaling procedures used in hydrological and meteorological sciences. After an introduction to the downscaling methodology, need and concept, different classifications of downscaling procedures is presented.Each type of downscaling procedure are then briefly explained along with necessary references that would provide more in-depth details. This review of downscaling procedures is in no way a comprehensive review of vast field of downscaling.

2.2. Downscaling

As a reference was made to the scales on which GCMs and RCMs operate in section 1.1, the need and importance of downscaling could be inferred from that. GCMs neither can be used nor are they designed for regional climate impact studies. One has to resort to some kind of downscaling procedure to make use of both the data (number of different meteorological variables) obtained/provided from/by GCMs and some locally measured variable. Two procedures/methods are commonly followed to combine large scale and local scale variables, dynamical downscaling and statistical downscaling. While the former is more or less a GCM on a regional scale the second make uses of different statistical procedures to reach to a conclusion about kind of relationship between large scale variable and local scale variable and then use that relationship in different spatial and temporal domain for intended studies.

2.2.1. Dynamical Downscaling

Synoptic climatology focuses on developing empirical-statistical associations to determine relationships between atmospheric circulation and surface environment. Empirical downscaling (statistical downscaling 2.2.2) on the other hand attempts to describe the relationship between the two precisely. Regional climate models are the dynamical downscaling tools that attempts to combine both the goals of synoptic climatology and empirical downscaling. Regional climate modeling presents the scientist with the opportunity to grasp the dynamics of individual synoptic systems and their interaction with surface environmental systems. Additionally they can also be used for predicting contemporary regional climates from large scale circulation data and developing regional scenarios for studying the impacts of climate change. First regional climate simulations were carried out by Dickinson et al. (1989) and Giorgi and Bates (1989), where downscaling was performed from global climate models for climate impact studies. Although the information downscaled from GCM is at a regional scale, the definition of regional scale is difficult. Different definitions are often implied in different contexts. For example, definitions can be based on geographical,

political or physiographic considerations, considerations of climate homogeneity, or considerations of model resolution. Because of this difficulty, an operational definition can be adopted from literature as follows.

Regional scale is here defined as describing the range of 10^4 km^2 to 10^7 km^2. The upper end of the range (10^7 km^2) is also often referred to as sub-continental scale, and marked climatic inhomogeneity can occur within sub-continental scale regions in many areas of the globe. Circulations occurring at scales greater than 10^7 km^2, also called "planetary scales", are clearly dominated by general circulation processes and interactions. The lower end of the range (10^4 km^2) is representative of the smallest scales resolved by current regional climate models. Scales smaller than 10^4 km^2 are referred to as "local scale" (Houghton et al., 2001). Ironically almost all hydrological processes occur at local scale or even sub-local scale. Hydrological models are frequently concerned with small, sub-catchment processes, occurring on spatial scale much smaller than those resolved in GCM or RCM. There is a need of further downscaling of information provided by RCM to better represent the catchments in hydrological models and hence reach to results which are representative. Keeping aside the issue of further downscaling of RCM data, we would in this section restrict ourselves only to the issue of regional climate modeling.

Regional climate models or limited area models use large scale and lateral boundary conditions from GCMs to produce higher resolution outputs (Figure 2.1). After the first successful demonstration of RCMs by Dickinson et al. (1989) and Giorgi and Bates (1989), much attention has been given to development, evaluation and application of RCMs. The main idea behind regional climate modeling is that given detailed representations of physical processes and high spatial resolution that resolves complex topography, land-sea contrast and land use, RCM can generate realistic regional climate information consistent with the driving large scale circulation supplied by either reanalysis data or a GCM. RCMs bridges the spatial gap between GCM and other modeling components such as hydrological models that require regional climate information. As such RCMs are critical component of climate modeling and climate impact prediction. RCMs usually resolve the forcings of GCMs to finer scale (typically $0.5°$ as opposed to $5.0°$ of GCM) of latitude and longitude and parameterize physical atmospheric processes (Fowler et al., 2007). Thus, they are able to realistically simulate regional climate features such as orographic precipitation (e.g. Frei et al. (2003)), extreme climate events (e.g. H.J.Fowler et al. (2005), Frei et al. (2006)) and regional scale climate anomalies, or non-linear effects, such as those associated with the El Nino Southern Oscillation (e.g. Leung et al. (2003)).

Almost all RCMs are grid point models which employ not only variety of staggerings for the wind components but also variety of time integrations schemes, including the split explicit scheme used in NCAR RegCM2 and semi-implicit schemes. Most of the RCMs are formulated using the hydrostatic primitive equations while few like PSU/NCAR mesoscale model (aka MM5) and Canadian regional climate model (CRCM) also include nonhydrostatic terms. Nonhydrostatics terms allow more accurate representation of phenomena such as deep convection and mountain waves which are thought to produce large vertical motions when fine grid are used. However, in

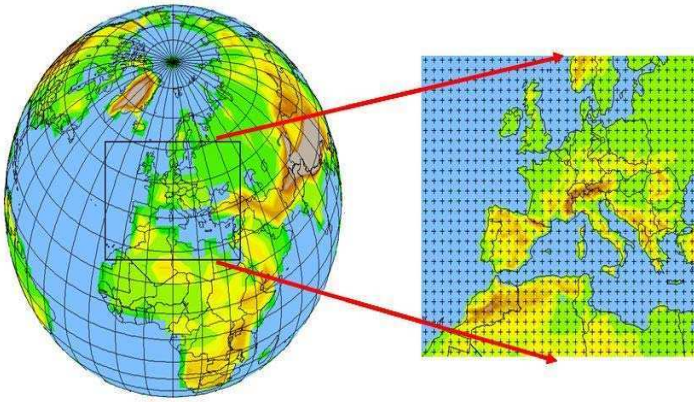

Figure 2.1.: A general picture of RCM embedded in a GCM. (Image source: World Meteorological Organization, Bulletin 57-2)

the context of regional climate modeling, improvement in the simulated climatology from the use of nonhydrostatic formulations has yet to be demonstrated as most RCMs have been applied at relatively coarse spatial resolution between 30 Km and 100 Km. Higher resolution modeling can be achieved through model nesting to telescopically zoom into finer spatial resolution with one or more level of nesting (Figure 2.1), and with the use of nonhydrostatic formulations (Grell et al., 2000). Two type of nesting methodologies are found in RCMs namely one-way nesting and two-way nesting.

In one-way nesting RCM is nested in a GCM in such a way that RCM could only receive the lateral boundary conditions/initial conditions from GCM without having any influence or feedback on the subsequent GCM runs/simulations. GCM is used to simulate the response of the global circulation to large scale forcings and RCM is used

1. to account for sub-GCM grid scale forcing like complex topographical features and land cover inhomogeneity in a physically-based way and

2. to enhance the simulation of atmospheric circulations and climatic variables at fine spatial scales.

With one-way nesting the RCM circulation may differ from that of host GCM e.g. when large domains are used or in the tropical regions where the boundary forcing is relatively weak. Weather this difference in circulation in RCM and GCM has an impact on the credibility of RCM is an issue and diverging views can be found in R.G.Jones and Noguer (1995) and McGregor (1997).

In two-way nesting, once RCM receives lateral boundary conditions from GCM, it feedbacks some of the results of finer resolution integrations to subsequent GCM runs. Although regional models can be run with two way interacting nested sub-domains, two way interacting experiments between global and regional models have seldom been attempted. One of the reason is the technical difficulty of coupling two physically complex models running at two different spatial and temporal resolution and because this technical difficulty outweighs the gains from such an exercise (Giorgi and Mearns, 1999). An alternate approach to two-way nesting is variable resolution global climate models,where the model's horizontal grid point spacing is gradually refined toward the area of interest.

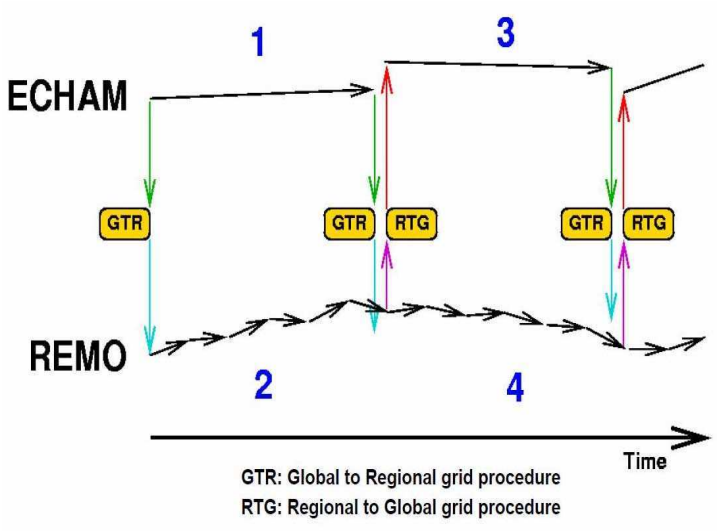

Figure 2.2.: One-way and two-way nesting of REMO model.

2.2.1.1. Short comings of dynamical downscaling

Although Regional climate models (RCMs) are important tool for dynamical downscaling of large scale forcings to regional scale due to superior and consistent inherit physics involved during the process, yet there are certain short comings of this procedure that can not be ignored;

1. RCMs are computationally intensive and requires expensive resources.
2. Limited number of scenarios ensembles are available from RCMs.
3. Results from RCMs are strongly dependent on GCM boundary forcings (hence making them biased).
4. Lack of two-way nesting may raise concern regarding completeness.

5. There occasionally are problems in maintaining viable parameterizations across scales.

2.2.2. Statistical Downscaling

Statistical downscaling is based on the view that regional climate is conditioned by two factors: the large scale climatic state, and regional/local physiographic features (e.g. topography, land-sea distribution and landuse; (Storch, 1995)). The main goal in statistical downscaling of GCM data is thus to define a relationship between large scale variable (derived from GCM e.g. geopotential height, generally called predictor) and local scale variable (observed and measured variable e.g. temperature, generally called predictant). Assuming that the developed relationship will hold in time, the relationship is used for future scenarios provided by GCMs. Given that statistical downscaling is computationally inexpensive compared to dynamical downscaling, multiple realization of future scenarios can be generated at local scale. Uncertainty of the realizations can thus be estimated. Another advantage is that they can be used to provide specific local information (e.g., points, catchments), which are generally most needed in many climate change impact studies (Mearns et al., 2003). With the development of general circulation models, came the realization of their inability to represent sub-grid, regional- and local-scale climate information. Although the long-term goal of numerical climate modellers is to develop accurate fine-grained model scenarios, it became obvious in the late 1980s that this goal might take decades to realize. Because climate impact assessors needed believable regional- and local-scale scenarios immediately, statistical downscaling became a workable alternative. Consequently, statistical downscaling, emerged as a stopgap effort in the late 1980s, and took on a life of its own in the 1990s (Brent et al., 2001).

Statistical downscaling of large scale variables is the topic that has evolved and developed tremendously over the last decade and a half. Different methods have been developed to ascertain the relationship between predictor and predictant. The most common form of the relationship has been the predictant as a function of predictor, but other relationships such as relationship between predictors and the statistical distribution parameters of the predictant (Pfizenmayer and Storch, 2001) or the frequencies of extremes of the predictant (Katz et al., 2002) have also been explored. The relationship can be expressed as a stochastic and/or deterministic function. In this thesis we restrict ourselves to most common practice of relationship identification i.e. predictant as a function of predictor. The following steps are commonly adopted for statistical downscaling model development and application (Zorita and Storch, 1997).

1. ***Downscaling model design:***
   a) Identification of surface variable S_{var}, e.g. Precipitation or temperature
   b) Selection of large scale variable L_{var} (reliably simulated by GCM) such that the relationship between L_{var} and S_{var} is of the type:

$$S_{var} = f\big(L_{var}, \alpha\big) + \epsilon \tag{2.1}$$

Where ϵ represents part of S_{var} that could not be described by the function f and α is a vector of unknown stochastic parameters $(\alpha_1, ...\alpha_m)$

c) Fitting of parameter α using paired samples (S_{var}, L_{var}) such that

$$|\epsilon| = \left|S_{var} - f\left(L_{var}, \alpha\right)\right| = minimum \tag{2.2}$$

d) Verification of the fitted model by means of independent data set

2. ***Downscaling model application:***

a) Getting large scale variable L_{var} from GCM

b) Checking if GCM reproduces the link between S_{var} and L_{var}

c) Calculation of surface variable S_{var} using

$$S_{var} = f\left(L_{var}, \alpha\right) \tag{2.3}$$

d) Using S_{var} in any impact model e.g. any rainfall-runoff model

Depending upon what kind of statistical tool is used to find the relationship between predictor and predictant, statistical downscaling has been grouped in different types. Regardless of the type of statistical downscaling that is employed to derive a relationship between predictor and predictant, there are certain important issues that need to be considered when working with statistical downscaling. In the following, after discussing the important issues in statistical downscaling, different kinds of statistical downscaling techniques are presented.

2.2.2.1. Issues in Statistical downscaling

1. ***Assumptions:*** The main assumption made in statistical downscaling is the stability of atmosphere-surface relationship over time. Yet, there are many reasons for this assumption to be wrong. The least probable explanation for transient relationships is a change in the underlying physics as climate changes (Brent et al., 2001). A more likely reason is that short-term relationships are conditional on longer-term variations in the climate system. Unstable relationships can be enhanced further when there are multiple factors responsible for a surface condition, each of which can change in their own way. Precipitation, for instance, is controlled not only by vertical ascent, but also by available atmospheric moisture.

   The second assumption is related to the belief in GCMs representation of the large-scale features of the atmosphere. Inherent in this assumption is that general circulation modelers have an adequate understanding of atmospheric physics and that the free atmosphere is not dominated by poorly resolved boundary conditions (Winkler et al., 1997). However it has been shown that even when large-scale circulation features are modeled, GCMs tend to produce significant errors. Heyen et al. (1996) and R.L.Wilby et al. (1998) are couple of references that present these errors.

   It is also assumed in statistical downscaling that the predictors fully represent the climate change signal.

2. ***Predictor variable selection:*** Importance should be given to the large scale variable selection during statistical downscaling procedure. During model development for present conditions, certain predictor may not seem important but future changes in that predictor may be critical in determining climate change. As an example local temperature change under a 2 x CO_2 scenario is dominated by change in atmospheric radiative properties rather than circulation changes (Schubert, 1998) but for local precipitation change the inclusion of low-frequency atmospheric predictors can produce enhanced simulations (R.L.Wilby, 1998). Circulation based predictors have been widely used in downscaling procedures owing to their long available records and reasonable skill of GCMs simulating these variables, but it is also acknowledged that circulation predictors alone may not be sufficient as they may fail to capture the mechanisms of precipitations that are based on thermodynamics and vapor content. Thus humidity should also be considered together with circulation based predictor (a practice that is followed in this thesis as well).

3. ***Predictor domain selection:*** It is important to give due consideration to the domain selection during downscaling procedure. The smaller the predictor domain, the more direct the influence of host GCM on the downscaled scenario. Additionally the positioning of the domain should reflect the dominant processes affecting the region in question. A study by Brinkmann (2002) suggests that, for studies where only one grid point is used, the optimum grid point location for downscaling may be a function of the timescale under consideration and is not necessarily related solely to location. If the position of downscaling domain is not adequate, subtle variations in present and future storm track positions may not be captured. R.L.Wilby and T.M.L.Wigley (2000) found that in many downscaling cases, maximum correlations between predictant (precipitation) and predictor (mean sea level pressure) occurred away from the grid box, suggesting that the choice of predictor domain, in terms of location and spatial extent, is a critical factor affecting the realism and stability of downscaled precipitation scenarios.

4. ***Model structure and Evaluation:*** The main step in statistical downscaling involves classifying the atmospheric data and determining the relationship between the atmosphere and the surface variable. Although there are a lot of ways to categorize the model, almost all fall along the two axes: one representing a continuum that ranges from lumped to split, and another that ranges from stochastic to deterministic. The traditional approach is to lump the circulation into discrete classes. Different techniques have been used to classify the weather-types including the manual and automated methods. The relationship between the lumped patterns and the surface environment is then defined either deterministically or stochastically. A more common approach however, has been to define stochastic relationships between the circulation patterns and the surface variable. The alternative to grouping the circulation into discrete groups is to consider the continuity of circulation where there are as many circulation classes as observations. Continuous-stochastic models though, have not received much attention (Brent et al., 2001).

No matter which technique is used in statistical downscaling, evaluating the methodology is a necessary (but problematic) step. It is important to demonstrate the validity of downscaling function under future climate and that the predictors represent the climate change signal. Unfortunately it is not possible because of insufficient empirical knowledge available. A comparison of downscaled information between recent and historical periods as well as with GCMs may provide the support for assumption that climate change signal is present. The traditional approach to validation remains the specification of downscaling technique from segment of available data and then assessing the performance of the model by comparing its predictions with independent observed values. This approach certainly needs long observational records which sometimes is not available.

2.2.2.2. Transfer Function

In this kind of statistical downscaling technique, a relationship is directly quantified between predictant and set of predictor variables. Individual downscaling schemes differ according to the choice of mathematical transfer function, predictor variables or statistical fitting procedure. Regression models are commonly used to derive a relationship between predictor and predictant. Both linear and nonlinear relationship could be obtained using regression methods. Although regression method offers comparatively simpler mean of obtaining the relationship, yet the complexity of the procedure can be increased by using other methods than regression. The amount of additional information that complex methods offer however, is sometimes not enough to justify the effort that is put into them.

In the simplest form multiple regression models are built using grid cell values of atmospheric variables as predictors for surface temperature and precipitation (Fowler et al., 2007). The main advantage of regression based methods is their ease of application and their use of observable trans-scale relationships. The downside of regression based methods is their inability to portray reasonable variability in the downscaled variable. Although there have been suggestions of incorporating additional variability using different statistical techniques. Yet there may still be an issue of downscaling of extreme events using regression models since events by definitions tend to lie at the margins (or even may be beyond the range of calibration data set).

As an example Zorita and Storch (1997) used canonical correlation analaysis (CCA) (for details of the CCA the reader is referred to the book *Statistical analysis in climate research* (Storch and Zwiers, 1999)), for expressing surface scale rainfall anomaly *S(i,t)* at certain location j and time t from large scale pressure anomaly *L(i,t)* at certain location i and time t. CCA basically identifies pairs of patterns whose time evolution is optimally correlated. if p_k and q_k are identified patterns for large and surface scale variables then first step in obtaining surface scale variable is to calculate amplitude a_k with which kth large scale CCA pattern appears. This was achieved by minimizing the sum of the squares in the following equation.

$$E = \sum_{t,i} \left[L\left(i,t\right) - \sum_{k} a_k(t) p_k(i) \right]^2 \tag{2.4}$$

Above equation is differentiated w.r.t E, equated to 0 and the resulting linear system of equation is solved by standard methods. The surface scale rainfall anomalies are then just the sum of the estimated amplitudes of the local CCA patterns.

$$R(j,t) = \sum_k c_k a_k(t) q_k(j) \tag{2.5}$$

Where c_k are the canonical correlations.

In addition to using CCA as a tool to derive a relationship between predictor and predictant, a large battery of traditional and modern statistical tools have been used as transfer functions in statistical downscaling procedures with varying success. Piecewise linear and non-linear interpolation techniques (Brandsma and Buishand (1997)), Logistic regression (Abaurrea and Asín (2005)), multi-way partial least squares regression (Bergant and Kajfez-Bogataj (2005)), Artificial neural network (ANN) (Zorita and von Storch (1999)), canonical correlation analysis (CCA) (Busuioc et al. (2001)) and expanded downscaling (Bürger (1996)) are some of the examples.

2.2.2.3. Weather Generator

Weather generators are not specifically developed for downscaling purposes. Weather generators are basically statistical models used for generating sequences of weather variables such as precipitation, maximum and minimum temperature, humidity, etc. Usually precipitation sequences are generated first, and other data sequences are derived using statistical relationships between these data and precipitation. Different relationships are used for wet and dry days. For downscaling purposes the precipitation occurrence in weather generators are conditioned on large scale circulation realized/simulated by a GCM. Weather generators may be driven by weather typing schemes. For example daily weather patterns have been identified from principal components of mean sea level pressure to condition a weather generator. Improvements in the modeling of the autocorrelation structure of wet and dry days were observed when the probability of rain is conditioned on the current circulation pattern and the weather regime of the previous day (Fowler et al. (2007)). As in other precipitation modeling methodologies, precipitation generation in weather generators are also divided in occurrence and amount processes. Most of the weather generators focus on daily time scale but there are also sub daily models also exist for example Katz and Parlange (1995).

Precipitation occurrence process is usually modeled in two ways, either using Markov chain approach or spell length approach. The performance of each method in realistically simulating precipitation occurrence depends much on the climatic properties of the area where each method is applied. For example Wilks (1999) found the first-order Markov model to be adequate for the central and eastern USA, but that spell length models performed better in the western USA.

Markov chain models (Figure 2.3a) are used in an attempt to realistically simulate the natural behavior of precipitation occurrence. Precipitation data exhibit distinc-

tive and difficult characteristics which complicate the statistical models needed to describe them. In addition to exhibiting the correlation between values at successive time periods that is typical of all weather variables, precipitation is unique in its mixed character as both a discrete and continuous variable. That is, precipitation is very often exactly zero, and hence there is a discontinuity in the probability distribution of precipitation data between the zero and the nonzero observations (D.S.Wilks and R.L.Wilby, 1999). The precipitation occurrence has understandably two states wet and dry, occurring in successive runs. This behavior can be reproduced using first order markov chain process (higher order markov chains are/can also be used). The first order process can be shown by the following two conditional probabilities (called transition probabilities as well).

$$p_{01} = pr\left\{precipitation\,on\,day\;t \mid no\,precipitation\,on\,day\;t-1\right\} \tag{2.6}$$

$$p_{11} = pr\left\{precipitation\,on\,day\;t \mid precipitation\,on\,day\;t-1\right\} \tag{2.7}$$

From these two probabilities two complementary probabilities could also be calculated as:

$$p_{00} = 1 - p_{01} \tag{2.8}$$

$$p_{10} = 1 - p_{11} \tag{2.9}$$

Where p_{00} is probability of dry day following a dry day while p_{10} is probability of dry day following a wet day. Two important and useful precipitation properties could be derived from four conditional probabilities shown in Equation 2.6 through Equation 2.9.

$$\pi = \frac{p_{01}}{1 + p_{01} - p_{11}} \tag{2.10}$$

and

$$r_1 = p_{11} - p_{01} \tag{2.11}$$

π represents the long run relative frequency of precipitation whle r_1 is first lag autocorrelation of the precipitation occurrence series. Given the natural precipitation phenomena, p_{11} is always greater than p_{01}, which makes $p_{01} < \pi < p_{11}$ and $r_1 > 0$. It is also assumed that the lengths of alternating wet and dry spells are distributed according to geometric distribution and that they are independent.

$$pr\left[X = x\right] = p\left(1-p\right)^{x-1}, x = 1, 2, 3, ... \tag{2.12}$$

Accordingly the probabilities for wet and dry spells are $p = p_{01}$ and $p = 1 - p_{11}$ respectively. Finally the average number of days (E) and variance of the number of days (Var) for certain length of consecutive wet days $N(T)$ are computed as:

$$E[N(T)] = \pi T \tag{2.13}$$

$$Var[N(T)] \approx \pi(1-\pi)T\frac{1+r_1}{1-r_1} \tag{2.14}$$

spell length models (Figure 2.3b) are another alternative for generating occurrence series of precipitation. This methodology generates the lengths of wet or dry spell not by operating on daily basis but instead in form of spells. Different probability distributions are fitted to observed relative frequencies of wet and dry spell lengths. Random numbers are then generated for each length of spell. A new spell length of opposite type is generated only when previous spell length has ended. The advantage of this method is that precipitation occurrence sequences with different statistical characteristics can be obtained using different distributions for the frequencies of spell lengths. Various distributions can be used for spell lengths e.g. truncated negative binomial, negative binomial distribution and mixed geometric distribution are some of the frequently used distributions.

Once a decision about the day being wet or dry is made, the next step is to generate precipitation amount on a wet day. Daily precipitation amount distribution is strongly skewed toward the right side, with small precipitation amounts occurring commonly and large precipitation amounts rarely. Different types of theoretical distributions have been used in weather generators to estimate non-zero precipitation amount. Most common and simple is the exponential distribution where only one parameter μ is needed.

$$f(x) = \frac{1}{\mu}exp\left[\frac{-x}{\mu}\right] \tag{2.15}$$

Average precipitation in equation 2.15 is μ and variance $\sigma^2 = \mu^2$. Comparatively complicated distributions such as gamma distribution (Equation 2.16) (with two parameters: the shape parameter α and scale parameter β and gamma function Γ evaluated at α. With distribution mean $\mu = \alpha\beta$ and variance $\sigma^2 = \alpha\beta^2$) and variant of exponential distribution (Equation 2.17) are also used for precipitation amount estimation. The probability density function of the two distributions are:

$$f(x) = \frac{(x/\beta)^{\alpha-1}exp[-x/\beta]}{\beta\Gamma(\alpha)} \tag{2.16}$$

$$f(x) = \frac{\alpha}{\mu_1}exp\left[\frac{-x}{\mu_1}\right] + \frac{1-\alpha}{\mu_2}exp\left[\frac{-x}{\mu_2}\right] \tag{2.17}$$

Equation 2.17 indicates a combination of two exponential distributions with respective means of μ_1 and μ_2. Third parameter α is called mixing parameter. First exponential distribution generates precipitation amount with probability α and the second one with $1-\alpha$. The distribution has mean $\mu = \alpha\mu_1 + (1-\alpha)\mu_2$ and variance $\sigma^2 = \alpha\mu_1^2 + (1-\alpha)\mu_2^2 + \alpha(1-\alpha)(\mu_1-\mu_2)^2)$ (first suggested by Woolhiser and Pegram (1979)). Although the mixed distribution is rarely used, it has been showed that it provides substantially better overall fits to daily precipitation data than the gamma distribution (e.g. Wilks (1998) and Foufoula-Georgiou and Lettenmaier (1987)).

The major disadvantage of WGs is that they are conditioned using local climate relationships and so may not be automatically applicable in other climates. They

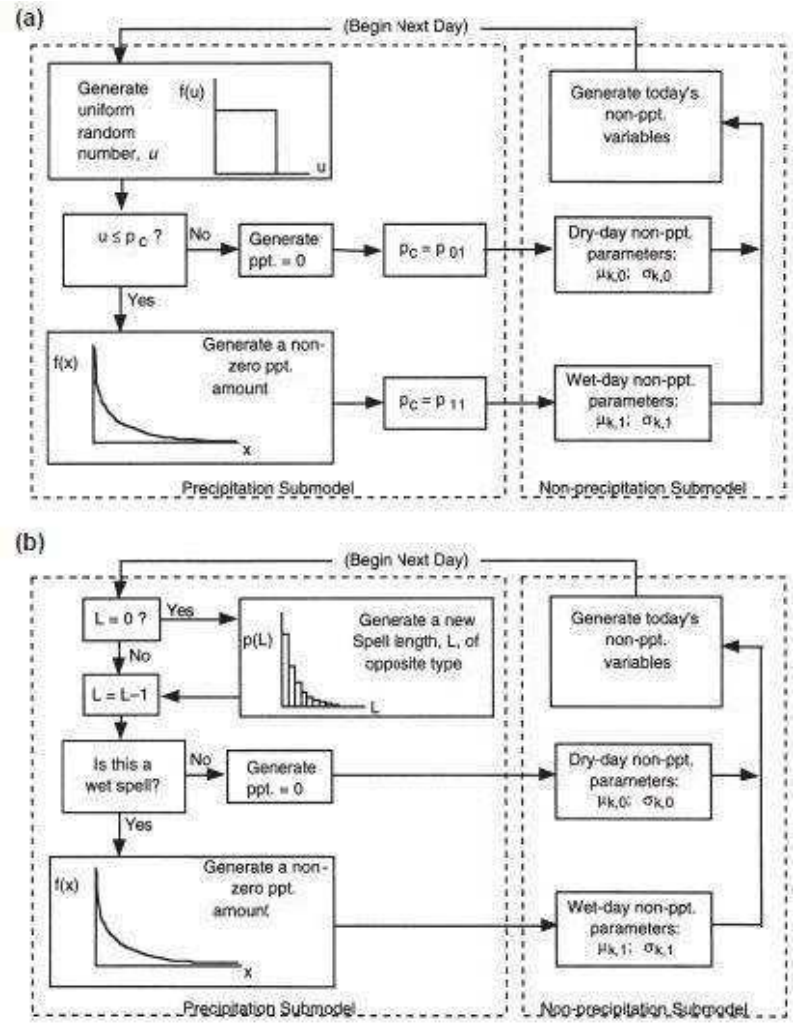

Figure 2.3.: Flow charts of precipitation occurrence process in weather generators using (a)Markov chain and (b) Spell length procedures (D.S.Wilks and R.L.Wilby, 1999)

also tend to underestimate inter-annual variability (Fowler et al. (2007)). Further, for future climate scenario studies it needs arbitrary adjustment in parameters. Changes in precipitation occurrence parameters may have unanticipated effects on other variables as well.

2.2.2.4. Analog Method

The idea of Analog downscaling is comparatively simple. The method is more applied in weather forecasting than in statistical downscaling of large scale variables. There are very few published examples of usage of analog method as a downscaling tool.Zorita et al. (1995), Cubasch et al. (1996) and Biau et al. (1999) are few

of the examples. The main idea of analog downscaling methodology is that similar general circulation patterns should provide similar local effects (Obled et al., 2002). Major task then in analog downscaling is to search for best analog of the given day in the historical archive and associate the corresponding reaction of that circulation pattern to given day's circulation pattern. Different similarity measures can be used to search for the best analog. E.N.Lorenz (1969) lists the following assumptions for analog search approach:

1. that there have been synoptic situations in the past that were not necessarily identical but similar to the current one for which a forecast is required

2. that during such situations, local variables, such as precipitation over a medium-sized mountain catchment, react partly in response to the synoptic situation, but also to more local features (e.g. orography, wind channeling, etc.)

3. that for this given day, the part explained by regional circulation will be similar to that observed in analogous situations.

The analog search and application of adopted analog are diagrammatically shown in figure 2.4 and figure 2.5. Given the synoptic patterns characterizing current day, the most similar past situations are looked up in comparatively long meteorological archive and a subset of analog is extracted. Assuming that precipitation amounts are the predictants of the downscaling process undertaken, for every day of this analog subset, the rainfall amounts collected over the specific catchment for these particular days are extracted from a hydrological archive. The resulting amounts provides an empirical sample of the amounts of rain for the current day's characteristic synoptic pattern. Any appropriate theoretical distribution can finally be fitted to the extracted amounts and a probabilistic forecast could be made. It should be noted that the process can be performed for the current day for which the synoptic patterns are either observed values or are simulated by GCM/RCM.

Often reported drawback of use of analog method for downscaling is the need of long homogeneous record of the large and local scale variables. It has been reported that due to the number of degrees of freedom of the large-scale atmospheric circulation, several thousand years of recorded data would be needed for finding appropriate analog. But it has been shown that using different statistical tools (e.g. empirical orthogonal analysis EOF) most of the degree of freedoms can be reduced as they are associated with background noise in the data and hence in comparatively shorter available records, analogs could be found.

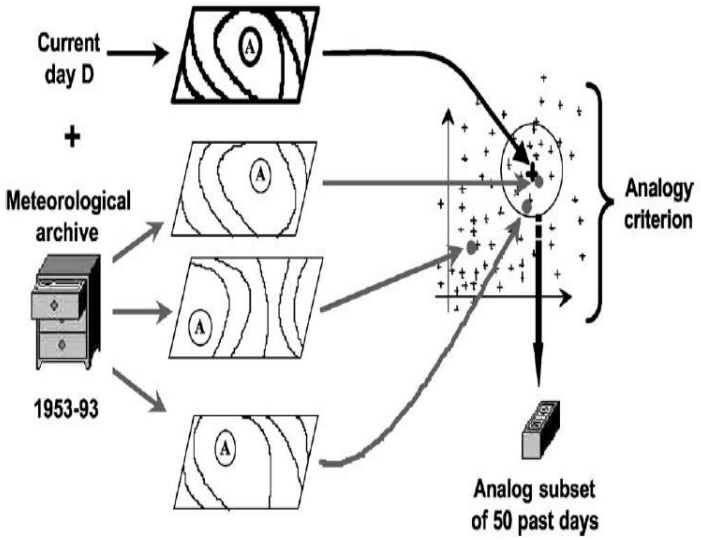

Figure 2.4.: Step one of analog search process Obled et al. (2002)

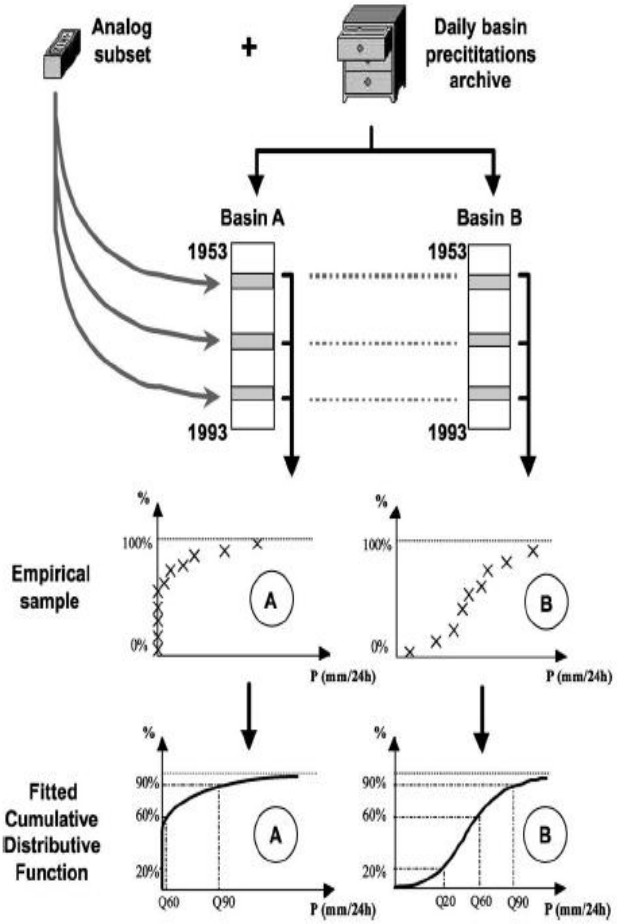

Figure 2.5.: Step two of analog search process Obled et al. (2002)

2.2.2.5. Weather typing

The basic idea of weather typing or classification is simple. Atmospheric circulations are classified in several classes using different schemes and criterions and a pool of historical observations is distributed into these defined classes. For downscaling purposes, atmospheric circulations simulated by GCMs are classified into the classes defined earlier. To each observed circulation there exists a simultaneous observation of the local variable, which could be assigned to the simulated circulation either as:

1. an average of all regional observations simultaneous to the elements of that class
2. or only the regional observations simultaneous to *one* element of the class, selected at random.

The choice among the two options depend upon the problem at hand. In case of simulation of daily rainfall, opting for case 1 above will in general lead to an underestimation of the local rainfall variance and extreme events. The rainfall probability distribution may also be different than the observed one. On the other hand, averaging over several elements of the class will filter out more effectively measurement errors at that station. Important aspect of weather typing is the methodology of classification employed for identification of classes. The classification can be subjective or objective.

The typical example of subjective classification schemes is the traditional *Grosswetterlagen* classification of the German Weather Service for the Western Europe North Atlantic sector (Zorita and von Storch, 1999). This classification has been used for downscaling purposes by Bárdossy and Plate (1992). Based on local expertise weather typing procedures have been developed by many national weather services for their particular regions. Subjective schemes of Schuepp (1953) for Switzerland and Lamb (1972) classification for the British Isles are the most important ones. Local surface variables, typically precipitation, are conditioned on daily weather patterns by deriving conditional probability distributions for observed statistics, e.g. *p(wet-wet)* or mean wet day amount, associated with a given atmospheric circulation. Climate change is estimated by evaluating the change in the frequency of the weather classes simulated by the GCM. The method assumes that the characteristics of the weather classes will not change (Fowler et al., 2007).

Depending upon the methodology employed for classification, objective classification can technically become quite complicated. Three major schemes of objective classification are:

1. classifications that only depend upon large scale circulation area
2. classifications that depend only on local scale variables
3. classifications that make use of both large scale and local scale variables

X.Cheng and Wallace (1993), used cluster analysis for classification of atmospheric circulation which is a typical example of first and second class of objective classification. In the first case the classes of the large-scale circulation are given directly

by the analysis. In the second case the elements of the large-scale circulation class are defined as the simultaneous circulation to each element of the local climate class. This second method has the advantage that the resulting large-scale classes should really correspond to different local situations, which is not necessarily the case in a classification based only on the large-scale patterns (Zorita and von Storch, 1999). Classifications that make use of both large scale and local scale variables are comparatively more complicated. Classification and regression trees (CART) used by Breimann et al. (1984), used for simulation of local daily rainfall is one example of this class. However, comparing with the first two categories it needs more computer resources.

2.2.2.6. Short comings of statistical downscaling

The major theoretical weakness of statistical downscaling methods is that their basic assumption is often not verifiable, i.e. that the statistical relationships developed for present day climate also hold under the different forcing conditions of possible future climates. Another caveat is that these empirically based techniques cannot account for possible systematic changes in regional forcing conditions or feedback processes. Long and reliable observed time series of predictant variable is required for estimation of reliable relationship between predictor and predictant. As is the case in RCMs, statistical downscaling methods are also affected by the biases in underlying GCM. some statistical downscaling techniques e.g. transfer function approaches and weather typing approaches suffer from under prediction of temporal variability.

3. Methodology

3.1. Preface

This dissertation employs statistical downscaling methodology to downscale large scale meteorological variable to local scale. Large scale variables (e.g. sea level pressure, geo-potential height etc.) are classified into certain groups representing different meteorological situations. These different meteorological situations are associated with different local scale variable's (e.g. precipitation, temperature etc.) reactions. The Weather typing approach of statistical downscaling was introduced in Chapter 2 (2.2.2.5), where different types of classification techniques, namely the subjective and objective classification, were presented. A fuzzy rule based objective classification method is used here to classify large scale circulation patterns (CPs). The fuzzy rule based classification system was developed by Bárdossy et al. (2002). The methodology is further developed in this dissertation to achieve a classification scheme that is representative of not only floods but droughts as well.

This chapter will present the methodology that is employed in fuzzy rule based classification of large scale circulation patterns and is followed by the developments made in the methodology. This chapter will also present the two statistical downscaling methodologies which make use of the improved classification system of critical circulation patterns explained in the first part of the chapter.

3.2. Fuzzy rule based classification of large scale circulation patterns

This type of classification of large scale circulation patterns is based on the concept of fuzzy sets defined by Zadeh (1965). Fuzzy logic works with imprecise/inconclusive statements and attempts to deduce meaning from them by assigning a membership function to each variable involved in a set. The membership function provides a measure to represent the degree up to which certain members of a set belongs to that set. It can be recalled that in conventional set theory a certain variable either belongs to a set or it does not. Detailed methodology of fuzzy rule based classification is presented in Bárdossy et al. (2002); here only a brief necessary background is presented.

The objective classification and optimization system necessarily consist of three steps;

1. Transformation of data

2. Definition of fuzzy rules for large scale circulation patterns

3. Classification

Assuming that we have certain large scale predictor data available over a regular grid in daily resolution, the first step is to normalize the data by calculating anomalies at each grid point i:

$$g(i,t) = \frac{h(i,t) - \overline{h}(i,t)}{s(i,t)} \tag{3.1}$$

Where *g(i,t)* is the normalized anomaly vector of the large scale predictor data *h(i,t)*, with a mean and standard deviation of $\overline{h}(i,t)$ and *s(i,t)*, respectively, for grid point i and time t.

Bárdossy et al. (2002) describes the fuzzy rules as more or less the same as classical expression based on logical operators except that in fuzzy rules the consequence and its opposite may both be "true" to a certain degree. Before the actual classification is performed, however, fuzzy rules of the type IF, THEN, ELSE are described first. The classification is then done by finding the most appropriate rule for the selected object (in this case, the calculated strength of daily anomalies). Daily anomalies are divided in following five classes:

1. Large positive
2. Medium positive
3. Medium negative
4. Large negative
5. Irrelevant

As the names would suggest, the first four describe the anomaly strength at any given location on the regular grid, while the last one defines the anomaly that does not make much impact on the class as such. A typical fuzzy rule for a certain large scale circulation pattern would thus resemble the following:

IF (AT LEAST A FEW of the locations (from all available locations) have very low pressure anomalies) AND (MOST OF the locations (from all available locations) have medium low pressure anomalies) AND (MOST OF the locations (from all available locations) have medium high pressure anomalies) AND (AT LEAST A FEW of the locations (from all available locations) have very high pressure anomalies) THEN the CP is i.

Thus a CP k on a day can be described as a vector that contains index values from 1 to 5, corresponding to anomaly strength at each grid point *i*, *v(k) = (v(1,k),...v(I,k))*. The rule system for all CPs can thus be represented by the matrix $\mathbf{V}$ as:

$$\mathbf{V} = \begin{pmatrix} v(1,1) & \cdot & \cdot & \cdot & v(I,1) \\ \cdot & \cdot & & & \cdot \\ \cdot & & \cdot & & \cdot \\ \cdot & & & \cdot & \cdot \\ v(1,K) & \cdot & \cdot & \cdot & v(I,K) \end{pmatrix} \tag{3.2}$$

Once the data transformation and fuzzy rule development is performed, the days are classified as belonging to distinct circulation patterns by calculating the degree of fulfillment (DOF) for each rule:

$$\mathbf{DOF}(\mathbf{k},\mathbf{t}) = \sum_{m=1}^{4} \left(\frac{1}{N_{k,m}} \sum_{v(i,k)=m} \mu_m(g(i,t))^{p_m} \right)^{(1/p_m)} \tag{3.3}$$

Assuming that fuzzy rules are developed such that there are m classes, then $N_{k,m}$ is the number of grid points that are assigned to each class in rule k. μ_m is the membership function of the anomalies corresponding to defined strength of anomalies, and p_m is used for taking care of small differences in calculation of exact location of the anomalies. The rule which obtains the highest value of ***DOF(k,t)*** is selected as governing CP for day t.

The fuzzy rule based classification was developed for downscaling the climate variables of precipitation and temperature. Circulation patterns were classified in number of different classes and based upon certain statistics, indicators and formulation of objective functions; critical circulation patterns (CPs) were distinguished from normal CPs. The indicators were developed keeping in mind the objective of the study, in most cases being floods. Hence a precipitation and temperature based classification was used for flood producing CPs. The methodology was further developed by Bárdossy and Filiz (2005) where, instead of precipitation, discharge was used to identify critical circulation patterns related to floods. The daily discharge time series was changed to a daily positive discharge increment series with a 1 day lag and used as the predictant. The idea behind using discharge based with a 1 day lag was to better capture the reaction of the catchment, as higher discharge may result because of precipitation that had occurred a day earlier. Hence the delayed reaction time of the catchment is attempted to be captured using this methodology. The daily discharge data set is first changed to discharge differences on 1 day lag (ΔQ), and a new variable *Z(t)* is used to classify large scale variable with:

$$Z(t) = \begin{cases} \Delta Q(t), & \text{if } \Delta Q(t) > 0; \\ 0, & \text{otherwise.} \end{cases} \tag{3.4}$$

The optimal rules were obtained in Bárdossy et al. (2002) who introduced the following two objective functions: one related to the occurrence of days with a large positive discharge increment (Equation 3.5), and second, related to the amount of discharge increment (Equation 3.6) as follows:

$$O_1 = \sum_{s=1}^{S} \sqrt{\frac{1}{T} \sum_{t=1}^{T} (p(z_0(CP(t)=i)) - \overline{p_{z_0}})^2} \tag{3.5}$$

$$O_2 = \sum_{s=1}^{S} \frac{1}{T} \sum_{t=1}^{T} \left| \overline{z(CP(t)=i)}\overline{z} - 1 \right| \tag{3.6}$$

$\overline{p}$ is the probability of an increase in discharge, exceeding threshold z_0 on a certain day, while *p(z(CP(t)=i))* is the same probability but conditioned upon the occurrence of CP i on day t. In the second equation, $\overline{z}$ is the mean increase of discharge increment amount on a certain day, while $\overline{z(CP(t) = i)}$ is the same amount but conditioned upon the occurrence of CP i on day t. Both Equation 3.5 and Equation 3.6 are summed over all the gauge stations S. Both of these objective functions would result in higher values if the relative increase in occurrence and amount of discharge increment given certain CP classification, is large than it is when no classification is considered at all. Both the objective functions are added to one objective function (with a possibility of giving different weights to each one, depending upon the need) and maximized with the help of a simulated annealing algorithm.

Above methodology was developed to obtain a classification that explains and identifies critical circulation patterns related to extreme flood events. Droughts are another extreme manifestation of a hydrological system that need to be considered in relation to large scale circulation pattern classification as well as downscaling. Floods are associated with certain meteorological and hydrological situations (frequent heavy rainfall, antecedent conditions, glacial melt) to which approximate degrees of certainty can be ascribed. Droughts, on the other hand, are associated with conditions which are difficult to predict. The time scales involved for these two extremes are very different in that floods could occur after a few hours of consistent heavy rainfall and pass through certain area within hours, whereas droughts are characterized by slow onset and unclear end. Thus bringing with them the impacts which are spread over larger geographical areas. Therefore droughts are rightly considered to be the most complex and least understood hydrological phenomenon of the two. In the following, two methodologies are presented for large scale circulation pattern classification that are hoped to give a more robust classification of large scale circulation patterns. The aim of the classification is to achieve a single classification system that gives distinct "critical" circulation patterns both for floods and droughts.

3.2.1. Low discharge based objective function

Low flow based objective function, as the name suggests, is based again on daily river discharge increments/decrements but instead of working with the discharge increments values above certain threshold value (like 95^{th} percentile value), here, limits on the probability distribution function of the discharge increments/decrements are used. As explained in the previous section, daily discharge values recorded at certain gauge stations can not be directly linked with atmospheric circulation. For a selected day, the river discharge amount is the function of several processes that include baseflow, interflow, antecedent soil moisture content and glaciel melt, etc. Hence, if a higher discharge has been recorded on a day at certain location x_1 this may probably be because of heavy precipitation occurring at location x_2 or glacier melting at x_3 due to higher temperatures . Therefore it might not be appropriate to relate the high discharge at location x_1 with flood producing large scale circulation pattern.

While discharge at a certain location x_1 and time t_1 can not be directly linked with the corresponding large scale active circulation pattern at the same time t_1, it

can, however, be written as a function of precipitation, which can be directly linked to atmospheric circulation. Hence, if for a certain catchment A the lag time Δt is known then the discharge can be written as:

$$Q(t) = \int_{t-\Delta t}^{t} \int_{A} h(P(x,t))dxdt + KQ(t-1) \tag{3.7}$$

where h is the rainfall-runoff transformation process, K represents memory of the discharge and is constant (usually equal to 1), *Q(t)* is the discharge amount at time t of catchment A which understandably is a function of precipitation P at certain location x. Discharge difference series can thus be formulated as:

$$\Delta Q(t) = Q(t) - Q(t-1) = \int_{t-\Delta t}^{t} \int_{A} h(P(x,t))dxdt - (1-K)Q(t-1) \tag{3.8}$$

Equation 3.8 represents daily discharge increments and is strongly related to the precipitation. It is very small for dry periods, positive for increasing limb of hydrograph and negative right after the flood wave. Figure 3.1 shows the discharge, discharge increment/decrement and positive discharge increment series for gauge station Ettlingen at Alb catchment in southern Germany for year 1982. It can be seen that the discharge increment/decrement series is closely related to precipitation. From this the following objective functions can thus be formulated:

$$O_3 = \frac{1}{T} \sum_{t=1}^{T} \left| \log \frac{dQ_+(CP(t))}{d\bar{Q}_+} \right| \tag{3.9}$$

$dQ_+(t)$ is the positive values of discharge increment series. This value is closely related to precipitation and increases as precipitation amount $dQ_+(t) = \max(0, dQ(t))$ increases. As mentioned earlier, this condition although is true, it is not always necessarily the case . Since discharge may increase due to other reasons. Different pre-event conditions stimulate different catchment reactions from the same precipitation event. Thus the second objective function to be defined takes in to account the occurrence of positive discharge increments as follows:

$$O_4 = \frac{1}{T} \sum_{t=1}^{T} (p_{dQ_+}(CP(t)) - p_{d\bar{Q}_+})^2 \tag{3.10}$$

Within the time period T, this objective function when maximized using optimization algorithms, will maximize the difference between CP conditioned relative frequency of $dQ_+(t) > 0$ ($p_{dQ_+}(CP(t))_i$ at station i) and the unconditional relative frequency $p_{d\bar{Q}_+}$ of a day with $dQ_+(t) > 0$ for all days.

For dry periods, the classification based on an objective function related with small discharge changes is presented. While the large positive discharge increment time series of a river indicates large amount of precipitation in the area, small discharge changes indicate the dry period in the river's catchment system. Additionally large positive discharge changes in regulated rivers can be misleading, as they might well be an anthropogenic change in the river discharge. Referring to the time series of

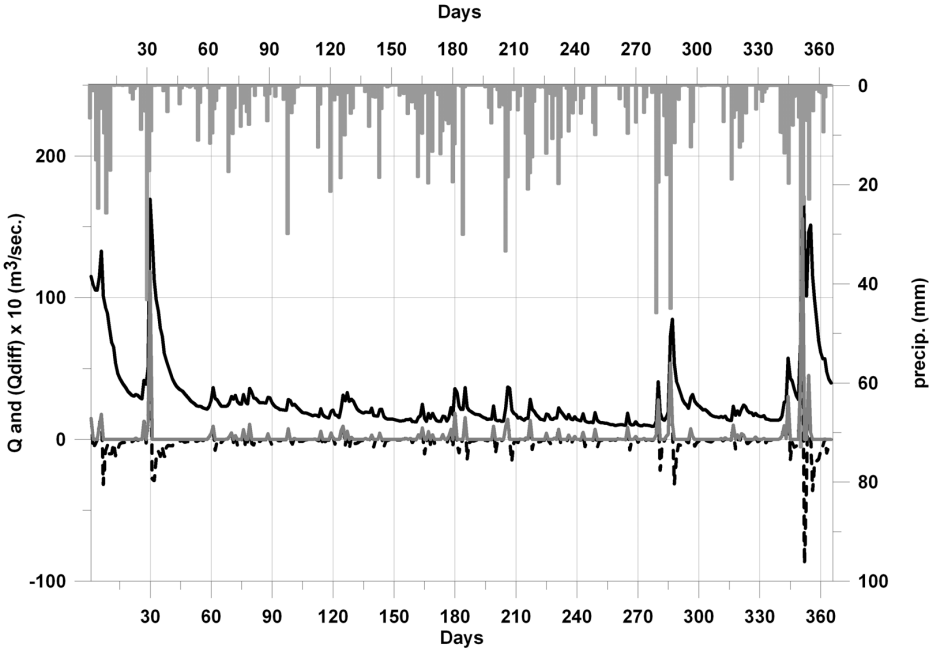

Figure 3.1.: Daily discharge (thick solid black line), discharge increment/decrement on 1 day lag (thick dashed black line), positive part of discharge increment on 1 day lag (thick solid gray line) and daily precipitation (thin gray solid lines) for Alb catchment for year 1982

discharge, discharge increment/decrement and positive part of discharge increment in Figure 3.1, one can see that most of the time series consist of small discharge changes, and they change to large changes only when there is additional water introduced in to the system. Hence the "equilibrium" state of the time series is disturbed either by additional precipitation coming from the atmosphere and/or from any river regulation authority managing the flow in the rivers. Hence, the extreme increase and decrease in the time series of discharge increment/decrement, displayed by curve in Figure 3.1 is specific to each river. This is because topography, land use, nature of catchment drained by the river, and antecedent state of the river plays an important role also. Small discharge changes, on the other hand, are always related to the dry state of atmosphere, that is independent of the catchment properties. Thus we can establish a mathematical link between discharge and the dry state of atmosphere by considering an objective function for classification of circulation patterns that is based on low flow or small discharge changes.

The dry state of atmosphere can thus be represented by an indicator $I_{dQ}(t)$:

$$I_{dQ\approx 0}(t) = \begin{cases} 1 & \text{if } p_{min} \leq F_{dQ}(dQ(t)) \leq p_{\max} \\ 0 & \text{else} \end{cases} \tag{3.11}$$

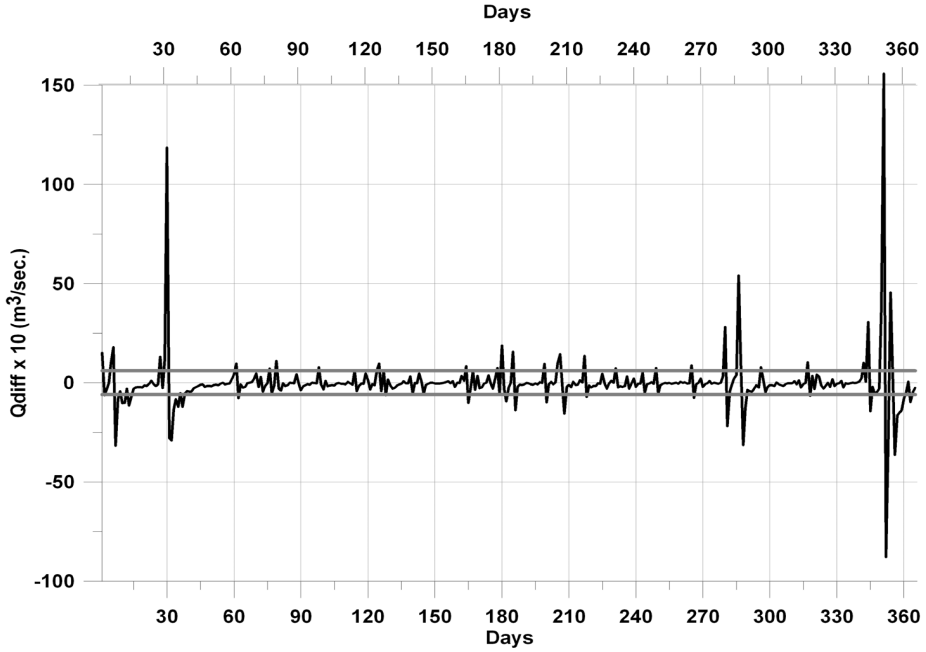

Figure 3.2.: Daily discharge difference series on 1 day lag (thick solid black line) along with the two limits (thick solid gray lines) representing the "equilibrium" state of Alb catchment for year 1982

Where F_{dQ} is the probability distribution function of the discharge differences. The equilibrium state of the catchment is represented by the limits p_{min} and p_{max} which are defined as $0 < p_{min} < p_{max} < 1$. Two conditions must be considered regarding the selection of p_{min} and p_{max}:

1. No major flood should have occurred/included between these limits

2. All non-natural discharge increments (or decrements) must remain in the interval $[F_{dQ}^{-1}(p_{min}), F_{dQ}^{-1}(p_{max})]$

A choice of $p_{max} = 0.75$ and $p_{min} = 0.25$ can be used if no specific information on discharge regulations is available. Figure 3.2 displays the discharge increment/decrement time series for 1982 of the Alb catchment along with the limits for the low discharge changes corresponding to $p_{max} = 0.85$ and $p_{min} = 0.20$.

The third objective function based on discharge can thus be written as:

$$O_5 = \frac{1}{T}\sum_{t=1}^{T}(p_{I_{dQ\approx 0}}(CP(t)) - p_{\bar{I}_{dQ\approx 0}})^2 \tag{3.12}$$

3.2.2. An objective function based on a cluster of precipitation stations

One potential problem with the optimization of the objective functions of the type presented in Equations 3.5 and 3.6, is that the shape of objective function obtained from them is extremely irregular. This might make it difficult for the optimization algorithm to reach to a global maximum (or minimum). It is especially true in case the algorithm attempts to optimize the objective function for each individual gauge station involved. An objective function with less irregular shape may result in better classification. Areal precipitation ($z_A(t)$) is one variable that can used instead of point precipitation. For a certain catchment A, the objective function based on areal precipitation ($z_A(t)$) can be written as:

$$O_6 = \frac{1}{T}\sum_{t=1}^{T}\left|\log\frac{z_A(CP(t))_i}{\bar{z_{Ai}}}\right| \tag{3.13}$$

Where

$$z_A(t) = \int_A z(x,t)\,dx$$

Large scale critical circulation patterns by definition affect larger areas. If a wet CP is considered then the area affected by it, in terms of amount of precipitation received, should be large. Some isolated precipitation events, although important, may not necessarily be because of a large scale circulation pattern and may just instead be a local phenomenon. Thus, an objective function should be developed to take into consideration total precipitation that is encompassed in a certain area by a certain rainfall event. This objective function should also not be affected by the high skewness of precipitation amounts. For a certain catchment, the ratio of wet precipitation stations (precipitation greater than certain threshold amount) to total precipitation stations in a neighborhood Δ is calculated and used in the objective function as:

$$C_\Delta(t) = \frac{\#\{x_i \,\big|\, x_i \in \Delta\ ,\ z(x_i,t) > 0\}}{\#\{x_i \,\big|\, x_i \in \Delta\}} \tag{3.14}$$

$$O_7(\eta) = \sqrt{\frac{1}{T}\sum_{t=1}^{T}(p_C(CP(t))_i - \bar{p_{Ci}})^2} \tag{3.15}$$

Where # is the total number of elements in a set of precipitation stations, $p_C(CP(t))_i$ is the relative frequency of the coverage exceeding a selected threshold η on a day with given CP at station i and $\bar{p_{Ci}}$ is the relative frequency of a day with coverage exceeding $0 \leq \eta < 1$ for all days without classification and within the time period T.

Wet and dry conditions in the catchment can be captured using the above objective condition by manipulating the value of η in Equation 3.15. If $\eta = 0$, the objective function then helps to identify situations where no precipitation in the neighborhood

Δ is found; this indicates prevailing dry situations. Alternatively, if η is close to 1, the objective function helps to identify situations where precipitation is found in whole of the neighborhood Δ; this indicates then very wet situations. Thus, the combination such as $O_4 = O_4(0) + O_4(0.999)$ provides an objective function that might lead to CPs corresponding to very wet and very dry situations.

3.3. Statistical downscaling of precipitation

Chapter 2 presented the need for downscaling of large scale variables from large scale to local scale. Different methodologies employed in downscaling were also presented, namely, statistical downscaling (2.2.2) and dynamical downscaling (2.2.1) along with the different procedures for each methodology. The initial part of this chapter presented the methodology for achieving a set of circulation patterns which describe as a whole the weather situation in a certain study area with emphasis on identifying critical circulation patterns related to floods and droughts. In this section, the statistical downscaling approach, based on the classification obtained from methodology in the first part, is presented. Two statistical downscaling methodologies are explained; one is based on Bárdossy and Plate (1992) and the PhD dissertation of Yang (2007), and the other methodology concerns the downscaling from RCM generated data using CP based quantile-quantile exchange of precipitation amounts for bias correction.

3.3.1. Statistical downscaling based on the conditional multivariate downscaling approach

The statistical downscaling is based upon multivariate autoregressive model, parameters of which depend upon atmospheric circulation pattern. Using this downscaling technique daily rainfall is modeled such that the spatial and temporal dependence of the original time series is maintained in the modeled time series. The spatial dependence is the model is captured by spatial covariance matrices. Temporal dependence in the model is captured by logistic regression technique which uses combined term of moisture flux (geostrophic wind and specific humidity) as regressor. In the following the components of model (occurrence model, amount model and spatial dependence structure) are briefly described.

Precipitation occurrence is modeled using logistic regression. Moisture flux (MF) is used as a predictor in the logistic regression equation. In previous studies, occurrence of precipitation was tied only to occurrence or non-occurrence of certain circulation patterns. Although precipitation occurrence probabilities achieved only from coupling of circulation patterns did provide reasonable results, they did result in a static model. Precipitation occurrence not only depends upon weather state, represented by circulation patterns, but also on multitude of other continuous variables. Moisture flux is thus used as an additional parameter and predictor in the logistic regression equation with rainfall probability as predictant. Moisture flux is supposed to catch within-type dynamic variability during classification of circulation patterns. It is a combined term achieved from geostrophic wind (summation of both **u** and **v** components of wind field) and specific humidity (sh). The moisture flux is thus supposed to describe the amount of water vapor transported by the wind in or out

of the selected area, and, consequently, influences the occurrence or non-occurrence of precipitation.

$$MF(x,t) = (\mathbf{u(x,t)} + \mathbf{v(x,t)}) \, .sh(x,t) \tag{3.16}$$

All the terms are for certain location x and time t. The logistic regression is defined as:

$$y(x,t) = \frac{1}{1 + exp(b_0(x,t) + b_1(x,t).MF_1(x,t) + b_2(x,t).MF_2(x,t) + ... + b_k(x,t).MF_k(x,t))} \tag{3.17}$$

$b_0, b_1 ... b_k$ are the parameters of the logistic regression equation and MF's are the moisture flux values considered for for location x and time t. They are approximated using fourier series.

$$b_0(t^*) = \frac{a_0(i,x)}{2} + \sum_{k=1}^{K} (a_k(i,u)cos(kwt^*) + b_k(i,u)sin(kwt^*)) \tag{3.18}$$

and

$$b_1(t^*) = \frac{c_0(i,x)}{2} + \sum_{k=1}^{K} (c_k(i,u)cos(kwt^*) + d_k(i,u)sin(kwt^*)) \tag{3.19}$$

a_k, b_k, c_k and d_k are the coefficients of harmonics of fourier series, b_0 and b_1 are the approximated parameters of the regression equation, i is the CP, x is the location, K is the total number of precipitation stations and t^* is the julian day of the year.

The precipitation amount distribution is highly skewed and unlike precipitation occurrence, which is modeled as discrete process, is a continuous process. Different probability distribution models have been used for the simulation of precipitation amounts e.g. weibull, transformed normal and gamma distribution. The exponential distribution model is used here for the precipitation amount process. For a certain variable value x,its probability density function can be written as:

$$f(x) = \lambda.exp(-\lambda.x) \tag{3.20}$$

Where x and λ are always greater than 0 . λ is the parameter of exponential distribution controlling the shape of distribution function and is estimated using the maximum likelihood estimator.

$$L(\lambda) = \sum_{Z(t,u) \leq Z_0} (\lambda(t,u).x) + \sum_{Z(t,u) > Z_0} (ln\lambda(t,u) - \lambda(t,u).x) \tag{3.21}$$

$$\lambda(t,u) = \frac{1}{\mu_0(t^*,u) + a.MF} \tag{3.22}$$

where $Z(t,u)$ is daily precipitation amount at time t and location u and $\mu_0(t^*,u)$ is the expectation of precipitation on the julian day t^*.

The spatial structure of precipitation is taken care of by using spatial covariance and auto-correlation. Instead of calculating the two measures directly from precipitation values, a binary indicator variable based on certain threshold value is used to regionalize the precipitation in certain catchment.

$$I(u,z) = \begin{cases} 1, & \text{if } z(u) \leq z; \\ 0, & \text{otherwise.} \end{cases} \tag{3.23}$$

$z(u)$ is the precipitation amount at certain location u and z is the cutoff corresponding to the conditional cumulative distribution of the precipitation amount. $I(u,z)$ is thus a binary variable which is used in the subsequent calculation of Γ_{0i}, the spatial covariance matrix, and Γ_{1i}, the space-time covariance for one day lag. Both Γ_{0i} and Γ_{1i} are calculated independently for each CP considered in the classification system.

$$\Gamma_{0i}(t^*) = E\Big[\Big(W(t) - w_i(t^*)\Big)\Big(W^T(t) - w_i^T(t^*)\Big)\Big] \tag{3.24}$$

$$\Gamma_{1i}(t^*) = E\Big[\Big(W(t-1) - w_i(t^*-1)\Big)\Big(W^T(t) - w_i^T(t^*)\Big)\Big] \tag{3.25}$$

Auto-correlation factor $r(t^*)$ links Γ_{0i} and Γ_{1i} as:

$$r(t^*) = \frac{\Gamma_{1i}(t^*)}{\Gamma_{0i}(t^*)} \tag{3.26}$$

The spatial structure of rainfall is described using Equation 3.27, where parameters p_i and q_i depend upon circulation pattern i and the day $t^*$of the year.

$$cov[W_x(t^*,u), W_y(t^*,u)]_i(t) = P_i(t^*)e^{-h(x,y)q_i(t^*)} \tag{3.27}$$

Where $h(x,y)$ is the distance between two considered stations x and y. Finally precipitation series is generated for each day using:

$$W(t,u) = r(t^*)(W(t-1,u) + C_i(t^*)\psi(t) \tag{3.28}$$

Where $\psi(t)$ is the random number of independent $N(0,1)$ random variables. A vector $\psi(t)$ can also be used to generate multiple realizations of precipitation for each day. $C_i(t^*)$ matrix takes spatial variability of the process into account and is related to W(t) through Equations 3.24 and 3.25 by:

$$C_i(t^*)C_i^T(t^*) = \Gamma_{0i}(t^*) - \Gamma_{1i}(t^*)\Gamma_{0i}^{-1}(t^*)\Gamma_{1i}^T(t^*) \tag{3.29}$$

Using the relation in Equation 3.26, one could reach

$$C_i(t^*)C_i^T(t^*) = (1 - r^2(t^*))\Gamma_{0i}(t^*) \tag{3.30}$$

The decomposition of $C_i(t^*)C_i^T(t^*)$ is detailed in Bárdossy and Plate (1992).

3.3.2. Statistical downscaling based on quantile-quantile bias correction approach

The second statistical downscaling approach is based on the bias correction of regional climate models (RCM) output using quantile-quantile correction. Chapter 2 introduced dynamical downscaling and Section 2.2.1.1, specifically, penned the drawbacks of the use of regional climate models as a downscaling tool. One of the shortcomings of RCM is the transfer of bias from the global circulation model (GCM),through which the bias present in the GCM generated data is systematically transferred to the underlying RCM.

Since GCMs are usually considered to yield unrealistic results on spatial scales smaller than several grid cells, there is in general little confidence in the simulated, regional-scale climate variability. In particular, the regional precipitation in the models is discounted, because precipitation can be strongly influenced by subgrid-scale processes, some of which are parameterized while others, such as details of the land-water distribution or topography, are not represented at all (Widmann et al., 2003). RCMs downscale the GCM provided data to the local scale assuming that the atmospheric variability on small spatial scale is conditioned by larger scales. Even if RCMs improve the realism of simulated regional climate properties, some important biases may still exist, especially concerning precipitation that need to be corrected (A.W.Wood et al., 2004). Houghton et al. (2001) mentions that GCMs display area-average biases that are highly variable from region to region and among models, with sub-continental area averaged seasonal temperatures biases typically within 4°C and precipitation biases mostly between -40% and +80% of observations. RCMs on the other hand while improving upon the spatial detail of simulated climate compared to GCMs show area-averaged temprature biases generally within 2°C and precipitation biases within 50% of observations. Nonetheless, RCMs are useful in impact studies whereby upon subjection of different forcings (approximation of patterns of development in future world and associated green house emission scenarios) they can provide useful insight in to the future projected climates. This particular property of RCM make them an important and necessary tool in climate change impact studies. Regarding their inadequency in simulation of different climatic variables, different statistical techniques can be applied to correct them. Michel (2007) proposes classes of correcting techinques that could be applied to outcomes of RCMs. Considering the output from the RCM model as M and some reference value as R, one can write the impact I as the difference of the two:

$$I = M - R \tag{3.31}$$

Given that M is provided (in most cases) by RCM and, as discussed earlier, that RCM inherit bias from GCMs, I would include that bias as well. Different statistical methods can be employed to bring the inherit bias in RCMs to some reasonable acceptable levels and thus giving more value to the I.

1. ***The delta method:*** In this method the terms M and R in Equation 3.31 (both can be considered as daily values), are replaced by $O + \overline{(M - R)}$ and O,

respectively. Where O is an equivalent series of (daily) observation data and represents a multi-annual average operator. This method of bias correction, although being very robust, assumes the availability of daily data. It also assumes that the climate variability is unchanged in the scenario projection.

2. ***The unbiasing method:*** The terms M and R in Equation 3.31 (both can be considered as daily values), are replaced by $M + \overline{(O - R)}$ and $R + \overline{(O - R)}$, respectively. This method although does corrects the mean error, it does assume that the variability of the RCM is good.

3. ***The regime method:*** Here the terms M and R in Equation 3.31 (both can be considered as daily values), are replaced by $O(d_2)$ and $O(d_1)$, respectively. d_1 and d_2 are dates chosen in the observation dataset. This method is also employed in cluster and analogue techniques. The drawback of this method is that, although it can change the frequency of the different meteorological events, it can not produce events that are not recorded. It is also not a very suitable method when working with extremely high temperatures or extremely high precipitation events.

The method used here is a CP based quantile-quantile exchange of RCM generated precipitation amounts in control runs with that of observed time periods. Hence it is a variable correction method that compares quantiles between two data sets. The terms M and R in Equation 3.31 are equated to $f(M(d)|O)$ and $f(R(d)|O)$, respectively. This way it is assumed that RCM is able to predict the ranked category of precipitation but not the actual value of precipitation. In other words the qualitative forecast/prediction of RCM can be trusted but not the quantitative part of that forecast/prediction. That is why there is the need of correcting that quantitative part of RCM, which in this case is the precipitation amount on the wet days. The precipitation distribution generated by RCM (control runs) is related to the precipitation distribution of the observed time series for the same time period. The precipitation amounts are corrected in control time periods of RCMs and for future scenarios the quantiles from control periods are used. This way, the downscaled precipitation signal becomes similar to the RCM generated signal and the bias is corrected. The downscaling process can be written as:

$$Z_D(x,t) = F_O^{-1}\left(F_R(Z_R(x,t),x),x\right) \tag{3.32}$$

Where $Z_R(x,t)$ is the precipitation at location x and day t simulated by the RCM, $Z_O(x,t)$ is the observed precipitation at location x and day t available for $t \leq T_O$. $F_O(z,x)$ is the distribution function of the observed precipitation amounts at location x while the corresponding RCM precipitation distribution for the control climate run is $F_R(z,x)$.

This kind of transformation ensures that if control period and observation period are identical and the model is able to reproduces the observations perfectly then:

$$Z_D(x,t) = Z_O(x,t) \tag{3.33}$$

else one can at least assume that

$$F_O(z, x) = F_D(z, x) \tag{3.34}$$

The transformation can be applied either universally without any added conditions on days, seasons etc., or for selected time periods (seasons) separately. The second case would naturally be the ideal choice, since one can reproduce season specific precipitation phenomena in the downscaled precipitation series. For precipitation distribution F_O, the following choices could be considered.

The first is to use the empirical distribution function. This method has of course the advantage that no distribution is needed to be fitted, but the possible critical disadvantage could be that the maximum observed precipitation amount can not be exceeded in the downscaled time series. The second possibility- which is a bit tedious- is to assign to each location (precipitation station, or grid point) a probability describing the location/grid point experiencing a dry day and then fitting a continuous distribution to amounts on the wet days. The problem of maximum precipitation in downscaled time series exceeding maximum observed in observational time series can be overcome, though at the cost of selecting an appropriate distribution and estimating its parameters for each location/grid point.Different continuous probability distributions can be used to fit to the amounts on wet days. Weibull distribution is selected to be used in this thesis owing to its relative simplicity in parameter estimation and its flexibility.

Weibull distribution is a two parameter distribution function closely linked with exponential and normal distribution. The two parameter Weibull probability density function with parameters δ and $\beta > 0$ is given by:

$$f_X(x) = \frac{\beta}{\delta}\left(\frac{x}{\delta}\right)^{(\beta-1)} exp\left[-(\frac{x}{\delta})^{\beta}\right] \tag{3.35}$$

for x > 0. For all other values the function equates to 0. The cumulative distribution function for $x > 0$ can be written as:

$$F_X(x) = 1 - exp\left[-(\frac{x}{\delta})^{\beta}\right] \tag{3.36}$$

The scale parameter δ controls the spread of the distribution, and the shape parameter β controls the form of the distribution. Weibull distribution is flexible in that at β value near 3.6, it closely approximates Gaussian distribution, while at β equal to 0, it approximates exponential distribution (Figure 3.3).

The bias in RCMs predominantly comes from the underlying GCMs. GCMs are known for not representing the effects of local scale phenomena such as topography, orography, near surface wind speed etc., in their simulations. On the other hand, large scale variables such as sea level pressure and geopotential heights are skillfully simulated by GCMs. In the first section of this chapter, identification of circulation patterns was discussed based on sea level pressure. The circulation patterns are believed to represent different climatic conditions efficiently. The errors in RCM simulations may come from different sources and it is believed that introduction of identified circulation patterns in the development of relationship between control period precipitation and observed precipitation, can bring physical meaning to and

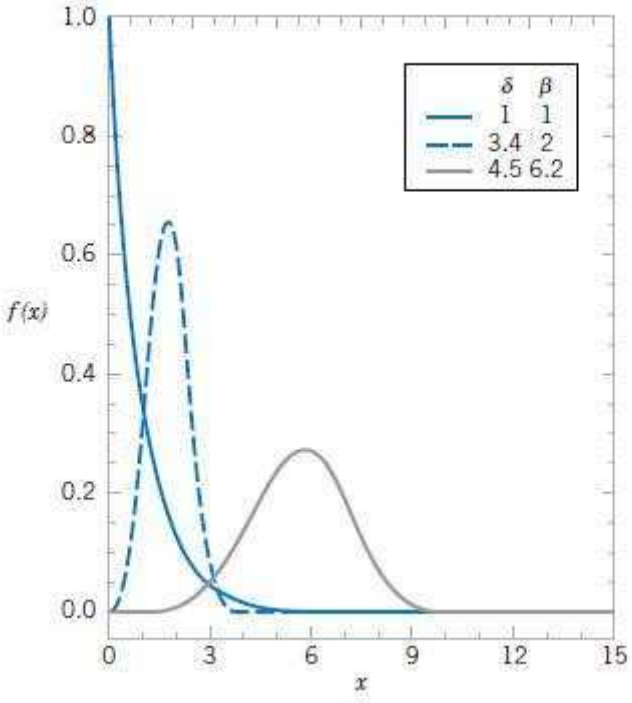

Figure 3.3.: Weibull probability density functions for different values of δ and β (D.C.Montgomery and Runger, 2002)

potentially improve the downscaling procedure which is purely a statistical correction. The fact that the precipitation amounts corresponding to different circulation patterns might change differently in the future,is taken into account in Equation 3.37. As non-stationary relationship is assumed between CPs and precipitation, the precipitation amounts would change if CP characteristics are changed.

$$Z_D(x,t) = F^{-1}_{O\alpha(t)}\left(F_{R\alpha(t)}(Z_R(x,t),x),x\right) \tag{3.37}$$

Where $\alpha(t)$ is the circulation pattern on day t for either the control or future runs of RCM generated data sets.

This methodology of bias correction and development of new scenarios from RCM data is applied to three different regional climate models for precipitation and temperature. RCMs used in this study are presented in the following chapter. The downscaled results and its application to regional hydrological model is presented in chapter 6 and Chapter 8 respectively.

4. Catchments and Data

This chapter presents the information regarding the catchments and precipitation and discharge stations therein, that are used in application of methodology presented in the previous chapter. Sources and availability of data is also discussed.

4.1. Catchments & Data

Two major sets of data and catchments were used for application of the methodologies developed and explained in Chapter 3. The first set of data was kindly provided by the Federal Ministry of Education and Research (Bundesministerium für Bildung und Forschung, BMBF.) funded project "Operational Discharge and Flooding Predictions in Head Catchments" (Operationelle Abfluss- und Hochwasservorhersage in Quellgebieten, OPAQUE). This set of data was used in development of identification of circulation patterns related with extreme hydrological and meteorological situations and downscaling using circulation pattern based autoregressive multivariate statistical method. The second set of data was kindly provided by European union (EU) funded 6th Framework program's project ENSEMBLES (contract number: GOCE-CT-2003-505539). This set was primarily used for application of identified critical circulation patterns and statistical downscaling of RCM data for new scenario generation.

4.1.1. OPAQUE Catchments & Data

One of the task in OPAQUE project was to better represent the hydrology of four important head catchments in different parts of Germany. Given that head catchments by definition have very short reaction time, it is important to have very precise operational prediction system. In addition to have better understanding of the hydrology of head catchments, it is also very necessary for forecast purposes to have very distinct set of critical circulation patterns based on which precise forecasts could be made.

Four head catchments, three present in southern Germany and one in the east were considered for identification of critical circulation patterns. The location of the catchments are shown in figure 4.1. The size (in Km^2) of each catchment is included in brackets.

Upper Danube catchment, mainly consist of two rivers Breg and Brigach that join at Donaueschingen to make river Danube. Daily and hourly discharge data for the two rivers of Breg and Brigach, shown in Figure 4.2, were provided from 1991 to 2006. Daily precipitation data was also provided for over 100 precipitation stations in this catchment with varying lengths of records. Table 4.1 shows the precipitation stations

Figure 4.1.: Location and size of catchments under study in OPAQUE Project.

used in classification and downscaling processes. These 7 stations were selected on the basis of length of precipitation data associated with each station.

Upper Danube floods are usually caused by the simultaneous effect of intense rain and snow melt in the Black forest region. The long-time average runoff at the gauge Donaueschingen/Danube is 9 m^3/sec. During the flood event of January 1995 the peak runoff of the Danube in Donaueschingen reached 312 m^3/sec, roughly equal to 50-year flood (Figure 4.3).

Table 4.1.: Selected precipitation stations of Upper Danube catchment.

X	Y	Alt. (m.a.s.l)	Station ID	Name
3478811	5304953	738	70194	Wellendingen
3436453	5307117	846	70204	Titisee
3440230	5310783	870	70206	Titisee-Langenordnac
3440153	5303372	818	70207	Lenzkirch
3451390	5305119	830	70208	Feldberg (Wst.)
3443947	5308892	928	70209	Friedenweiler
3450079	5297718	875	70210	Bondorf

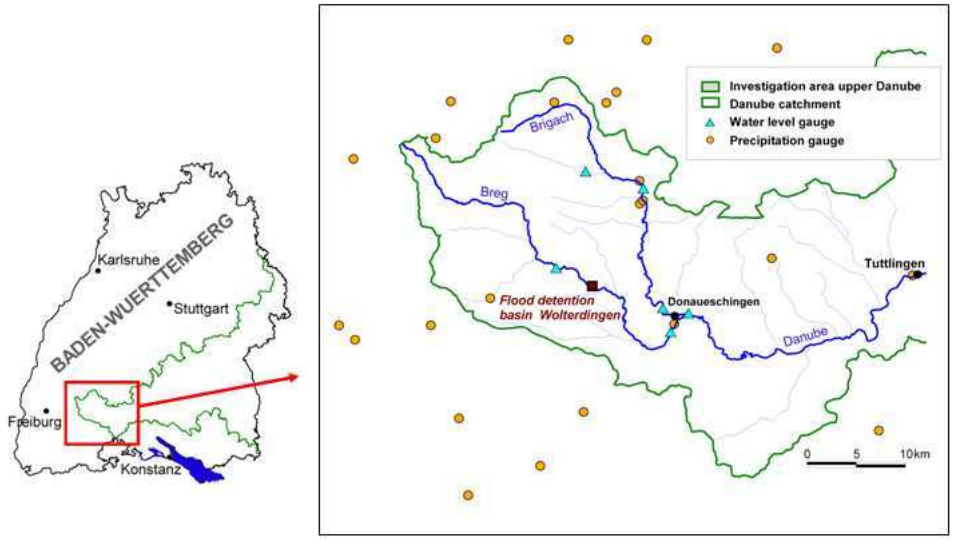

Figure 4.2.: Upper Danube catchment in detail.

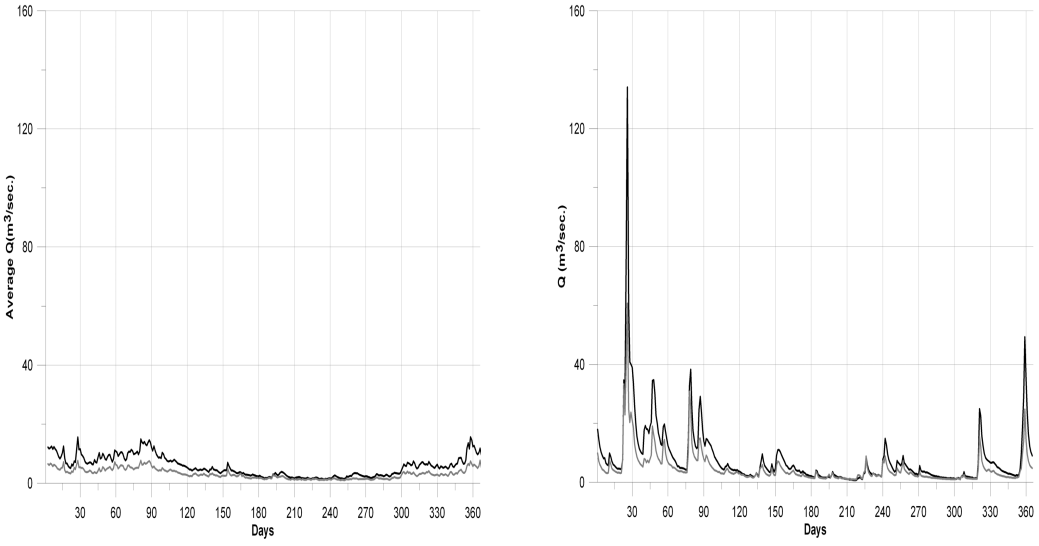

Figure 4.3.: Daily average discharge (to the left) and 1995 flood event discharge (to the right) for River Breg (Black) and Brigarch (Gray). Daily average is calculated from 1991-2006, excluding flood year 1995.

Weisseritz catchment is another head catchment which was studied for extreme flooding events. Weisseritz catchment is drained by two rivers called Rote Weisseritz and Wilde Weisseritz originating in the eastern ore mountains at the Czech-German border close to Altenberg. The two branches join at the city of Freital to form the United Weisseritz (Vereinigte Weißeritz). Daily mean and monthly mean discahrge data for number of gauge stations was available for this catchment. The temporal length of data varied from gauge station to gauge station. Daily precipitation station data for 7 stations were provided from 1947 to 2006. The details of the precipitation stations are provided in Table 4.2. The main flooding event in this catchment was August 2002 flood which was 100 year flood event and caused significant damage to property and life. The location of the rivers are shown in Figure 4.4 while mean daily discharge calculated for period 1971-2001 at location Freital and daily discharge for flooding year of 2002 at the same location are shown in Figure 4.5.

Figure 4.4.: Weisseritz catchment in detail.

Table 4.2.: Selected precipitation stations of Weisseritz catchment

X	Y	Alt. (m.a.s.l)	Station ID	Name
5421640	5654650	114	41080	Dresden-hosterwitz
5411750	5623281	877	41135	Zinnwald
5406202	5641924	365	41242	Dippoldiswalde
5412504	5667779	227	41524	Dresden-Klotz.
5382836	5646108	380	42235	Freiberg
5394025	5619901	615	42351	Neuhausen
5391632	5618095	593	42354	Neuhausen-Erzbeg.

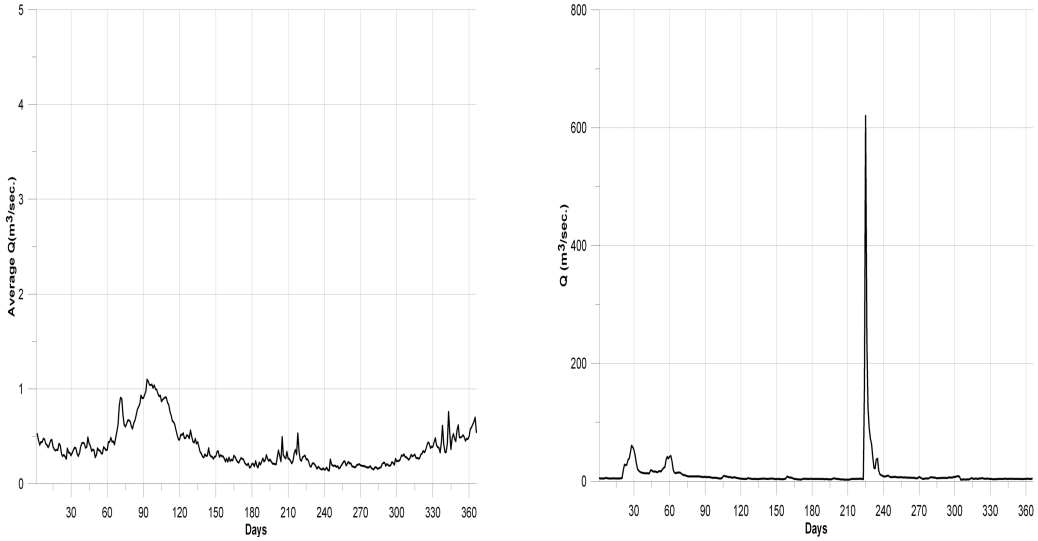

Figure 4.5.: Daily average discharge (to the left) and 2002 flood event discharge (to the right) for all the rivers in Weisseritz catchment. Daily average is calculated from 1971-2001.

Iller river is in Southwestern Germany. It is on German-Austrian border and is one of the most important tributary to the German part of Danube. The highest point of the catchment is at 3000 m.a.s.l while the lowest is at 650 m.a.s.l. Daily and sub-daily data, both for precipitation and discharge was available for number of precipitation and dischrage stations along the upper Iller river. The precipitation stations used for classification and downscaling purposes are tabulated in Table 4.3. Iller has alpine and sub-alpine flow regime with low flows in winter, medium flows in summer and high flows during the snow melt season of spring. Among the number of floods that have occurred in this river the most important one in terms of destruction and loss of lives was the summer flood of May 1999. The peak discharge at gauge station Kempton was 850 m^3/sec (mean annual flow at gauge Kempten is 47 m^3/sec). This was 100 year flood event. The flood of August 2005 had a return period of 300-400 years (peak discharge at gauge station Kempton =900 m^3/sec) but had significantly smaller associated losses because of the flood protection measures taken after 1999 flood.

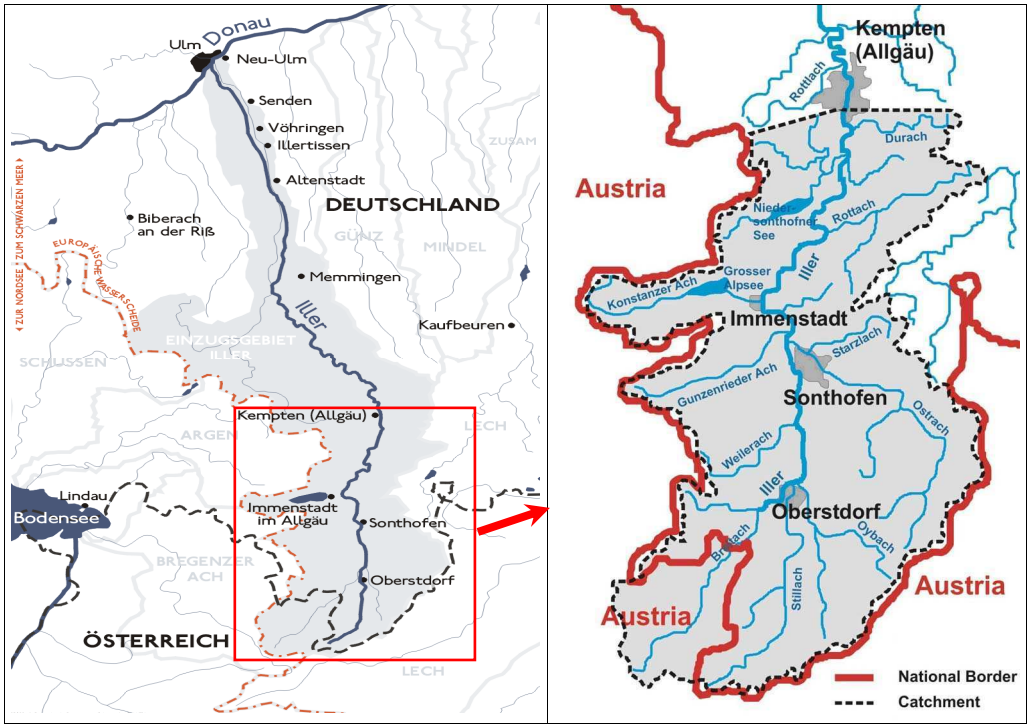

Figure 4.6.: Iller catchment in detail. Whole catchment is to the left and upper Iller catchment to the right.(Left figure courtesy of http://de.wikipedia.org/wiki/Iller)

Table 4.3.: Selected precipitation stations of Iller catchment

X	Y	Alt. (m.a.s.l)	Station ID	Name
4369046	5245938	950	90215	Oberstdorf-Birgsau
4369947	5252498	810	90216	Oberstdorf
4369641	5259487	757	90226	Fischen
4371550	5265315	754	90233	Sonthofen
4378410	5262048	828	90243	Hindelang
4356042	5270527	745	90251	Oberstaufen
4365169	5269073	935	90252	Immenstadt (Wärterhaus)
4366367	5270219	731	90253	Immenstadt (Liststr.)
4380871	5284116	896	90254	Durach
4373961	5273264	865	90256	Rettenberg

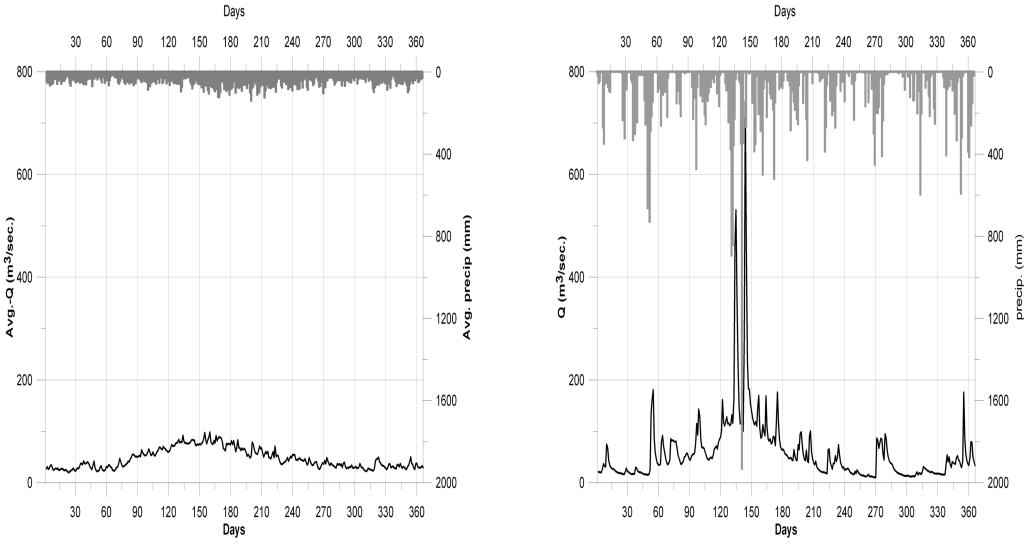

Figure 4.7.: Daily average discharge (to the left) and 1999 flood event discharge (to the right) of all the rivers in Iller catchment(gauge:Kempton). Daily average is calculated from 1971-1991.

Alb catchment is another head catchment studied for extreme hydrological conditions in this study. Alb is to the west of Black forest in southern Germany. It has its source in the northern black forest at about 750 m.a.s.l and leaves black forest near Ettlingen entering into the Rhine valley. Daily discharge data at gauge station Etllingen from 1980 to 2009 and daily precipitation for the stations Tabulated in Table 4.4 from 1971 to 2009 was available for the forthcoming analysis of classification and downscaling. The major floods in this catchment were in 1995 and 1998 (Figure 4.8).

Table 4.4.: Selected precipitation stations of Alb catchment

X	**Y**	**Alt. (m.a.s.l)**	**Station ID**	**Name**
3524930	5357540	740	61314	Hohenstein
3461030	5392270	600	61373	Enzkloesterle
3446160	5391410	750	61377	Forbach
3466000	5401485	740	61485	Wildbad
3462750	5406450	717	61529	Dobel

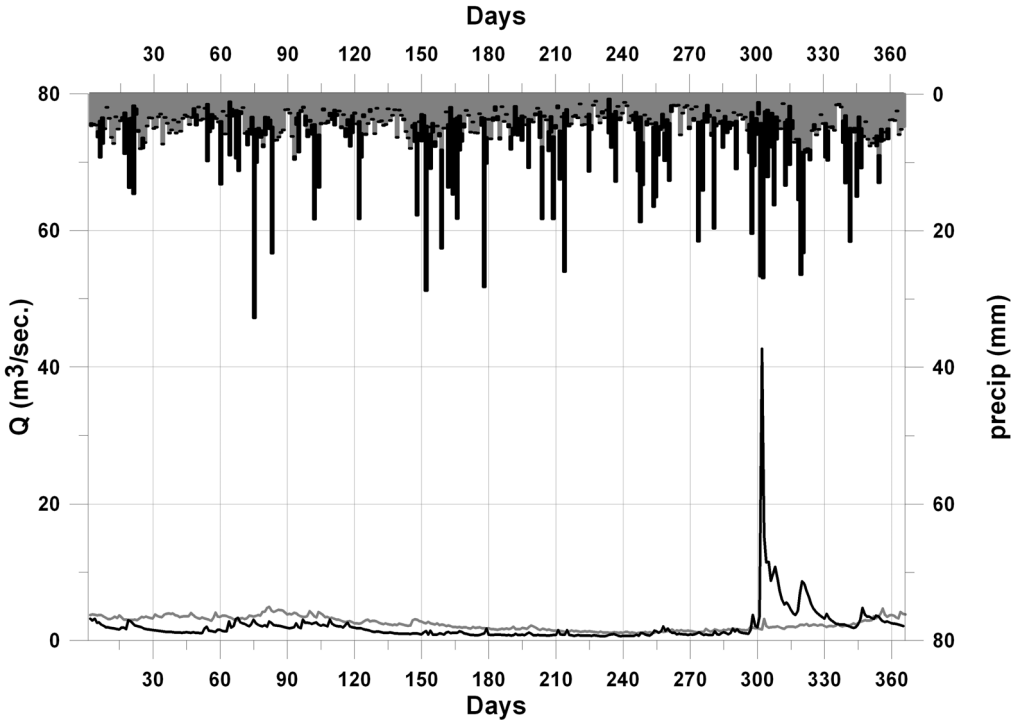

Figure 4.8.: Daily average precipitation and discharge (in gray) and 1998 flood event precipitation and discharge (in black) of river Alb . Averages are calculated from 1971-1995, excluding flood year 1998.

All the four catchments are small head catchments that are drained by small rivers named above. All these rivers on its way either join or turn into some of the largest rivers in Central Europe (Rhine, Danube, Elbe). Therefore its is very important to understand the climatological conditions that result in large scale floods in these head catchments. Given that there are huge population concentration along these big rivers it becomes more important to identify the circulation patterns that result in extremely large floods and use that information for predicting future flows.

4.1.2. ENSEMBLES Catchments & Data

This set of data, in addition to analysis for extremes, was also used in application of quantile-quantile basede bias correction of RCM data for downscaling purposes. The data was kindly provided by EU funded project 6th Framework program's project ENSEMBLES (contract number: GOCE-CT-2003-505539). The results presented here are part of the results that were submitted to ENSEMBLES deliverable No. D5.36 titled "Optimization of the objective drought CP classification" and deliverable No. D5.37 titled "Validation of critical CPs associated with hydrological extremes". The deliverables were submitted while working for research theme 5 (RT5) of the project. The aim of RT5 was to perform a comprehensive and inde-

pendent evaluation of the performance of the ENSEMBLES simulation-prediction system against analyses/observations, including the production of a high-resolution observational dataset necessary to perform the task. The evaluation was supposed to cover all spatial scales and seasonal to decadal timescales in an integrated way. The evaluation was also supposed to be performed fully independently from the ENSEMBLES system and to consider processes and phenomena, forecast quality, extreme events in observational and RCM data, and impact models when forced with downscaled ERA-40, hindcasts and gridded observational datasets. (ENSEMBLES RT5 web page: http://www.knmi.nl/samenw/ensembles_rt5/)

Keeping in view the aim of the project, different research teams were responsible for different research themes (RT). RT5 provided the observational gridded dataset for precipitation and temperature over European continent over two different grid sizes (Haylock et al. (2008)) of 25km x 25Km and 50km x 50Km. The daily time series was prepared using data from 2191 meteorological and hydrological stations located in Europe and the Mediterranean. Figure 4.9 shows the location of precipitation and temperature stations used in generation of daily gridded data set for observational data.

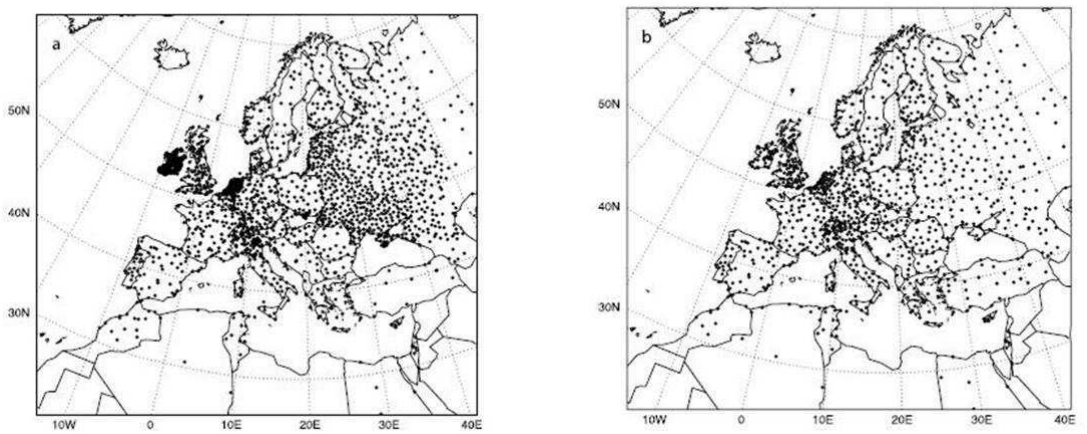

Figure 4.9.: Precipitation (a) and temperature station (b) location used in generation of daily observational gridded data set Haylock et al. (2008).

RCM data sets for ERA40 driven control runs and Special report on Emission Scenarios (SRES) A1B scenario runs were provided by researchers working for RT3 and RT2B respectively. The output of three different regional climate models HadRM3 (developed by Hadley center for Climate prediction and research, Met office UK. Model description reference Collins et al. (2005) **?** and M. Noguer and Murphy (1998)), RACMO2 (developed by the Royal Netherlands Meteorological Institute, KNMI. Model description reference Meijgaard et al. (2008)) and REMO (developed by Max-Planck-Institute für Meteorologie, MPI-M. Model description reference Jacob (2001)) were considered in this study. The RCM data sets predominantly cover the European continent to different extents and with spatial resolutions of 25 km x 25 km and 50 km x 50 km grid sizes. Unlike observational gridded data set which

was available only on daily scale, the RCM data sets were available on more extended temporal scales of 6 hourly, 12 hourly, daily and monthly mean. All RCMs that were used in this study provided data on rotated spherical coordinate system with a north pole latitude placed at $-39.25°$ and longitude at $18°$. The extent of coverage with this rotated grid system was different for each RCM used.

The downscaling methodology was applied to German part of Rhine basin. River Rhine is approximately 1320 Km long and rises in Switzerland as a fast flowing mountain river, being fed by the melting waters of glaciers and snow in the Alps. It drains almost 185,000 Km^2 of area, of which more than 100,000 Km^2 lies in Germany. Approximately 50 million people live in the Rhine basin. It is one of the largest river in Europe, fed by rainwater and glacial melt from 9 countries and flows out into the North Sea in Netherlands. About 50% of the area from the Rhine basin is utilised for agriculture, about 33% is covered by forest, 11% is built-up area and the remaining is composed of surface water. It is estimated that the assets in the flood prone area are worth 1500 billion Euro. So, it is very important to consider this area for both the extremes of floods and drought. Figure 4.10 displays the total area drained by the Rhine basin.

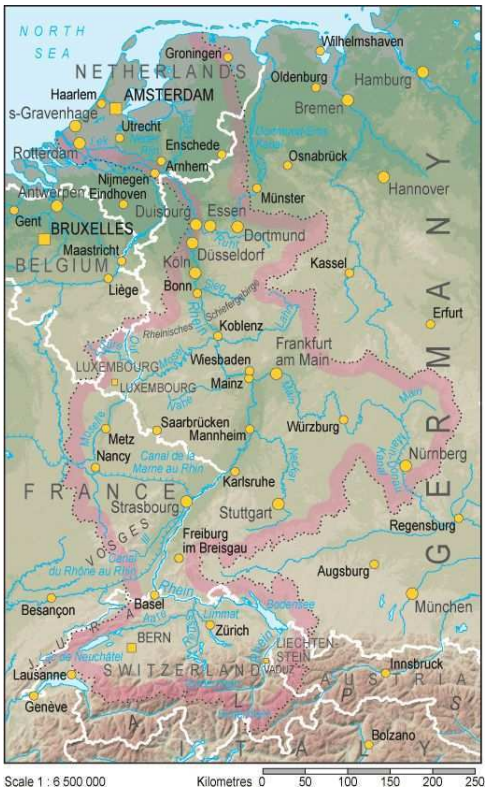

Figure 4.10.: Rhine catchment (Image retrived on 12.03.2010 from United Nations Environment Programme's (UNEP) collaborating center. http://www.grida.no/

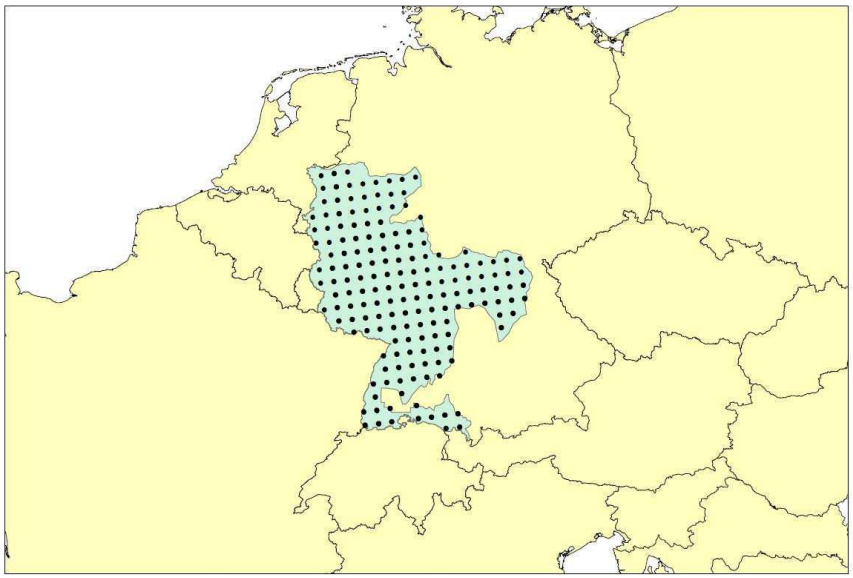

Figure 4.11.: selected grid points in German part of Rhine basin

Based on 25 km x 25 km grid resolution, 172 grid points were selected within the catchment for analysis and evaluation (Figure 4.11). For observational and RCM control runs the analysis was based on a common time period of 1961-1990 while for SRES future scenario run, different time periods between 2001-2100 (2001-2099 in case of HadRM3 transient futures runs) were considered for evaluation. Given that the considered RCMs provide different meteorological variables over the European continent on a rotated grid system, the data was first transformed to the geographical longitude latitude grid using the Bi-cubic spline interpolation method before they were used for classification and downscaling purposes. Climate data operators (CDO) (https://code.zmaw.de/projects/cdo/) developed by Max-Planck-Institut für Meteorology (MPI) were used for interpolation.

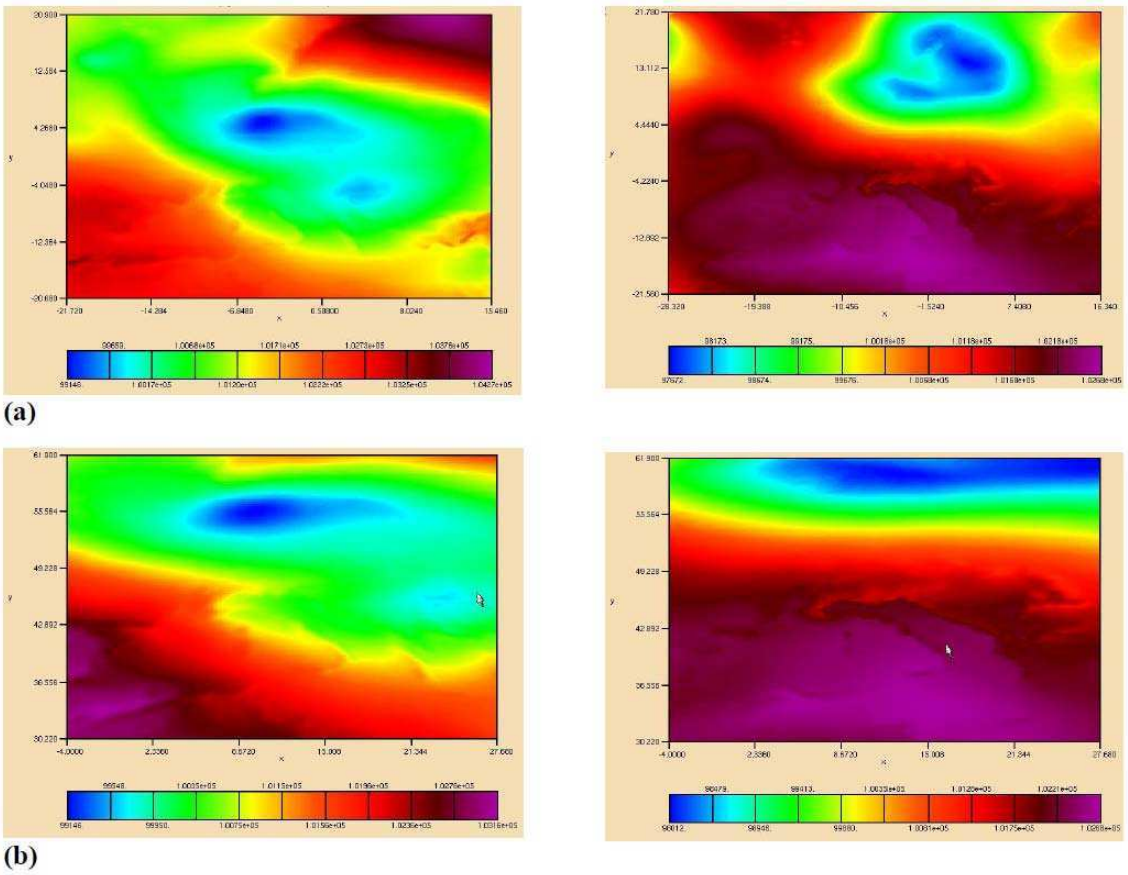

Figure 4.12.: Mean sea level pressure (MSLP) of 01.01.2001.(a) Original RCM MSLP of RACMO on left and HadRM on the right (b) MSLP Interpolated to geographic coordinates of RACMO on the left and HadRM on the right.

5. Results-Circulation pattern classification

5.1. Preface

This chapter presents the results obtained from the application of improved classification method of critical circulation patterns discussed in Chapter 3 . The methodology is applied to both the data sets described in Chapter 4 titled "About Catchments and Data" i.e. to gauge station based data of OPAQUE and grid point based data of ENSEMBLES.

5.2. Classification of critical circulation patterns

Chapter 3 described the methodology used for classification of critical circulation patterns and introduced certain objective functions that were used in automated procedure of fuzzy rule based classification system. Two sets of objective functions based on daily values of precipitation and discharge were introduced. Given that the aim of classification of atmospheric circulation patterns was to associate some of the circulation patterns with the extremes of hydrological system and that in both the projects (introduced in chapter 4) the aim was to identify in the respective catchments critical circulation patterns, it was thought that instead of optimizing the fuzzy classification rules for each individual gauge station of each catchment of OPAQUE project, or for each of the grid point in the German part of Rhine basin of ENSEMBLES project, a single set of rules obtained from independent data set representing the same area would both be logical and less tedious.

For this purpose the discharge data at two rivers and precipitation data at 294 stations in Baden Württemberg, Germany is used for fuzzy rule optimization. The location of river Rhine (at Maxau) and Neckar (at Plochingen) used for discharge and 294 precipitation stations are shown in Figure 5.1. The figure also shows the topography of the region. The catchment area of the upper Neckar at Plochingen is 3995 km^2. The climate is temperate and humid with an annual mean temperature of 8.7 °C and a mean annual precipitation of 870 mm. Precipitation shows a weak annual cycle. Due to the marked annual cycle of radiation and temperature discharge has strong annual cycle with maxima around February and minima in September-October. The Rhine at Maxau on the other hand has a catchment area of 50196 km^2, most of which is upstream the Lake Constance in Switzerland. Flows from the Black Forrest also contribute to the discharge and are responsible for quick increases. These increases are different from those slow and long lasting increases caused by floods in the Swiss part of the catchment.

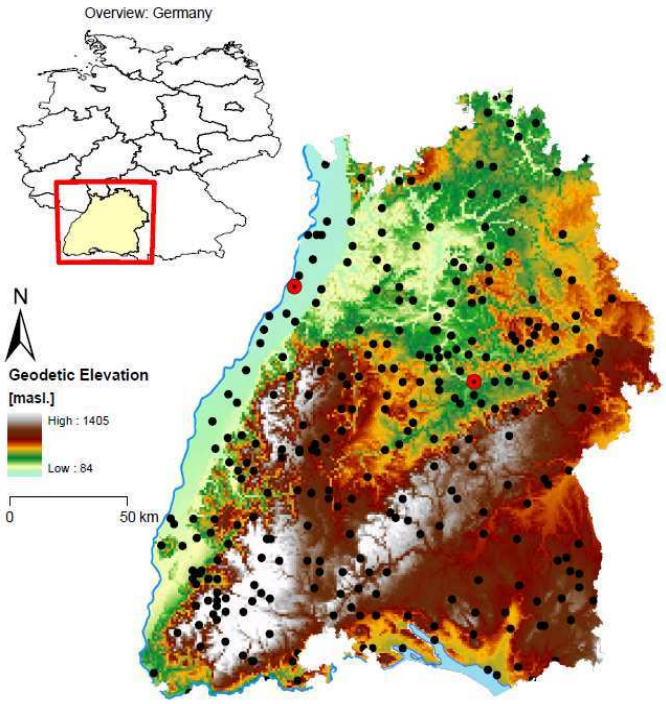

Figure 5.1.: Topographic map of the state of Baden Württemberg, along with the precipitation (in black) and discharge (in red) stations

Daily mean sea level pressure (MSLP) from National Center for Atmospheric Research (NCAR), National Centers for Environmental Prediction (NCEP) and European Centre for Medium-Range Weather Forecasts (ECMWF) has been used as large scale predictor in different cases. The grid resolution of both the data sets are 2.5°. The lower left and upper right corners of the spatial window used for MSLP are (35°N,15°W) and (65°N,40°E). The two discharge gauges shown in Figure 5.1 were used for discharge based objective functions (Equations 3.5 through 3.12) while precipitation stations shown in Figure 5.2 were used for precipitation based objective functions. For the rainfall coverage based objective functions (Equations 3.13 and 3.15) the two sets of precipitation stations are marked in Figure 5.2.

For classification, discharge measured at two locations - Maxau (river Rhine) and Plochingen (river Neckar) were selected. The time series of the discharge differences dQ(t) for the two gauges are shown in Figure 5.3. The limits corresponding to the 25% and 75% value of the distributions are marked with the two horizontal lines. One can see that the two gauges have quite similar behaviour. The number of days falling within the limits for both locations is very high - which indicates that both rivers are simultaneously in a quasi equilibrium state.

Selecting appropriate number of circulation patterns to be defined by the automated fuzzy rules is very important. Too many classes of CPs may average out the associated extreme conditions and hence may hide the true critical CPs. Too few

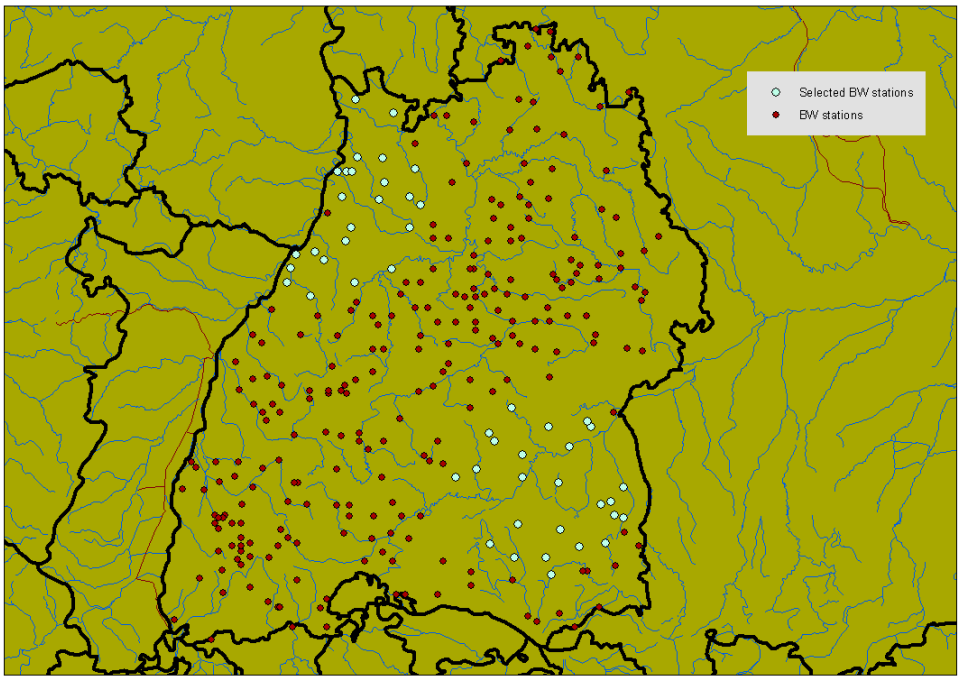

Figure 5.2.: Two sets of precipitation stations in Baden Württemberg used for precipitation coverage based objective functions

on the other would clearly be not enough do describe the unique characteristics of different circulation patterns active in certain area. Therefore different information measures were used to assess the optimum number of CPs that should be used to define certain catchment/area with. These measures should help in better representation of quality of each considered number of patterns both in space and time. A good classification should ideally lead to classes which differ from climatological mean for the selected variable.

For precipitation amounts a selected number of thresholds $0 \leq z_0 < \ldots < z_k$ can be selected. For each circulation pattern α and each location x the probability of the precipitation not exceeding $z_i(x)$ is denoted as $p_{\alpha,i}(x)$. The probability of not exceeding $z_i(x)$ calculated over all days is $p_i(x)$. The quality measure with respect to z_i is defined as:

$$I_{P_i}(x) = \sum_{\alpha} h_{\alpha,i}(p_{\alpha,i}(x) - p_i(x))^2 \tag{5.1}$$

The more the CP conditioned probability of precipitation increment $p_{\alpha,i}(x)$ differ from unconditioned probability incrment $p_i(x)$, the bigger I_{P_i} gets.

Another measure related to the mean precipitation amounts can also be introduced. Let $\bar{z}(x)$ be the mean daily precipitation amount at location x while $\bar{z}_\alpha(x)$ be the CP α conditioned daily precipitation amount at the same location. The ratio

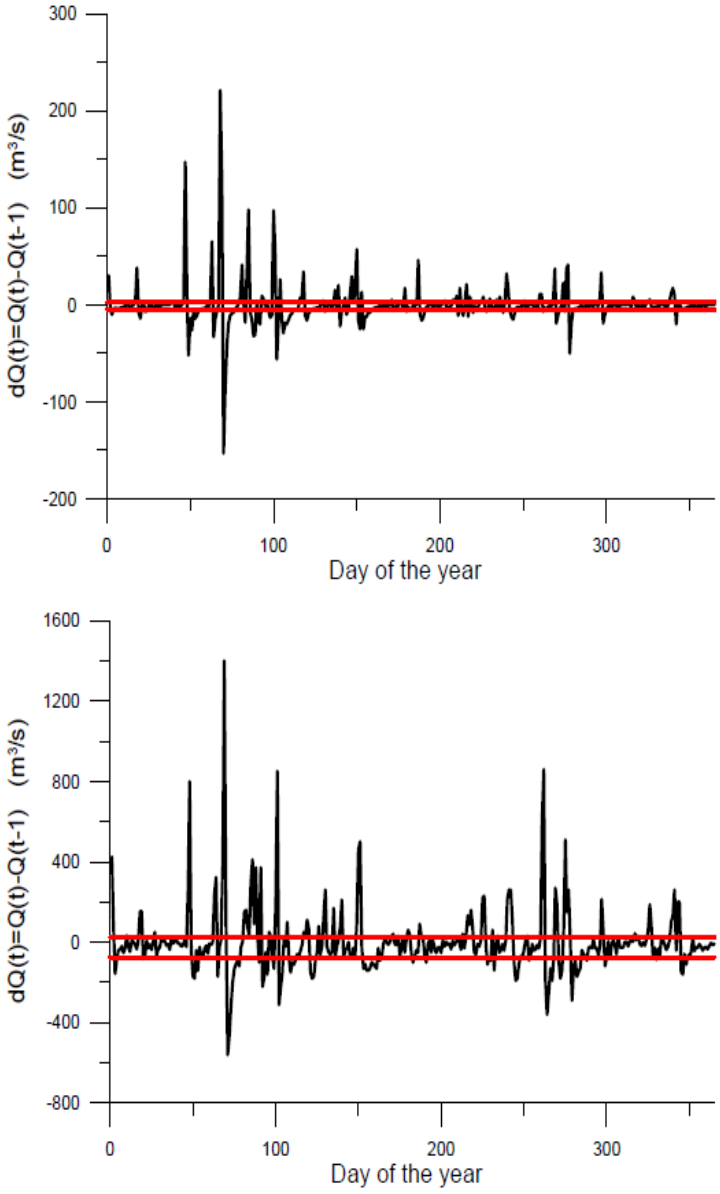

Figure 5.3.: Daily discharge differences along with 25%-75% lines (red) for Plochingen (on river Neckar) and Maxau (on river Rhine) for year 2006 (Plochingen in upper panel).

of these two quantities

$$w_\alpha(x) = \frac{\bar{z}_\alpha(x)}{\bar{z}(x)} \tag{5.2}$$

is an indicator for the relative wetness of a pattern and referred to as wetness index. A pattern with wetness index 1 does not provide additional information at site compared to climatology. For extreme wet patterns $w_\alpha(x)$ should ideally be far greater than 1 (e.g. to the order 2 or 3, implying that the CP which has a wetness index equal to 3 is bringing in thrice the amount of precipitation comparing with a CP with wetness index 1). For dry circulation patterns $w_\alpha(x) < 1$. The smaller the wetness index is, the drier CP would it represent. In a given classification the more the values differs from 1 the better the classification describes precipitation behavior.

The overall performance of a classification can be measured using the following two equations:

$$Z_{1P}(x) = \sum_\alpha h_\alpha \left| \frac{\bar{z}_\alpha(x)}{\bar{z}(x)} - 1 \right| \tag{5.3}$$

or

$$Z_{2P}(x) = \sum_\alpha h_\alpha \left| \log\left(\frac{\bar{z}_\alpha(x)}{\bar{z}(x)} \right) \right| \tag{5.4}$$

Both $Z_{1P}(x)$ and $Z_{2P}(x)$ measure the difference from the unconditional mean, the former describing the overall wetness of the classification system while the later explains the extent of dryness of the classification system in question.

With the precipitation and discharge data described above, the quality measures outlined in equations 5.1 through 5.4 and NCEP-NCAR daily MSLP from 1979-1988, different number of CPs were used to classify the atmospheric circulations with and their quality assessed. For the quality assessment of each classification, precipitation data from Baden-Württemberg at 294 stations shown in Figure 5.1 were used from 1958-2000. Classification quality measures defined in equations 5.1 through 5.4 were used for different precipitation threshold values (e.g. z_1=0 mm, z_2=1 mm, z_3 =5 mm and z_4=10 mm). Z_{1P} and Z_{2P} were calculated for each precipitation station in order to compare the different classification results. Subsequently sum of each of these measures was calculated using all available measurement stations as an overall performance measure. Two of the calculated quality measures are shown in Figure 5.4 where mean of I_{P3} (in black) and Z_{1P} (in gray) are plotted for different number of patterns investigated. Given the heuristic nature of the optimization method, both curves show random fluctuations but generally both the measures increase with the increase of number of classification patterns. Both the measures peak at around 17 and afterward either decrease or stay the course.

17 CP classification was thus considered for further classification of OPAQUE and ENSEMBLES catchments and data sets respectively. The CP classification is obtained using precipitation and discharge based objective functions. The analysis (validation) is made using only the precipitation data. CP classification based on 17 CPs was made using both NCEP's reanalysis and ECMWF's ERA40 MSLP. The

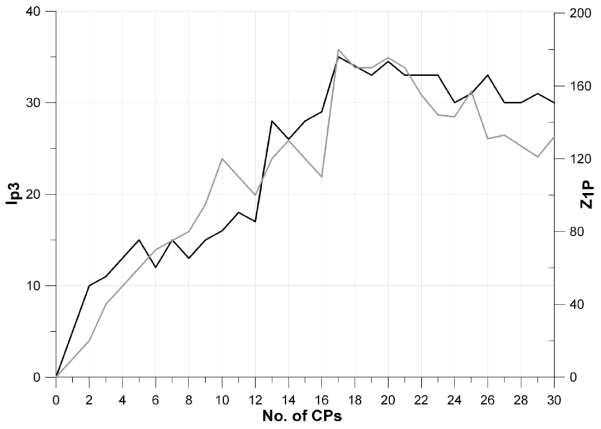

Figure 5.4.: Information measures I_{p3} (solid black line) and Z_{1p} (solid gray line) for different number of CPs.

resulting CPs from both data sets displayed similar characteristics. Further classification for ENSEMBLES and OPAQUE data sets and catchments were made using ERA40 MSLP as all the control runs provided by different RCM's in ENSEMBLE data set were also driven by ERA40 data. ERA40 daily MSLP are available from 1958-2001 while for NCEP's reanalysis are available from 1957-2009. In some cases when longer CP classification time series was needed, NCEP's MSLP has also been used. Optimized fuzzy rules were obtained using the data from 1979-1988. For validation purposes different time periods for the two data sets of ENSEMBLES and OPAQUE has been used and would be noted in respective sections.

5.2.1. ENSEMBLES data sets classification

All ENSEMBLES data sets have been analyzed for extremes using the classification obtained from methodology presented in chapter 3. RT5 observational gridded data set has been considered as standard against which all other RCM data sets have been compared. Comparisons have been made by calculating the wetness indices for each individual data sets, for each grid point considered in the German part of Rhine basin and for winter (November to April) and summer (May to October) half years.

5.2.1.1. RT5 observational data set classification

As discussed in previous chapter in section 4.1.2, RT5 data set is the interpolated gridded data set for European continent obtained from 2191 meteorological and hydrological stations located in Europe and the Mediterranean. The data set would thus be called observational gridded data set. Based on 25 km x 25 km grid resolution, 172 grid points were selected within the catchment for analysis and evaluation. The grid points are shown in Figure 4.11 and the location of each grid point are tabulated in Table A.1 of Appendix A. Both NCAR's NCEP and ECMWF's ERA40 Daily MSLP was available to be used as large scale variable for classification purposes. Classi-

fication was made using both the data sets and close similarity was found between the two. Table 5.1 shows the contingency table between two classifications for all 17 CPs. CP18 is the unclassified CP in both cases. ERA40 CPs are in rows and NCEP CPs in columns. It can be seen that for all CPs both classifications have agreement in terms of occurrence on a certain day. Given that control runs of all RCMs studies in this thesis are also based on ERA40 data, subsequent observational gridded data set's classification is also based on ERA40 daily MSLP for comparison of results.

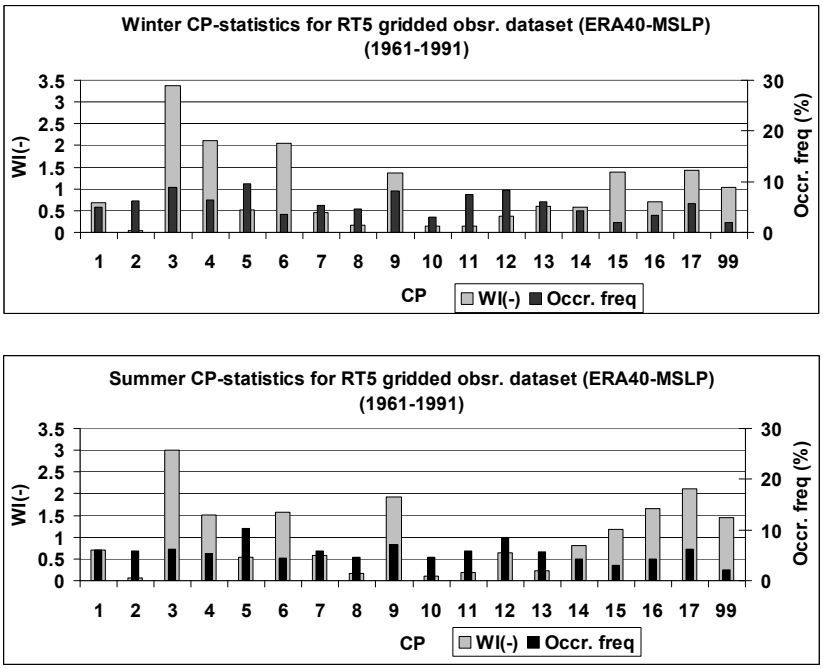

Figure 5.5.: Wetness indices (WI) and occurrence frequencies of all CPs for winter (Nov.-April) and summer (May-Oct.) half year.

Table 5.1.: Contingency Table for ERA40 and NCEP based classification of CPs

CP/CP	1	2	3	4	5	6	7	8	9	10	11	12	13	14	15	16	17	18
1	**406**	14	8	9	8	36	9	6	11	6	14	3	46	12	28	0	0	4
2	21	**457**	0	2	22	4	42	21	3	20	41	14	8	8	0	1	0	14
3	9	0	**670**	42	1	51	0	0	21	2	1	4	3	7	9	1	20	9
4	14	1	78	**432**	33	8	0	4	8	7	3	0	50	2	16	0	13	0
5	7	13	15	80	**818**	1	7	23	16	42	19	1	13	6	14	19	29	1
6	28	4	41	13	2	**260**	11	4	12	1	2	19	16	17	10	1	7	6
7	12	51	0	0	6	13	**418**	17	7	3	11	44	0	17	2	11	15	15
8	2	17	1	1	27	0	10	**372**	0	29	32	6	13	3	0	3	3	6
9	5	2	31	7	5	23	7	1	**658**	2	3	16	0	23	25	14	34	9
10	6	12	0	13	41	2	5	37	1	**285**	12	4	14	2	3	1	2	3
11	12	38	0	1	31	0	7	26	4	7	**579**	10	12	8	1	1	0	6
12	5	40	0	0	1	22	49	5	13	2	23	**725**	1	28	1	28	5	3
13	36	12	2	18	22	5	2	24	0	15	25	0	**478**	1	18	0	0	3
14	13	11	4	1	6	13	23	8	10	5	23	14	0	**321**	6	9	5	4
15	18	1	11	6	1	11	0	0	22	1	3	0	21	3	**184**	0	3	5
16	1	0	8	2	6	4	24	1	45	2	3	40	0	17	0	**252**	18	1
17	0	1	39	12	15	6	11	2	31	1	1	6	1	22	5	8	**500**	13
18	0	2	9	0	0	2	8	6	15	0	2	0	0	3	7	0	8	**164**
No. of classified days=11315, Cramer's V=0.679																		

Figure 5.5 shows the CP statistics in terms of wetness indices and occurrence frequency for Grid point 1 (for grid point location please refer to Table A.1 of Appendix A) of grid system used. Wetness index was defined in Equation 5.2 as the ratio of CP conditioned precipitation amount and unconditioned precipitation amount. Higher values of wetness index generally would portray wet CPs and lower values would represent dry CPs. For identifying wet CPs we have selected 1.5 as the threshold value for wetness index. Any CP having wetness index value larger or equal to 1.5 would be regarded as wet CP. For Dry CP the corresponding threshold value for wetness index has been set as 0.5. In terms of wetness indices, CP03 is the wettest CP followed by CP04, CP06 and CP17 in winter while the same CPs are wet in summer half year except that CP09 (wet in winter as well) also appears as one of the more wetter CP. CP02, CP08, CP10, CP11, CP12 and CP13 are the driest CPs both in winter and summer. The occurrence frequencies of individual CPs are also shown in Figure 5.5. Dry CP's frequencies remain more or less the same in both seasons while wet CPs behavior is not very clear. While for most wet CP the frequency in winter is more than in summer, for other wet CPs the frequencies tend to increase in summer.

Table 5.2 and Table 5.3 show in addition to wetness indices and occurrence frequencies, some other basic statistics of all CPs. These are averaged values over all 172 grid points of German part of Rhine basin. For each CP the table (it also holds for subsequent CP statistics tables for different RCMs) show the CP number (table column heading: CP), number of days belonging to each CP out of total analysis period (table column heading: Days), number of missing data days out of total CP days (table column heading: No_data), total CP days minus the missing number of days (table column heading: CPdays), number of dry and wet days based upon threshold precipitation value of 1 mm. (table column headings: Dry and table column heading: Wet), the occurrence frequency of each CP throughout the time period (table column heading: Freq), the occurrence frequency of each CP throughout the identified wet days (table column heading: dQfreq), probability of precipitation associated with each CP (table column heading: prob.), contribution to precipitation increase for each CP (table column heading: Cont.), wetness index (table column heading: WI), total precipitation sum associated with each CP (table column heading: Sum), Mean daily precipitation amount associated with each CP (table column heading: Mean), standard deviation (table column heading: St.Dev.) and finally the maximum precipitation amount that was associated with each CP during the analysis period (table column heading: Max).

In terms of wetness indices it can be seen that although the degree of wetness and dryness change to some extent when compared with the values shown in Figure 5.5, yet wet CPs remain wet and dry CPs remain dry. This shows the classification is robust in a sense that each class of CP consistently represent a particular type of behavior. The wettest CP in winter has wetness index value of 3.36 for Grid point 1, but when averaged the value reduces to 2.98. This shows that there are certain areas in the catchments where local effects influences the degree of wetness of wet CPs. The spatial behavior of each CP would be shown later which would help to identify areas where individual CP tend to differ to its general behavior. On the other

hand CP07 (identified dry CP) when averaged over all the grid points becomes even drier in winter (from a wetness index value of 0.48 to 0.43). Comparing sum, mean and maximum precipitation for each CP in winter and summer show that winter classification seem to be more representative than summer classification. For wet CPs the total sum, mean and maximum precipitation in winter have larger values than in summer and similarly dry CPs are drier in winter than in summer.

Table 5.2.: Basic CP statistics averaged over all 172 grid points of German part of Rhine basin for winter

Average CP statistics over 172 grid points of German part of Rhine basin (observational data set) (Winter)														
CP	Days [-]	No_data [-]	CPdays [-]	Dry [-]	Wet [-]	Freq [%]	dQfreq [%]	Prob. [%]	Cont. [%]	WI [-]	Sum [mm]	Mean [mm]	St.Dev. [-]	Max [mm]
01	280	0	280	196	84	5.00	3.47	30.08	2.79	0.56	335.11	3.96	3.37	18.16
02	347	0	347	323	24	6.20	1.01	7.11	0.62	0.10	74.09	2.99	2.40	10.64
03	497	0	497	58	439	8.80	18.26	88.35	26.37	2.98	3155.20	7.16	5.51	36.37
04	361	0	361	63	298	6.40	12.41	82.77	14.52	2.26	1738.14	5.78	4.42	30.06
05	539	0	539	239	300	9.60	12.44	55.73	9.42	0.98	1142.52	3.72	2.93	20.54
06	205	0	205	77	128	3.60	5.33	62.79	5.28	1.45	632.20	4.86	3.87	24.03
07	304	0	304	232	72	5.40	3.00	23.89	2.33	0.43	280.26	3.83	2.98	15.32
08	264	0	264	226	38	4.70	1.58	14.53	1.07	0.23	128.11	3.36	2.43	10.97
09	460	0	460	214	246	8.20	10.23	53.64	9.40	1.15	1127.61	4.51	3.74	23.76
10	174	0	174	131	43	3.10	1.77	24.79	1.03	0.33	124.93	2.89	2.31	12.55
11	413	0	413	360	53	7.40	2.23	13.06	1.59	0.22	190.52	3.50	3.10	17.37
12	469	0	469	391	78	8.30	3.22	16.64	2.64	0.32	319.06	4.01	3.85	23.09
13	336	0	336	233	103	6.00	4.27	30.84	3.65	0.61	433.61	4.06	3.38	19.11
14	239	0	239	171	68	4.30	2.84	28.78	1.99	0.47	238.60	3.43	2.97	16.85
15	112	0	112	58	54	2.00	2.23	48.23	1.89	0.95	224.78	4.16	2.98	14.57
16	184	0	184	89	95	3.30	3.96	51.78	3.27	1.00	390.43	4.02	3.05	16.01
17	321	0	321	86	235	5.70	9.78	73.40	9.43	1.65	1142.40	4.79	3.79	26.95
99	113	0	113	66	47	2.00	1.97	42.07	1.76	0.87	215.80	4.43	3.18	15.42

Table 5.3.: Basic CP statistics averaged over all 172 grid points of German part of Rhine basin for summer

Average CP statistics over 172 grid points of German part of Rhine basin (observational data set) (Summer)														
CP	Days [-]	No_data [-]	CPdays [-]	Dry [-]	Wet [-]	Freq [%]	dQfreq [%]	Prob. [%]	Cont. [%]	WI [-]	Sum [mm]	Mean [mm]	St.Dev. [-]	Max [mm]
01	340	0	340	242	98	6.00	4.27	28.84	3.93	0.66	510.02	5.18	4.26	22.50
02	331	0	331	303	28	5.80	1.24	8.66	0.85	0.15	112.64	3.83	3.07	13.51
03	353	0	353	72	281	6.20	12.27	79.77	15.63	2.53	2025.56	7.18	5.68	38.36
04	308	0	308	105	203	5.40	8.89	66.23	9.08	1.68	1177.16	5.77	4.72	27.57
05	585	0	585	296	289	10.30	12.58	49.51	10.16	0.99	1343.28	4.54	3.72	26.93
06	249	0	249	123	126	4.40	5.52	50.99	5.27	1.21	680.25	5.33	4.26	23.43
07	338	0	338	260	78	5.90	3.42	23.33	3.10	0.52	405.56	5.11	5.09	30.31
08	261	0	261	228	33	4.60	1.43	12.69	1.00	0.22	135.91	3.95	2.94	12.98
09	405	0	405	143	262	7.10	11.40	64.74	12.46	1.76	1636.93	6.19	5.69	43.40
10	269	0	269	223	46	4.70	2.01	17.25	1.33	0.28	173.89	3.72	2.97	14.36
11	330	0	330	286	44	5.80	1.94	13.52	1.82	0.31	242.70	5.25	4.63	22.47
12	482	0	482	393	89	8.50	3.87	18.57	3.58	0.42	475.54	5.19	4.49	25.20
13	325	0	325	263	62	5.70	2.70	19.19	1.76	0.31	228.30	3.70	2.92	14.69
14	237	0	237	158	79	4.20	3.46	33.62	3.02	0.73	392.34	4.90	3.95	20.56
15	178	0	178	85	93	3.10	4.06	52.41	3.84	1.23	501.93	5.37	4.94	27.76
16	240	0	240	92	148	4.20	6.45	61.71	7.50	1.78	975.70	6.54	6.22	42.12
17	353	0	353	85	268	6.20	11.69	76.08	12.78	2.07	1674.42	6.20	4.90	31.33
99	120	0	120	56	64	2.10	2.82	53.93	2.91	1.38	381.29	5.85	5.04	26.65

To assess the long term occurrence behavior of wet and dry CPs, the identified extreme wet and extreme dry CPs were grouped together. For wet CP group, CP03, CP04, CP06, and CP17 where combined, while CP02, CP08, CP10, CP11, CP12 and CP13 were combined together to form a dry CP group. The occurrence frequencies of the combined wet and dry CPs for each year are plotted in Figure 5.6. The gradual increase in dry CP frequency can be seen even for the comparatively shorter time period of 30 years. The wet CP group on the other hand remain inconclusive in terms of increasing or decreasing trend in occurrence frequency. These frequencies would later be compared with the frequencies achieved in SRES RCM control and A1B scenario runs in the following sections. This will be important in a sense that RCM control run comparison would give an indication towards the skill of the individual model used and comparison with SRES A1B scenarios would provide potential trend of extremes of climate in future.

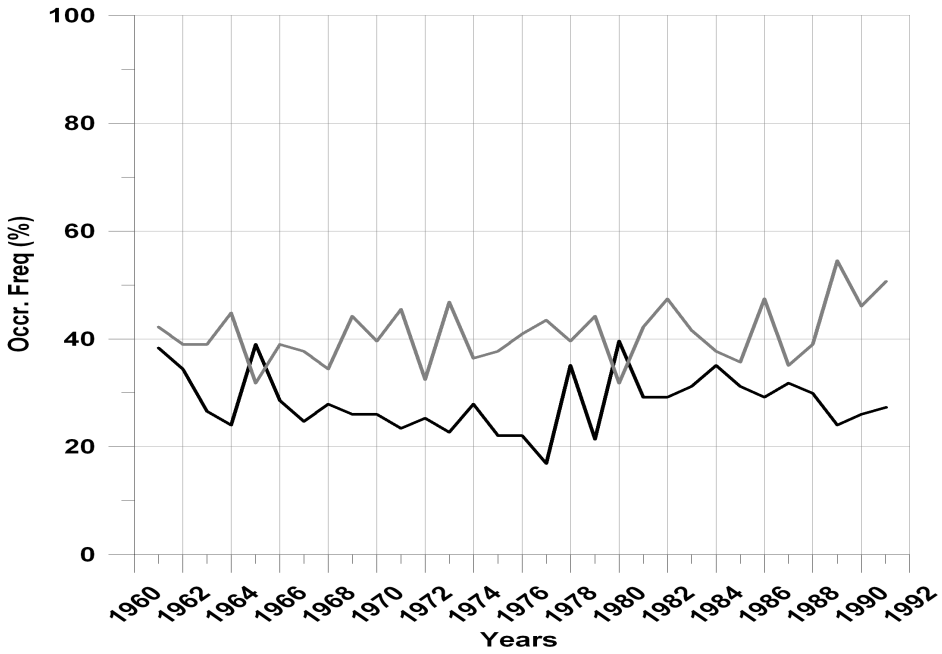

Figure 5.6.: Combined wet (black line) and dry (gray line) CP frequencies for each year.

Mean sea level pressure anomaly maps of all the CPs are shown in Figure 5.7 which corresponds quite well to wet and dry CP classification based on the wetness index. The anomaly maps are created from 1961-1991 daily normalized MSLP. The wet group of CPs (CP03, CP04, CP06 and CP17) have marked low pressure centers either at north Atlantic or central Europe (in case of CP17). Dry group of CPs (CP02, CP08, CP10, CP11, CP12 and CP13) on the other hand have predominantly higher pressure anomaly centered over eastern British isles and changing its position in north-south direction. The pressure system causes a weak air movement and transports dry air masses from eastern Europe to central Europe. CP02 is the driest

CP with minimum precipitation probability in both winter and summer (7.11% and 8.66%) and minimum contribution to precipitation increase (0.62% in winter and 0.85% in summer). The occurrence frequency of CP02 tend to marginally increase in winter (6.2% in winter against 5.8% in summer).

The two wettest CPs are CP03 and CP04. Both CPs have strong negative pressure anomalies over north of British Isles and high pressure anomalies over eastern Atlantic ocean (with slight difference in location of pressure centers). This is a typical wet pressure system and causes a typical west cyclonic transport of moist ocean air masses from the Atlantic Ocean to Central Europe. The two CPs have highest probability of precipitation in both winter and summer (88.35% and 82.77% in winter and 79.77% and 66.23% in summer for CP03 and CP04 respectively). They also contribute more than any other CPs to total precipitation in both winter in summer. The contribution to precipitation for the two CPs are 26.37% and 14.52% in winter and 15.63% and 9.08% in summer.

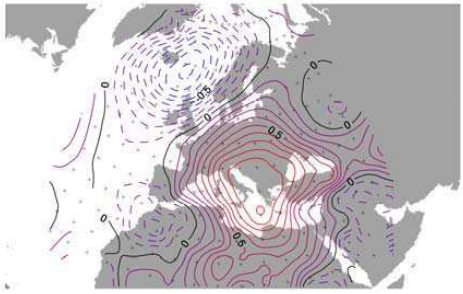
CP01

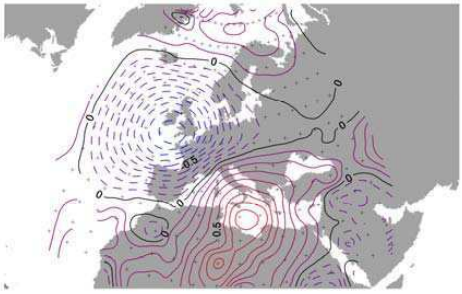
CP06

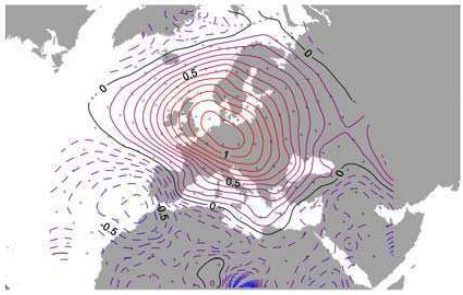
CP02

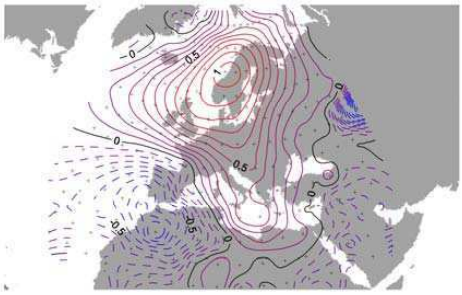
CP07

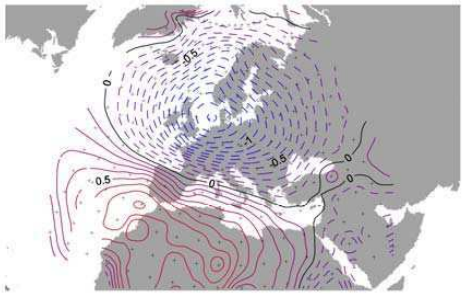
CP03

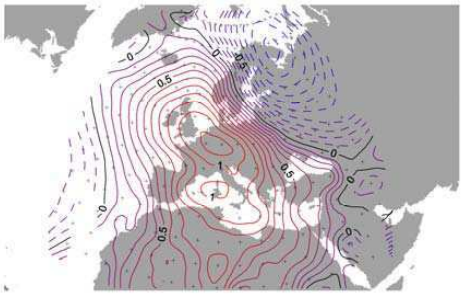
CP08

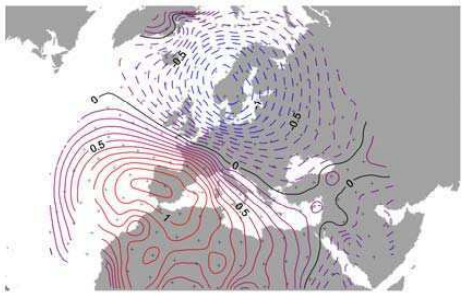
CP04

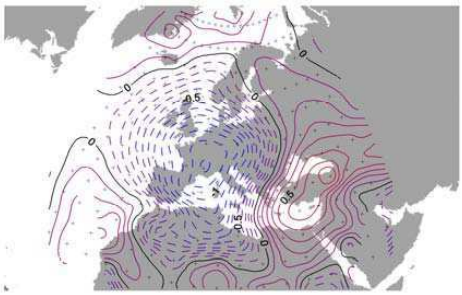
CP09

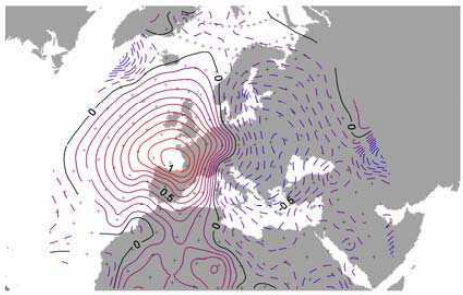
CP05

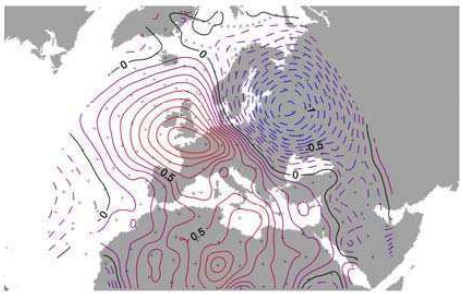
CP10

Figure 5.7.: Mean sea level pressure maps of all CPs (contd...)

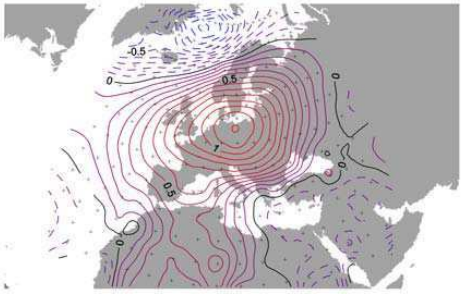

CP11

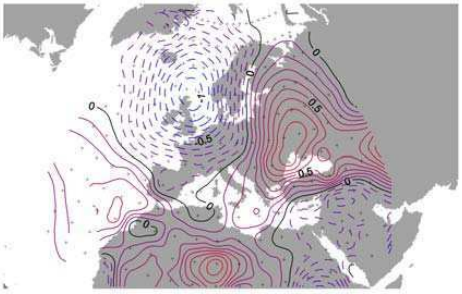

CP15

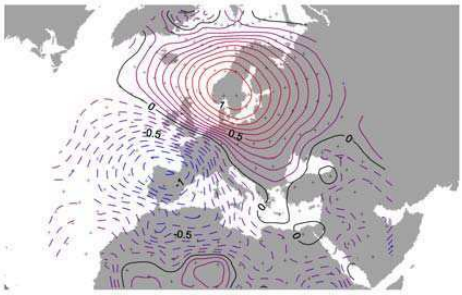

CP12

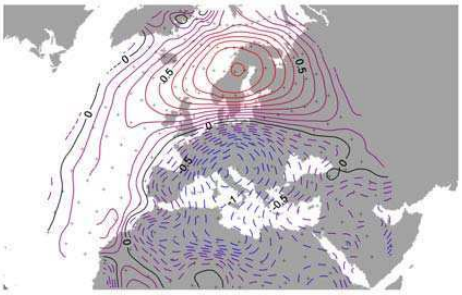

CP16

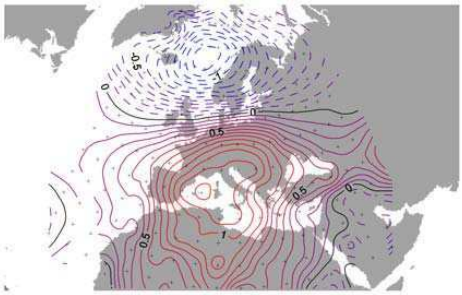

CP13

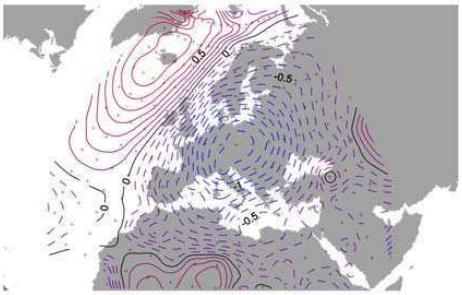

CP17

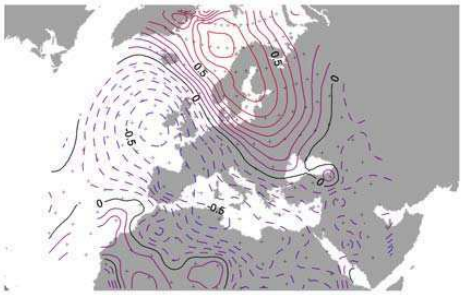

CP14

Figure 5.7.: Mean sea level pressure maps of all CPs

Figure 5.8 shows the CP conditioned precipitation distribution for summer and winter of wettest and driest CPs. The distribution clearly show difference of precipitation associated with each identified critical CP.

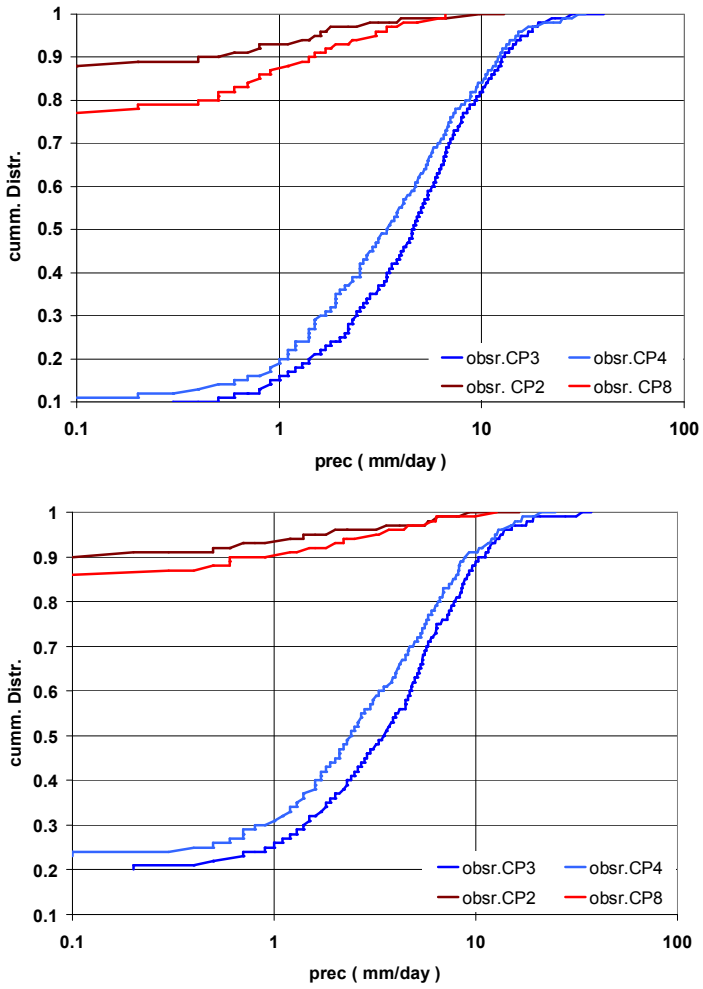

Figure 5.8.: CP conditioned precipitation of two wettest and driest CP for winter (above) and summer (below).

Given that dry spells usually are characterized by long spells of no precipitation, only the precipitation amounts, means and precipitation contribution to total precipitation associated with certain identified dry CP in certain area may not be the only way of showing worthiness of dry CP identification. Thats why in Table 5.4, the two historical drought spells in summer of 1976 and 1991 along with the classification of CPs is shown. It can be clearly seen that identified critical dry CPs (background shaded in gray) dominate the two dry spells. The cells shaded light gray are also identified dry CPs but they have wetness indices slightly above 0.5. e.g. CP07 has average wetness index of 0.52 in summer and 0.43 in winter.

In order to investigate the spatial relationship between CPs and daily precipitation the wetness indices were calculated for each CP and grid point and interpolated using external drift kriging (Ahmed and Marsily (1987)). The topographic elevation was used as external drift and calculations were carried out for the winter and summer half years separately. The results for winter are shown in Figure 5.9 while Figure 5.10 displays the same for summer.

It can be seen that regardless of the season, dry CPs remain dry while wet CPs remain wet. Additionally dry CPs show more spatial homogeneity than wet CPs mainly because of the physical nature of two phenomena. High pressure anomalies usually are more widely spread with mild gradients and effect larger areas as compared to low pressures which are localized and have steep gradients. Dry CPs remain dry both in winter and summer and are homogeneous in their spread of WI values except CP13 which is considerably dry in summer than it is in winter. In fact in north-western part there are areas which have WI values larger than 1 for CP13 in winter. In terms of wet CPs, the biggest difference in spatial distribution of wetness index can be seen in CP17 where it is more wetter with more even spread of wetness in summer than it is in winter.

Table 5.4.: Historical European drought spells of 1976 and 1991 and associated identified dry CPs (in shaded boxes)

Date	1976 CPs	1991 CPs
1.06	CP04	CP08
2.06	CP05	CP17
3.06	CP05	CP03
4.06	CP02	CP06
5.06	CP11	CP03
6.06	CP13	CP09
7.06	CP02	CP03
8.06	CP12	CP06
9.06	CP14	CP04
10.06	CP01	CP13
11.06	CP07	CP06
12.06	CP13	CP06
13.06	CP10	CP01
14.06	CP13	CP01
15.06	CP01	CP09
16.06	CP07	CP09
17.06	CP10	CP05
18.06	CP01	CP04
19.06	CP15	CP03
20.06	CP01	CP13
21.06	CP08	CP15
22.06	CP08	CP14
23.06	CP02	CP04
24.06	CP02	CP13
25.06	CP07	CP03
26.06	CP07	CP17
27.06	CP11	CP05
28.06	CP02	CP05
29.06	CP07	CP13
30.06	CP07	CP11
1.07	CP07	CP07
2.07	CP12	CP12
3.07	CP12	CP12
4.07	CP06	CP12
5.07	CP12	CP12
6.07	CP12	CP12
7.07	CP12	CP06
8.07	CP17	CP01
9.07	CP14	CP02
10.07	CP14	CP14
11.07	CP12	CP01
12.07	CP16	CP04
13.07	CP16	CP05
14.07	CP14	CP05
15.07	CP06	CP10
16.07	CP01	CP05
17.07	CP06	CP05
18.07	CP06	CP06
19.07	CP01	CP10
20.07	CP04	CP10
21.07	CP09	CP02
22.07	CP05	CP14
23.07	CP05	CP17
24.07	CP05	CP17
25.07	CP11	CP05
26.07	CP11	CP11
27.07	CP05	CP12
28.07	CP05	CP12
29.07	CP10	CP12
30.07	CP06	CP16
31.07	CP09	CP03
1.08	CP05	CP05
2.08	CP13	CP05
3.08	CP13	CP05
4.08	CP10	CP02
5.08	CP11	CP13
6.08	CP11	CP01
7.08	CP08	CP05
8.08	CP07	CP10
9.08	CP99	CP13
10.08	CP99	CP01
11.08	CP99	CP04
12.08	CP06	CP10
13.08	CP07	CP02
14.08	CP07	CP11
15.08	CP07	CP05
16.08	CP12	CP15
17.08	CP05	CP10
18.08	CP08	CP10
19.08	CP07	CP13
20.08	CP07	CP13
21.08	CP12	CP12
22.08	CP12	CP01
23.08	CP12	CP08
24.08	CP07	CP02
25.08	CP07	CP12
26.08	CP07	CP12
27.08	CP16	CP12
28.08	CP07	CP12
29.08	CP12	CP12
30.08	CP04	CP12
31.08	CP03	CP06

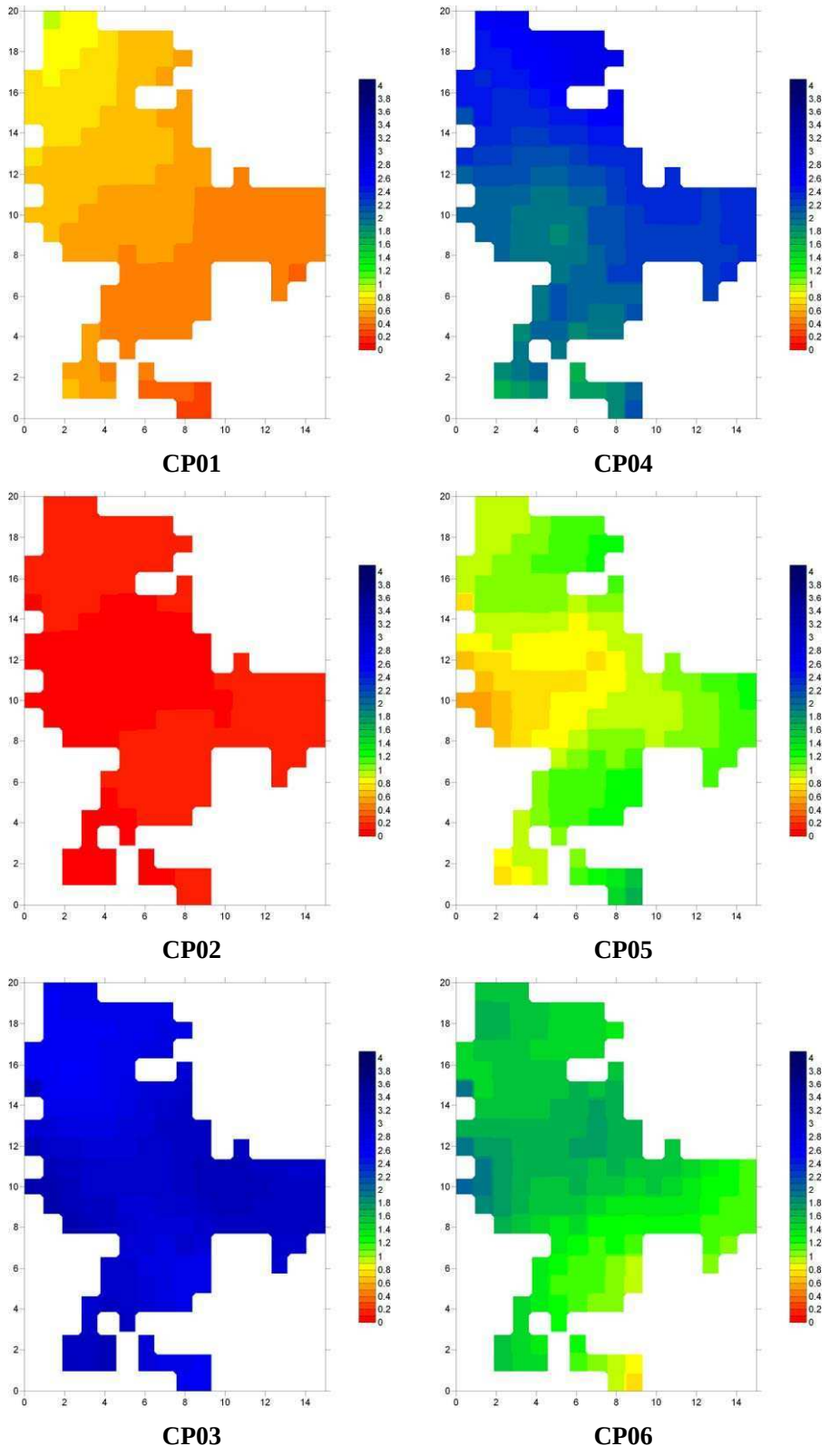

Figure 5.9.: Spatial distribution of wetness index for each CP for winter

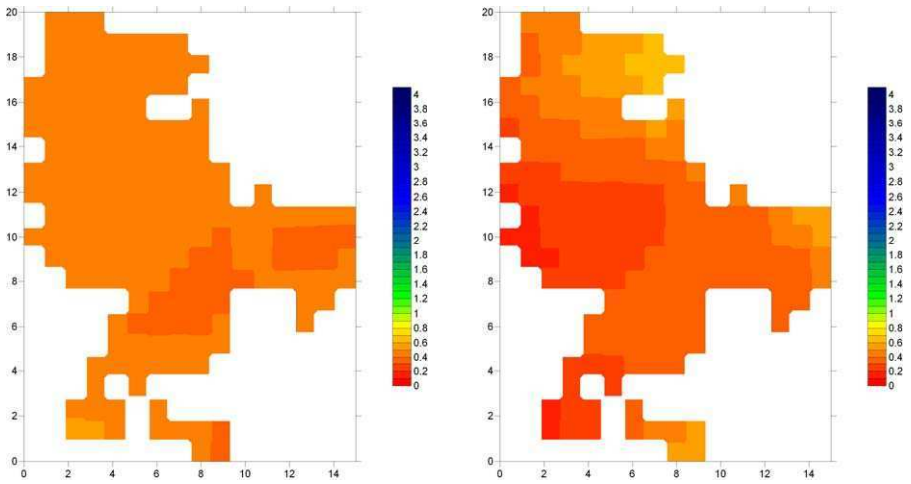

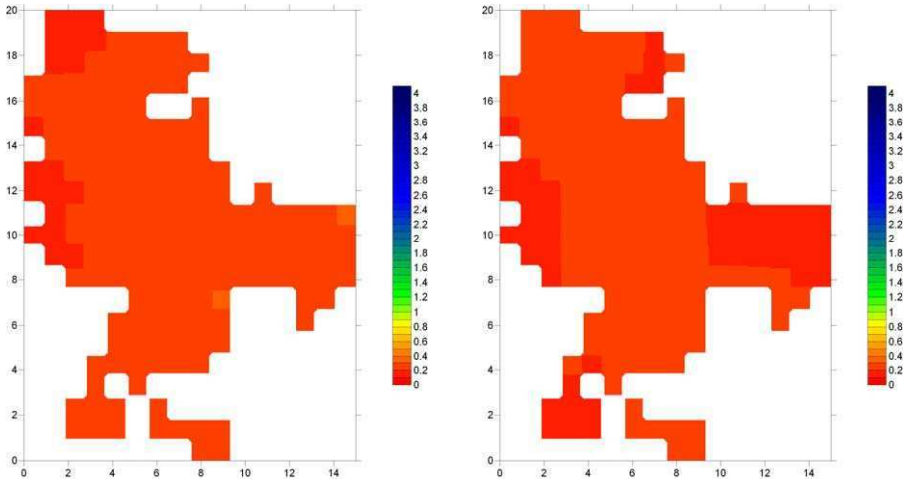

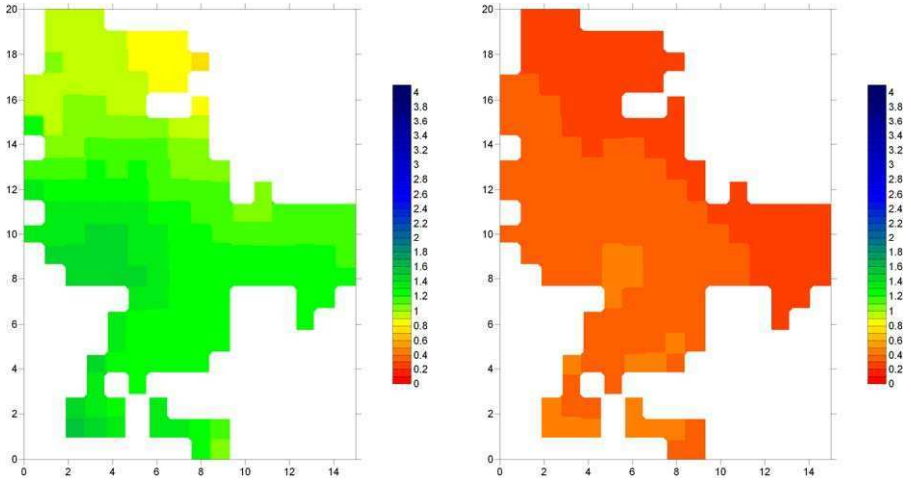

Figure 5.9.: Spatial distribution of wetness index for each CP for winter. Contd...

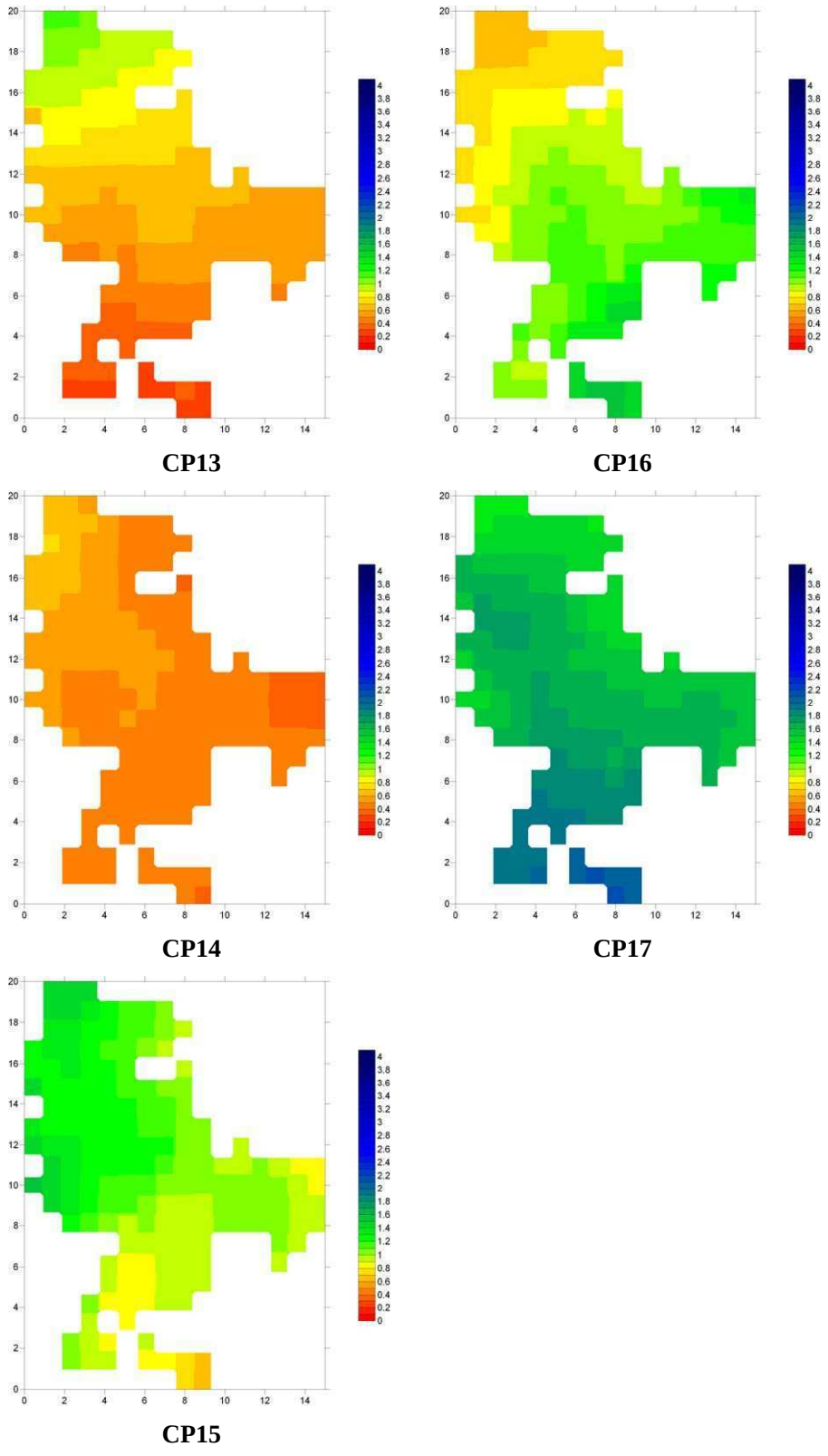

Figure 5.9.: Spatial distribution of wetness index for each CP for winter. Contd...

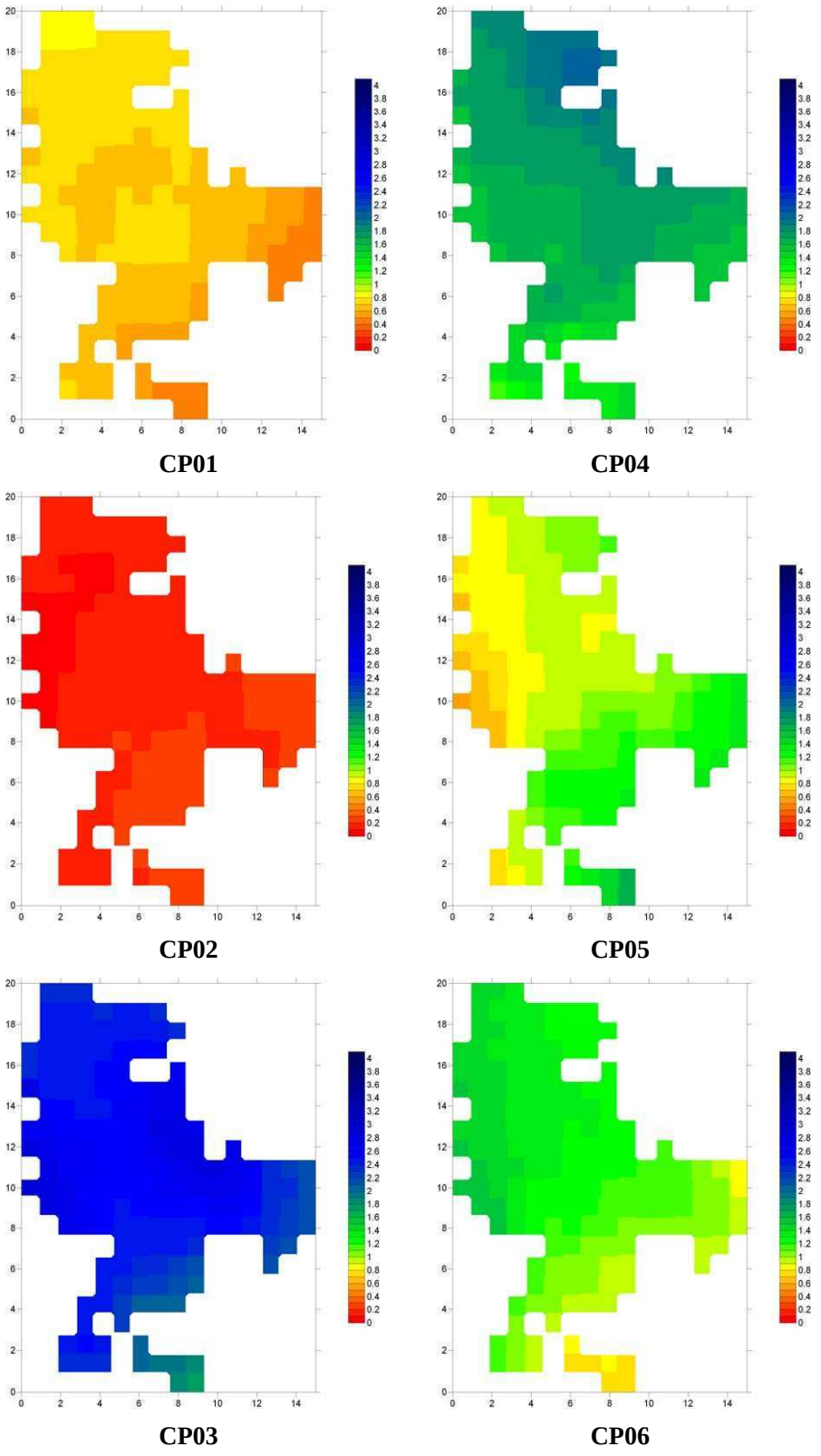

Figure 5.10.: Spatial distribution of wetness index for each CP for summer.

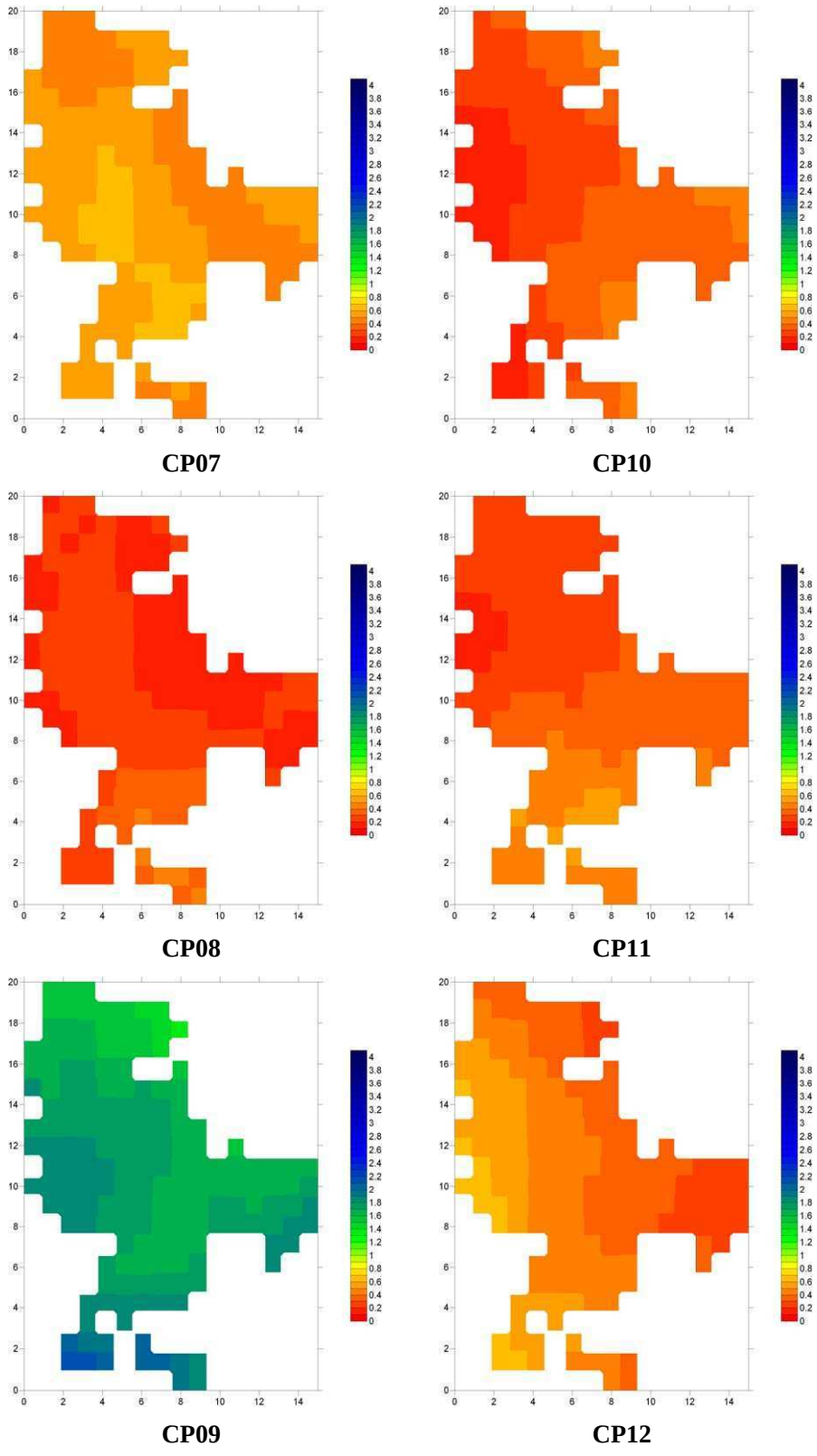

Figure 5.10.: Spatial distribution of wetness index for each CP for summer. Contd...

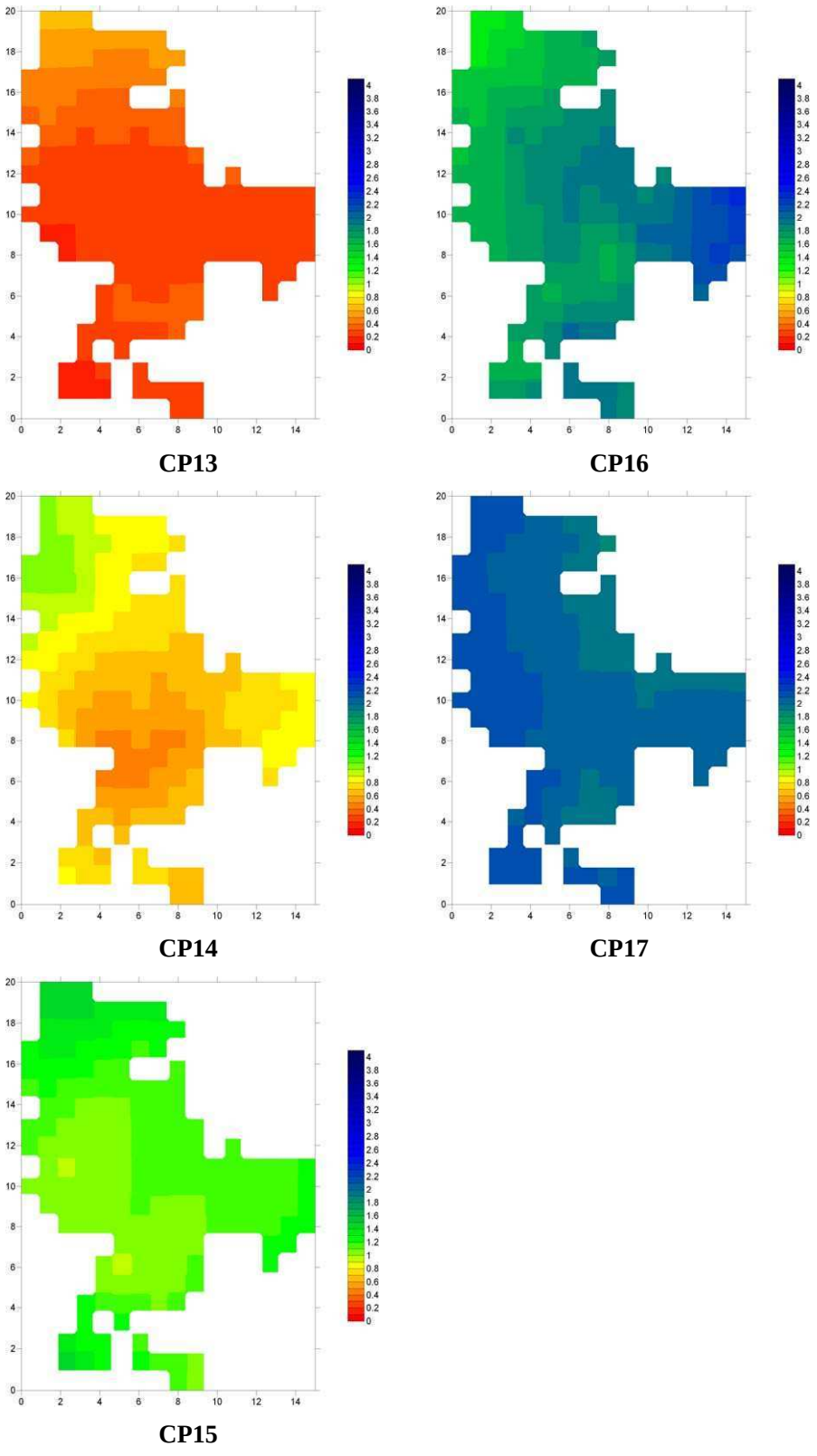

Figure 5.10.: Spatial distribution of wetness index for each CP for summer. Contd...

5.2.1.2. RACMO data set classification

RACMO is the regional climate model developed by the Royal Netherlands Meteorological Institute, KNMI. The details of the model, its resolution, underlying physics and driving GCM can be found in Meijgaard et al. (2008). Daily mean sea level pressure and daily precipitation values available on 0.22° regular grid resolution have been used for classification purposes. RACMO provides all its data on rotated spherical coordinate system with a north pole latitude placed at −39.25° and longitude at 18°. On a rotated grid system the data is provided with lower left corner at (−21.72 , −20.68) and upper right corner at (15.46 , 20.90) as its x and y coordinates. This grid corresponds to (4.806W , 26.719N) and (58.32E , 67.365N) window on a geographic coordinate system with irregular coordinates spacing. To convert the data to regular grid spacing of 0.22° on geographical coordinate system the data was interpolated to a working window with (4W , 30N) and (27.68E , 61.68N) as lower left and upper right corners respectively. With interpolated geographic coordinate system, German part of Rhine basin is represented by 172 grid points shown in Figure 4.11.

Comparing the individual grid point based results with observational gridded data set results shown in Figure 5.5 it can be seen that the basic CP statistics for this Grid point have been maintained by RACMO control run data set. Wet CPs remain wet and dry CPs remain dry in both observational and RACMO gridded data set albeit some small differences. For example CP03 remains the wettest CP both in winter and summer but the degree of wetness decreases from 3.4 in observational gridded data set to 3.0 in RACMO data set for winter and from 3.0 for observational to 2.5 for RACMO data set for summer. Similarly CP06 has also lower wetness index value in both winter and summer. RACMO data set's dry CPs are the same as observational gridded data set except that the degree of wetness for dry CPs is slightly larger in RACMO. Figure 5.11 displays the averaged values of different important statistics of all CPs for winter and summer. These values are averaged over all the 172 grid points to obtain the general picture of RACMO classification for each CP. The same picture of reduced degree of wetness index values for wet CPs arise here. Except CP16 which increases slightly (significantly) in wetness index all other classified wet CPs have lower index value in RACMO classification in winter (summer). In terms of occurrence frequencies on the other hand RACMO tends to have higher values for the two wettest CPs than observational gridded data set for both winter and summer and considerably lower values for other wet CPs. Looking specifically into the dry CPs it is found that on average RACMO overestimates (4%) the occurrence frequencies of combined dry CPs in winter while there is negligible overestimation (0.5%) in summer.

Three times periods are selected for classification for assessing how the extreme CPs change over time in selected RCM. 2021-2050 and 2071-2100 are the two shorter time periods selected in the initial and later part of 21st century. Finally the whole time period made available by each RCM (2001-2100) was selected for performing CP classification. For the same time periods, averaged values of important CP statistics are displayed for each season in Figure 5.12 through Figure 5.14. In terms of "inter-time period" changes among the CP statistics, except some few instances, most of the

values does not alter that much. Wet CPs classified in observational gridded data set and in RACMO control run data set remain wet here although with smaller values of wetness indices. Two of the wettest CPs have lower wetness index value than they were either in observational gridded data set or in RACMO control run data set. Except CP06 which has higher value of wetness index than it had in observational or RACMO control run. The increase is more in 2021-2050 time period than in 2071-2100. This increase though is only in winter and in summer it more or less remains stable. Occurrence frequencies of both wet and dry CPs remain on average the same. Year wise occurrence frequencies of combined wet and dry CPs in control and A1B scenario would be shown later. The biggest change in occurrence frequency in dry CPs occur in CP02 which has increased in A1B scenario. In winter the increase in 2021-2050 is more than 2071-2100 while in summer the opposite is true. In terms of "inter-season" changes, it can be seen that the classification is quite homogeneous in that wet CPs remain wet and dry remain dry both in summer and winter but in some cases the strength of wetness indices fluctuates. Case in point CP13, where it is twice as dry in summer as it is in winter in almost all the cases of RACMO control and three time periods of RACMO A1B scenario .

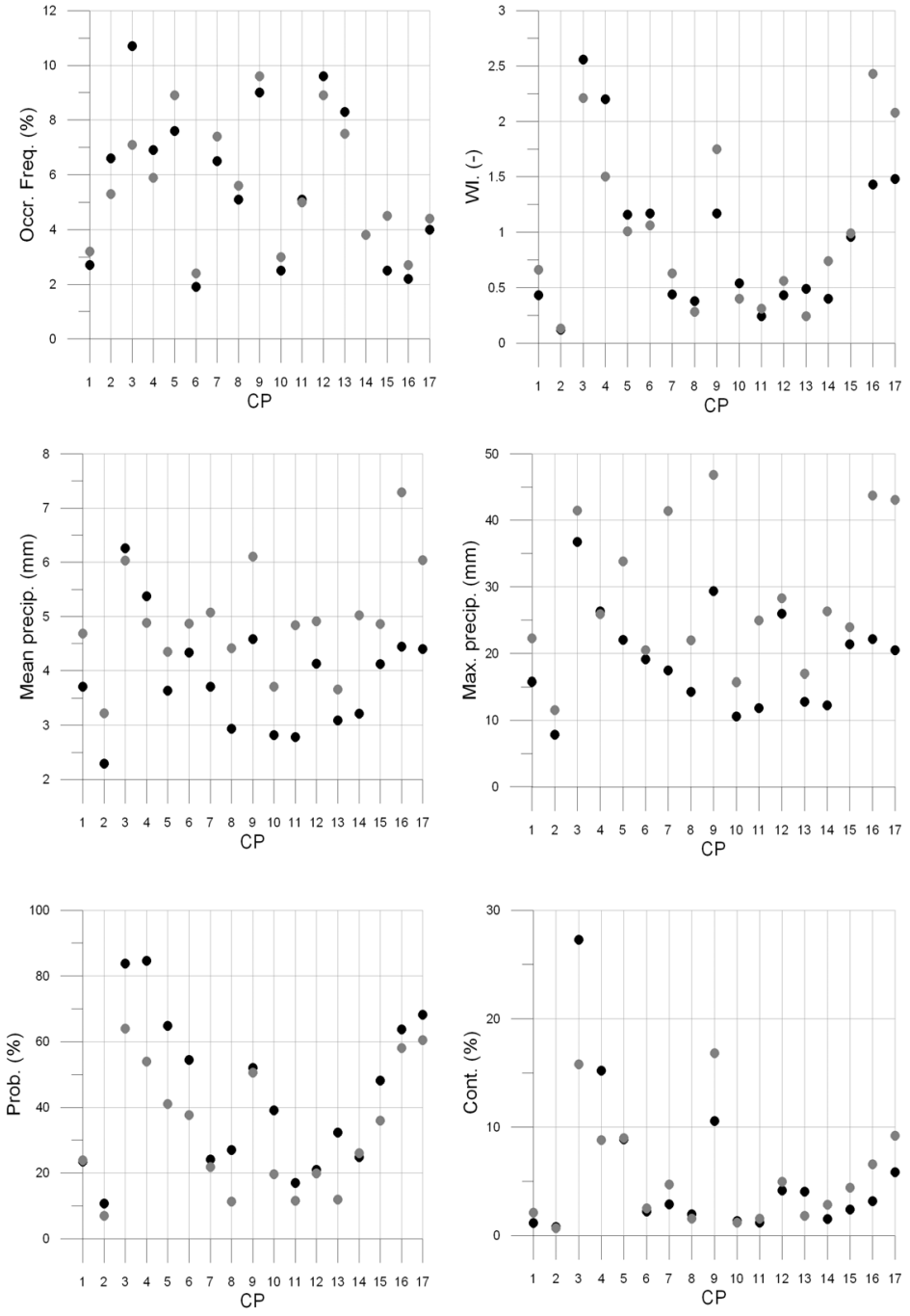

Figure 5.11.: Basic CP statistics averaged over all 172 grid points of German part of Rhine basin for winter (black circles) and summer (gray circles) for RACMO control run scenario (1961-1991) dataset

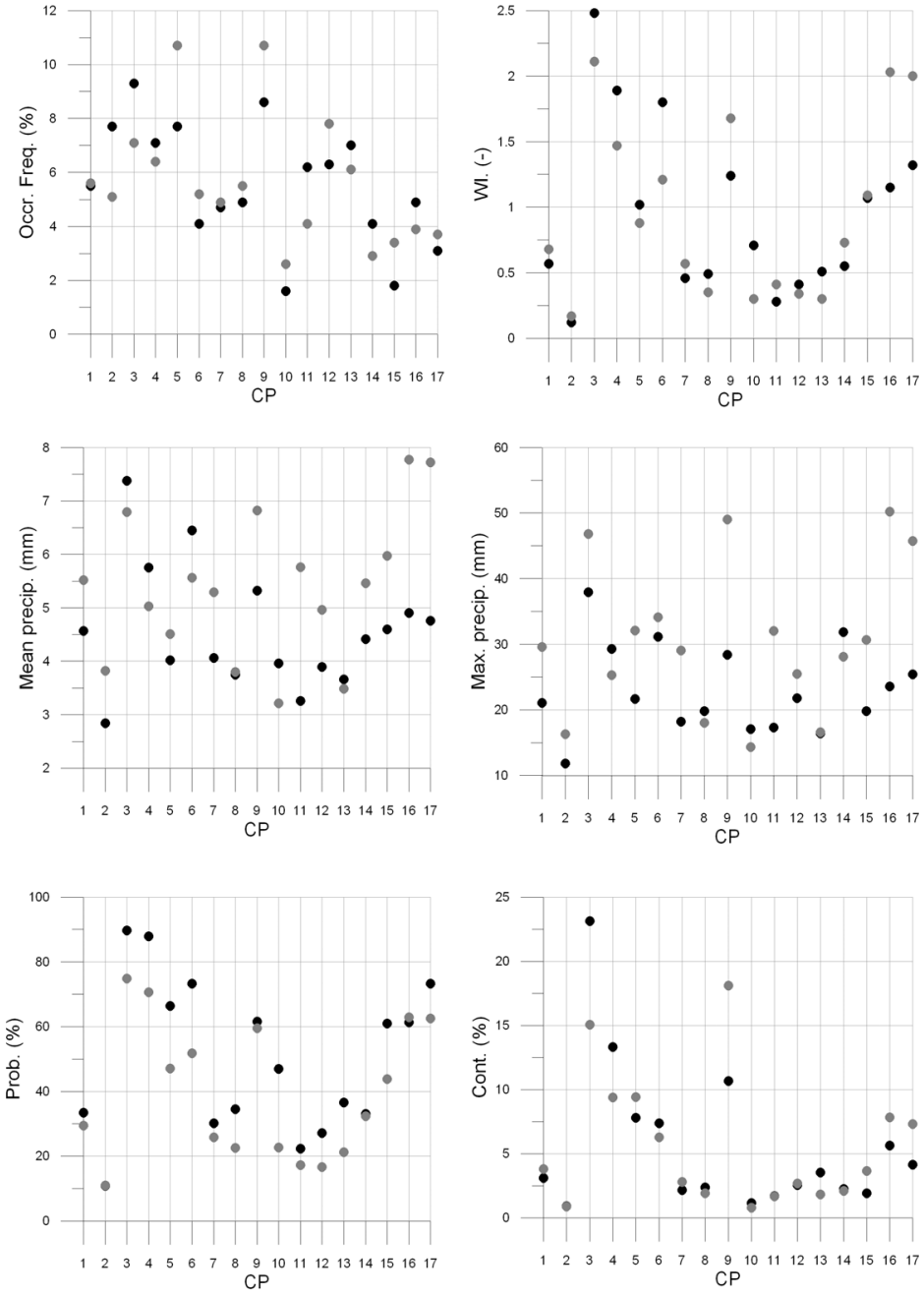

Figure 5.12.: Basic CP statistics averaged over all 172 grid points of German part of Rhine basin for winter (black circles) and summer (gray circles) for RACMO SRES A1B scenario (2021-2050) dataset

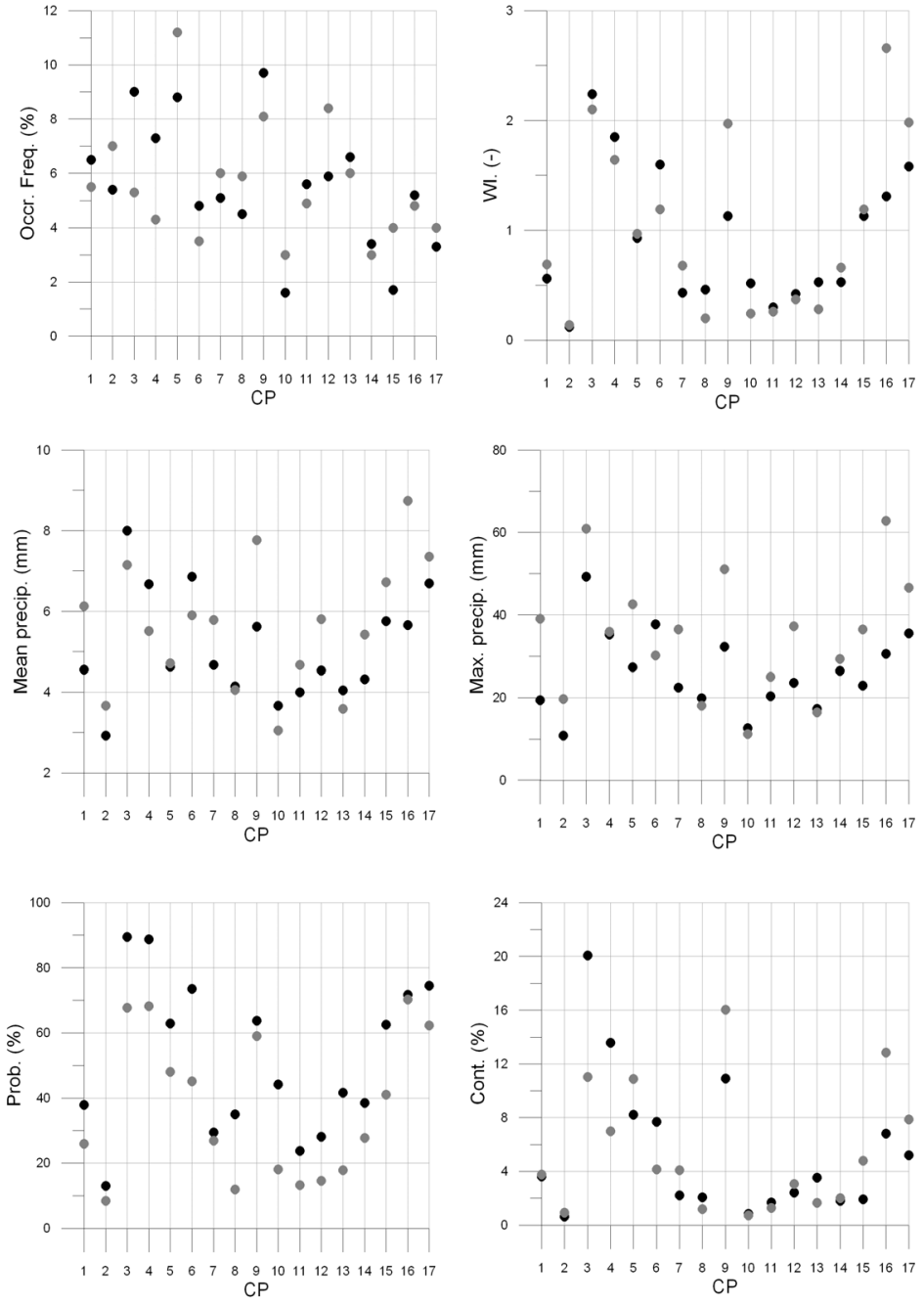

Figure 5.13.: Basic CP statistics averaged over all 172 grid points of German part of Rhine basin for winter (black circles) and summer (gray circles) for RACMO SRES A1B scenario (2071-2100) dataset

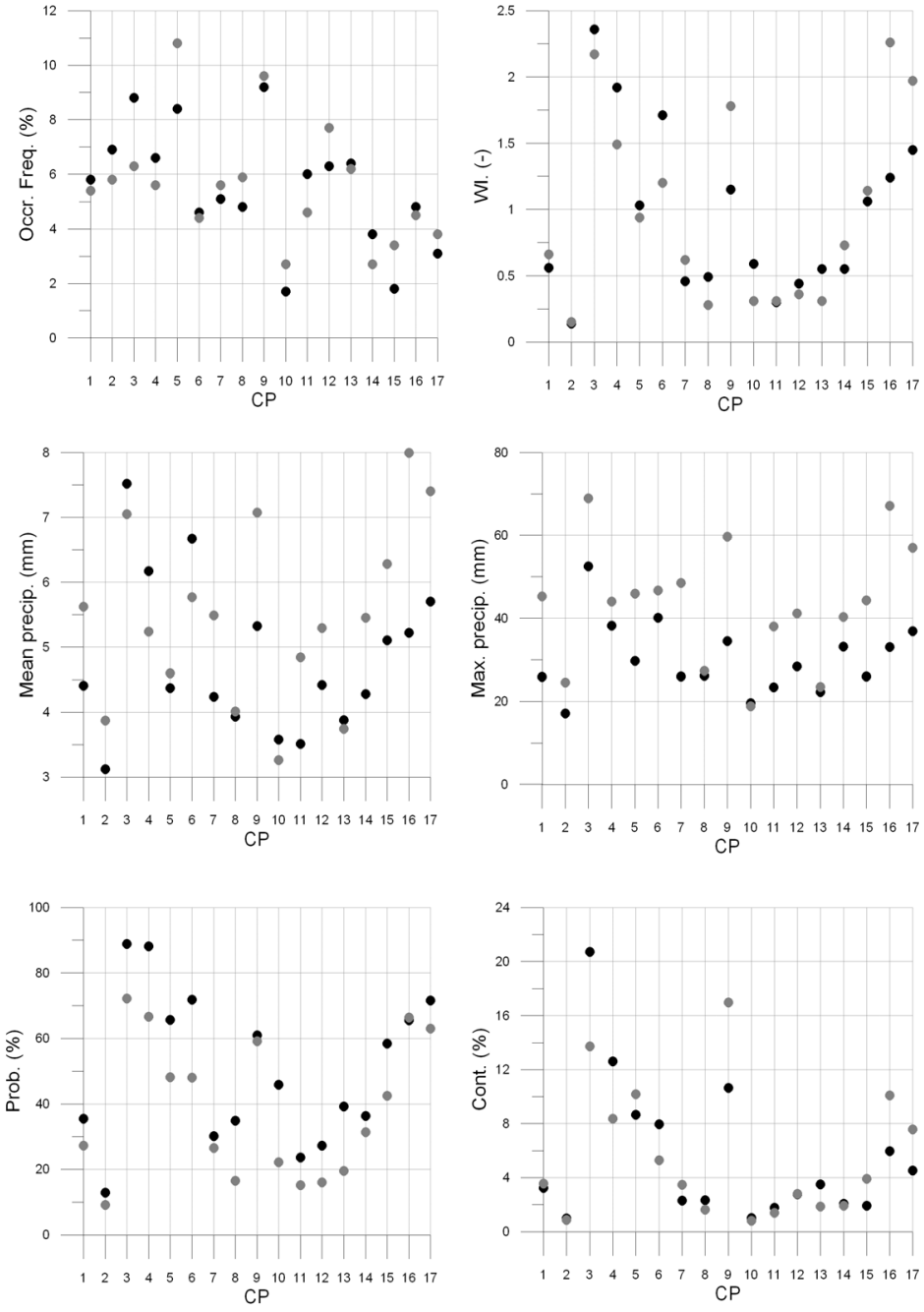

Figure 5.14.: Basic CP statistics averaged over all 172 grid points of German part of Rhine basin for winter (black circles) and summer (gray circles) for RACMO SRES A1B scenario (2001-2100) dataset

Figures 5.15 and 5.16 shows the combined dry and wet CP occurrence frequencies for observational (solid black line) and RACMO (solid gray line) gridded data set respectively. Control period of RACMO and SRES A1B scenario have both been included in the figures along with the linear trend (shown in dashed black line). It can be seen that during the control period of 1961-1991 RACMO simulates the occurrence frequency of combined dry and wet CP's reasonably well. Given that RACMO control runs are driven by ERA40 data, the similarity with observational frequency (also obtained from ERA40 MSLP classification)is not surprising. Although the pattern of increase and decrease are simulated well, yet there are some consistent underestimation of combined wet CP occurrence frequencies during the control time period. In case of combined dry CP occurrence frequencies though, there are no consistent under or over estimation and increase and decrease in occurrence frequency is well simulated. In case of RACMO A1B scenario occurrence frequencies for combined wet and dry CPs, the two figures show contrasting and interesting behavior. In case of wet CPs there is visible downward trend in occurrence of extreme wet CPs over 2001-2100 period and increasing trend of extreme dry CPs. RACMO thus predicts a more drier situation in coming 90 years.

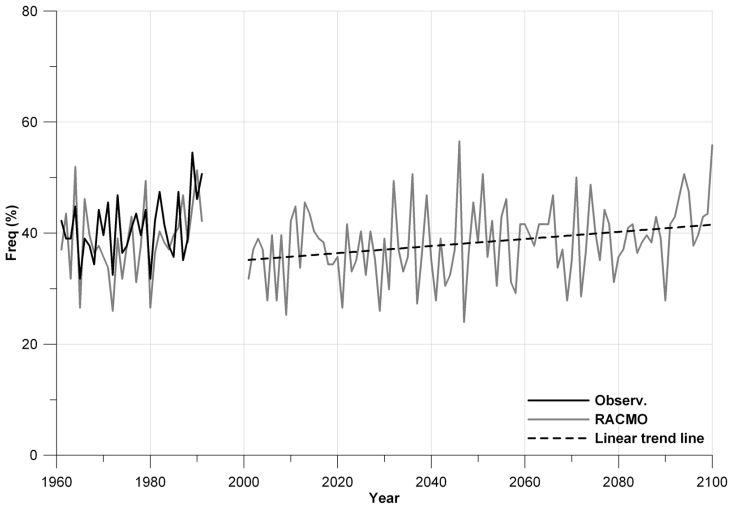

Figure 5.15.: Occurrence frequencies of combined dry CPs for observational gridded (solid black line) and RACMO control and SRES A1B scenario (solid gray line) data sets

Spatial structure of wetness indices for all CPs and for each season are presented in Appendix B. Section B.1 presents spatial maps for both control and SRES A1B scenario runs with Figure **??** and B.2 showing control run maps for winter and summer while Figure B.3 and Figure B.4 showing the same for A1B scenario respectively. It can be seen that extreme CPs are predominantly remaining very homogeneous and depending upon the extreme CP one is looking at remain wet or dry over the whole region. Considering dry CPs of CP02 and CP10 in summer, it can be seen that in southern part of German part of Rhine basin (Black forest and Alps) the CPs

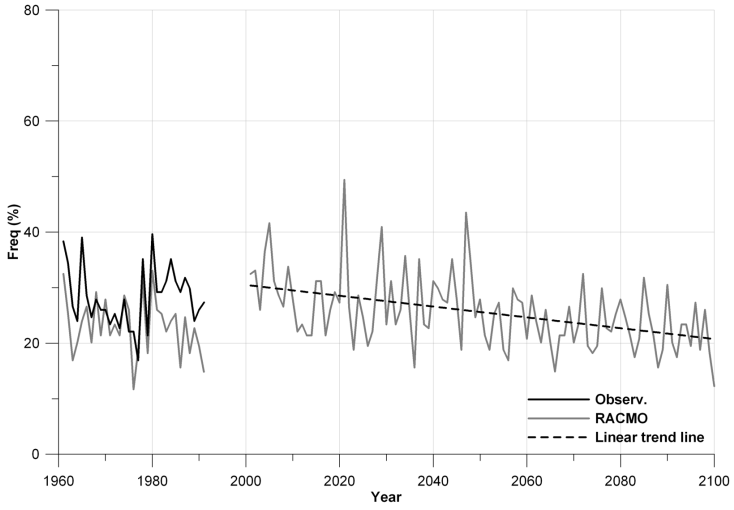

Figure 5.16.: Occurrence frequencies of combined wet CPs for observational gridded (solid black line) and RACMO control and SRES A1B scenario (solid gray line) data sets

are marginally wetter than they are in northern areas. This difference is more in control run than observational gridded data set and more in A1B scenario run than in control run. Giving an indication of possible bias in the model. In some CPs (for example CP06, both in winter and summer) the spatial behavior of wetness index corresponds very well with the topographical nature of the catchment with distinct areas of comparatively wet and dry situation in northern and southern part of the basin. CP16 and CP17, both wet CPs, show considerable inter-season variation in terms of wetness index for both control and A1B scenario runs. Both CPs are considerably wet in summer than in winter.

Appendix B Table C.1 presents the contingency table between ERA40 based CP classification and RACMO control run classification.

5.2.1.3. REMO data set classification

REMO is the regional climate model developed by the Max-Planck-Institute für Meteorologie, (MPI-M). Model description, resolution and underlying GCM information can be found in Jacob (2001). REMO is based on the "Europamodell" D. (2008), the former numerical weather prediction model of the German Weather Service (Deutscher Wetterdienst, DWD.). MPI-M made further development of the model, where the physical parameterisations from ECHAM4/T106 were implemented into the Europamodell code in addition to the ones which already existed. REMO can be used both in forecast and in climate mode. REMO provides different meteorological variables for control and SRES A1B scenario runs in different temporal and spatial resolutions. Daily mean sea level pressure and daily precipitation values

available on 0.22° regular grid resolution have been used for classification purposes. As was the case with RACMO, REMO also provides all of its modeled data on rotated spherical coordinate system with a north pole latitude placed at −39.25° and longitude at 18°. The data was first interpolated to geographical coordinate system before being used for classification purposes.

The general picture for control runs classification remains very much the same as RT5 observational gridded data set. Wet CPs remain wet and dry CPs remain dry in REMO simulations. Figure 5.17 shows the more detailed CP statistics averages over all 172 grid points of Rhine basin for control winter and control summer period. Comparing with RT5 observational gridded data set's averaged CP statistics, it can be seen that wet CP occurrence frequencies tend to increase in REMO control runs while dry CP occurrence frequencies tend to decrease a bit. CP08 is exceptionally dry CP in summer which is increasing in occurrence as well. The wetness indices of both wet and dry CP remain more or less stable but generally in dry CPs case the wetness indices are a bit higher, indicating less dryness. Figure 5.18 through Figure 5.20 show averaged CP statistics value for SRES A1B scenario for three time periods of 2021-2050, 2071-2100 and 2001-2100 for winter and summer half years respectively. In case of wet CPs the occurrence frequencies for all three time periods remain in the same range as observational gridded dataset showing not a marked difference in future. But in case of dry CPs the occurrence frequencies of two most dry CPs i.e. CP02 and CP08 tend to increase both in summer and winter. Other dry CPs either remain in the range that were observed in observational gridded data set or decrease a bit. The increase in occurrence frequencies of these two CPs affect the overall behaviour of dry CP occurrence. The same can be seen in the combined dry and wet CP frequencies in Figure 5.21 and Figure 5.22 respectively. The clear increasing and decreasing trends in the two figures for SRES A1B scenario run are more or less the same as was the case in RACMO model.

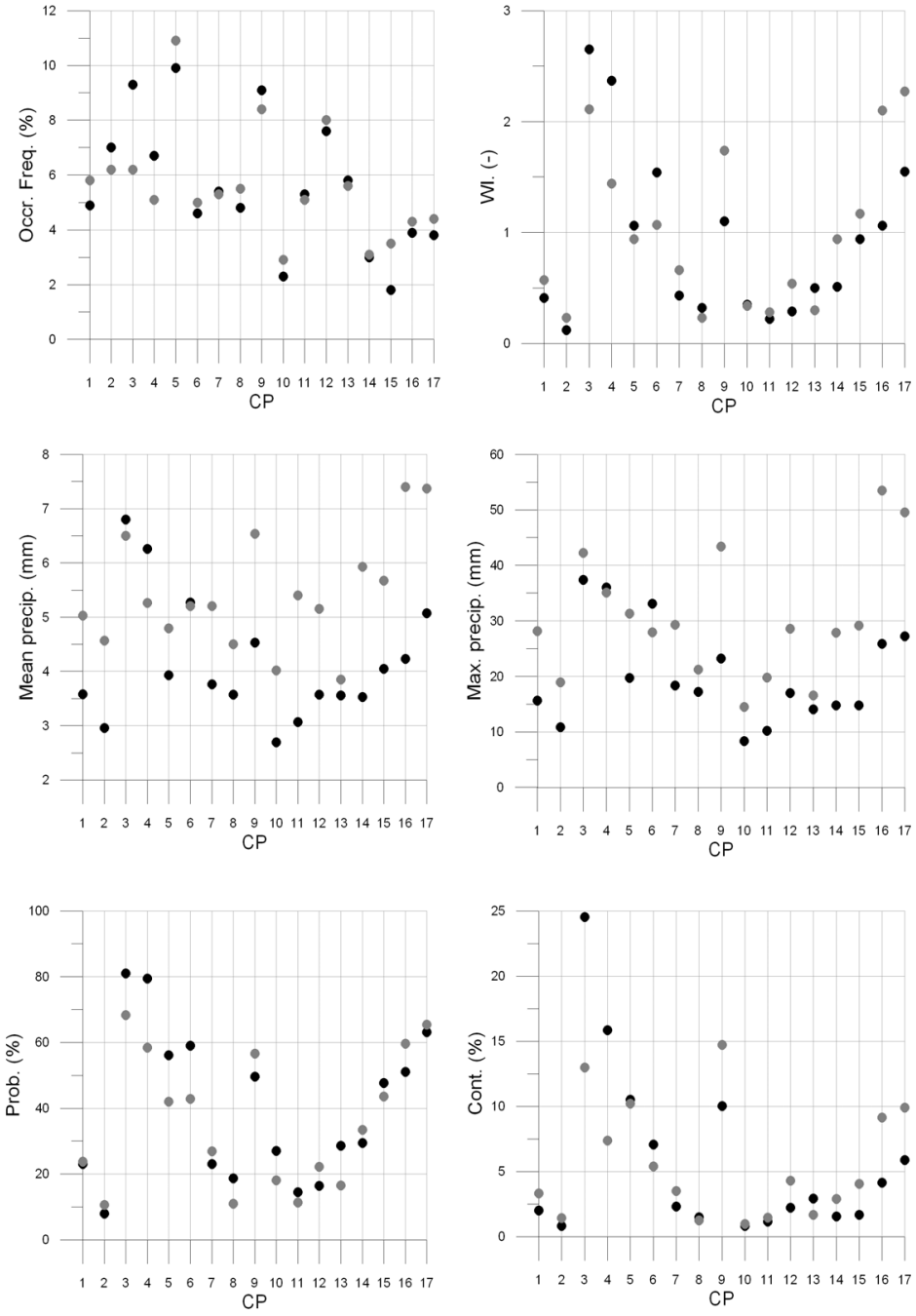

Figure 5.17.: Basic CP statistics averaged over all 172 grid points of German part of Rhine basin for winter (black circles) and summer (gray circles) for REMO control run scenario (1961-1991) dataset

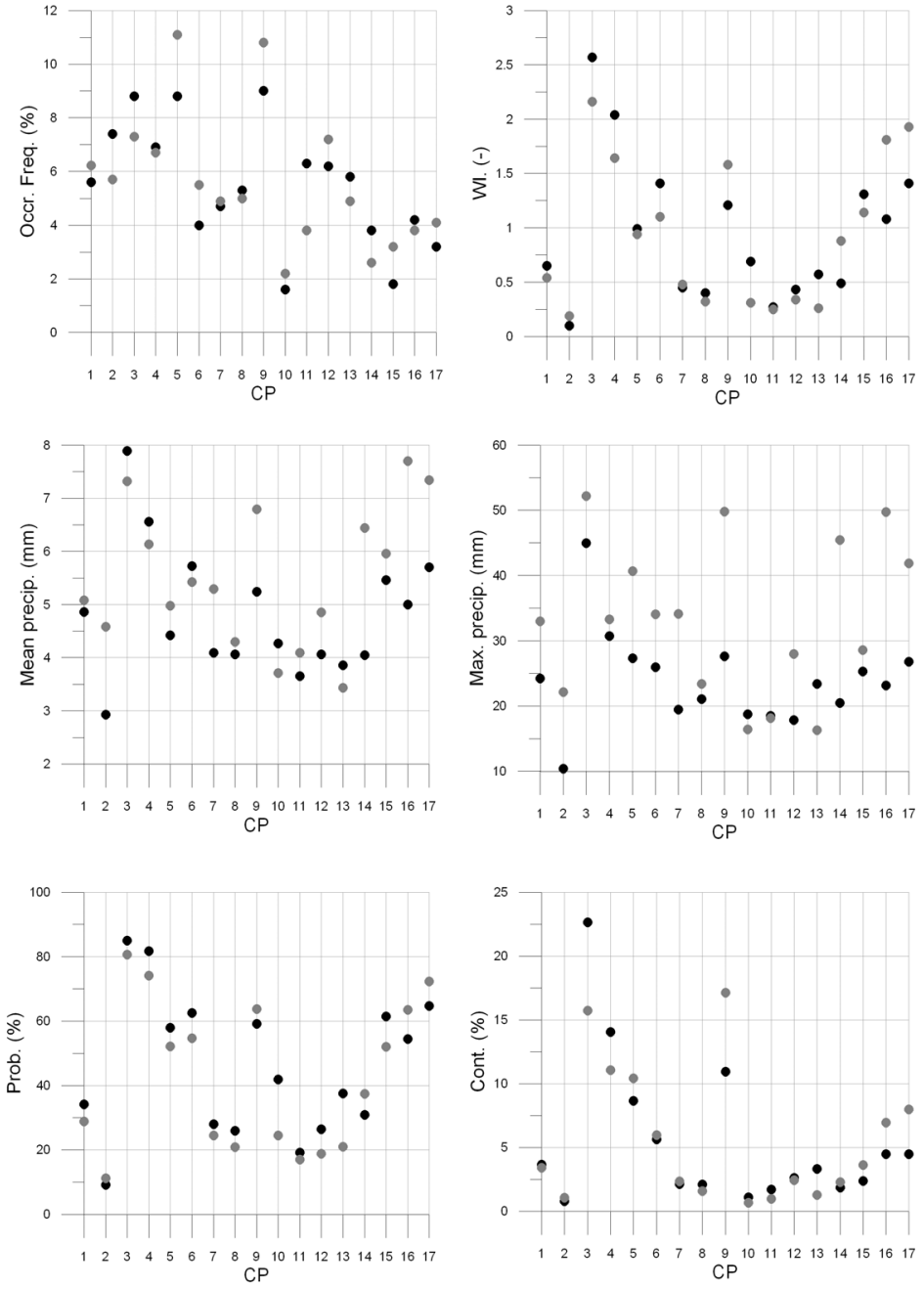

Figure 5.18.: Basic CP statistics averaged over all 172 grid points of German part of Rhine basin for winter (black circles) and summer (gray circles) for REMO SRES A1B scenario (2021-2050) dataset

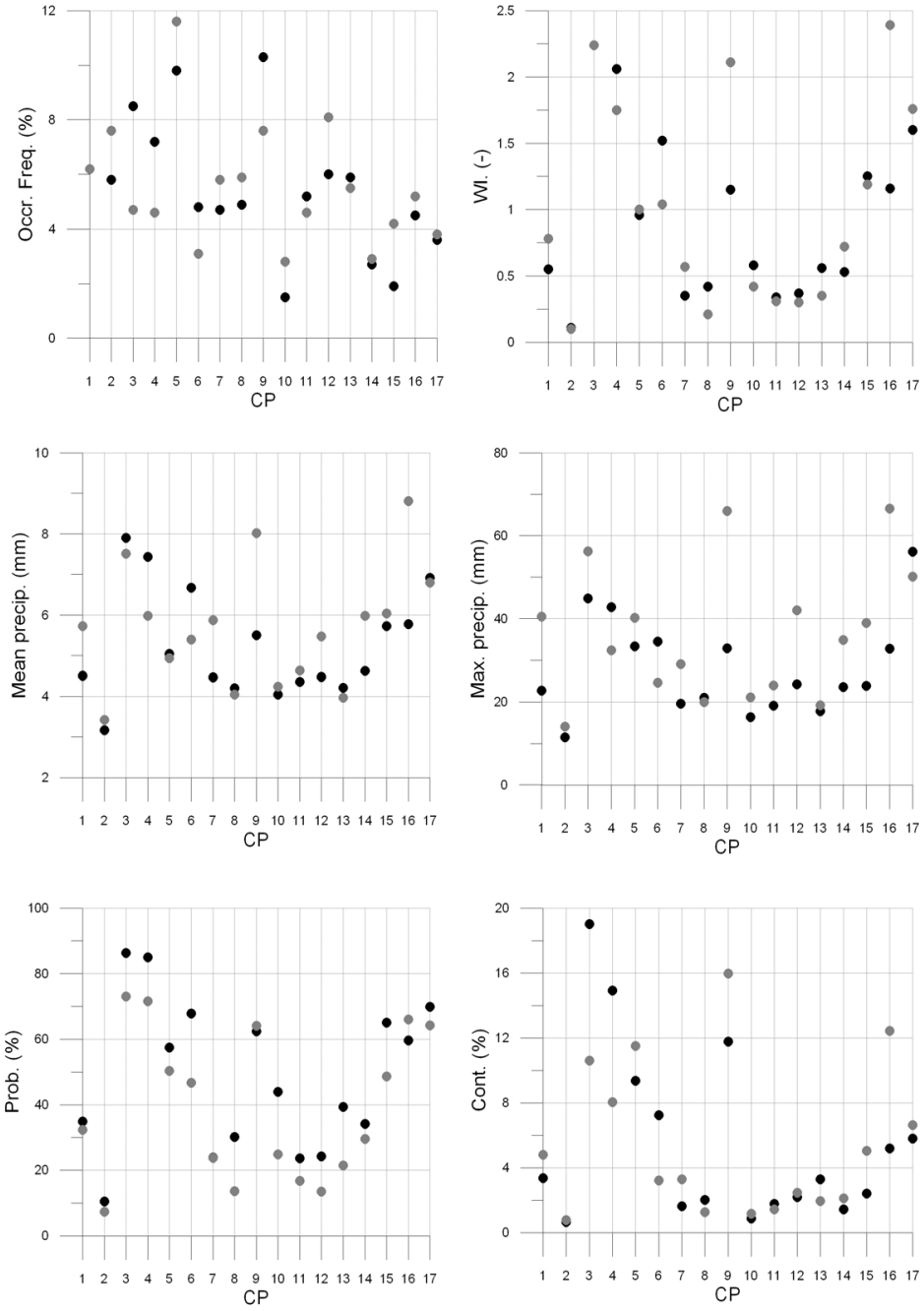

Figure 5.19.: Basic CP statistics averaged over all 172 grid points of German part of Rhine basin for winter (black circles) and summer (gray circles) for REMO SRES A1B scenario (2071-2100) dataset

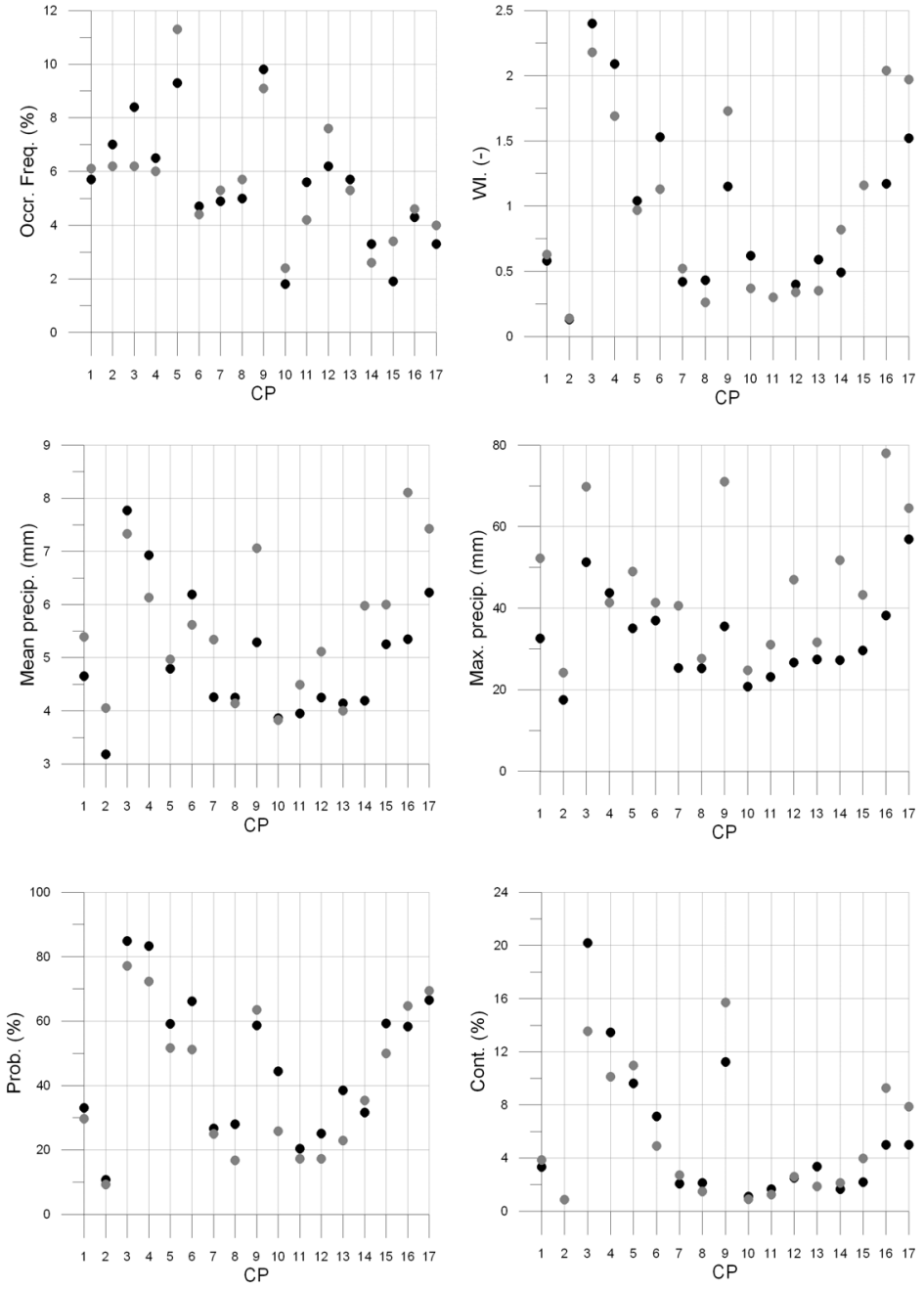

Figure 5.20.: Basic CP statistics averaged over all 172 grid points of German part of Rhine basin for winter (black circles) and summer (gray circles) for REMO SRES A1B scenario (2001-2100) dataset

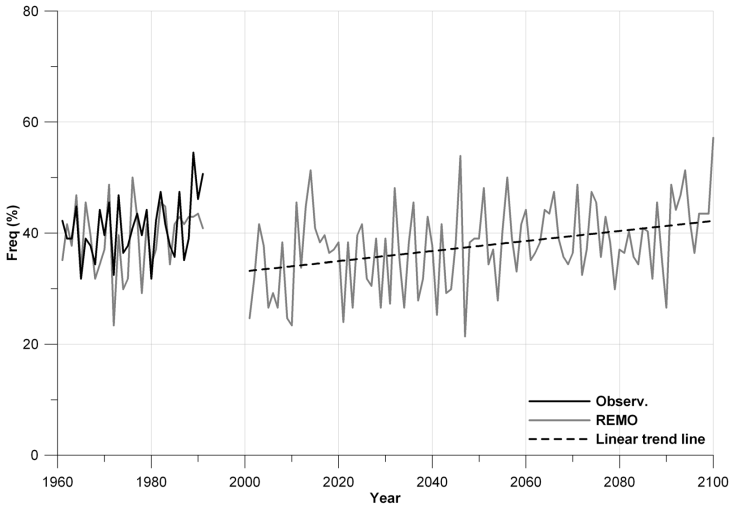

Figure 5.21.: Occurrence frequencies of combined dry CPs of observational gridded (solid black line) and REMO control and SRES A1B scenario (solid gray line) data sets

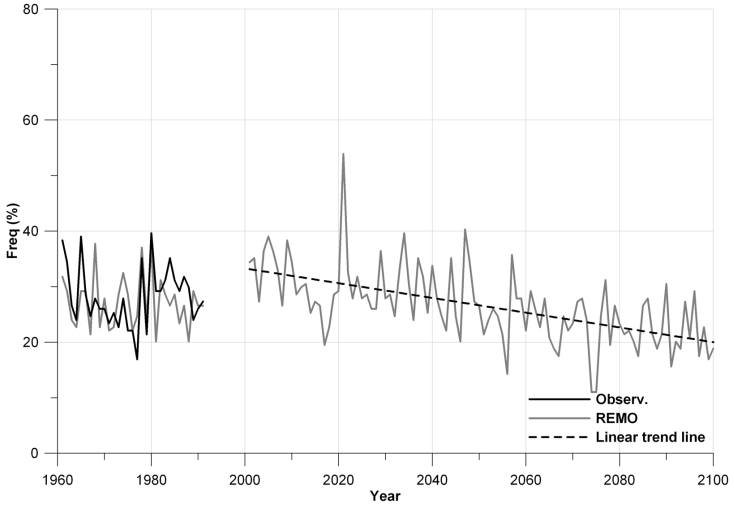

Figure 5.22.: Occurrence frequencies of combined wet CPs of observational gridded (solid black line) and REMO control and SRES A1B scenario (solid gray line) data sets

Appendix B contains the spatial distribution maps of wetness index for all CPs and winter and summer seasons obtained from REMO classification. B.5 and B.6 are winter and summer maps for control runs while B.7 and B.8 are the two set of maps for SRES A1B scenario run. REMO simulates the control period quite well. The spatial structure of wetness index follow the patterns that were witnessed in observational gridded data set. Spatial maps for winter are especially well simulated. In summer there are certain CPs which have different structure of wetness index maps. The two wettest CPs of CP03 and CP04 are less wetter throughout the basin than control run. Similarly the two classified dry CPs of CP08 and CP13 are also less drier than control run maps. Inter-season differences can be seen for CP16 and CP17 which are more wetter in summer than in winter. CP14 (not recognized as one of the extreme wet or dry CP) show big difference in wetness index distribution in summer and winter. In winter it has average wetness index value of 0.51 while in summer it shoots up to almost 1. The spatial maps of REMO control run shows the difference more clearly. SRES A1B scenario maps show the possible future as depicted by REMO model. Almost all classified wet CPs are less wetter in A1B scenario and classified dry CPs are more drier both in winter and summer. For example CP16 and CP17 both classified wet CPs, are less wetter in A1B scenario run than in control run. This difference is more pronounced in summer though. In case of dry CPs also A1B scenario seem to predict more dry future. In control runs some of the dry CP spatial maps do show some areas where the wetness index is larger than the mean CP wetness index for the same CP but in A1B scenario maps the dry CPs are more homogeneously dry.

Appendix B Table C.2 presents the contingency table between ERA40 based CP classification and REMO control run classification.

5.2.1.4. HadRM data sets classification

The results presented in this section are obtained from analysis and classification of data obtained from Hadley regional climate model (HadRM). HadRM is developed by Hadley center for climate prediction and research, Met office UK. Model description can be found in Collins et al. (2005). HadRM provide several atmospheric variables in different temporal formats of 6 hourly, 12 hourly, daily and monthly data. The data is available in different spatial resolutions and extents. The data is available both in regular grid of 0.22°(roughly 25Km square) and 3.75° x 2.5° grid. Both resolutions are based on spherical rotated coordinate system. Before using the data for classification purposes the data is converted to geographic coordinate system. HadRM provides extensive sets of atmospheric variables in three different flavors. These flavors are achieved by forcing the regional climate model by GCM which is run under different climate sensitivity [1] parameter.Each GCM possesses a

[1]The term "climate sensitivity " refers to the steady-state increase in the global annual mean surface air temperature associated with a given global-mean radiative forcing. It is common practice to use CO2 doubling as a benchmark for comparing GCM climate sensitivities. Thus in practice the climate sensitivity may be defined as the change in global-mean temperature that would ultimately be reached following a doubling of carbon dioxide concentration in the atmosphere (e.g. from 275 ppmv to 550 ppmv, where ppmv is parts per million by volume). The Intergovernmental Panel on Climate Change (IPCC) 4th Assessment Report reported the likely

different climate sensitivity, depending on the representation of various feedback processes in the model. It is generally assumed that the climate sensitivity of a model is approximately constant over the range of forcings expected for the next century. Three climate sensitivity runs (namely low, normal and high climate sensitivity) are provided by HadRM for control and SRES A1B scenario run and each of them are considered for classification of extreme CPs. For SRES A1B scenario runs HadRM provides data from 2001-2099 with 360 days in a year.

Figure 5.23 presents the classification results for HadRM control run while **??**, 5.25 and 5.26 provide the same for SRES A1B scenario for low, normal and high climate sensitivity runs. All the values are averaged over 172 grid points of German part of Rhine basin. Given that in previous cases the difference between three different time period analysis of 2021-2050, 2071-2100 and 2001-2100 was not too much, only the analysis from 2001-2099 (HadRM provide SRES A1B scenario runs from 2001-2099) are shown in these tables for winter and summer half years.

Both the wetness indices and occurrence frequencies of extreme wet and dry CPs in HadRM control runs are closely matching with the values of observational gridded data set. Wet CPs classified in observational gridded data set remain wet here as well, with the only difference that instead of CP04 being the second most wettest CP, CP06 is the second wettest one. Also the wetness index values are a bit on the lower side as compared to observational gridded data set. But this was the case in both the RCMs of RACMO and REMO as well. Dry CPs do not show much difference from the dry CPs of observational gridded data set. Comparing the averaged values of winter and summer with the averaged value of observational gridded data set (please refer to Table 5.2 and Table 5.3 for observational mean CP statistics for winter and summer respectively), it can be seen that in both winter and summer the occurrence frequencies of wet CPs have increased in HadRM control run and at the same time the wetness indices have decreased. The only exceptions are CP16 in winter and CP16 and CP17 in summer. The inter-season difference between CP16 and CP17 is also quite big, with both CPs marginally wet in winter but extreme wet in summer. This picture is seemed to be repeated in all three RCMs. Dry CPs on the other hand also show increased occurrence frequencies and higher wetness indices (meaning on average dry CP of HadRM is less drier than observational gridded data set's dry CP). The increased occurrence frequencies are specially visible for two of the extreme dry CPs.

The low climate sensitivity runs of HadRM predicts on average lower occurrence frequencies values for extreme wet CPs in winter and comparable or slightly larger values in summer than control run statistics. Wetness indices values on the other hand are larger than control runs. Except CP16 and CP17 in summer which have slightly lower wetness index values. Mean wet day precipitation amounts of low climate sensitivity runs for wet CPs are clearly larger than control run amounts. In summer the picture is more or less same as CP16 and CP17 have lower wet day precipitation amounts. Maximum precipitation associated with each wet CP is clearly

range for this quantity to be between 2° and 4.5°C, with a 'best' estimate of 3°C.

larger than control run statistics for both winter and summer (the only exception again are CP16 and CP17 in summer). So although wet CPs remain wet in HadRM low climate sensitivity run, the degree of wetness comparing to its control run are lower and are less frequent. However, whenever these extreme wet CP bring rain in the catchment it tends to be more extreme. Probability of rain associated with occurrence of wet CPs remain more or less the same in low climate sensitivity runs during winter periods of 2001-2099. In summers though, probabilities tends to come down. Contribution to precipitation increase are also shown in the Figure 5.24 through Figure **??** and the pattern closely follows that of wetness indices. Except CP03 for which the contribution to precipitation increase has lower value than control time period, all other wet CPs have larger or equivalent values both in winter and summer. Extreme dry CPs on average have larger occurrence frequencies and lower or equivalent values of wetness indices. Low climate sensitivity run of HadRM thus predicts even drier dry CPs occurring more frequently than present or previous occurrences. Mean daily precipitation amounts associated with days with active dry CPs have larger values than control period of HadRM in winter. In summer the picture is not conclusive and in some cases the amounts are decreasing and in some cases increasing.

Normal climate sensitivity and high climate sensitivity runs of HadRM SRES A1B scenario on average paints the same picture for future as low climate sensitivity runs in terms of wet and dry CPs and their important statistics. Referring to Figure 5.27 and Figure 5.28 which are the combined figures for all three climate sensitivity runs and HadRM control run, it can be seen that in most of the cases the three circles associated with SRES A1B scenario tend to stick together on either side of the black crosses (representing HadRM control run). Hence most of the discussion associated with low climate sensitivity runs and its statistics in previous paragraph also hold for normal and high climate sensitivity runs. There are some marginal exceptions though. For example the maximum precipitation amounts related to each CP in winter predicted by all three SRES scenario are far larger than control run amounts. In some cases high climate sensitivity run provides the largest maximum (e.g. CP17 in winter) while in some cases it is the smallest maximum (e.g. CP03 in winter). But this does not change the overall picture.

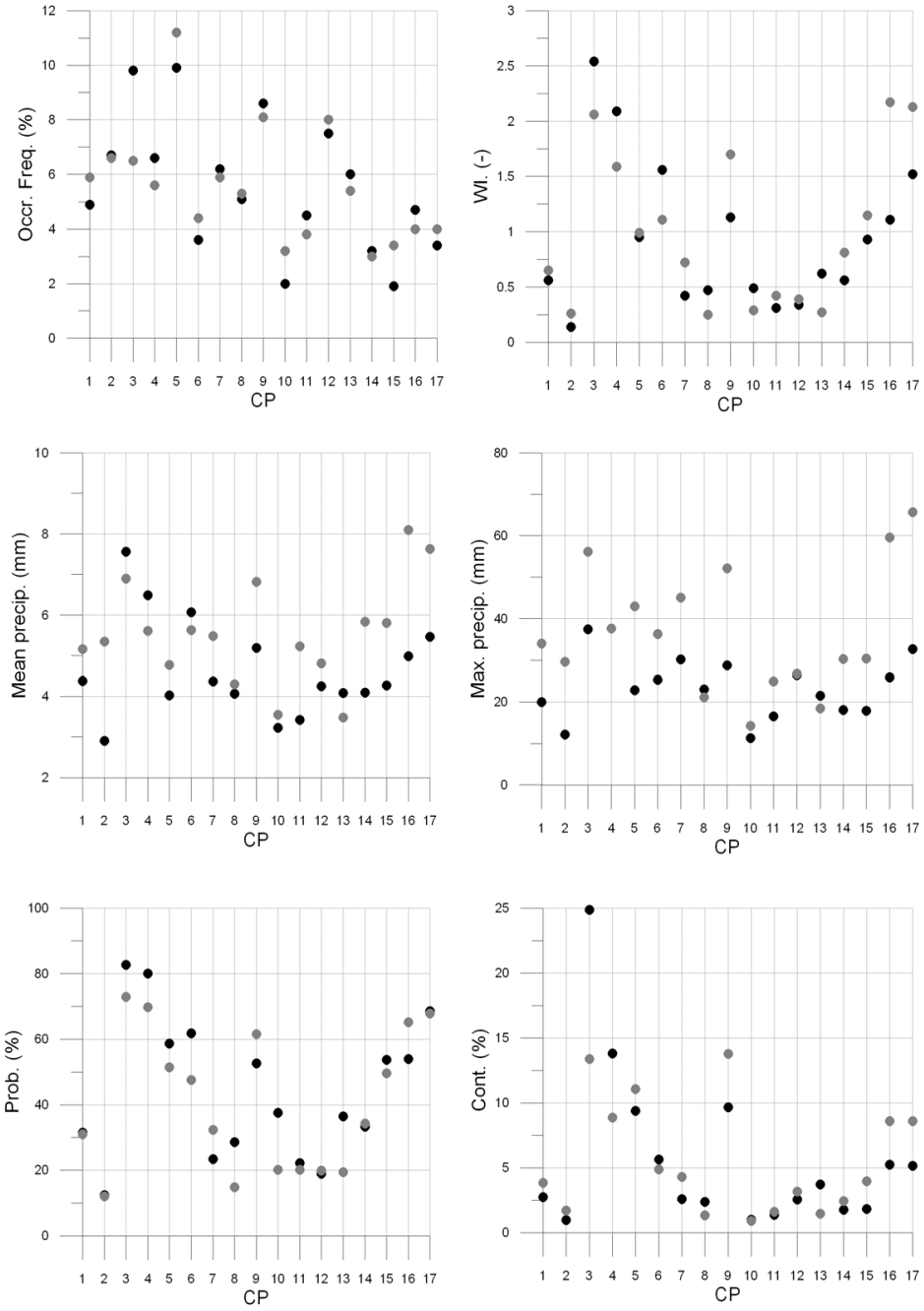

Figure 5.23.: Basic CP statistics averaged over all 172 grid points of German part of Rhine basin for winter (black circles) and summer (gray circles) for HadRM control run scenario (1961-1991) dataset

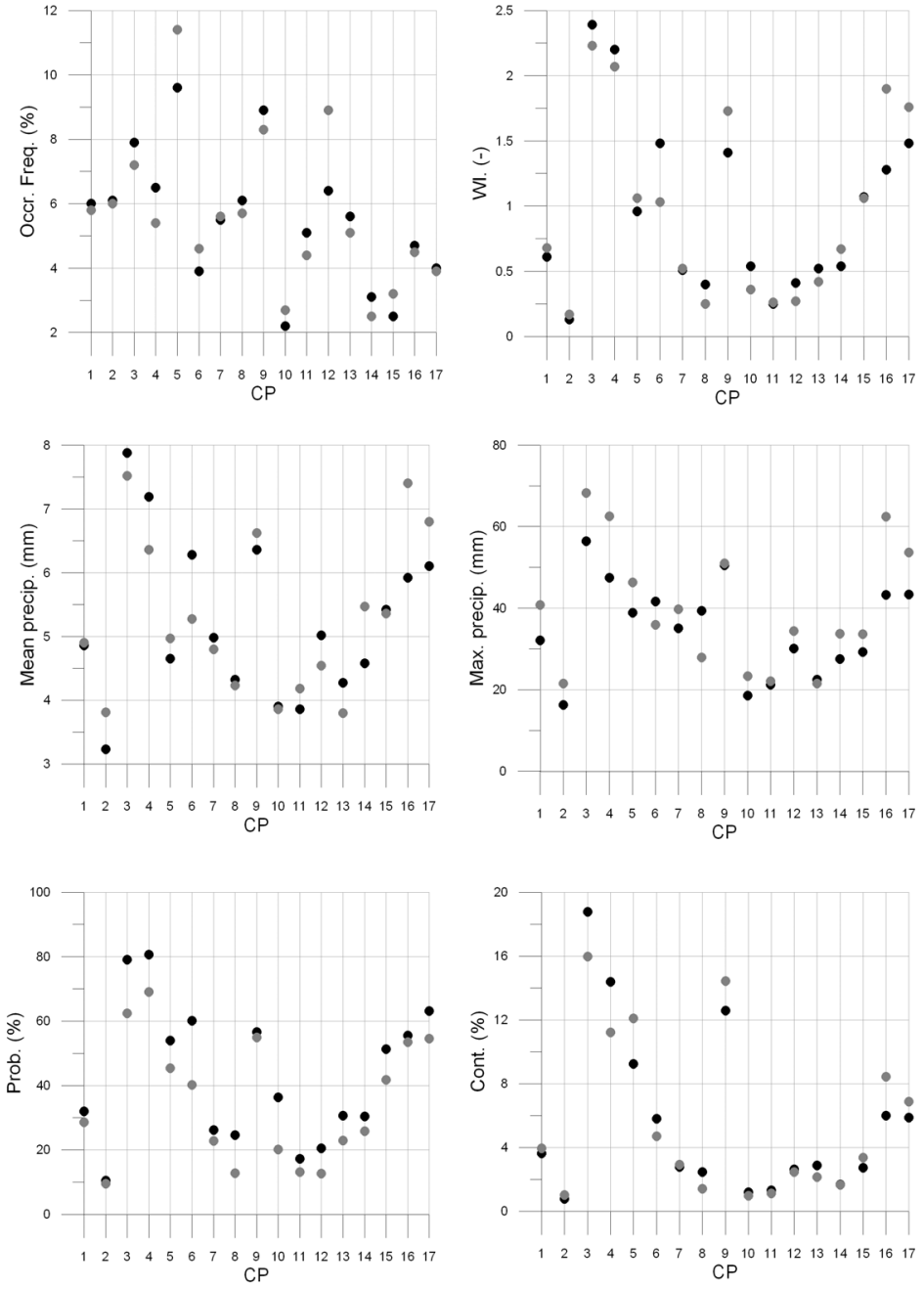

Figure 5.24.: Basic CP statistics averaged over all 172 grid points of German part of Rhine basin for winter (black circles) and summer (gray circles)for HadRM SRES A1B low climate sensitivity scenario (2001-2099) dataset

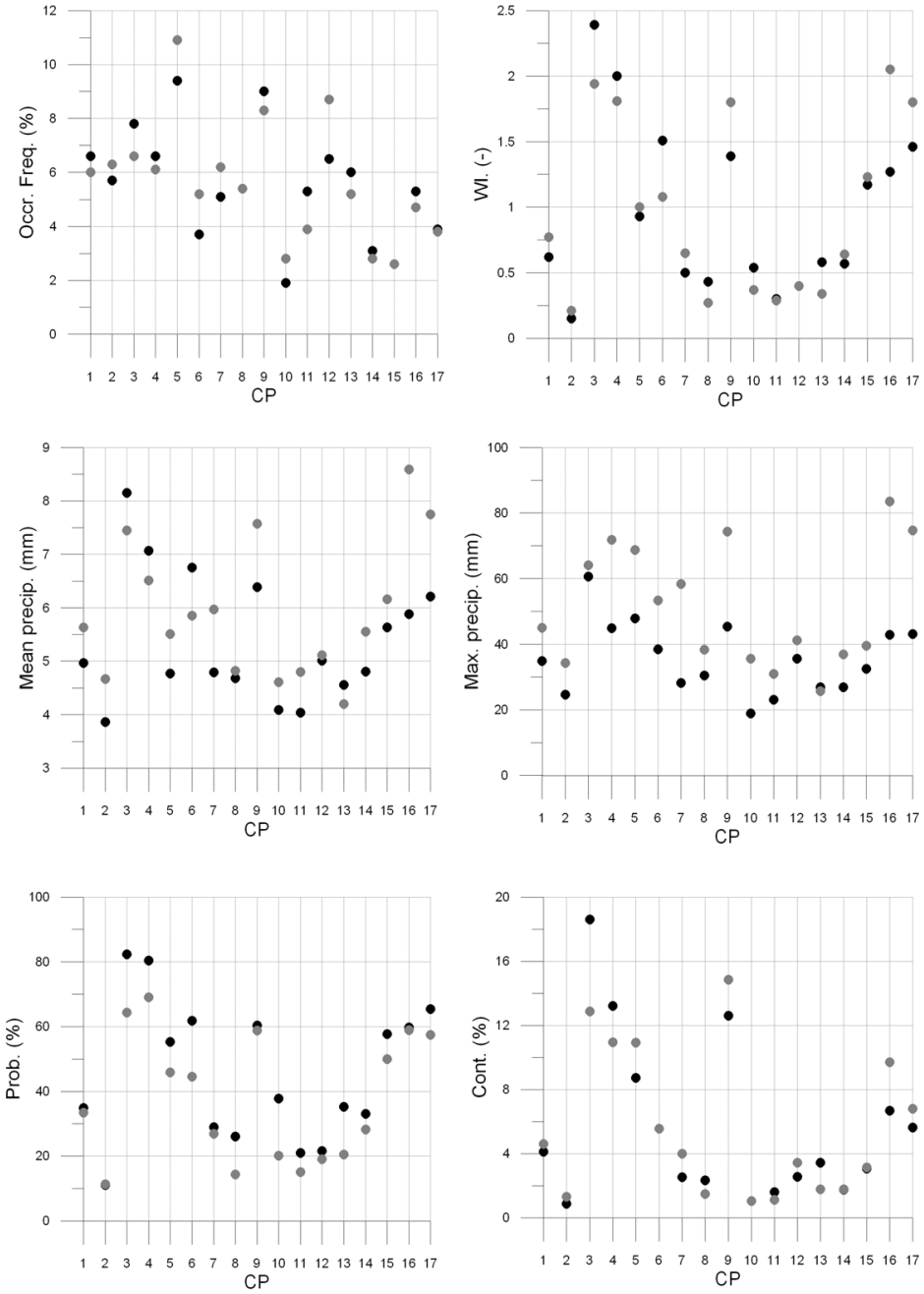

Figure 5.25.: Basic CP statistics averaged over all 172 grid points of German part of Rhine basin for winter (black circles) and summer (gray circles)for HadRM SRES A1B normal climate sensitivity scenario (2001-2099) dataset

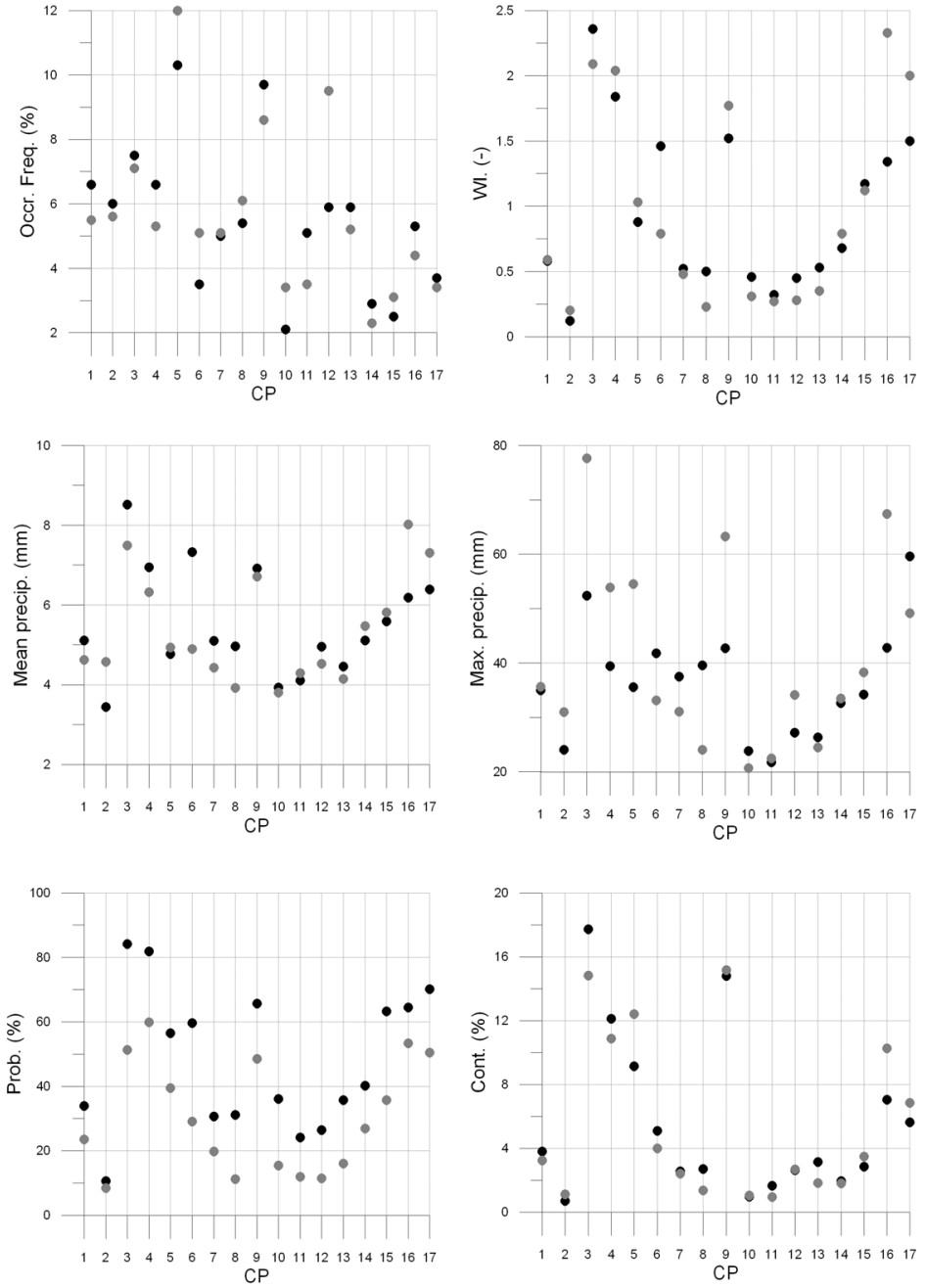

Figure 5.26.: Basic CP statistics averaged over all 172 grid points of German part of Rhine basin for winter (black circles) and summer (gray circles)for HadRM SRES A1B high climate sensitivity scenario (2001-2099) dataset

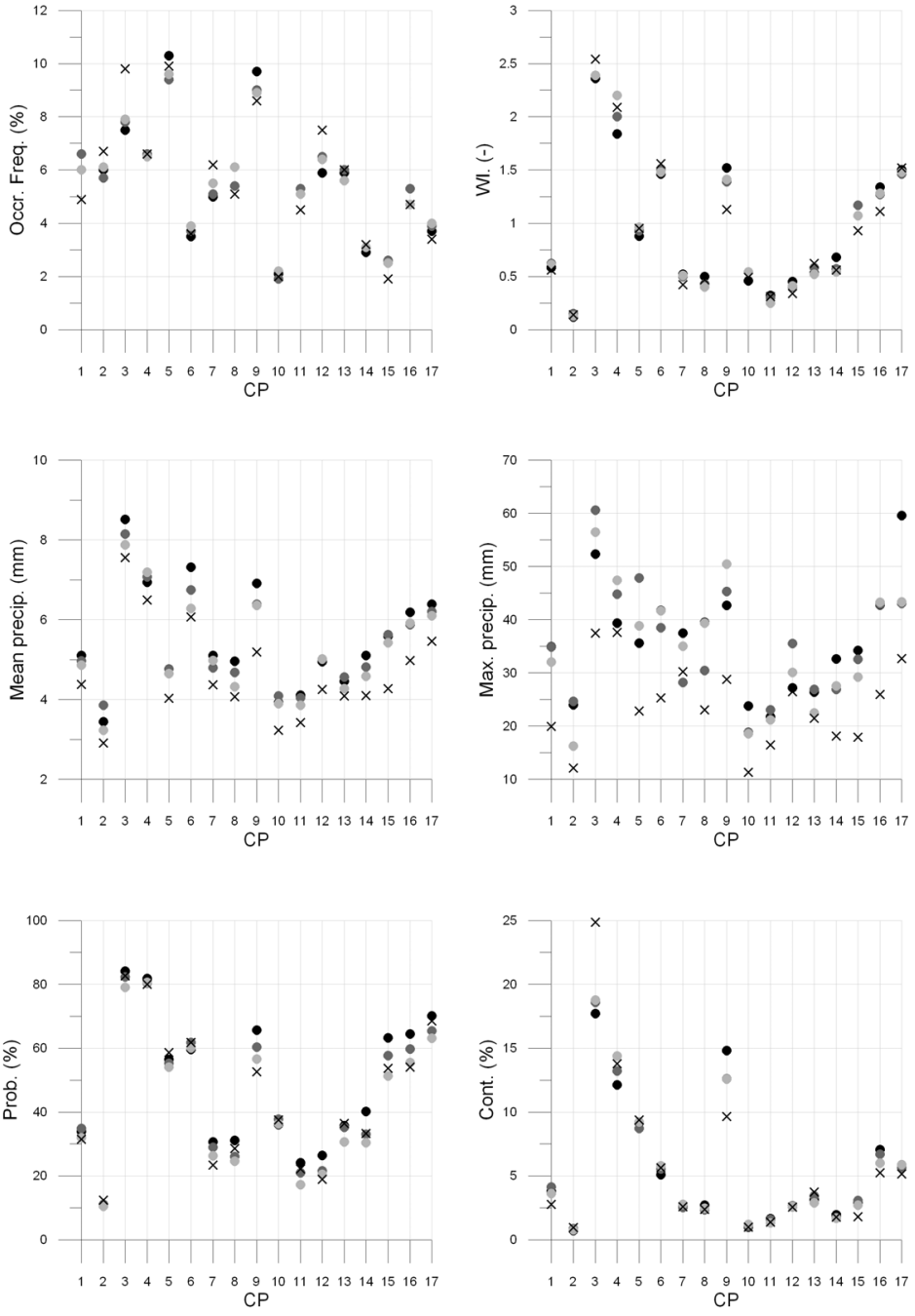

Figure 5.27.: Basic CP statistics averaged over all 172 grid points of German part of Rhine basin for winter for HadRM control (black cross) and three SRES climate scenarios of HadRM of low climate sensitivity (light-light gray circles), normal climate sensitivity (light gray circles) and high climate sensitivity (black circles) datasets

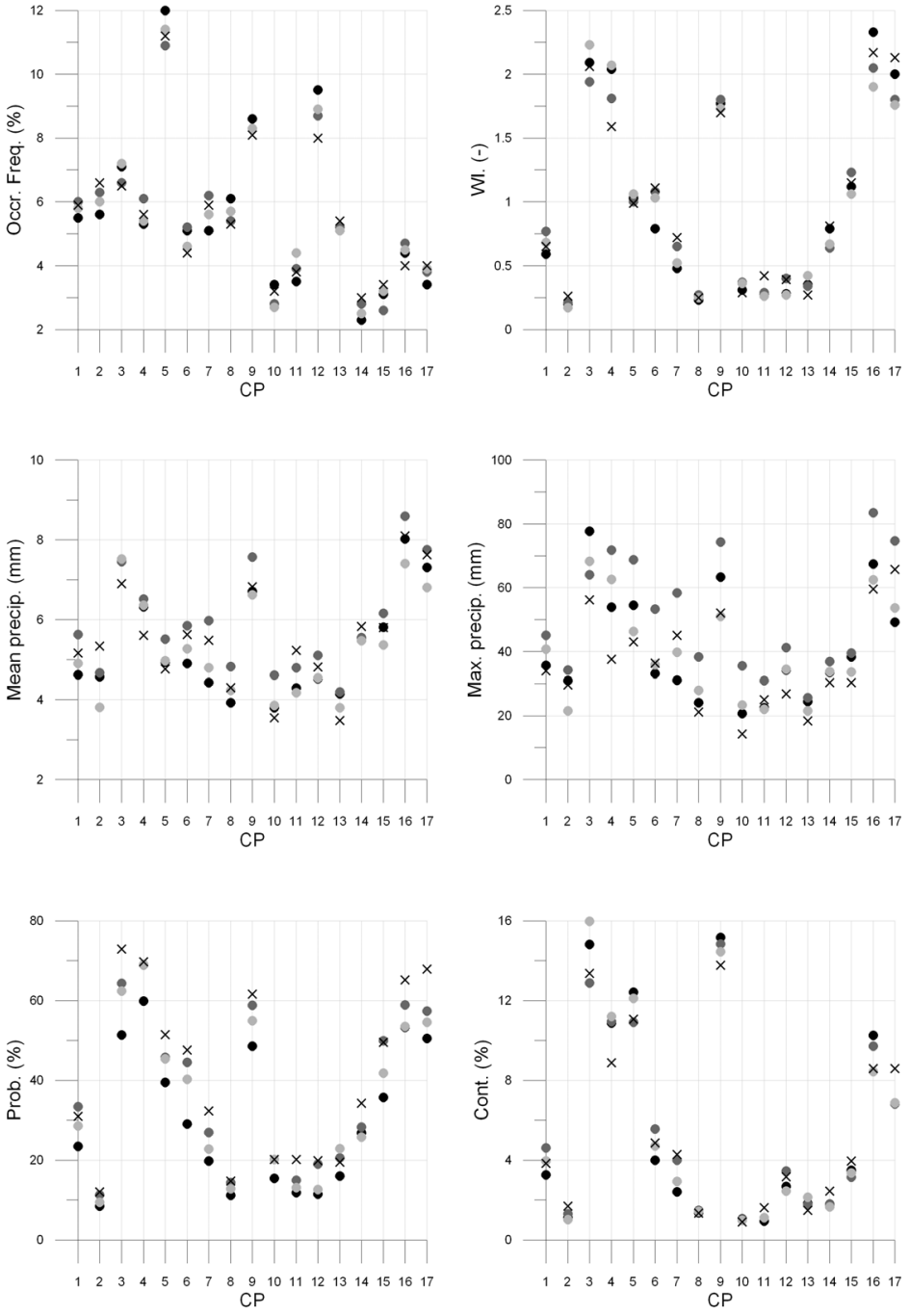

Figure 5.28.: Basic CP statistics averaged over all 172 grid points of German part of Rhine basin for summer for HadRM control (black cross) and three SRES climate scenarios of HadRM of low climate sensitivity (light-light gray circles), normal climate sensitivity (light gray circles) and high climate sensitivity (black circles) datasets

Figure 5.29 through Figure 5.34 present the combined wet and dry CP yearly frequencies for all the three climate sensitivity runs of HadRM along with control and observation gridded data set's frequencies. The three figures are considerably different than the ones presented in Figure 5.15 through Figure 5.16 for RACMO and Figure 5.21 through Figure 5.22 for REMO. RACMO and REMO both predicted increasing trends in occurrence frequencies of combined dry CPs and decreasing trends in combined wet CP frequencies. HadRM related combined occurrence frequencies are different in three different climate sensitivity runs. For low climate sensitivity runs there is an increasing trend visible in combined dry CP occurrence but it is not as steep as it was for RACMO and REMO. Further the control run dry CP frequencies also does not capture the observational CP frequencies that well. For combined wet CP's a mild decreasing trend can be detected in occurrence frequencies. For normal climate sensitivity runs both wet and dry combined CP frequencies show decreasing trend while in high climate sensitivity the trend for combined dry CP frequency is almost negligible while for wet CPs it is a clear decreasing trend. So although in terms of some basic statistics there are similarities in three climate scenarios, for yearly occurrence frequencies the three runs differ considerably from each other (in some cases they are even exhibiting contradictory results).

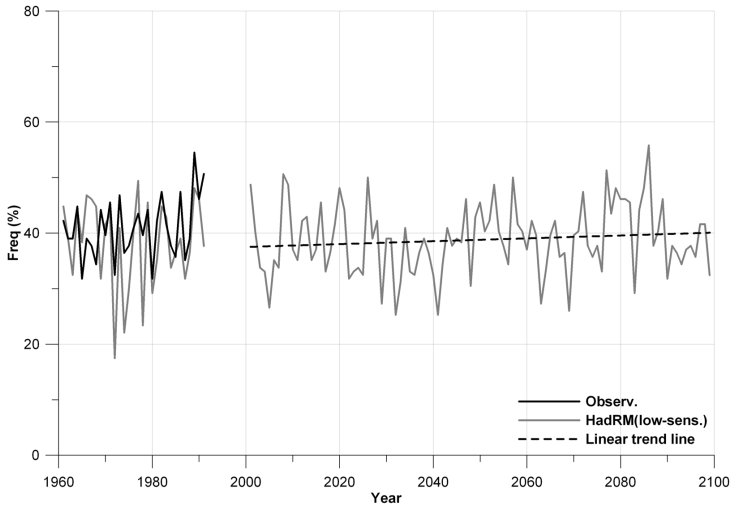

Figure 5.29.: Occurrence frequencies of combined dry CPs of observational gridded (solid black line) and HadRM control and SRES A1B scenario (solid gray line) of low climate sensitivity data sets

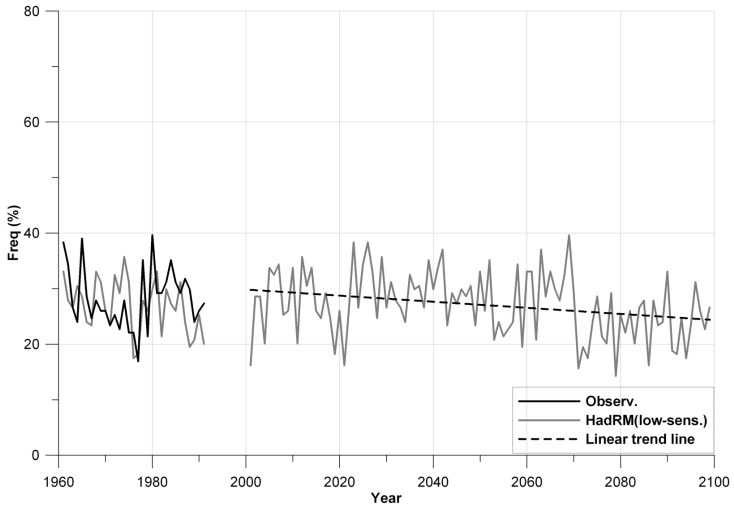

Figure 5.30.: Occurrence frequencies of combined wet CPs for observational gridded (solid black line) and HadRM control and SRES A1B scenario (solid gray line) of low climate sensitivity data sets

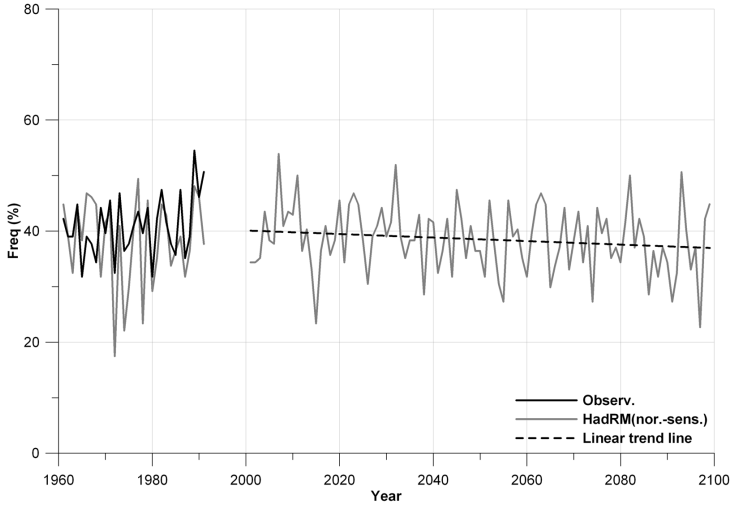

Figure 5.31.: Occurrence frequencies of combined dry CPs for observational gridded (solid black line) and HadRM control and SRES A1B scenario (solid gray line) of normal climate sensitivity data sets

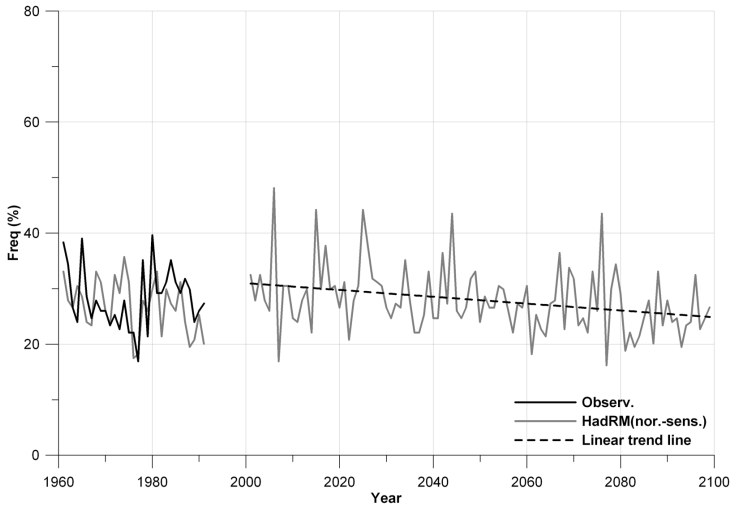

Figure 5.32.: Occurrence frequencies of combined wet CPs for observational gridded (solid black line) and HadRM control and SRES A1B scenario (solid gray line) of normal climate sensitivity data sets

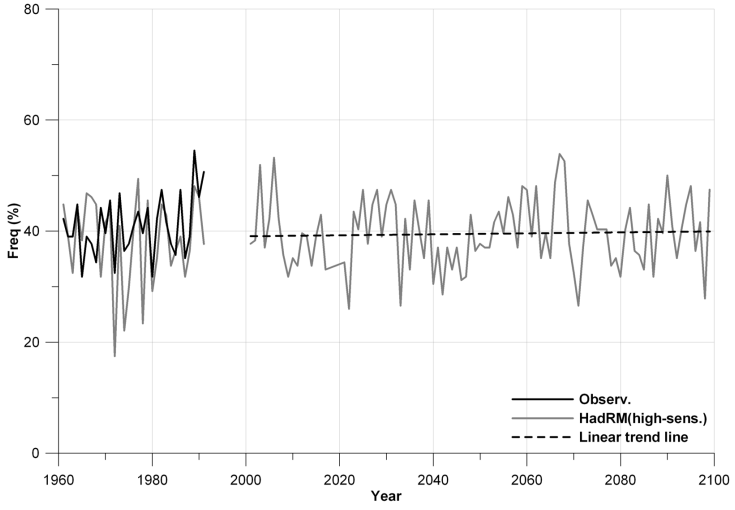

Figure 5.33.: Occurrence frequencies of combined dry CPs for observational gridded (solid black line) and HadRM control and SRES A1B scenario (solid gray line) of high climate sensitivity data sets

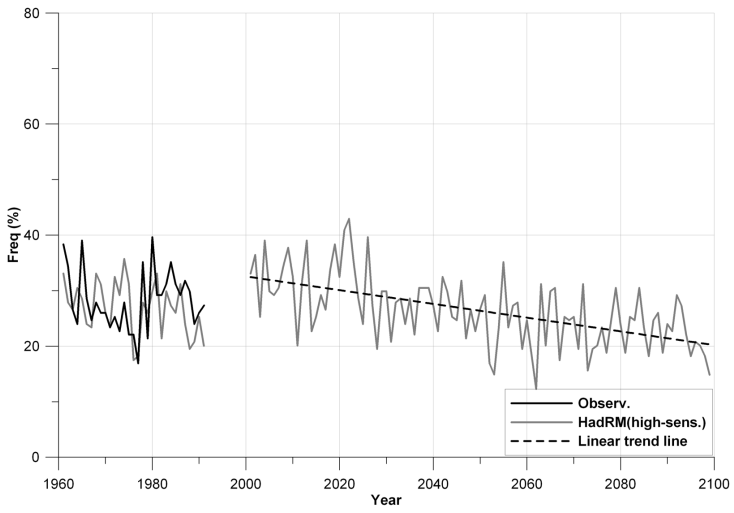

Figure 5.34.: Occurrence frequencies of combined wet CPs for observational gridded (solid black line) and HadRM control and SRES A1B scenario (solid gray line) of high climate sensitivity data sets

Spatial maps of wetness indices of three sets of HadRM SRES A1B scenario for winter and summer are presented in Appendix B Section B.3. Spatial distributions of wetness indices vary slightly in some cases and considerably in others. CP08 which is very dry in observational gridded data set is not that dry in HadRM control and SRES A1B low climate sensitivity runs in winter. Similarly CP16 is more wetter in SRES A1B low climate scenario in winter than it is in observational gridded data set or HadRM control run. Comparing summer distributions of wetness indices differences can be seen for CP11, CP12 and CP14 where they are more drier in A1B scenario than either observational and control data sets. Inter-season differences are also visible, specially for CP16 and CP17 which are markedly wetter in summer than in winter. Normal climate sensitivity run related spatial maps are shown in Figure B.13 for winter and Figure B.14 for summer. CP08 is less drier both in control and SRES A1B normal sensitivity scenario. CP04 which is uniformly wet throughout the catchment in winter for observational gridded data set is progressively decreasing in uniformity of wetness from control run to normal climate sensitivity run. Inter-season differences are dominant in wet CPs of CP16 and CP17, where they are considerably wet in summer than in winter and for dry CPs of CP08 and CP10, which are considerably dryer in summer than in winter. This particular feature of inter-season difference is well captured in all three climate sensitivity runs of HadRM. Figure B.15 and Figure B.16 showing the spatial maps of wetness indices for high climate sensitivity runs of HadRM SRES A1B scenario for winter and summer respectively, depicts the same spatial behavior as was shown by the other scenario runs.

The differences between the three climate sensitivity runs of HadRM are not very large. There are subtle differences but they are more in CPs which are not classified

as extreme wet or dry CPs. For example comparing the three sets of figures for summer, one can see differences for CP01 and CP06 for summer which are getting drier in intensity over the catchment when moving from low climate sensitivity to high climate sensitivity . Both the CPs are not extreme CPs, CP01 is closer to dry CPs in its anomaly map structure and CP06 to wet CPs. The spatial structure of wetness indices in winter are surprisingly identical. Even when comparing the small details of local intensities of wetness indices for each CP in the region, there seem to be quite good convergence between the results.

5.2.2. OPAQUE catchments classification

The results presented in this section are related to the head catchments that are briefly described in Chapter 4, Section 4.1.1. The main objective of this study was to identify critical circulation patterns responsible for creating flood like situation in the head catchments. The four head catchments of upper Danube, Iller, Alb and Weisseritz are studied for critical wet CPs and the resulting circulation patterns are used in statistical downscaling explained in Chapter 3, Section 3.3.1.

5.2.2.1. Upper Danube catchment classification

The same set of circulation patterns classification obtained in Section 5.2 has been used of Upper Danube catchment owing to the same area of interest. Validation of the classification is performed by analyzing daily precipitation data of seven precipitation stations of upper danube catchment (for precipitation station details, please refer to Table 4.1). Important statistics obtained from validation (1971-1991) and averaged over all the seven precipitation stations are shown in Figure 5.35. CP03, CP04, and CP17 comes out to be the most wettest CPs for Upper Danube catchment both in winter and summer. These CPs were also identified as wet CPs in validation process of ENSEMBLES RT5 observational gridded data set for German part of Rhine basin. Figure 5.35 also displays mean and maximum precipitation associated with wet CPs for both winter and summer half years. It can be seen that the difference between winter and summer mean and maximum precipitation for CP03, CP04 and CP09 is considerable. CP17 related values on the other hand, seem to be much closer together regardless of the season. CP03 and CP04 are more wet in winters than in summer while CP09 which is also a wet CP, is more wet in summer. CP17 remains wet both in winter and summer. Mean sea level pressure anomaly maps for these CPs can be seen in Figure 5.7.

Figure 5.35 displays the precipitation associated with winter floods of 1990 and 1995 in upper Danube catchment along with associated CPs. It can be seen that almost all the days with peak precipitation values are associated with CPs which are classified as wet CPs. Additionally the days prior to occurrence of peak precipitation are also associated with extreme wet classified CPs.

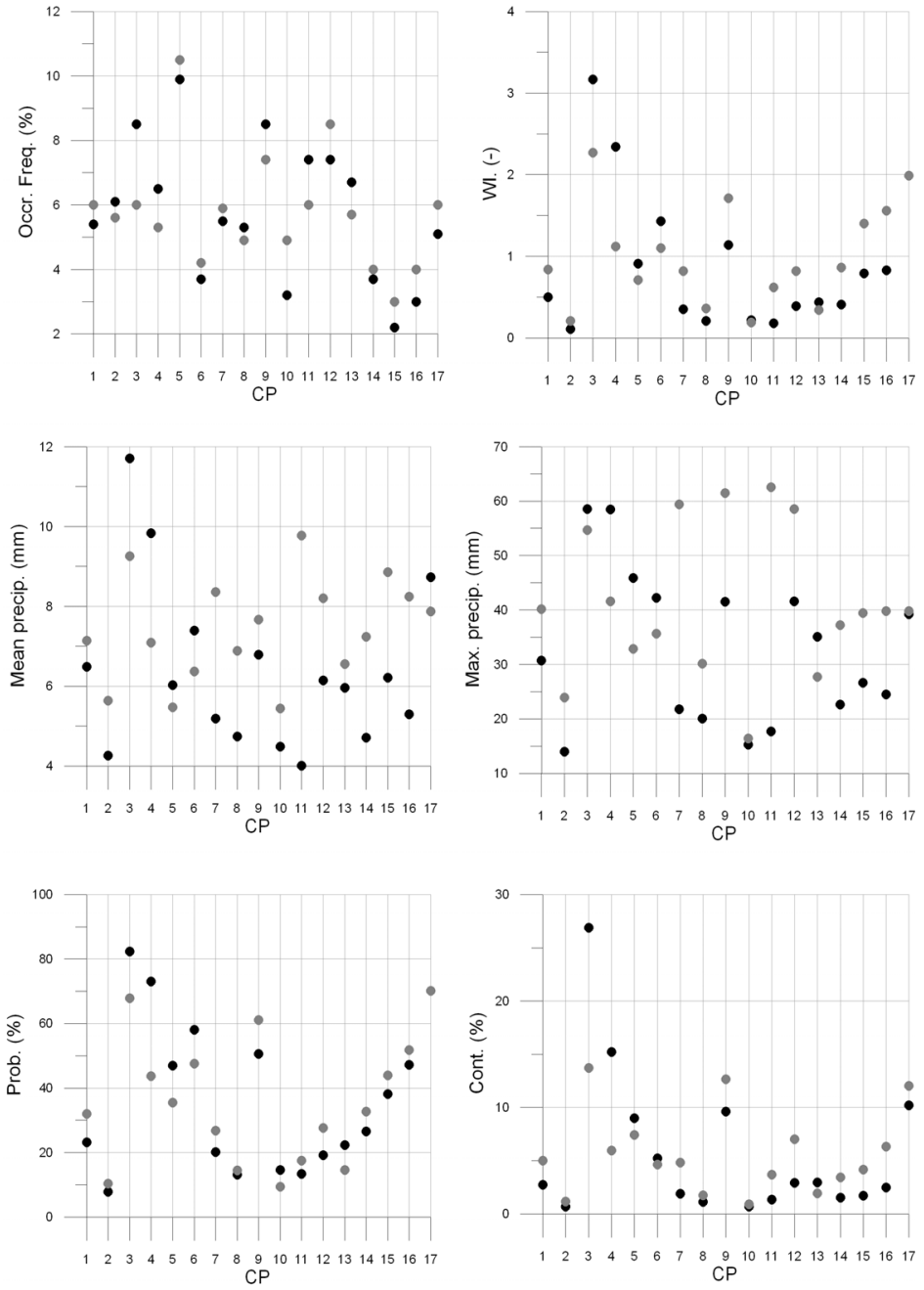

Figure 5.35.: Basic CP statistics averaged over all precipitation stations of Upper danube catchment for winter (black circles) and summer (gray circles).

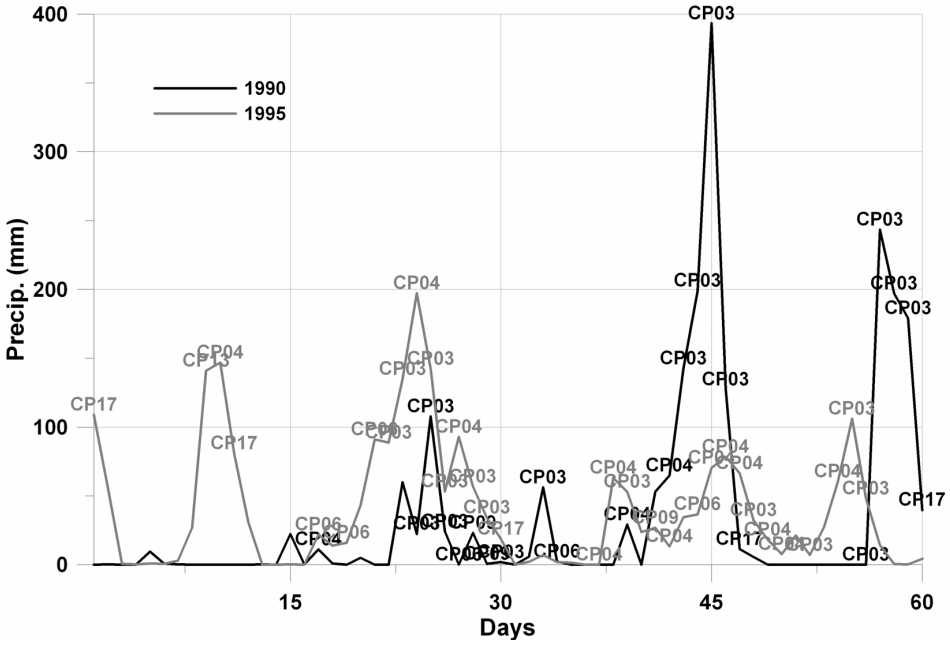

Figure 5.36.: Daily total precipitation over 7 precipitation stations of Upper Danube catchment associated with the winter floods of 1990 (in Black) and 1995 (in Gray). Associated CPs are marked as well. Only January and February days are included.

5.2.2.2. Alb catchment classification

17CP classification obtained from extreme hydrological condition (Section 5.2) is used for Alb catchment as well. Figure 5.40 displays the important CP statistics validated through Alb precipitation. 5 precipitation stations (Table 4.4) were used for analysis from 1961-2000. The values shown in Figure 5.40 are averaged over these precipitation stations. In terms of wetness indices the results look quite similar to the ones obtained for Upper Danube catchment. Owing to the proximity of two stations the patterns look very similar and the same set of CPs i.e. CP03, CP04 and CP17 are the most wettest CPs. Mean and maximum precipitation associated with each CP are also shown in Figure 5.40 and it can be seen that the difference between winter and summer mean precipitation is not as large as was the case in Upper Danube catchment classification. Probability of precipitation occurring in presence of a wet CP and contribution to total precipitation are higher in winter than in summer. Precipitation associated with summer flood of 1998 is shown in Figure 5.37 along with the associated CPs. Classified wet CPs can be clearly seen associated with the days with maximum precipitation and days prior to occurrence of precipitation peak. CP09 and CP16 are also marked in this figure as they are also identified wet CPs.

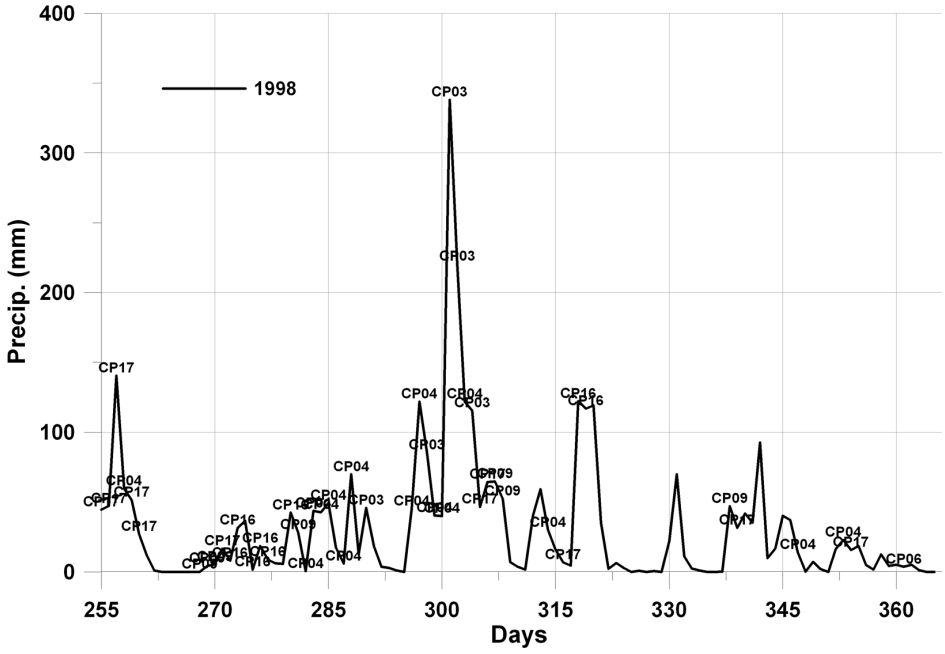

Figure 5.37.: Daily total precipitation over 5 precipitation stations of Alb catchment associated with the summer flood of 1998 . Associated CPs are marked as well.

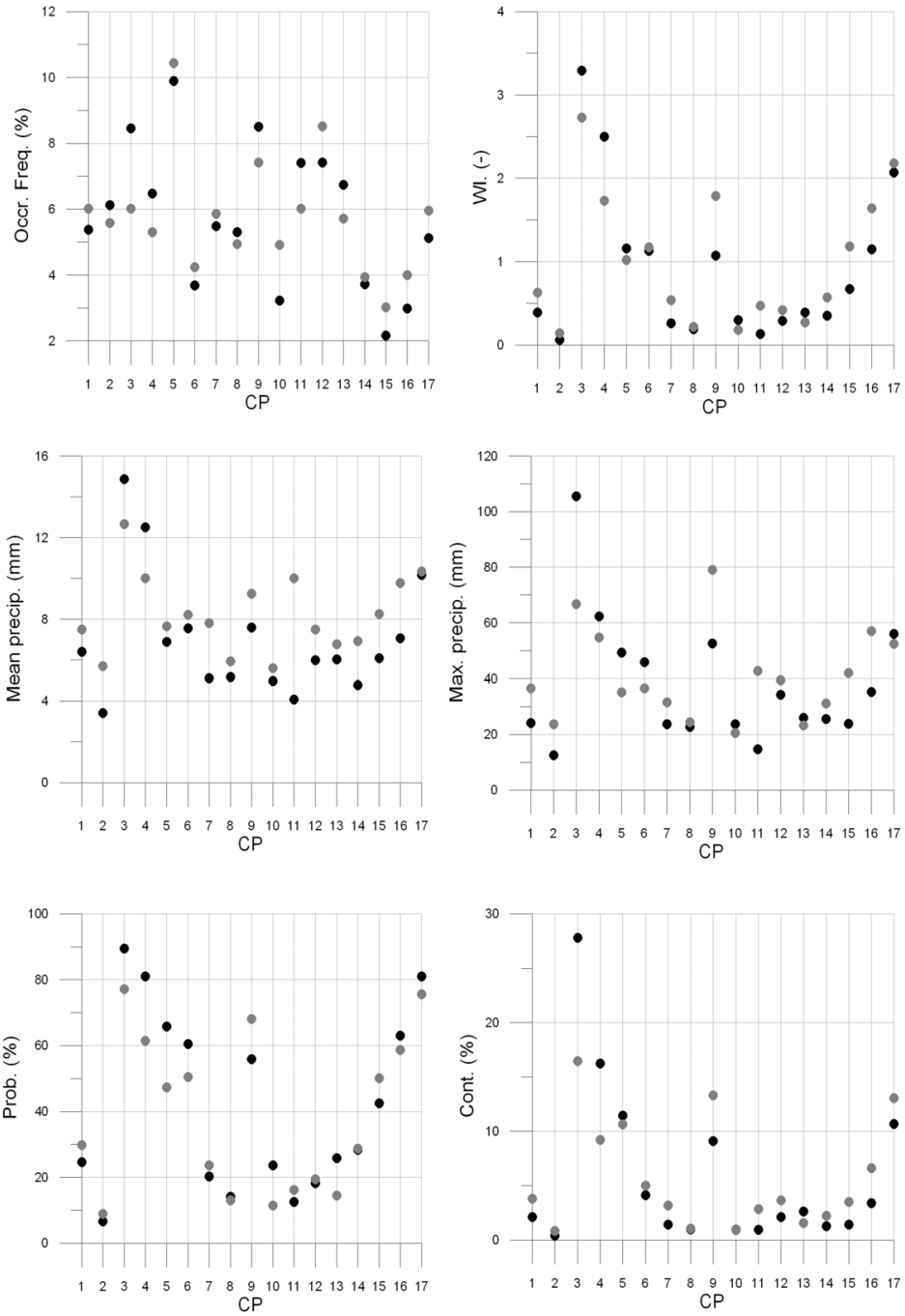

Figure 5.38.: Basic CP statistics averaged over all precipitation stations of Alb catchment for winter (black circles) and summer (gray circles).

5.2.2.3. Iller catchment classification

Although wetness indices calcualted from Iller catchment's precipitation stations are on slightly lower side, yet the distinction between wet and dry CPs is very clear. CP03, CP04, CP05, CP16 and CP17 are the most wet CPs while the rest are clearly dry CPs. Averaged CP statistics over 10 precipitatin stations (for precipitation stations used, please refer to Table 4.3). Validation for 17 CP classification was performed from 1961-2000. Surprisingly CP05 also turns out to be one of the wet CPs. This CP was not classified as wet CP either in previous two head catchments nor when classification was performed for ENSEMBLES RT5 observational gridded data set of German part of Rhine basin. Probability of ocuurrence of rain with CP05 is higher than with CP16 and CP17 which were wet CPs in all the previous cases. Similarly it contributes more to total precipitation increase than CP04, CP16 and CP17. Figure 5.39 displays total daily precipitation over 10 precipitation stations associted with two historical flood events of 1999 and 2005 along with the CPs. Again wet classified CPs seem to active on these critically wet days.

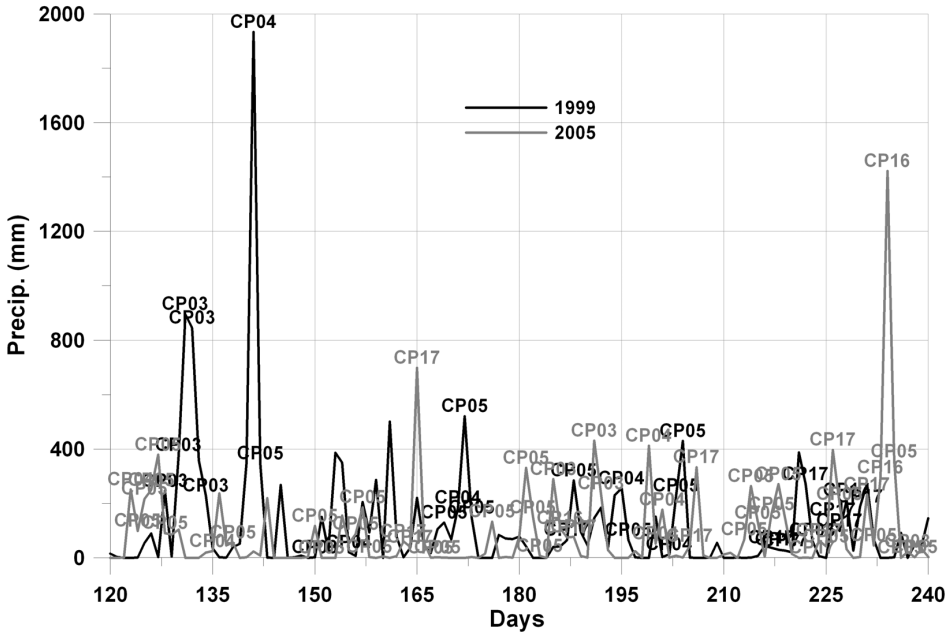

Figure 5.39.: Daily total precipitation over 10 precipitation stations of Iller catchment associated with summer floods of 1999 (in Black) and 2005 (in Gray). Associated CPs are marked as well.

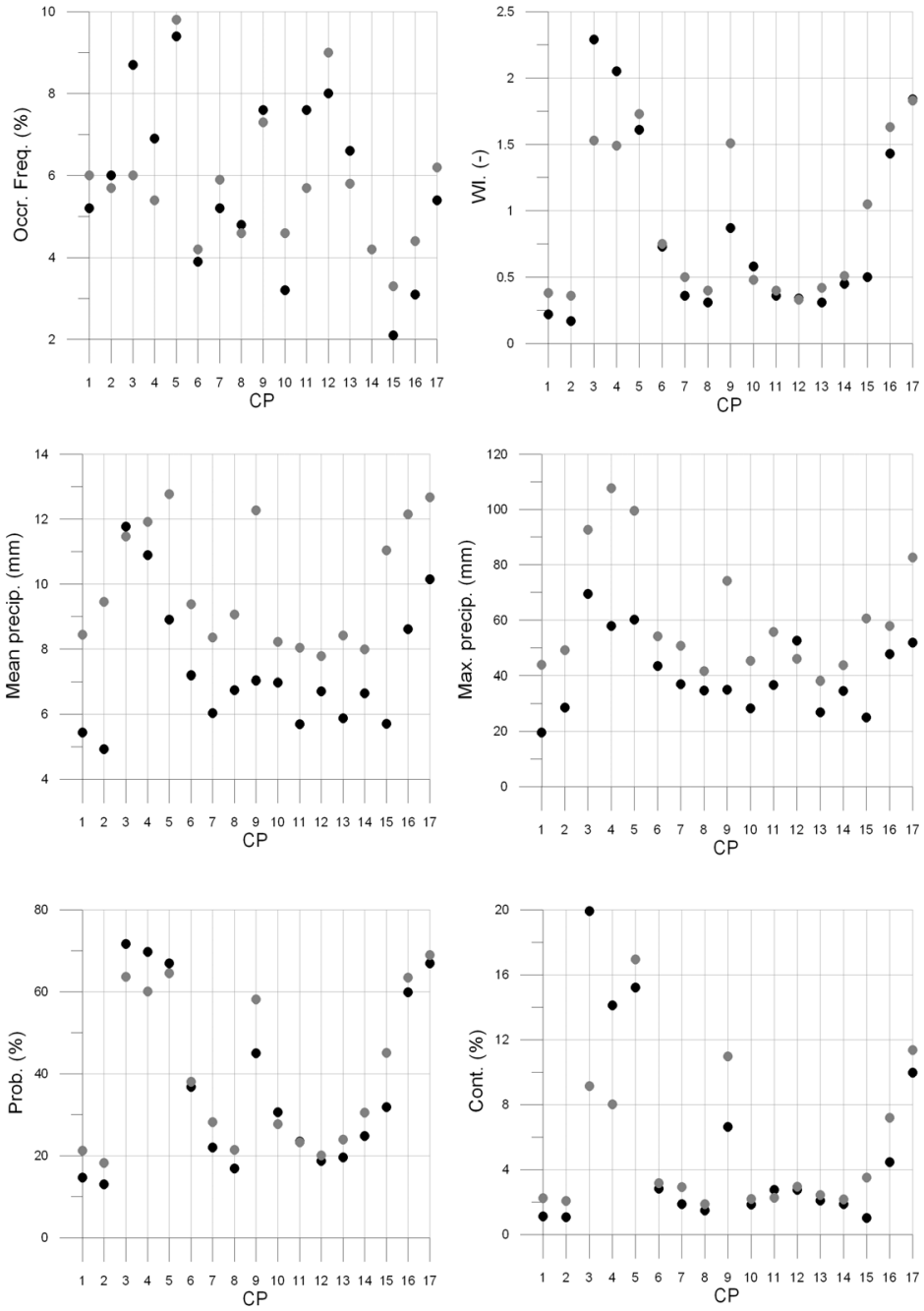

Figure 5.40.: Basic CP statistics averaged over all precipitation stations of Iller catchment for winter (black circles) and summer (gray circles).

5.2.2.4. Weisseritz catchment classification

CP04, CP05, CP16 and CP17 are most wet CPs for weisseritz catchment. CP03, which was wettest CP in all cases of classification so far is taken over by CP04 as wettest CP. All of these wet CPs have higher wetness indices in winter than summer except CP17 which has opposite behaviour. Additionally there are certain CPs for example CP09 and CP15 which show big difference in wetness index values between summer and winter. Both these CPs have extremely low wetness index in winter making them almost dry CPs, but in summer they are reasonably wet. This is also shown in Figure 5.41 where precipitation corresponding to summer flood of 2002 is plotted along with the associated CPs. It can be seen that in addition to the wet CPs that are active on peak precipitation days in this flooding event, CP15 and CP09 are occuring on days prior to extreme precipitation day. Additionally CP conditioned maximum precipitation shown in Figure 5.42 also confirms this, where the difference between winter and summer maximum precipitation for some CPs is exceptionally great.

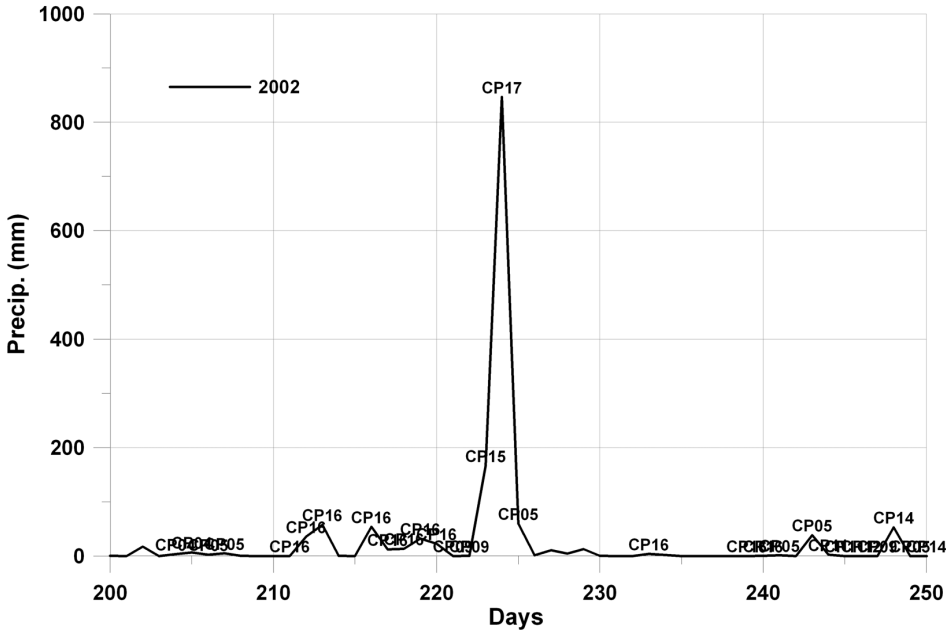

Figure 5.41.: Daily total precipitation over 7 precipitation stations of Weisseritz catchment associated with August floods of 2002 . Associated CPs are marked as well.

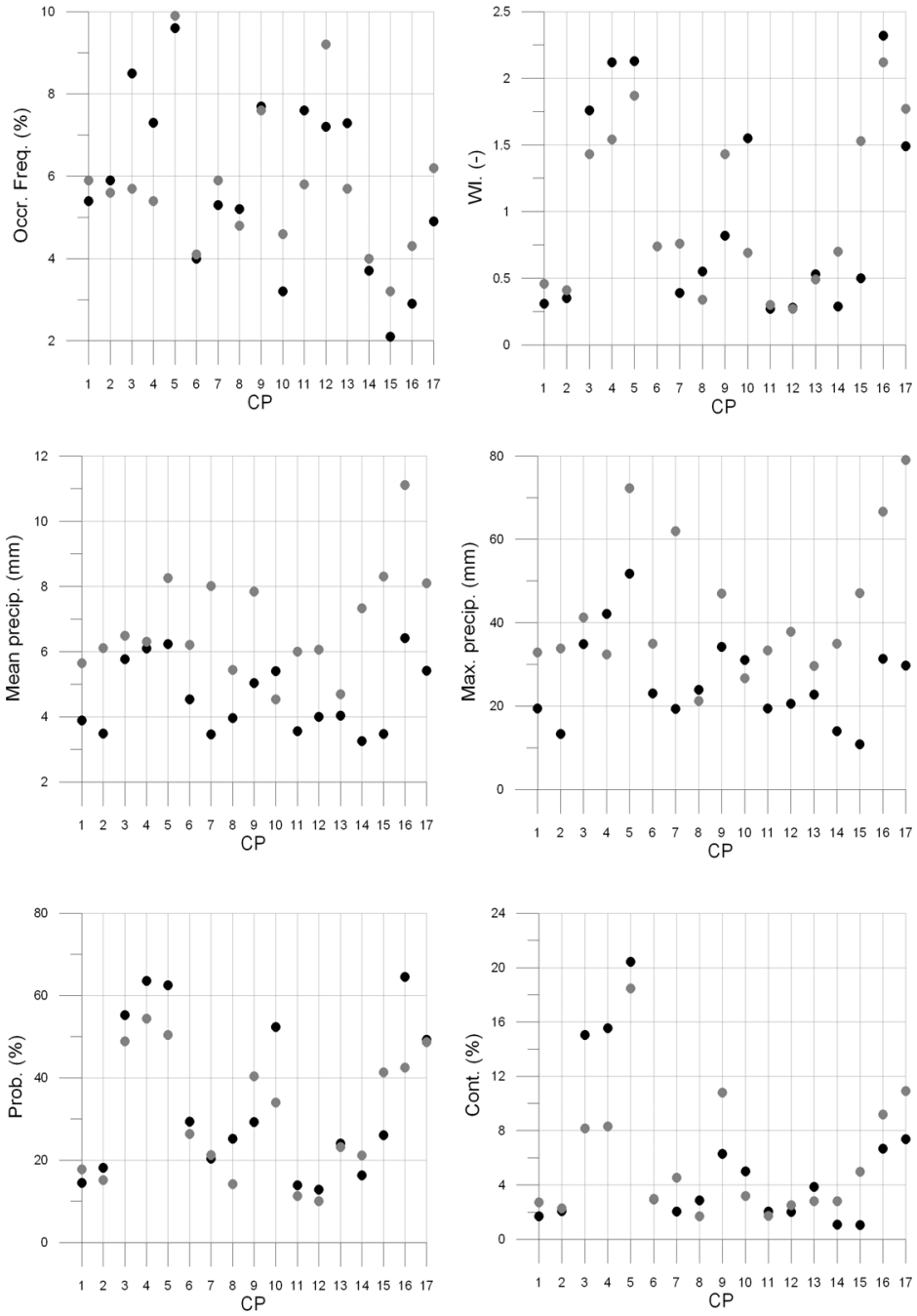

Figure 5.42.: Basic CP statistics averaged over all precipitation stations of Weisseritz catchment for winter (black circles) and summer (gray circles).

5.3. Conclusions

The new optimization methodology for classification and identification of circulation patterns, developed in this thesis is applied in this chapter. The classification obtained from precipitation and discharge data of Baden Württemberg was applied to several smaller head catchments of Germany and to the number of data sets obtained from three different RCMs for German part of Rhine basin. This served as the validation of the process and the results prove the methodology to be effective and robust for classification of circulation patterns. The identified extreme wet and dry CPs remained the same in different cases with slight changes in wetness index and occurrence frequency. The observed extreme events of floods and droughts were clearly identified by the classification with almost all floods occurring simultaneously with identified extreme wet CPs. In majority of the cases the preceding days of maximum flood were also classified as extreme wet CP day. This makes the classification important for forecasts and warnings. Additionally this also reflect that the natural phenomena of clustering of wet days is well represented and captured by the classification system. The same classification is also analyzed for drought years and the extreme summer heat waves of European continent during 1976 and 1991 are well captured by identified extreme dry CPs. The single classification can thus be used for identification of both wet and dry conditions.

6. Results-Downscaling

6.1. Preface

This Chapter presents the results obtained from application of the downscaling methodologies presented in Chapter 3. Multivariate statistical downscaling technique presented in Section 3.3.1 is applied to OPAQUE classified data while bias correction method presented in Section 3.3.2 is applied to ENSEMBLES gridded data sets of all the RCMs.

6.2. Downscaling based on bias correction in RCMs using quantile-quantile exchange of simulated variables

The need of downscaling of different variables simulated by GCMs from global scale to local scale was presented in Chapter 2. Two main methodologies adopted for downscaling were also presented along with the shortcomings of each one of them. Section 2.2.1.1 specifically penned down the shortcomings associated with dynamical downscaling. One of the most serious and well reported drawback of dynamical downscaling is the transfer of bias from global to local scale. GCMs are inheritly biased and it is but natural for RCM, run by certain GCM to inherit this bias. In spite of this drawback, the output of RCMs (specially if outcome is precipitation and/or temperature) is finally used in hydrological and/or impact assessment models which at the minimum could be described as questionable approach. The approach is questionable because hydrological cycle is known to be highly non linear and same climatic signal applied to a biased baseline could produce completely different hydrological signal. Given that regional hydrology is extremely sensitive to precipitation and temperature (in some cases temperature is conditioned upon the presence or absence of precipitation), small biases may change the whole hydrological equilibrium.

Different RCMs produce different simulation of different hydrological and meteorological variables. Unfortunately the accuracy of these simulations, specially in case of precipitation and temperature, are not that accurate. Example of this in terms of mean daily wet day precipitation for winter and summer is shown in Figure 6.1 and Figure 6.2 respectively. For German part of Rhine basin three RCMs studied in this thesis produce different realization of precipitation. It can be seen that neither spatial patterns nor amounts of precipitation are modeled adequately. All RCMs are considerably different from observational gridded data set and also from each other. Perhaps because of the biases that each model inherit from its parent GCM. The goal of bias corrected downscaling is thus to bring the bias to some reasonable limit by relating the distribution of precipitation amounts generated by RCMs during the

control runs with the distribution of observed amounts. For the future scenario runs of each RCM then, this "corrected" quantile of control run is used to develop a new future scenario. Given that the bias of the model would have been corrected in the first step, it is believed that the future scenario would be more plausible.

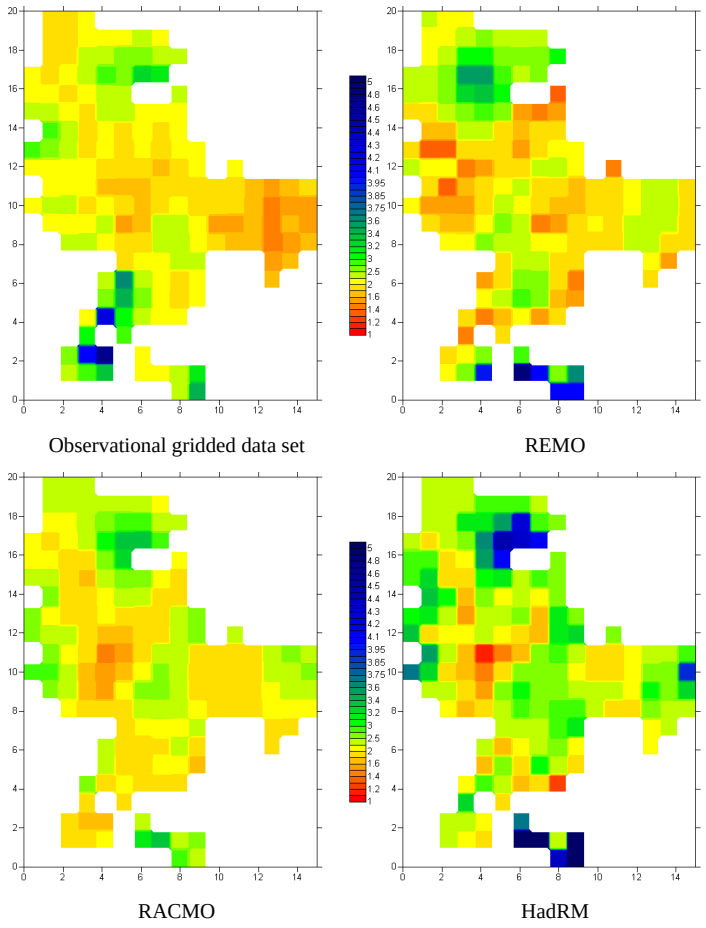

Figure 6.1.: Mean daily wet day precipitation of observational gridded data set and RACMO, REMO and HadRM RCMs. Averages are calculated for winter from 1961-1991.

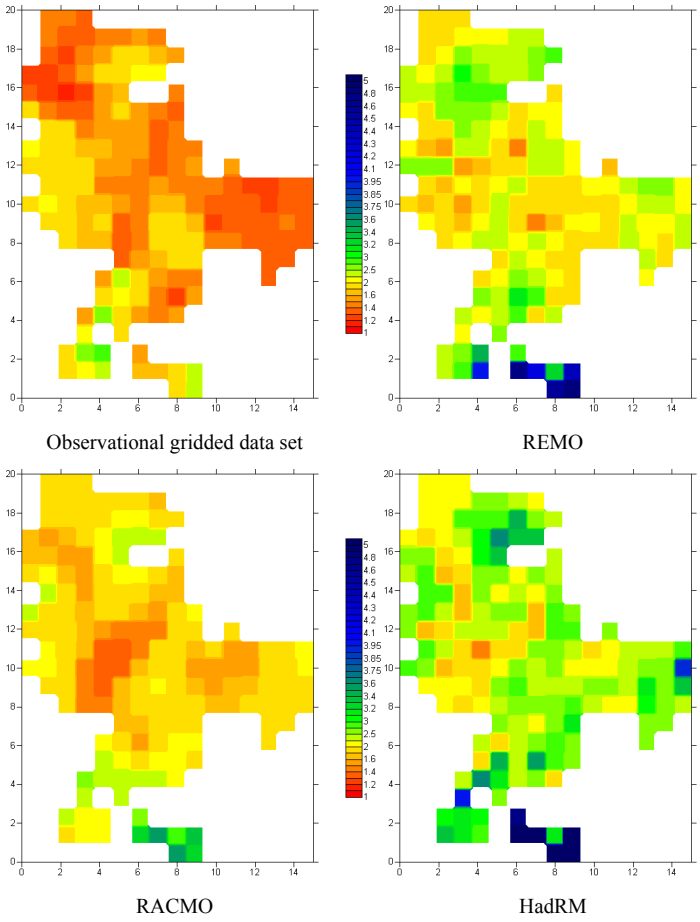

Figure 6.2.: Mean daily wet day precipitation of observational gridded data set and RACMO, REMO and HadRM RCMs. Averages are calculated for summer from 1961-1991.

Circulation patterns for control period of each RCM were presented in Chapter 5, Section 5.2.1.2, Section 5.2.1.3, Section 5.2.1.4 for RACMO, REMO and HadRM respectively. Figure 6.3 and Figure 6.4 display the wetness indices for wet and dry CPs for observational gridded data set and control runs of three RCMs. Comparing with Figures 6.1 and Figure 6.2 of precipitation amounts, it can be seen that wetness indices maps of wet and dry CPs are more skillfully represented in RCMs. Conversely one can also say that CPs can successfully capture the same behavior for each RCM. Thus conditioning the bias correction on CPs would bring more robust downscaling results.

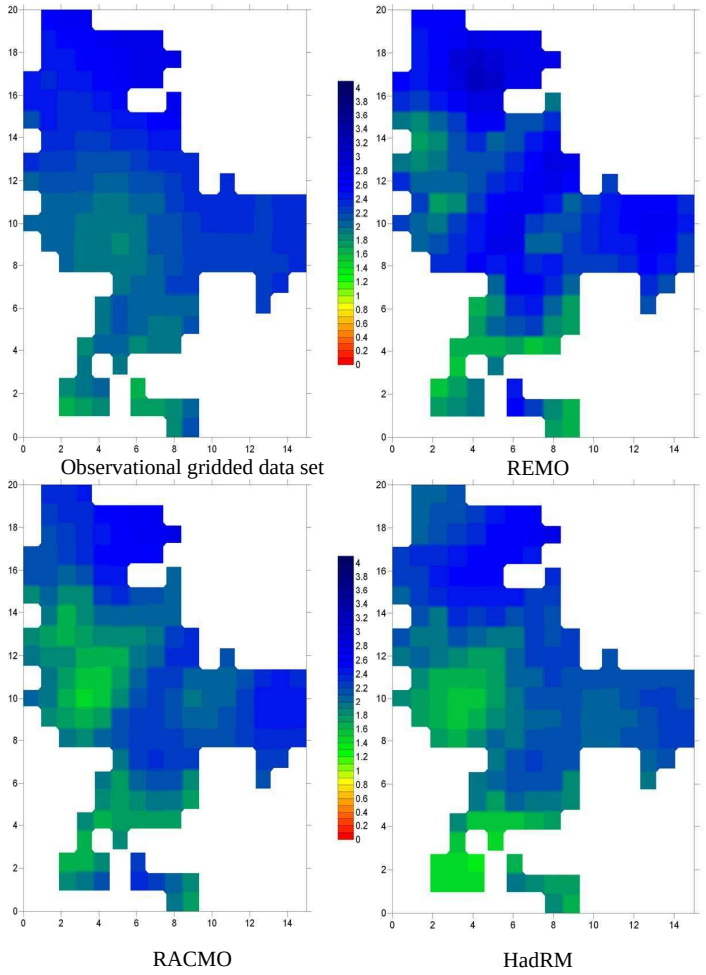

Figure 6.3.: Wetness index maps of wet CP (CP04) for observational, RACMO, REMO and HadRM control runs.

Two approaches are considered for the application of the above idea. One is development of relationship between quantiles of observational gridded data and RCM generated precipitation amounts without any additional condition on any of the two

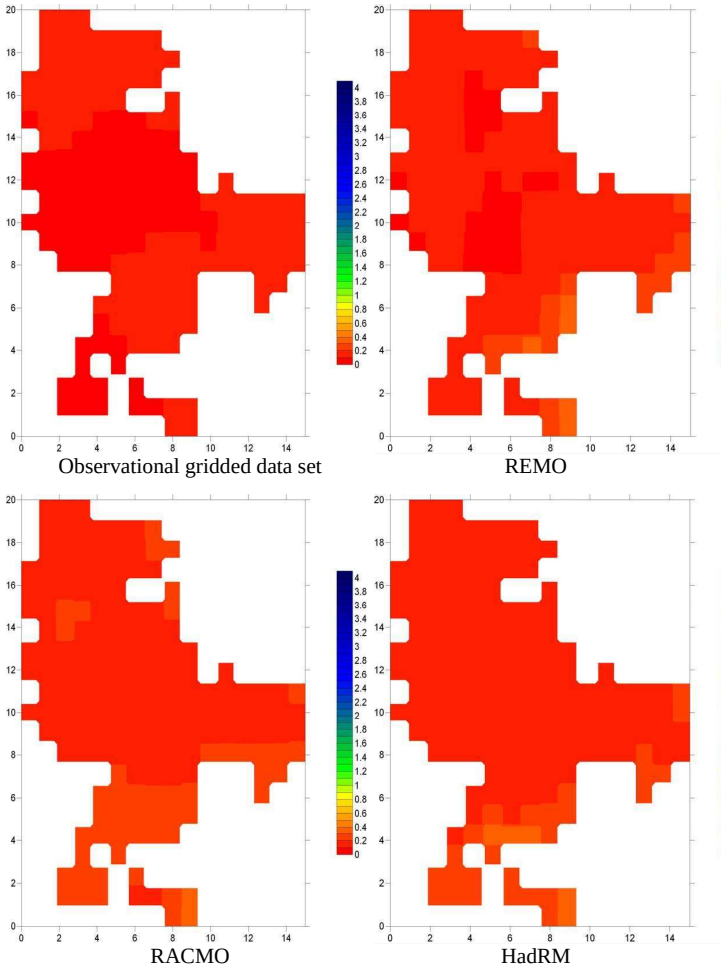

Figure 6.4.: Wetness index maps of dry CP (CP02) for observational, RACMO, REMO and HadRM control run.

quantiles, called as "Universal approach" and the second one is the development of relationship conditioned on circulation pattern called "CP based approach". The reason of conditioning the development of relationship on circulation pattern is that circulation patterns represents different climatic conditions in terms of precipitation amount skillfully and thus by adding this information the relationship between the amounts of observational gridded data set and RCM control run would be more representative. In both the approaches, Weibull distribution, defined in section 3.3.2, is fit to the precipitation amounts for each grid point, season and dataset. The scale parameter δ and shape parameter β are shown for each data set in Figure 6.5. As mentioned earlier, the scale and shape parameter controls the spread and shape (appearance) of the distribution. It can be seen that for observational gridded data set (bold solid blue for winter and bold solid red for summer) the shape parameter consistently hover around value 1 for each station in both seasons, thus following a distribution very close to exponential. As expected the RCM generated precipitation's distribution parameters for control period are different than the observed ones. RACMO, REMO and HadRM based parameters are shown in first, second and third row. It can also be noted that while in case of observational precipitation amounts the shape and scale parameters are not that far away from each other for winter and summer, in case of RCMs the differences between summer and winter values are considerable.

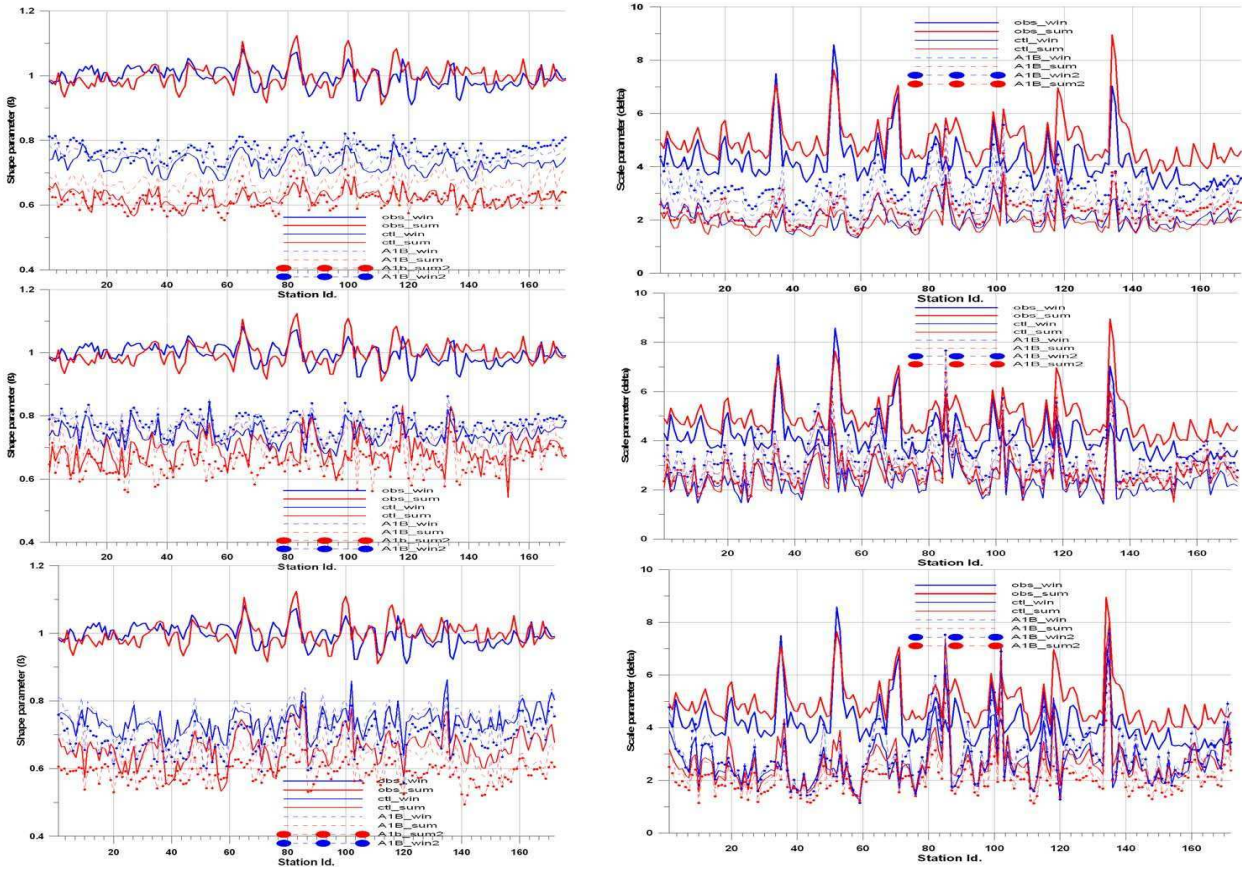

Figure 6.5.: Shape (left column) and scale (right column) parameters for RACMO (top row), REMO (middle row) and HadRM (bottom row) RCMs for each station. Parameters are estimated for Winter (blue) and Summer (red) seperately. Observational gridded data set is represented in bold solid line, control run in solid line and SRES A1B scenario (2001-2030) in dashed line. Parameter values of SRES A1B scenario for time period 2069-2099 are shown in dashed line with symbols.

Before the results of downscaling are presented and analysis are made, Figure 6.6 is presented which shows the distribution of observed and RCM modeled precipitation. This figure is shown as an example of substantial differences between the models simulation for control runs and observational gridded data set. Considering also Figures 6.1 and 6.2 one can conclude that not only RCMs have problems in simulating spatial patterns and amounts but also grid point based distributions. This discrepancy is further translated to the simulations of future scenarios. The quantile-quantile method of downscaling is supposed to bring this discrepancy to reasonable limits.

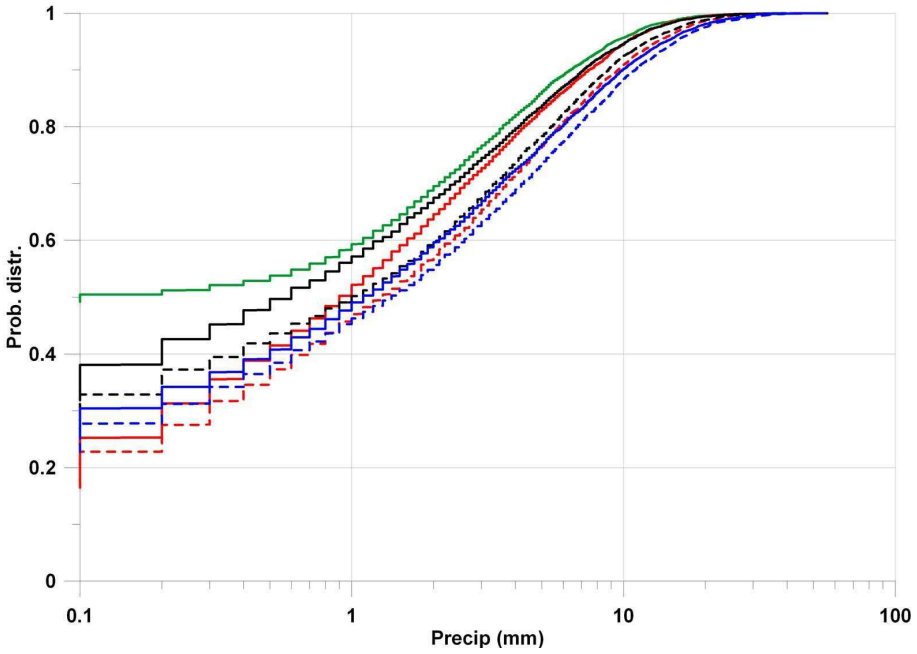

Figure 6.6.: Precipitation distributions for Grid point 2 (selected randomly, grid point shown in Figure 6.7) of observational (solid Green color) and RCMs gridded data sets for winter. RACMO is shown in red, REMO in black and HadRM in blue. Control runs are shown in solid lines and SRES A1B scenario (2001-2031) in dashed. For observational and RCM control data sets, the time period is from 1961-1991.

The results from both "universal" and "CP based" approaches for downscaling are analyzed by considering each of 172 grid points in German part of Rhine basin independently and also by delineating smaller catchments inside the German part of Rhine basin and considering their areal properties. For the grid point analysis, the results are mostly presented for the grid points shown and labeled in the left panel of Figure 6.7. These grid points are selected in different areas (and different sub catchments) of German part of Rhine basin exhibiting different hydrological properties. The right panel of the same figure shows the grid points associated with smaller sub catchments of German part of Rhine basin. The areal properties are calculated for these sub catchments.

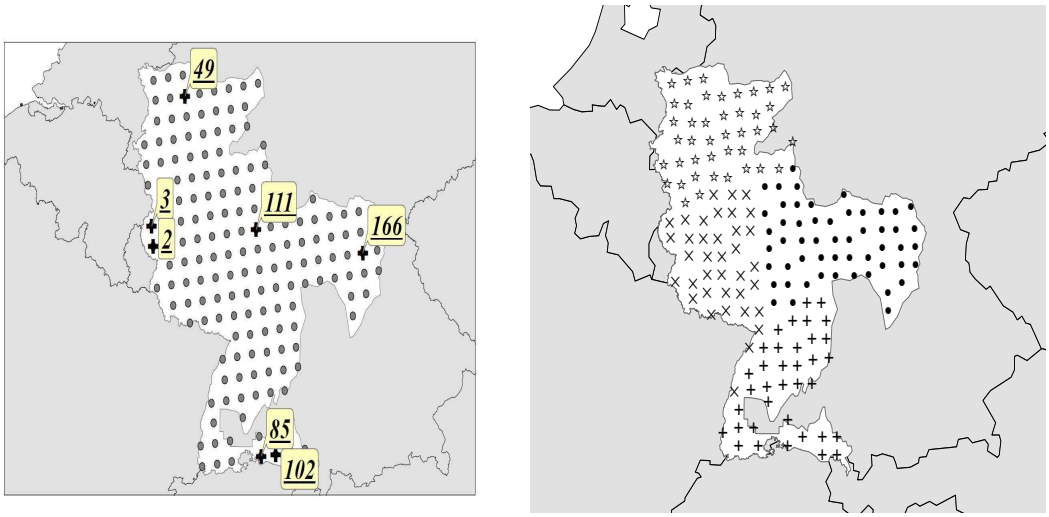

Figure 6.7.: Selecting grid points (shown in the left as labeled plus signs) for point based analysis and sub catchments (to the right sub catchment Main is shown as black dots, Necker as plus sign, Rhineland-Pfalz as crosses and Nordrhein-Westfalen as stars) for areal based analysis of the downscaled data

For grid point based analysis, measures such as annual maximum precipitation and annual precipitation sums are calculated for downscaled precipitation series while for catchment scale analysis, average areal precipitation sums, maximum areal precipitation sums and antecedent precipitation index are calculated. While average and maximum areal precipitation measures, portray the wet situations in the model simulated and downscaled scenarios, antecedent precipitation index represent the dry situation in the two series. Antecedent precipitation index (API) can be formulated as:

$$API(x,t) = \eta API(x,t-1) + Z(x,t) \tag{6.1}$$

For a certain day t and location x, API indicate dry situation by considering precipitation *Z(x,t)*. Lower API values would indicate drought situation and by considering minimum API values for two series, the drought situation in original and downscaled series can be compared.

6.2.1. Grid point based analysis

Figure 6.8 displays annual maximum daily precipitation for all RCMs from 2001 to 2030 (in upper panel) and from 2070 to 2099 (in lower panel) for randomly selected grid point 2 (left) and 49 (right). It can be seen that all RCMs understandably produce different annual maxima.Both universal downscaling approach and CP conditioned downscaling approach tends to lower the annual extreme of precipitation for each RCM. CP conditioned downscaling reduces the annual maximum precipitation more than universal downscaling approach. Comparing the two time periods it can

also be seen that annual maximum daily precipitation tend to touch higher precipitation amounts more frequently in later time periods than in earlier time periods. Looking at the annual precipitation sums represented in Figure 6.9, one can see a big difference in raw RCM scenarios. HadRM and REMO models predicts considerable wet years than RACMO for grid point 85 located close to Lake constance in southern Germany. The downscaling process reduces the annual precipitation amounts of all RCMs to almost the same level.

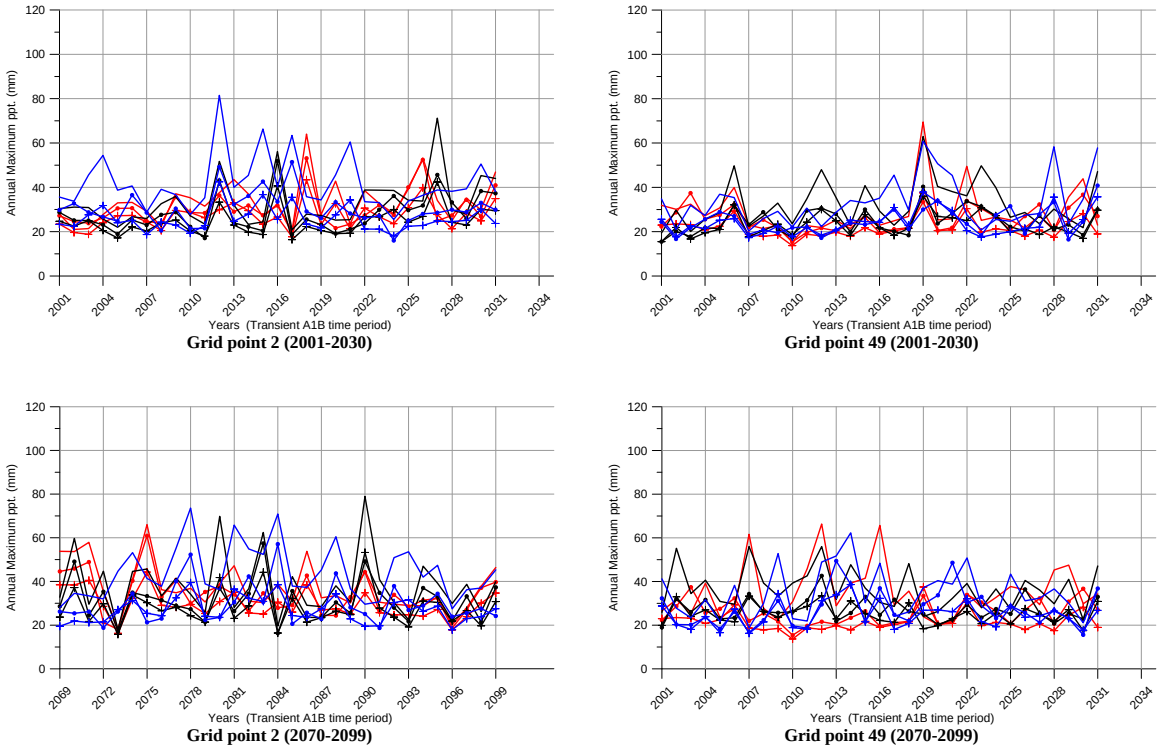

Figure 6.8.: Annual maximum precipitation plots of raw and downscaled precipitation scenarios for all RCMs. RACMO is in red, REMO in black and HadRM in blue. Plots obtained from universal downscaling application are shown with dots as symbol while CP conditioned downscaling based results are shown with plus sign as symbol.

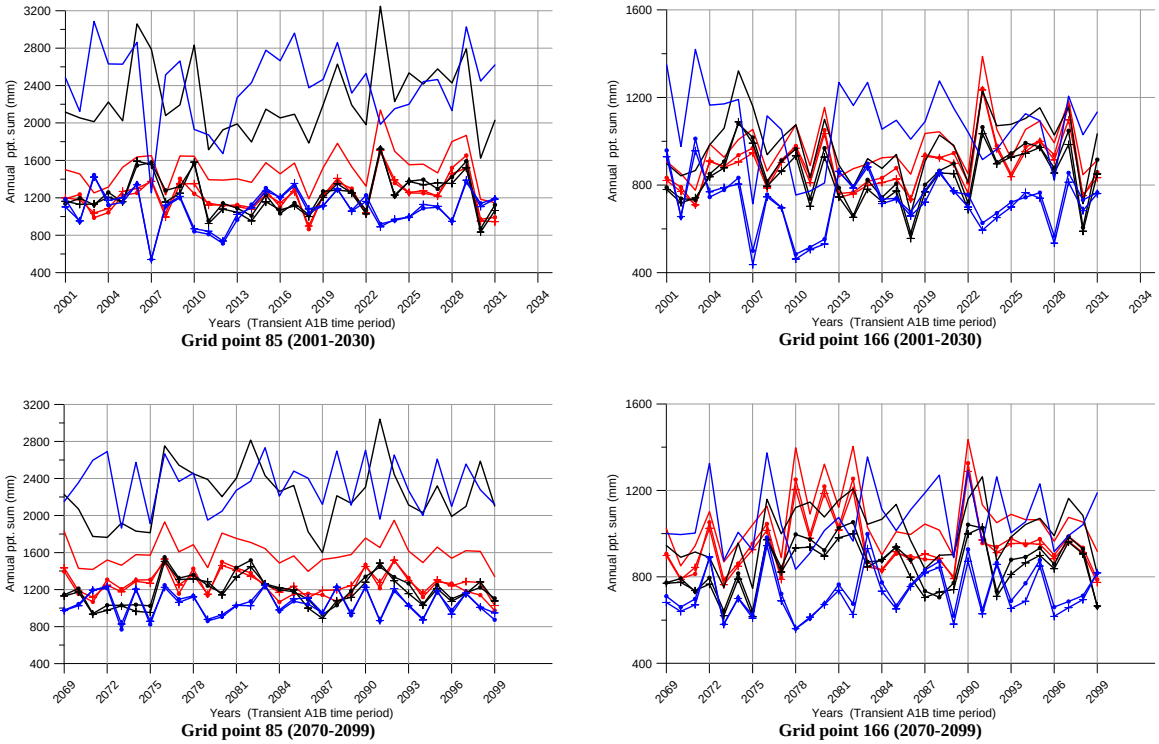

Figure 6.9.: Annual total precipitation plots of raw and downscaled precipitation scenarios for all RCMs. RACMO is in red, REMO in black and HadRM in blue. Plots obtained from universal downscaling application are shown with dots as symbol while CP conditioned downscaling based results are shown with plus sign as symbol.

6.2.2. Sub catchment based analysis

To consider the effects of downscaling on sub catchments of German part of Rhine basin, areal precipitation and antecedent precipitation index (API) were calculated for four different areas within larger basin. Yearly maximum areal precipitation and minimum API are shown for time period 2001-2030 and 2070-2099 for all RCMs, downscaled scenarios and observational gridded data set in Figure 6.10 to Figure 6.13. Maximum areal precipitation portrays the extreme wet situation while minimum API shows the driest situation within the area. It can be seen that all models show increase in absolute value of maximum areal precipitation for all four areas from 2001-2030 to 2070-2099.Additionally unlike the downscaling effect on grid point based yearly maximum precipitation values where mostly the extreme values were reduced, the downscaling affect here on areal based maximum yearly precipitation is different. In some cases (e.g. RACMO in Figure 6.10 for Main catchment) the downscaling increase the areal maximum yearly precipitation values (for 2016) and in some cases decrease the amount (2005). The effect of downscaling process on minimum API index is not significant for time period between 2001-2030. But for time period 2070-2099 the two downscaling processes tend to differ much from each other. HadRM is more sensitive to CP conditioned downscaling process than RACMO and REMO.

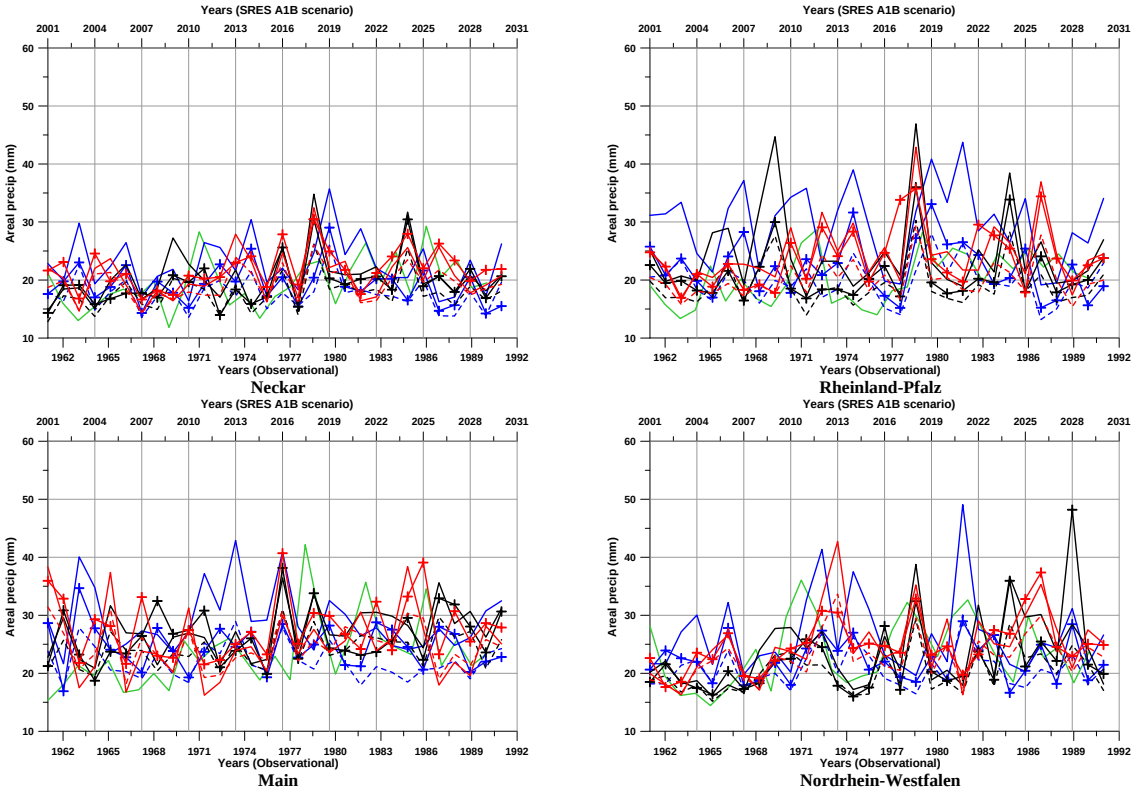

Figure 6.10.: Maximum areal precipitation of raw and downscaled precipitation scenarios of all RCMs and for selected sub catchments within German part of Rhine basin . RACMO is in red, REMO in black and HadRM in blue. plots obtained from universal downscaling application are shown with dashed lines while CP conditioned downscaling based results are shown with plus sign as symbol. All results are based on time period 2001-2030

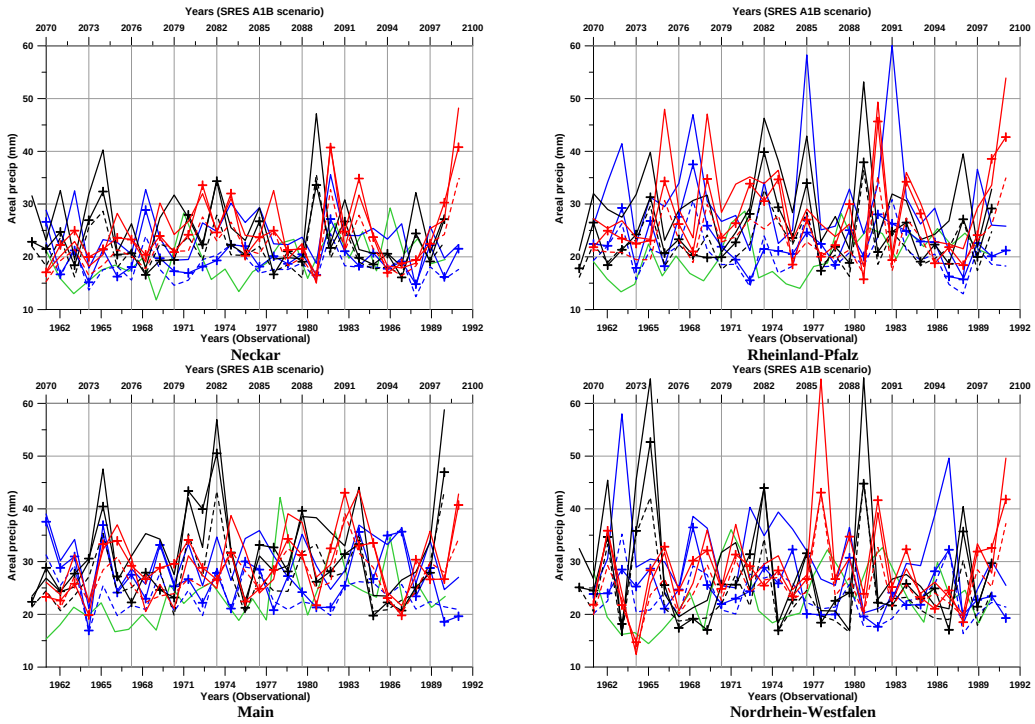

Figure 6.11.: Maximum areal precipitation of raw and downscaled precipitation scenarios of all RCMs and for selected sub catchments within German part of Rhine basin . RACMO is in red, REMO in black and HadRM in blue. plots obtained from universal downscaling application are shown with dashed lines while CP conditioned downscaling based results are shown with plus sign as symbol. All results are based on time period 2070-2099

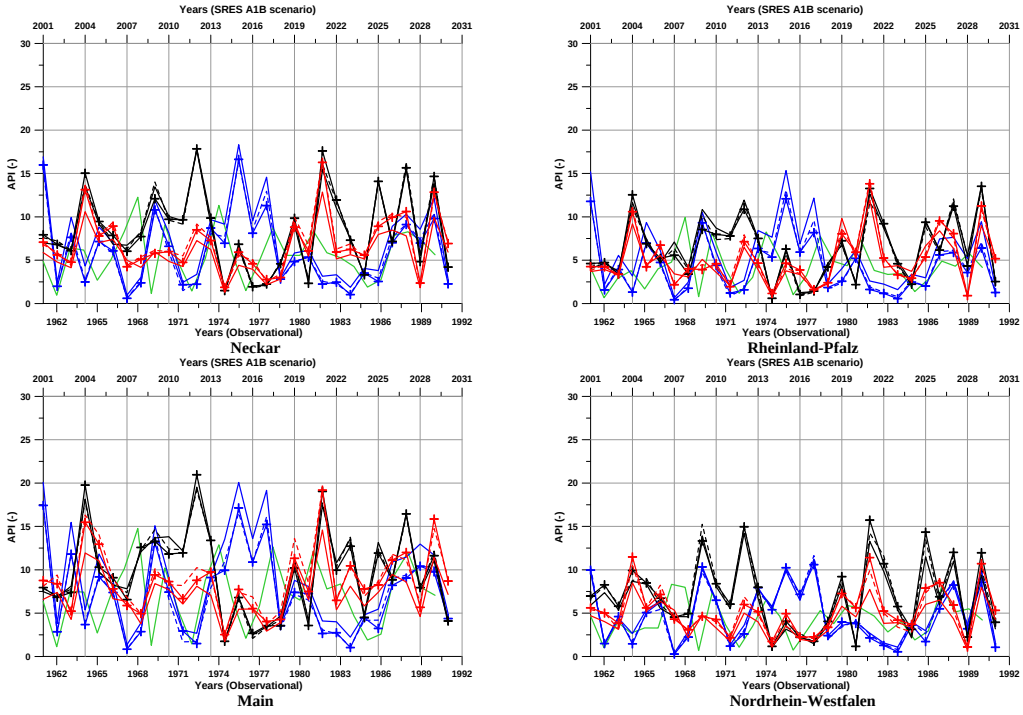

Figure 6.12.: Minimum API of raw and downscaled precipitation scenarios of all RCMs and for selected sub catchments within German part of Rhine basin . RACMO is in red, REMO in black and HadRM in blue. plots obtained from universal downscaling application are shown with dashed lines while CP conditioned downscaling based results are shown with plus sign as symbol. All results are based on time period 2001-2030

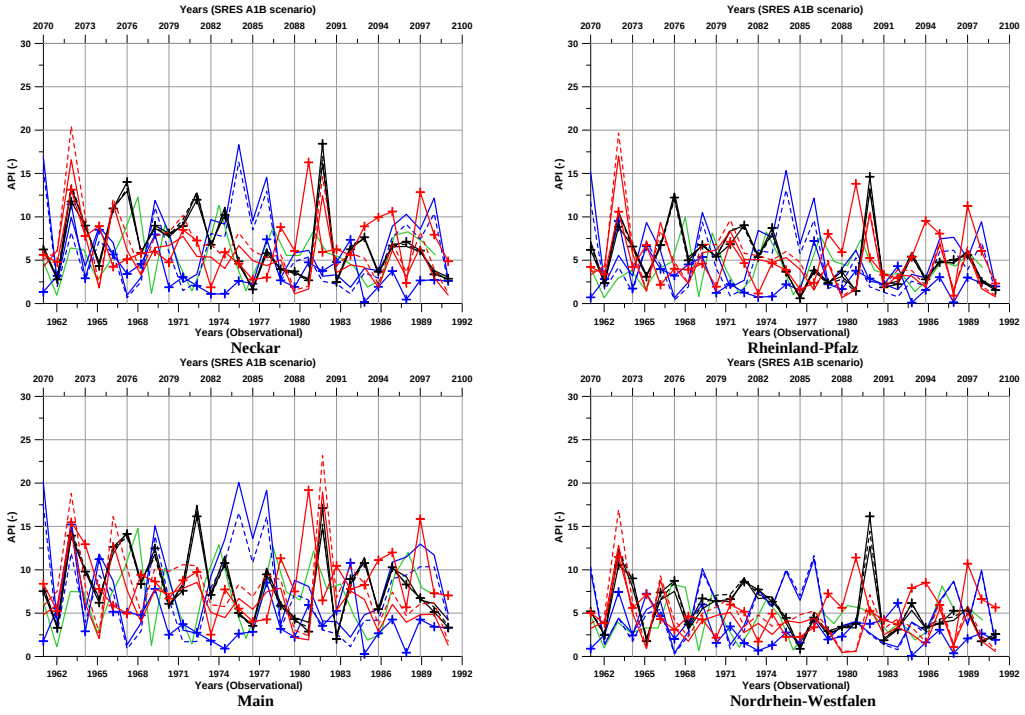

Figure 6.13.: Minimum API for raw and downscaled precipitation scenarios for all RCMs and for selected sub catchments within German part of Rhine basin . RACMO is in red, REMO in black and HadRM in blue. plots obtained from universal downscaling application are shown with dashed lines while CP conditioned downscaling based results are shown with plus sign as symbol. All results are based on time period 2070-2099

6.3. Downscaling based on CP conditioned Autoregressive multivariate technique considering Moisture Flux

This downscaling methodology is applied to OPAQUE catchments for precipitation forecast (for information regarding catchment and precipitation stations therein, please refer to Chapter ch:A, Section A:catch:opaque). The methodology is based upon multivariate autoregressive model. The components of the model such as precipitation occurrence and precipitation amount are explained in Chapter 3, Section 3.3.1. The circulation pattern classification obtained earlier and explained in Section 5.2 is used here as well. Given that the circulation patterns were classified based on completely independent data set, the downscaled precipitation simulations discussed below can be taken as kind of validation.

In addition to MSLP, Moisture flux (MF) is also used as large scale predictor. Moisture flux is the product of geostrophic wind and specific humidity at a given location. **U** and **V** components of wind and MSLP is obtained from NCEP NCAR reanalysis data. Reanalysis data provide **U** and **V** components of wind at different pressure levels. To find out the most appropriate pressure level for MF, Yang et al. (2010) analyzed correlation between local rainfall events and MF calculated at different levels. MF calculated at 700 hpa. was found to strongly correlated with precipitation comparing with other levels. Given that the area of interest in both studies is almost the same, the MF at 700 hpa. is also used here as large scale predictor.

The methodology is further improved in this thesis and it is now possible to have multiple realizations of daily precipitation amount. This way it would be possible to carry out uncertainty analysis on predicted results. Downscaling is performed for all OPAQUE catchements, but the results are only shown for Upper Danube and Alb Catchments.

6.3.1. Upper Danube Catchment

Information about Upper Danube catchment and precipitation stations therein are presented in Section 4.1.1. Simulations are performed from 1971-1991. All the precipitation stations in upper Danube catchment are located approximately at 48°05′38.64″N, 08°15′55.90″E. MF is calculated at 47°30′N, 09°30′E for all the stations. Figure 6.14 presents mean and variance of observed and simulated precipitation for summer and winter for all precipitation stations. The figure contains the simulations made with and without considering MF. It can be seen that multiple simulations made considering MF are more closer to the observed values. The difference between simulations made with and with out considering MF are more clear in the variance of precipitation.

Figure 6.15 shows monthly precipitation sums of observed and simulated precipitation for four of the upper Danube precipitation stations. The difference between two simulation methodology is quite evident in this figure. Observed monthly precipitation sums are almost without exception bounded by the multiple simulations made

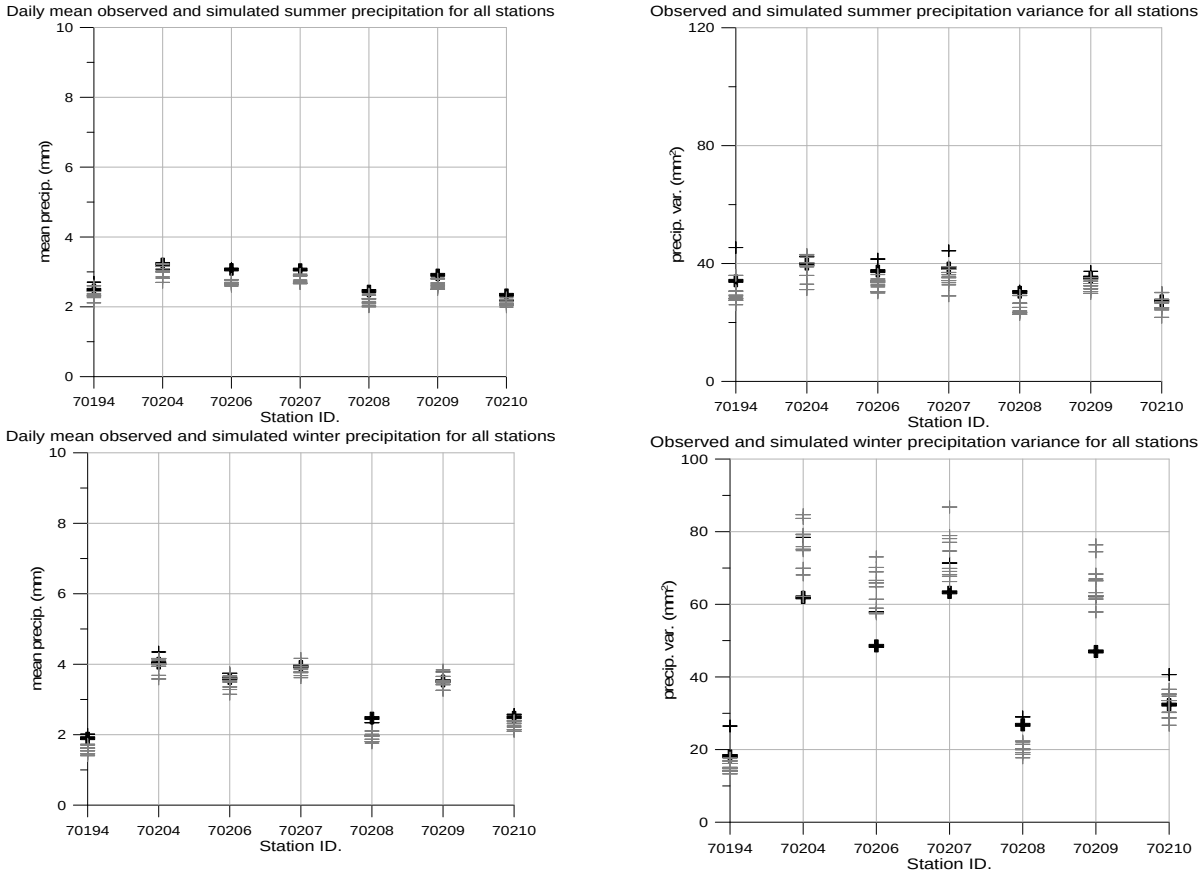

Figure 6.14.: Mean and variance of observed and simulated precipitation of all precipitation stations of upper Danube catchment for summer and winter season. Dark black cross represent observed values, light black represent simulation without considering MF, while gray crosses represent multiple realizations of precipitation considering MF.

considering MF. The downscaling methodology is able to capture the seasonal variability of precipitation amounts whether the simulations are made with or without considering the MF. The multiple realizations of MF considered simulation additionally gives the information about the possible range of monthly precipitation amounts.

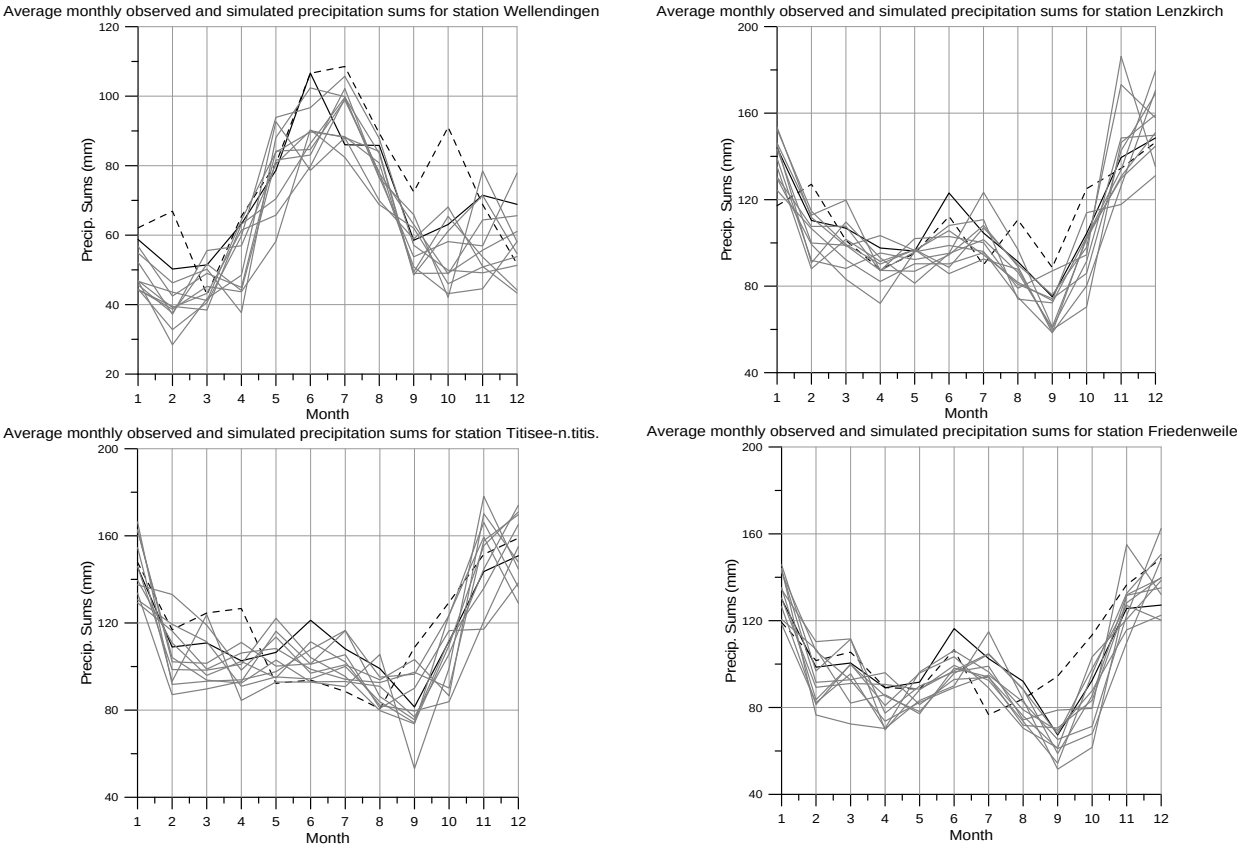

Figure 6.15.: Monthly observed and simulated precipitation sums of four precipitation stations of upper Danube catchment. Solid black line represent observed values, dashed black line represent simulation without considering MF, while gray lines represent multiple realizations of precipitation considering MF.

Figure 6.16 finally compares yearly areal observed and simulated precipitation. Areal precipitation is calculated from gauge precipitation as:

$$AP_i = \sum_{j=1}^{tot.st._i} \frac{P_{ij}}{tot.st._i} \tag{6.2}$$

Where AP is areal precipitation in units $[mm]$ for certain catchment i, $tot.st.$ is total number of precipitation gauge station located in catchment i and P is the precipitation amount in $[mm]$.

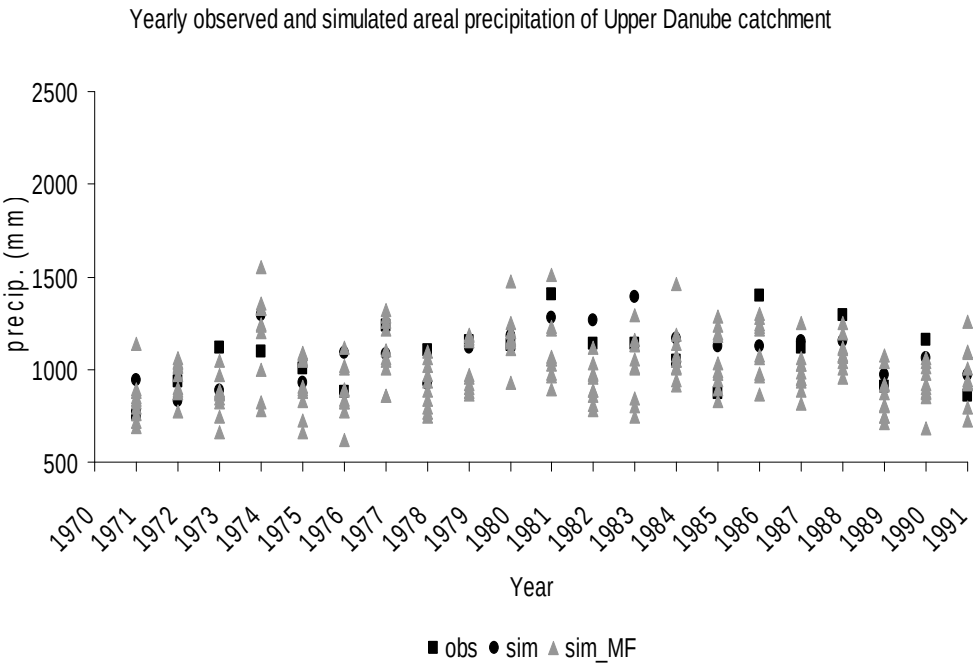

Figure 6.16.: Yearly observed and simulated areal precipitation sums of upper Danube catchment. Squares represent observed values, circles represent simulation without considering MF, while gray triangles represent multiple realizations of precipitation considering MF.

6.3.2. Alb Catchment

Downscaling was performed from 1971-1991 for Alb catchment. The precipitation stations used in Alb catchments are tabulated in Table 4.4. The mean precipitation amounts and variance of precipitation of simulated precipitation are shown in Figure 6.17. The results show that both the statistics are nicely captured by the downscaling methodology for all catchments and for winter and summer. Unlike upper Danube catchment results, where winter precipitation variance was not simulated adequately for some of the catchments, here the same is simulated efficiently for all stations. Monthly precipitation sums and areal precipitation for the catchment shown in Figure 6.18 and Figure 6.19 respectively are also efficiently simulated. The additional effort of including moisture flux as additional predictor in the downscaling process can be justified by considering Figure 6.20. The figure displays, as an example, the basic statistics of summer precipitation of four precipitation stations. It can be seen that the basin statistics based on MF conditioned downscaling process are more in agreement with the observed precipitation than they are with the simulation where MF is not considered.

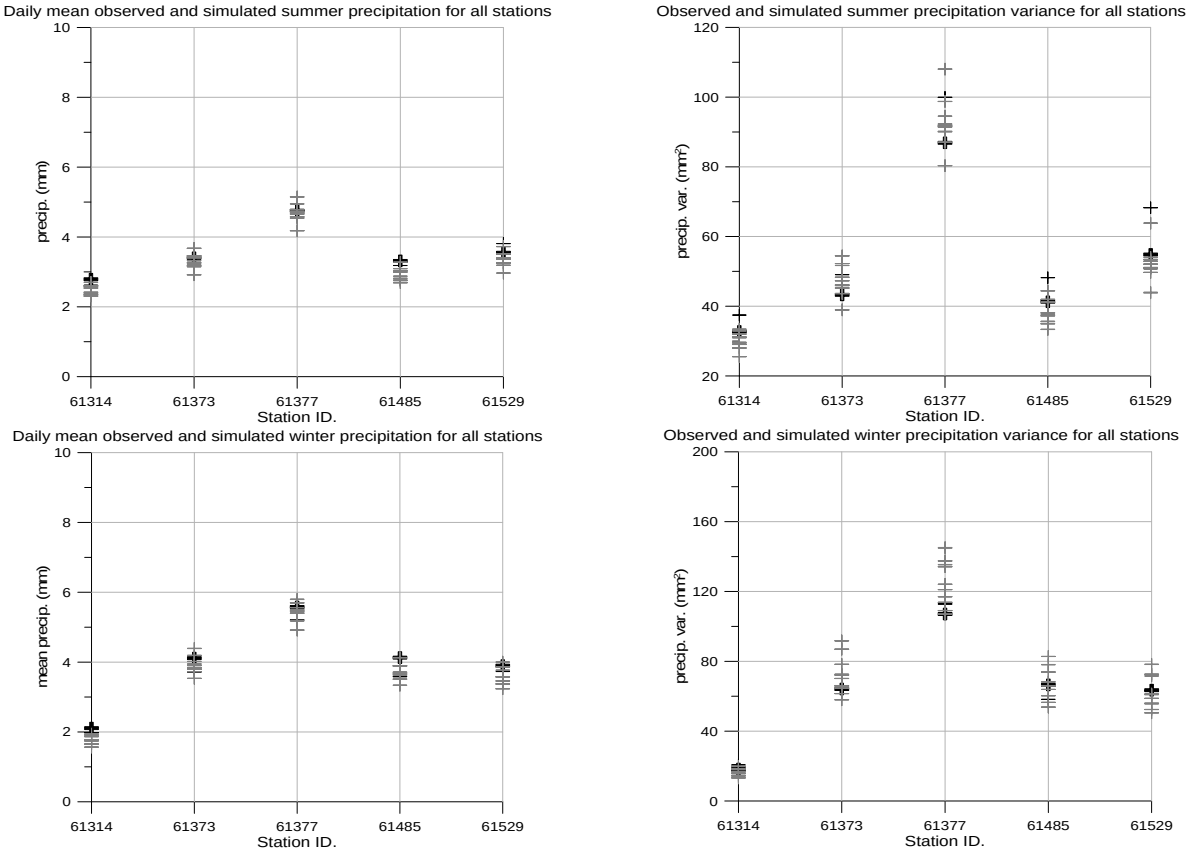

Figure 6.17.: Mean and variance of observed and simulated precipitation of all precipitation stations of Alb catchment for summer and winter season. Dark black cross represent observed values, light black represent simulation without considering MF, while gray crosses represent multiple realizations of precipitation considering MF.

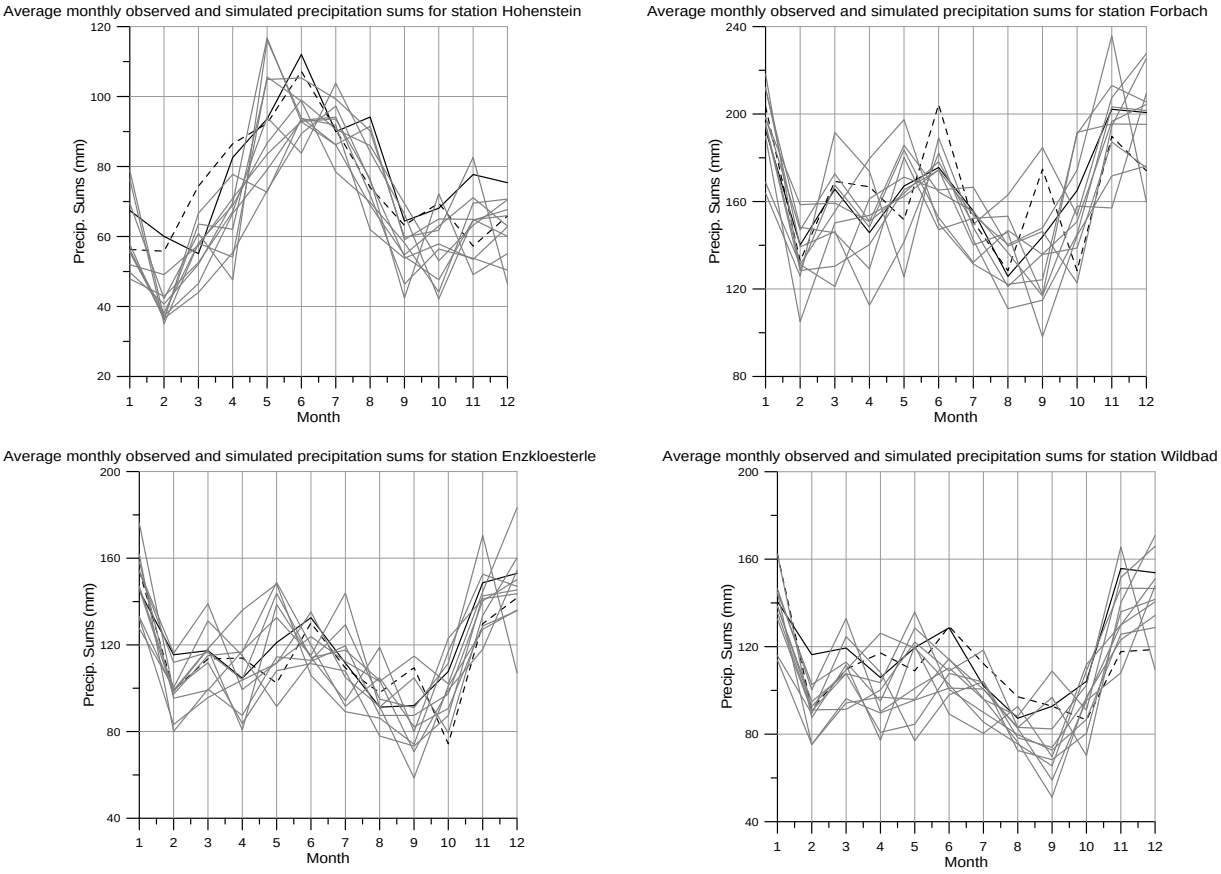

Figure 6.18.: Monthly observed and simulated precipitation sums of four precipitation stations of Alb catchment. Solid black line represent observed values, dashed black line represent simulation without considering MF, while gray lines represent multiple realizations of precipitation considering MF.

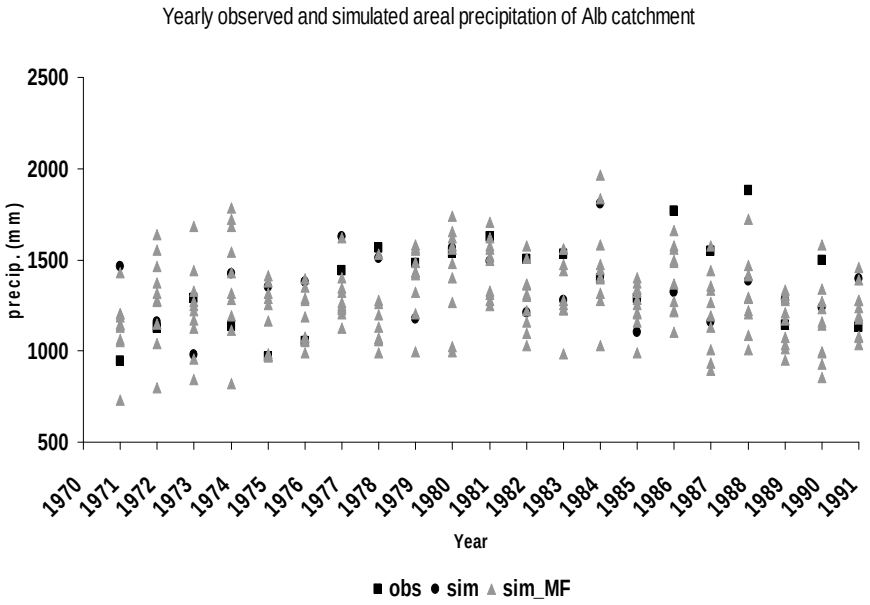

Figure 6.19.: Yearly observed and simulated areal precipitation sums of Alb catchment. Squares represent observed values, circles represent simulation without considering MF, while gray triangles represent multiple realizations of precipitation considering MF.

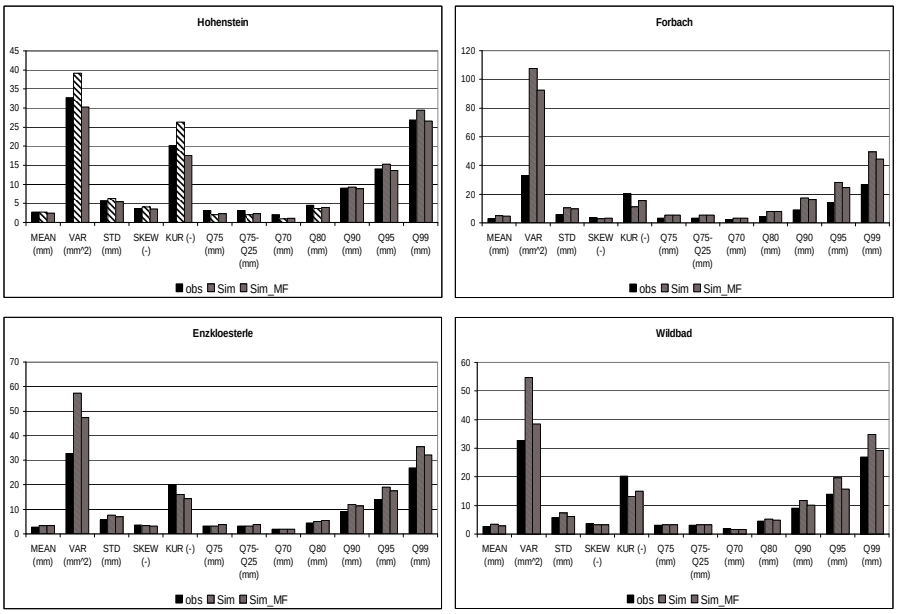

Figure 6.20.: Observed and simulated (with and with out considering MF) precipitation statistics of Alb precipitation stations for Summer.

7. Drought Analysis

7.1. Preface

Reference was made to drought as one of the manifestation of extreme hydrological situation in chapter 1. Comparing with floods, the other manifestation of extreme hydrological situation, drought situation are difficult to be represented in precipitation simulations. A reference to this difficulty was also made during circulation pattern classification methodology in Chapter 3 where it was mentioned that classification of circulation patterns for drought situation can not be efficiently made owing to complex nature of droughts. Floods can directly be associated with extreme short events of precipitation which is a measurable and observable meteorological event. Droughts on the other hand are difficult to be directly associated with any one of meteorological event. Rather it is a result of occurrence of some and non occurrence of other meteorological events over a long period of time. E.L.Tate and Gustard (2000) acknowledges that there is no universally accepted definition of drought and that the definition of drought strongly depends upon the region in which it is considered and on the aim of the study for which it is considered. Different definitions have been put forward for droughts and similarly number of measures or indices have been developed to characterize drought situations. T.A.McMahon and Diaz (1982) defined drought as "a period of abnormally dry weather sufficiently prolonged for the lack of precipitation to cause a serious hydrological imbalance, carrying connotations of a moisture deficiency with respect to man's usage of water". As can be noted this definition circumscribes a lot of areas and needs clarification for words like "abnormally","sufficiently","lack","serious" etc. Clarification of all these terms would clearly make drought definition more complex. In the following different kinds of droughts classified in literature and some frequently used drought indices are outlined.

7.2. Classification of droughts and frequently used indices

Drought is site specific phenomena in that if certain precipitation deficit is considered as a drought onset criteria at certain place than the same criteria can not be directly applied to other areas as drought indicator. A classification of different types of droughts thus should consider its type, intensity, duration and spatial extent in conjunction with its perceived impact (E.L.Tate and Gustard, 2000). Following categories of drought are usually found in literature.

7.2.1. Climatological drought

Climatological droughts are usually defined on the basis of precipitation deficits. Previously defined site specific precipitation limits are considered as threshold values

along with the duration taken to reach this limit. Once these limits are crossed, climatological drought is declared to be on. The main advantage of this type of classification is that it only needs precipitation as input meteorological variable. Comparing with other variables like temperature and evapotranspiration, longer observation records for precipitation can easily be found. The draw back of using precipitation deficit based drought definition is that antecedent moisture conditions are not taken into account. Laux (2008) used effective precipitation based drought index for drought studies for Volta basin in West Africa. Although effective precipitation is more useful than pure precipitation based indicators but then again one is in need of available evapotranspiration data. Palmer drought severity index (PDSI) (W.C.Palmer, 1965), (sec. 7.3) is one the most widely used drought severity index that uses precipitation as drought indicator along with other data. Number of other indicators have been developed based on PDSI and used around the world. Other indicators based on precipitation anomalies have also been developed in areas where precipitation is normally received at fairly frequent interval. For example Hulme (1996) plotted precipitation trends from 1900 to 1995 as percent anomalies from 1961-90 average. Similarly Welsh National Water development Authority gauged Wales drought of 1975-1976 as percentage of average of 1941-1970 period (Anon, 1977).

7.2.2. Hydrological drought

Hydrological droughts are sub divided usually in stream flow drought and ground water drought. The effect of hydrological drought usually lag behind in terms of its first appearance in time series than climatological and Agro-Meteorological droughts. Stream flow droughts are primarily related to the effect of precipitation deficit on surface and subsurface water supply. Flow frequency curves (Ben-Zvi, 1987), Gumbel's extreme minimum flow analysis (T.J.Chang and Stenson, 1990) and discrete markov analysis (Sen, 1980) are some of the methods that are used to describe drought based on stream flow.

Ground water drought on the other hand is represented by lower than average annual recharge for more than one year. Ground water drought characterization is highly subjective and comparing with its importance as a water source, its consideration in drought study is very minimal. Calow et al. (1999) and van Lanen and Peters (2000) uses ground water drought indices for ground water management strategies which are primarily dependent upon ground water levels. Three kind of parameters can be investigated for ground water characterization i.e. recharge, ground water level and ground water discharge. Hydrological drought is out of phase with climatological and agro-meteorological drought, and ground water drought is slower component of hydrological drought cycle. Given its slow reaction to natural precipitation and temperature inputs, only major droughts would show up as a ground water drought.

7.2.3. Agro-Meteorological drought

As the name suggests this classification of drought primarily deals with agriculture. It links various categories of meteorological and hydrological droughts to its impacts on

agriculture out put. Any water deficiency in the soil (root zone) that is going to affect the normal cropping behavior in certain area is considered as Agro-meteorological drought. As such this kind of drought usually use indicators based on soil water and differences between actual and potential evapotranspiration for drought onset. The deficiency in root zone is expressed by the water content of the soil profile per meter depth. Different indices have been developed to cater for the definition of onset of agro-meteorological drought. FAO water satisfaction index (Frére and Popov, 1979) is used for crop monitoring and yield prediction and make use of 10 day based soil moisture balance indicator. Although this measure is used in different studies but number of short comings of this indicator have been documented by E.L.Tate and Gustard (2000). Petrasovits (1990) uses the so called agrohydropotential of certain crop which is a ratio of actual water consumption and the optimal water requirement of a crop. The advantage of this index is that it is possible to prepare comparative drought prognoses for any crop and also to estimate the degree of drought susceptibility by the frequency of occurrence (Petrasovits, 1990).

7.3. Palmer drought severity index (PDSI)

Previous section outlined different kinds of classification of droughts and associated drought indices used. Perhaps the most used and best known among them is Palmer drought severity index (PDSI). PDSI is a meteorological drought index and W.C.Palmer (1965) defined drought period as "an interval of time, generally of the order of months or years in duration, during which the actual moisture supply at a given place rather consistently falls short of the climatically appropriate moisture supply". Based on this definition and the fact that PDSI takes into account evapotranspiration and soil moisture conditions in addition to precipitation, the PDSI can also be used as hydrological drought index as noted by Fieldhouse and Palmer (1965). The index can be related to water supplies in streams and rivers and hence be of interest equally for hydrologists, meteorologists and climatologists. The main advantage of PDSI is that it is a standardized drought index and can be readily compared with the same index calculated in other regions.

The PDSI is based on water balance equations on monthly or weekly basis. The underlying concept is that the amount of precipitation required for the near normal operation of the established economy of an area during some stated period is dependent on the average climate of the area and on the prevailing meteorological conditions both during and preceding the period under consideration (E.L.Tate and Gustard, 2000). The weighted difference between actual precipitation and required precipitation for certain area is accumulated and related with severity index. In addition to its ease in comparison with PDSI calculated in other areas, PDSI is useful in the sense that it can be used for identifying wet situations as well. PDSI is widely used in USA and is routinely calculated by the NOAA (National Oceanic and Atmospheric Administration) for all the states. Additionally the index is also used by private industry for real-time drought management and planning (Karl, 1991). Based on the PDSI concept following indices have been developed;

1. Palmer drought severity index (PDSI)

2. Palmer hydrological drought index (PHDI)
3. Monthly moisture anomaly index (ZINX)
4. Colorado Palmer Drought index (CPDI)

These indices respond differently to changes in supply and demand for moisture and thus represent different kinds of droughts. ZINX is used primarily for agricultural drought, CPDI is developed for areas with lower elevations while PHDI is modified form of PDSI that is used for drought impacts on river flow, groundwater availability and lake or reservoir levels. All these variables are derived from water balance equations with complex calculation procedures. A brief review of the procedure for 1 month time step is given here which is based directly on original paper of W.C.Palmer (1965).

For each month of the year, four values are computed related to the soil moisture along with with their complementary potential values. The eight values are computed assuming a two stage bucket model of the soil and the computed values are evapotranspiration (ET) and potential evapotranspiration (PE), recharge (R) and potential recharge (PR), runoff (RO) and potential runoff (PRO), loss (L) and potential loss (PL). Thornthwaite's (Thornthwaite, 1948) method of calculation of potential evapotranspiration is used. The upper layer is assumed to hold 25mm of water. The potential values are weighted according to the climate of the area using α, β, γ and σ to obtain the so called climatically appropriate for existing conditions (CAFEC) potential values. The four coefficients are called water- balance coefficients and are found as follows:

$$\alpha_i = \frac{\overline{ET_i}}{\overline{PE_i}} \tag{7.1}$$

$$\beta_i = \frac{\overline{R_i}}{\overline{PR_i}} \tag{7.2}$$

$$\gamma_i = \frac{\overline{RO_i}}{\overline{PRO_i}} \tag{7.3}$$

$$\sigma_i = \frac{\overline{L_i}}{\overline{PL_i}} \tag{7.4}$$

Where i is the month and the bar over the values suggest an average value over all the time period. From potential values and water-balance coefficients the so called CAFEC precipitation $\hat{\mathrm{P}}$ is calculated which is assumed to represent the amount of precipitation needed to maintain a normal soil moisture level for certain month.

$$\hat{P} = \alpha_i PE + \beta_i PR + \gamma_i PRO - \sigma_i PL \tag{7.5}$$

Moisture departure thus is then the difference between actual precipitation P fell in a specific month and $\hat{\mathrm{P}}$.

$$d = P - (\alpha_i PE + \beta_i PR + \gamma_i PRO - \sigma_i PL) \tag{7.6}$$

The moisture departure d is mainly used in calculating PDSI for different regions and for different times. Given that same d will mean different things at different times and location, straight forward comparisons could not be made. To correct for this W.C.Palmer (1965) suggest weighting d with K, the climatic characteristic. K corrects for the deviations in values of d due to climate of the region. The resulting index is called moisture anomaly index and is the measure of wetness or dryness during a single month.

$$Z = dK \tag{7.7}$$

Using Z for month i, the PDSI for corresponding month is thus calculated as:

$$X_i = 0.897X_{i-1} + \left(\frac{1}{3}\right) Z_i \tag{7.8}$$

All the weighting factors (W.C.Palmer (1965) calls them the duration factors) in above equation and in estimating values for K are empirically derived by W.C.Palmer (1965) but are frequently treated as fixed parameters regardless of the climate regime in which the index is computed (Wells et al., 2004). The following limits for PDSI were finally set.

Table 7.1.: Classification of PDSI.

PDSI values	Category
Above 4.00	Extreme wet spell
3.00 to 3.99	Severe wet spell
2.00 to 1.99	Moderate wet spell
1.00 to 1.99	Mild wet spell
0.50 to 0.99	Incipient wet spell
0.49 to −0.49	Normal
−0.50 to −0.99	Incipient drought
−1.00 to −1.99	Mild drought
−2.00 to −2.99	Moderate drought
−3.00 to −4.99	Severe drought
Below −4.99	Extreme drought

7.4. Application of PDSI to raw RCM and downscaled RCM data

A FORTRAN-90 routine was written based on above methodology and applied to all data sets. Both Observational gridded data set and RCM (control and SRES A1B

scenario) datasets were analyzed for drought situations in German part of Rhine basin. Figure 7.1 shows the yearly averaged PDSI values for observational and control run of all RCMs for one randomly selected grid point of Rhine basin. Observed historical floods (summer floods of 1965, 1968, and 1995) and droughts/major heat waves (1964,1976,1991) within 1960 and 2000 are captured by PDSI. Major European heat wave of 2006 is also captured by PDSI but is not shown in Figure 7.1. The control runs of RACMO, REMO and HadRM mimics the observed record to different degrees. For example although the drought of 1964 is captured by RACMO and REMO, both the models seem to miss the timing of 1991 drought. HadRM seem to miss completely these droughts. Similarly for floods the three control runs although capture the summer floods of 1965 and 1966, they seem to highly exaggerate and portray extreme wet conditions in other wise relatively less wet conditions.

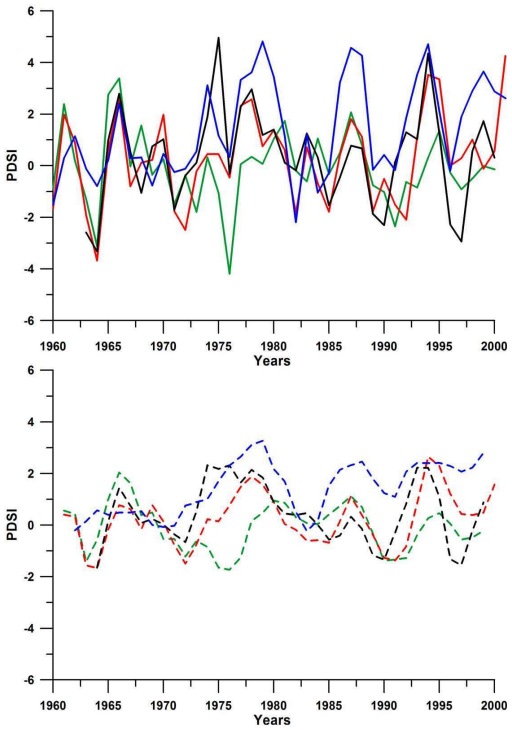

Figure 7.1.: Yearly averaged PDSI values of observational gridded data set (green) and control runs of RACMO (red), REMO (black) and HadRM (blue) datasets. PDSI values are on top and running average of the same based on 3 year window are on bottom. The values are for one randomly selected grid point in German part of Rhine basin.

Figure 7.1 showed the time series of PDSI at one randomly selected location. To look at the spatial behavior of all RCMs for extreme flooding and drought years, Figures 7.2 and 7.3 are presented for floods and droughts respectively. Three historically wet years of 1965, 1966 and 1995 are shown in Figure 7.2 for observational gridded data set and for control runs of three RCMs. According to calcualted PDSI 1965 and 1966 were moderate to extreme wet years for German part of Rhine basin.

While all RCMs portray the same thing for 1966, they fail to mimic the observed meteorological situation for 1965 and the severely wet year is classified as slightly wet. The situation for 1995 winter floods of river Rhine is different where all RCMs highly exaggerate the wetness.

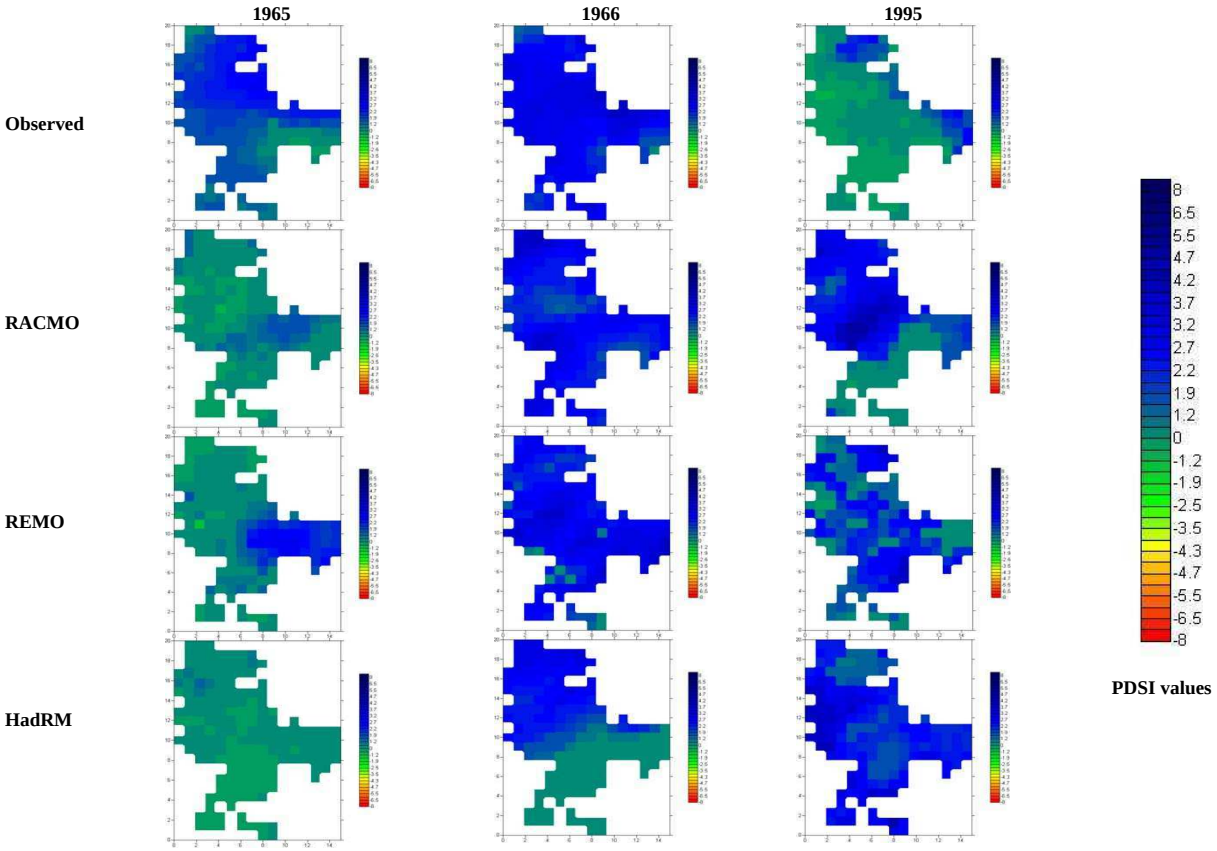

Figure 7.2.: Calculated PDSI for three extremely wet years of German part of Rhine basin. PDSI based on observational gridded data set and control runs of three RCMs are shown.

Considering the historical dry years of 1964, 1976 and 1991, one can see in Figure 7.3 that RCMs generally tend to simulate more wet conditions than they really are. Moderate to severe droughts of 1964, 1976 and 1991 are simulated by control runs of RACMO, REMO and HadRM as incipient to slightly dry situation.

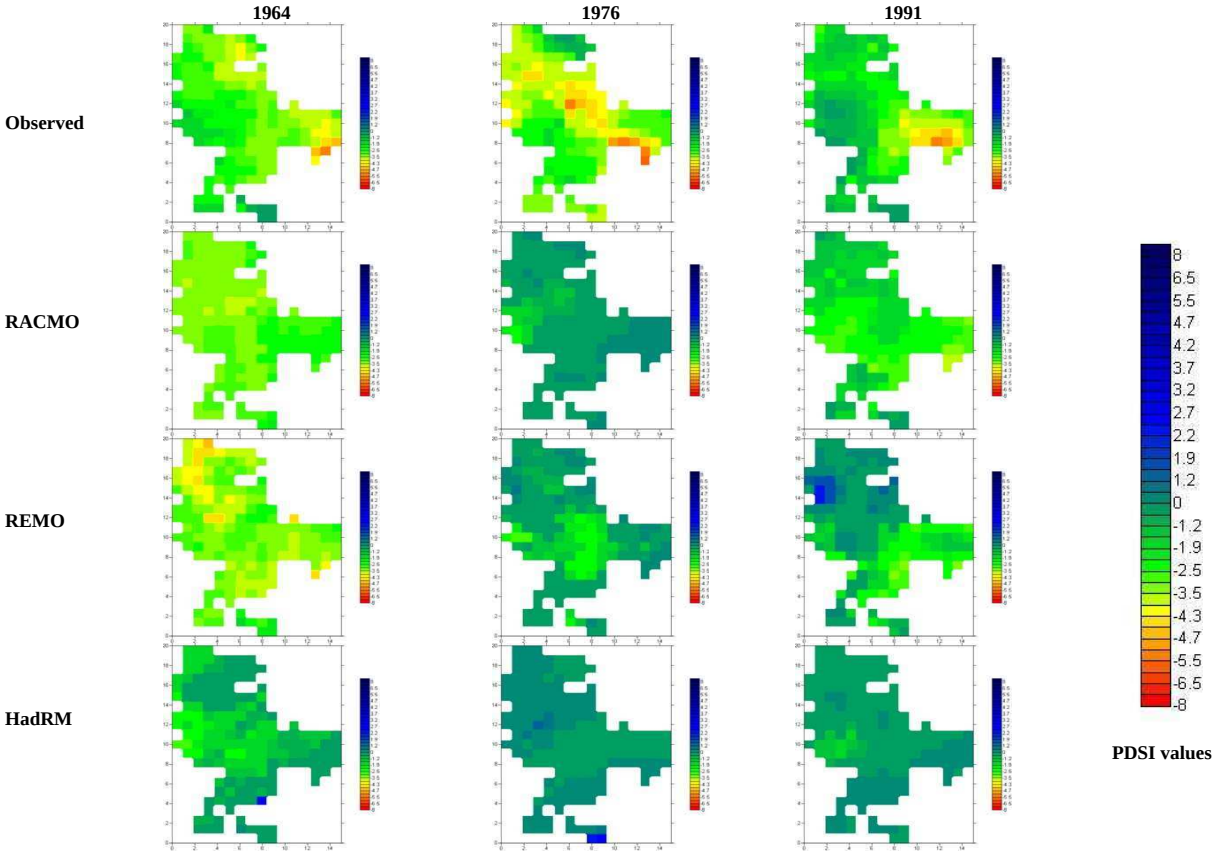

Figure 7.3.: Calculated PDSI for three extremely dry years of German part of Rhine basin. PDSI based on observational gridded data set and control runs of three RCMs are shown.

Figure 7.4 shows PDSI calculated for all RCMs' SRES A1B scenario. Downscaled precipitation and temperature are also analyzed for PDSI and plotted in the same figure. The monthly PDSI values at each grid point are averaged to get one yearly PDSI value for each grid and then for each year all grid points values are averaged to get one PDSI value for whole German part of Rhine basin. Understandably all RCMs have different time series for PDSI but the common thing is the similarity in the fitted linear trend line. All RCMs tend to forecast more drier conditions for German part of Rhine basin. The same result was also reached to when occurrence frequencies of combined dry circulation patterns were plotted for the same RCMs in chapter 5. HadRM SRES A1B scenario show more fluctuation in PDSI than RACMO and REMO.

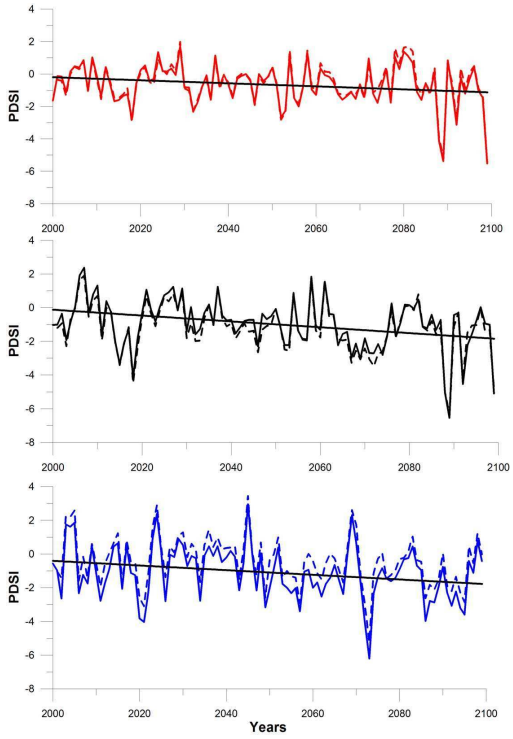

Figure 7.4.: Time series of PDSI for all raw and downscaled RCM data sets. RACMO is shown on the top, REMO in the middle and HadRM in the bottom. PDSI based on downscaled data are shown as dashed lines and linearly fitted trend line is shown as solid black line in all three plots.

8. Application of raw and downscaled RCM information to hydrological model

8.1. Preface

This chapter presents a brief introduction to the distributed version of conceptual hydrological model HBV used in this thesis. Model is calibrated for German part of Rhine basin and raw RCM data and downscaled RCM data are fed to calibrated model to analyze the change in hydrological regime of this important European river.

8.2. HBV model

HBV is a multi-purpose conceptual hydrological model. It has been widely used in different climatic regions of the world for different objectives such as flood forecasting, hydro power plant planning, hydraulic structure designing, pollutant transport and irrigation planning. It is also been widely used for climate change impacts on hydrological regimes of rivers.

The model was initially developed for comparatively smaller catchments in Sweden for rainfall-runoff modeling at Hydrologiska Byråns Vattenbalansavdelning (Hydrological water balance section, former section of Swedish Meteorological and Hydrological Institute SMHI). The name of the model HBV is adapted from institute name where it was developed. According to SMHI [1] website, different versions of HBV have been developed in over 40 countries for specific purposes. Bergström (1976), Bergström (1995) and Lindström (1997) provide the particulars of original and improved HBV model in detail. An independent version of HBV is also maintained and continuously developed at Institute of hydraulic engineering, Stuttgart University (IWS-STU). The model is used for water balance studies, rainfall-runoff modeling and climate change impact studies for German rivers like Neckar, Rhine, Rems etc. The developments made in HBV model at IWS-STU can be found in Yi (2008) and Hundecha and Bárdossy (2004). Distributed version of HBV model is further developed in this thesis to cater for the inflow into Rhine river and is adapted to the 25Km square grid. Below are the salient features of HBV described.

[1] http://www.smhi.se/sgn0106/if/hydrologi/hbv.htm

8.3. HBV Model description

HBV model describes the itinerary of water from atmosphere to the surface of earth and below. The model tries to simulate the natural flow of water on the surface of earth and part of water going into deeper earth taking into account the change in its state and its dependence on temperature. An attempt has been made to translate the natural processes into mathematical formulae by developing smaller interacting routines for snow accumulation and snow melt depending upon temperature, soil moisture accounting, evapotranspiration, production of runoff and finally routing of flow between subcatchments. As such the input data required to run the model are observations of precipitation and temperature and long term estimates of mean evapotranspiration of the area. Daily time step is used for the mentioned data. Like all hydrological models, HBV is based on water balance equation:

$$P - ET - I - Q = SP + SM + GWS_u + GWS_l + SurS \tag{8.1}$$

Where P is precipitation, ET is evapotranspiration, I is interception, Q is runoff, SP is snow pack, SM is soil moisture, GWS_u is upper groundwater storage, GWS_l is lower groundwater storage and $SurS$ is surface storage. The main processes of the model described below are adapted mainly from Yi (2008).

8.3.1. Snow accumulation and snow melt process

This routine mainly caters for the state of water once it reaches earth surface. Depending on air temperature, the routine either accumulates the incoming precipitation as snow to already existing snow pack, or starts the melting process and add to runoff. The decision between either of the two options is reached to using degree day approach. For snow melt to occur a threshold temperature(TT) is set which need to be exceeded by air temperature. Hundecha and Bárdossy (2004) also included the effect of additional energy introduced by falling rainfall that may increase the snow melt rate. Degree day factor is then modified as a linear function of precipitation.

$$S_{melt} = DD(T - TT) \tag{8.2}$$

Where S_{melt} is snow melt in $[mm/day]$, DD is degree day factor in $[mm/^{\circ}C.day]$, T is daily average air temperature in $[^{\circ}C]$ and TT is the threshold temperature again in $[^{\circ}C]$.

$$DD = \begin{cases} DD_{\circ} + kP, & \text{if } P \leq \frac{D_{max} - DD_{\circ}}{k}; \\ D_{max}, & \text{else.} \end{cases} \tag{8.3}$$

Where D_{max} is maximum limit to the degree day factor in $[mm/^{\circ}C.day]$ and is used to avoid unrealistically high snow melt during intense rainfall event, $DD_{\circ}$ is degree day factor in the absence of rainfall in $[mm/^{\circ}C.day]$, k is positive constant coefficient with units $[(^{\circ}C.day)^{-1}]$ and P is the daily precipitation amount with units $[mm]$.

8.3.2. Soil moisture process

In any precipitation event not all precipitation reaches the ground surface and affects the soil moisture. Some parts of precipitation is intercepted before it reaches the ground mainly by vegetation along with other factors. Given that vegetation is the main factor of interception, fixed values of interception are defined for each land use and month. It is assumed that if $T \leq TT$ then there would be no interception and total precipitation amount would be considered in soil moisture accounting process. Precipitation must be corrected before using in soil moisture equation in case if there is intercepted precipitation. The relationship between runoff formation R in $[mm]$ and precipitation is described as follows:

$$\frac{R}{P-I} = \left(\frac{SM}{FC}\right)^{\beta} \tag{8.4}$$

Where I is intercepted water storage, SM is actual soil moisture and FC is field capacity. All three are in $[mm]$. β is model a parameter.

8.3.3. Evapotranspiration

ET is calculated using a product of long term mean monthly average ET and adjusted coefficient. The adjusted coefficient in turn is made up of product of difference of daily temperature and long term mean monthly temperature and a model parameter. The parameter in evaptranspiration formula takes into account vegetation and elevation etc.

$$PE_A = (1 + C_{ET}(T - T_M))PE_M \tag{8.5}$$

Where PE_A and PE_M are daily potential evapotranspiration and long term mean monthly evapotranspiration in units of $[mm/day]$ and $[mm/month]$. T and T_M are mean daily and long term mean monthly air temperature in units $[^{\circ}C]$ while C_ET is a model parameter with units $[(^{\circ}C)^{-}1]$.

In case if intercepted precipitation is greater than 0, then it would also contribute to evapotranspiration such that:

$$E_{int} = min(I_{act}, PE_A) \tag{8.6}$$

Where E_{int} and I_{act} are evaporation from intercepted storage and total amount of intercepted storage respectively. Both have $[mm/day]$ as units. So PE_A can now be adjusted taking into account E_{int} as:

$$P\acute{E}_A = PE_A - E_{int} \tag{8.7}$$

Finaly ET can be obtained as:

$$ET = \begin{cases} min(SM, P\acute{E}_A), & \text{if } SM > PWP; \\ min(SM, \frac{SM}{LP}P\acute{E}_A), & \text{else.} \end{cases} \tag{8.8}$$

Where PWP is the minimum soil moisture at which plant wilts. This is the minimum SM at which potential ET takes place from the soil water.

8.3.4. Runoff production and concentration process

The HBV-IWS model uses two reservoirs system for runoff generation. The two reservoirs, upper and lower reservoir, arranged one above the other are connected to each other through a constant percolation rate and are considered linear with a constant recession coefficient. The upper reservoir has two outlets, one above the other, simulating near surface runoff ($Q_\circ$) and interflow (Q_1) respectively. The two outlets of upper reservoirs are separated by threshold depth, exceeding which the reservoir starts outflow from upper outlet. The lower reservoir simulates the baseflow (Q_2) and takes input from the upper reservoir as percolation flow (Q_{perc}). The outflow equations follow Darcy's flow and are outlined below as:

$$Q_\circ = \begin{cases} \frac{1}{K_\circ}\left(S_u - L\right)A, & \text{if } S > L; \\ 0, & \text{else.} \end{cases} \tag{8.9}$$

$$Q_1 = \frac{1}{K_1} S_u A \tag{8.10}$$

$$Q_{perc} = \frac{1}{K_{perc}} S_u A \tag{8.11}$$

$$Q_2 = \frac{1}{K_2} S_l A \tag{8.12}$$

Where $K_\circ$, K_1, K_{prec} and K_2 are the recession coefficients for each outflow in $[(day)^-1]$ units, all outflows are in $[m^3/day]$ units, S_u, S_l and L are upper reservoir water level, lower reservoir water level and threshold water level for near surface flow to occur respectively. A is the catchment area.

The three runoffs are added to have a combined value and smoothed by a triangular transformation function. The base of the function is defined with a parameter called $MAXBAS$ [days], which approximates the delayed time required for runoff concentration at the outlet of the catchment.

$$Q = g(t, MAXBAS)(Q_\circ + Q_1 + Q_2) \tag{8.13}$$

Finally Muskinghum method of routing is applied to route the flow between the catchments.

8.4. Results

HBV model was calibrated for German part of Rhine basin from 1981-1990, while validation was performed for the years 1991-1995. Grid points used for the distributed HBV model are shown in Figure 8.1. These are the same grid points that were used for CP classification and downscaling. The inflow into Rhine river system was considered at Rheinfelden while outflow, against which the system was calibrated and validated, was considered at Lobith on German-Netherlands border (Figure 8.1). Observed daily discharge data was obtained from Global runoff data

center (GRDC) [2]. The mean river flow at the two locations is 1070 m^3/sec and 2480 m^3/sec respectively. The model was first calibrated using daily precipitation and temperature data obtained from ENSEMBLES RT5's observational gridded data set (Sec. 4.1.2). After validating the model, gridded precipitation and temperature data obtained from control runs of three RCMs i.e. RACMO, REMO and HadRM were also analyzed for their behavior in reproducing the observed daily discharge. Figure 8.2 shows the time lines of observed and simulated daily discharge at Lobith for the whole calibration and validation process and also for one year alone from the two series. Observational gridded data set of RT5 seem to capture the dynamics of daily river flow. This is confirmed by Nash-Sutcliffe (NS) coefficient (Nash and Sutcliffe, 1970) of 0.70 and correlation of 0.84 between observed and simulated discharge. The calibration year 1988 time series shows that simulated runoff tend to under estimate the peaks while simulating the low flow periods efficiently. During validation process both the NS coefficient and correlation improves further for observational gridded data set. Validation for control runs of all RCMs shows that NS coefficient decreases while correlation improves marginaly. Table 8.1 tabulates the basic calibration and validation statistics.

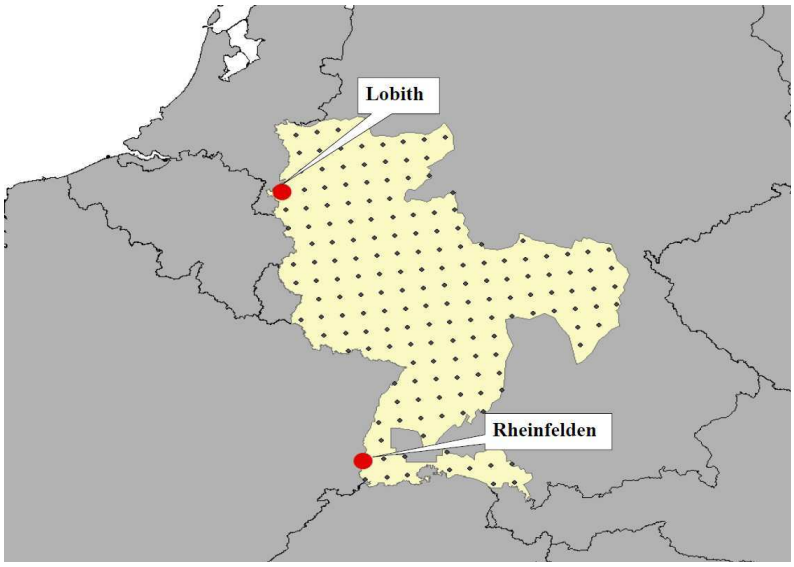

Figure 8.1.: Considered grid points in German part of Rhine basin for hydrological modeling and location of Rheinfelden and Lobith.

Among the three RCMs, RACMO and REMO simulate the dynamics of observed daily discharge better than HadRM. HadRM simulates a hydrological regime of river Rhine that is quite different than observed, RACMO and REMO based simulations. The difference is more clear when validation results for year 1995 (flood year) are observed. RACMO and REMO capture the flood of 1995 to some extent both in magnitude and timing. HadRM on the other hand seem to miss this particular flood. The basic discharge based statistics of observed and simulated daily discharge are shown in Figure 8.3 and Figure 8.4 for calibration and validation runs of the model. The model simulates yearly statistics of mean, minimum and maximum

[2] http://www.bafg.de/GRDC/EN/Home/homepage__node.html

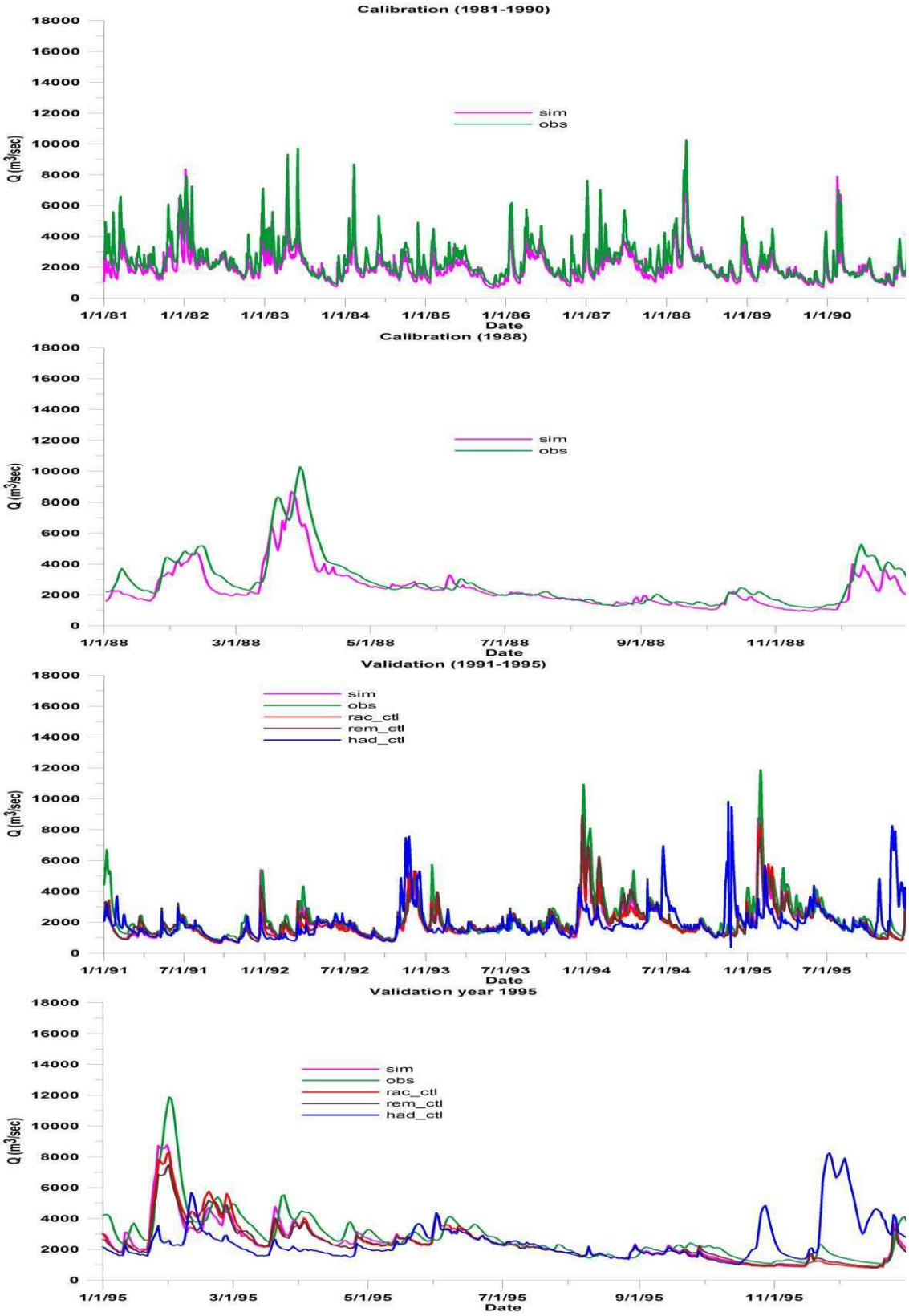

Figure 8.2.: Time series of observed and simulated discharge during calibration and validation for observational gridded data set and control runs of all RCMs. For a closer look, a time series of only one year both from calibration and validation time periods are also shown.

satisfactorily. The yearly difference between the 75^{th} and 25^{th} quantiles are not that skillfully simulated. During validation on the other hand, except maximum yearly discharge all other basic statistics are simulated satisfactorily.

Table 8.1.: Basic statistics for calibration and validation process of HBV model for German part of Rhine basin.

Data set	Obs. mean	Obs. Std.	Sim. mean	Sim. Std.	NS	Corr.
Calibration (1981-1990)						
Obs.gridded data set	2480.89	1274.04	2409.37	1011.45	0.70	0.84
Validation (1991-1995)						
Obs.gridded data set	2220.98	1321.74	2338.31	1116.67	0.74	0.86
RACMO-ctl	2220.98	1321.74	1860.55	1005.00	0.68	0.87
REMO-ctl	2220.98	1321.74	2011.44	1038.98	0.73	0.87
HadRM-ctl	2220.98	1321.74	1962.80	1233.06	-0.44	0.25

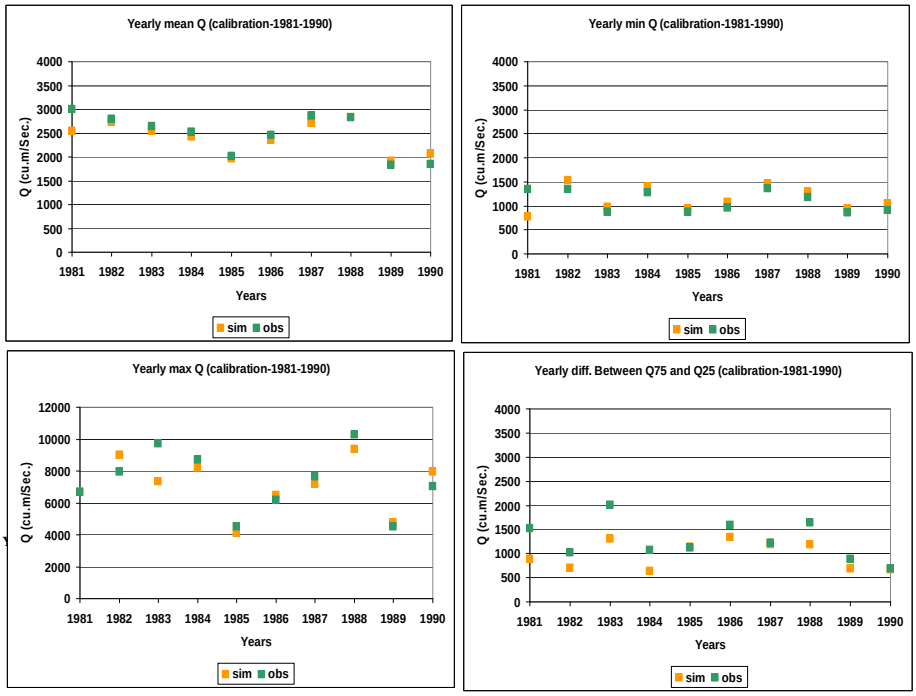

Figure 8.3.: Yearly mean, minimum, maximum and difference between the 75^{th} and 25^{th} quantiles of observed and simulated discharge during calibration.

SRES A1B scenarios of daily precipitation and temperature of all three RCMs were then fed to the HBV model to analyze the resulting discharges of river Rhine. The model was run from 2001 to 2099. Unlike RACMO and REMO which provide

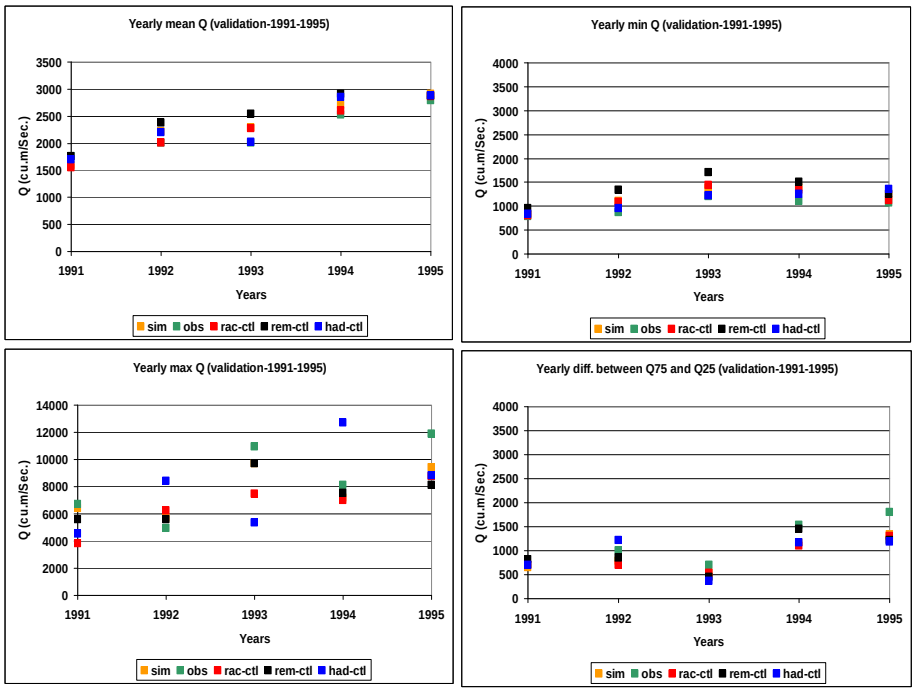

Figure 8.4.: Yearly mean, minimum, maximum and difference between the 75^{th} and 25^{th} quantiles of observed and simulated discharge during validation.

one realization of future, HadRM provides three realization of precipitation and temperature based upon model's sensitivity to increase in CO_2 concentrations. Low, normal and high climate sensitivity runs of HadRM were analyzed for hydrological regime behavior. Although the model was run from 2001-2099, results below are presented for two selected time periods of 30 years each from 2001-2030 and 2070-2099. Table 8.2 provides the mean and standard deviation of daily discharge for the three SRES A1B scenarios. It can be seen that all three models predict increased mean daily discharge for Rhine river in future. The increase in later 30 years is more than the initial 30 years of 21st century.This behavior of increased discharge is in accordance with analysis of SRES A1B precipitation simulation of all RCMs except for the normal and high climate sensitivity runs of HadRM. The increased precipitation amounts is understandably translated into increased discharge.

Table 8.3 and 8.4 tabulates the mean and standard deviations of unconditional and CP conditioned downscaled precipitation and temperature based results. The downscaled precipitation and temperature scenarios, result in the increase of mean daily discharge both for unconditional and CP conditioned downscaling procedure. The difference between the two downscaling procedures in terms of mean daily discharge is not that big but differs considerably from raw SRES A1B scenarios. Looking at Figure 8.5 and 8.6 on the other hand, it can be seen that among different RCMs the yearly mean, minimum, maximum and variance vary considerably. The results from downscaled precipitation and temperature closely follow the raw RCM based results. For RACMO and REMO, the downscaling process results in yearly mean, maximum and minimum values which are larger than raw RCM based results, while

Table 8.2.: Basic statistics of daily simulated discharge obtained from SRES A1B scenarios of daily precipitation and temperature of RACMO, REMO and HadRM for German part of Rhine basin.

Data set	Sim. mean	Sim. Std.
SRES A1B scenario (2001-2030)		
RACMO	2302.81	1110.72
REMO	2309.14	1054.17
HadRM (low cli. Sens.)	2183.61	1010.28
HadRM (normal cli. Sens.)	2398.39	1058.81
HadRM (high cli. Sens.)	2455.62	1087.69
SRES A1B scenario (2070-2099)		
RACMO	2511.60	1202.46
REMO	2416.55	1113.54
HadRM (low cli. Sens.)	2204.25	982.66
HadRM (normal cli. Sens.)	2373.91	1054.72
HadRM (high cli. Sens.)	2312.01	1059.70

for HadRM the same are lower than raw RCM results. This perhaps is because CP based downscaling process corrected the precipitation and temperature values for bias in different directions for different RCMs.

Table 8.3.: Basic statistics of daily simulated discharge obtained from unconditional downscaling of SRES A1B scenarios of daily precipitation and temperature of RACMO, REMO and HadRM for German part of Rhine basin.

Data set	Sim. mean	Sim. Std.
SRES A1B scenario (2001-2030)		
RACMO	2496.48	1186.51
REMO	2320.17	1054.17
HadRM (low cli. Sens.)	1881.05	800.83
HadRM (normal cli. Sens.)	2047.23	874.84
HadRM (high cli. Sens.)	2098.97	860.00
SRES A1B scenario (2070-2099)		
RACMO	2686.27	1286.39
REMO	2406.73	1104.25
HadRM (low cli. Sens.)	1899.27	771.38
HadRM (normal cli. Sens.)	2015.01	827.20
HadRM (high cli. Sens.)	1960.61	808.78

Table 8.4.: Basic statistics of daily simulated discharge obtained from CP conditioned downscaling of SRES A1B scenarios of daily precipitation and temperature of RACMO, REMO and HadRM for German part of Rhine basin.

Data set	Sim. mean	Sim. Std.
SRES A1B scenario (2001-2030)		
RACMO	2550.44	1264.90
REMO	2390.00	1102.38
HadRM (low cli. Sens.)	1973.58	891.76
HadRM (normal cli. Sens.)	2139.66	958.30
HadRM (high cli. Sens.)	2191.63	961.61
SRES A1B scenario (2070-2099)		
RACMO	2717.47	1352.28
REMO	2465.97	1154.38
HadRM (low cli. Sens.)	1993.87	869.70
HadRM (normal cli. Sens.)	2098.42	932.73
HadRM (high cli. Sens.)	2037.18	900.33

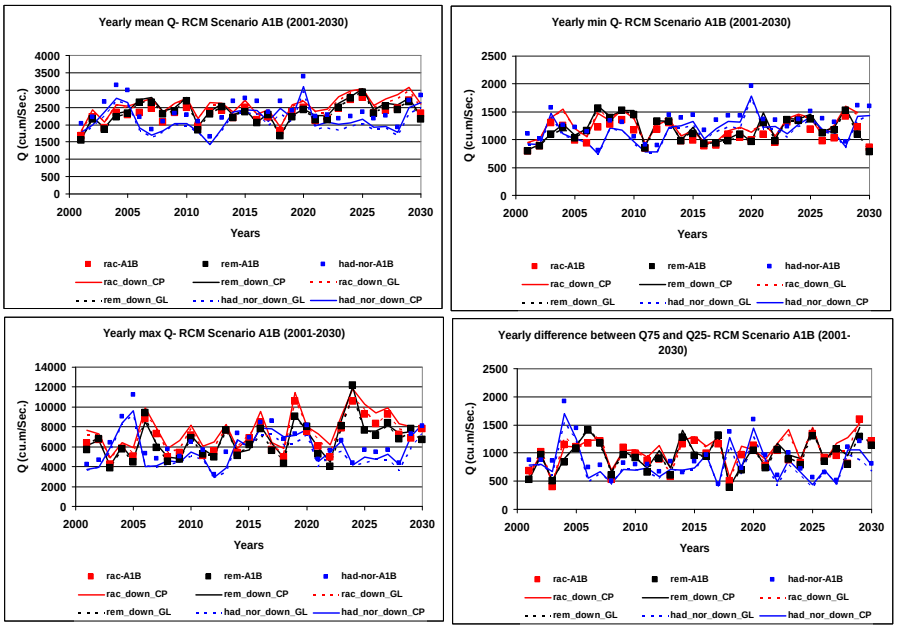

Figure 8.5.: Yearly mean, minimum, maximum and difference between the 75^{th} and 25^{th} quantiles of observed and simulated discharge for raw and downscaled RCM data. Raw RCM based results are shown as blocks, unconditioned downscaled as dashed line and CP conditioned downscaled as solid line. RACMO is in red, REMO in black and HadRM in blue. The results are from 2001-2030.

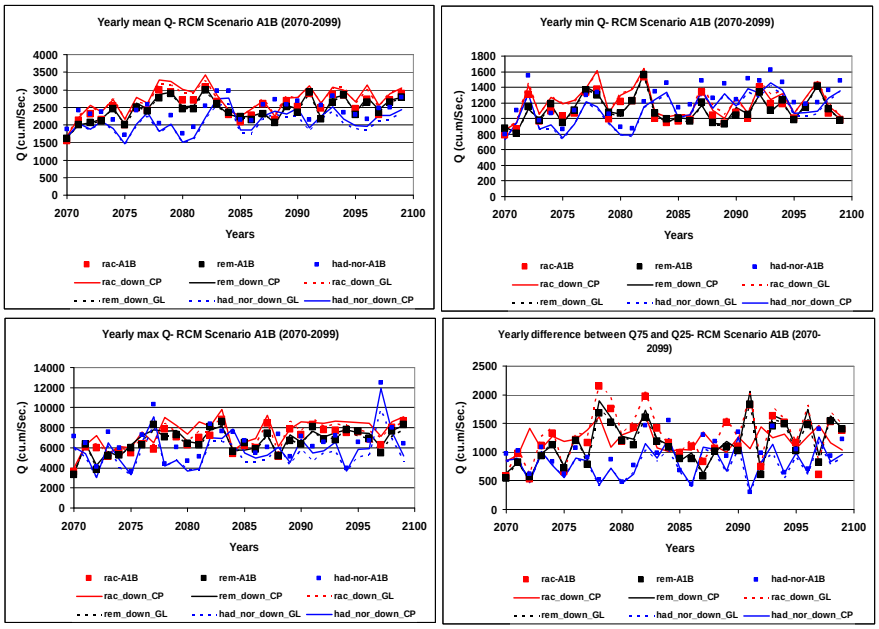

Figure 8.6.: Yearly mean, minimum, maximum and difference between the 75^{th} and 25^{th} quantiles of observed and simulated discharge for raw and downscaled RCM data. Raw RCM based results are shown as blocks, unconditioned downscaled as dashed line and CP conditioned downscaled as solid line. RACMO is in red, REMO in black and HadRM in blue. The results are from 2070-2099.

8.5. Conclusions

Observational gridded dataset, control, SRES A1B and downscaled SRES A1B scenarios of three RCMs were analyzed for the daily discharge of river Rhine at Lobith. Control runs of all three RCMs underestimate the mean daily discharge at Lobith. Analyzing the daily discharge values for 2001-2099 time period, each RCM result in increased discharge from its corresponding control run during initial time period of 2001-2030. RACMO, REMO and three climate sensitivity runs of HadRM (low, normal and high) increase by 23%, 14%, 11%, 22%, and 25%. For the later period of 21st century the increase is more for RACMO, REMO and low climate sensitivity run of HadRM, with the percent increase of 35%, 20%, 12%, 20%, and 17% in the same order of RCMs. The downscaling process result in further increase of daily mean discharge at Lobith, with CP conditioned downscaling process bring in more water than unconditional downscaling of precipitation and temperature. The increase though is not considerable. The increased discharge in raw SRES A1B scenarios based results are in perhaps becasue of the increase in temperature in 21st century. The increase in temperature results in increased snow melt in Alpine regions of Rhine basin thus increasing the discharge in winter. This automaticaly results in damped increase in summer.

9. Conclusions and Outlook

9.1. Conclusions

This thesis presented an improved methodology for circulation pattern classification. Additionally different information measures were developed which help in quantifying worth of classification system. Critical circulation patterns were identified from set of circulation patterns using wetness index. Classification pattern methodology was improved using new objective functions based on daily precipitation and discharge values. While the former was used to identify the coverage extent of certain precipitation event, low values of the later were used to identify the equilibrium state of catchment and use it as an objective function. The resulting classification of circulation patterns was found to be robust and representative in that extreme hydrological situations such as flood and droughts were represented in them. The classification system was tested on completely independent data sets and was found to capture the extreme situation efficiently. Classification scheme was further used in future scenarios of different RCMs and frequency analysis were made with regards to occurrence of critical CPs. It was concluded that comparing with earlier periods of 21^{st} century, there would be more occurrence of dry period in the later part of 21^{st} century.

A new statistical downscaling methodology was also developed with the main aim of removing bias from RCM simulated data sets. The downscaling methodology was conditioned upon previously achieved classified set of circulation patterns. It was shown how different RCMs produce different realization of past observed precipitation amounts and that perhaps that was because of bias that each RCM inherits from driving parent GCM. Downscaling methodology was applied to three different RCMs, comprising of five gridded data sets of precipitation and temperature. Downscaling of data was performed both in "Global mode" and in "CP conditioned" mode. Investigation were made with regards to the difference in precipitation amount change that each methodology brings in RCM simulation.

A FORTRAN-90 code was developed based on Palmer drought severity index to analyze the data for extreme situations in future. All gridded data sets were analyzed for drought severity and it was concluded (and earlier findings confirmed) that in later 21^{st} century there would be more occurrences of dry periods in the study area.

A distributed version of conceptual hydrological model was calibrated for German part of Rhine basin and raw and downscaled precipitation and temperature scenarios were analyzed for possible hydrological regime change in the study area.

9.2. Outlook

Although the results obtained from the new improved classification methodology were quite encouraging, there are, as always, certain possibilities that can make the process even more effective. One possibility would be to add to the existing methodology the concept of data depth. Data depth is a statistical technique developed originally by Tukey (1975) to order multivariate data sets. The details of the methodology and its usage in hydrological studies can be found in Zhang (2002) and Chebana and Ouarda (2008) respectively. Briefly, the methodology assigns greater depth to points which are deeper inside the data cloud and assigns lower depth to ones on peripheries. Hence unusual data points can be identified from the cloud. Given that the circulation patterns are defined by the anomalies of large scale predictor such as mean sea level pressure at certain locations, the anomalies can be ordered with respect to observed precipitation at the same location. Data depth technique would be useful in a sense that one can order multi-dimensional data (e.g. mean sea level pressure data obtained from multiple grid points around precipitation station) with respect to precipitation at the same time. Ordering of multi-variate data of more than two dimensions is always a difficult task. With this technique one can attempt (and has been attempted by this author) to order multi-variate data set with nine dimensions. Specific to circulation pattern classification methodology, If one only consider the mean sea level pressure anomalies of already defined critical circulation pattern, and order the data with respect to precipitation amounts, one can practically filter out even more critical days out of already declared/identified critical days. Hence additional condition with respect to certain days' anomaly depth can be put during classification methodology which can help for forecast purposes.

There is also a possibility of using other large scale predictors than mean sea level pressure. It has been reported and and also mentioned Chapter 3, that role of some of the large scale predictors which are not used in the training period of the downscaling methodology might be more important in the future perturbed climate (e.g. humidity). Hence the statistical relationship developed during the training period may not hold to the same degree in the future. One of the selection criteria of large scale predictor is that it should be reliably simulated by GCM. Geopotential height is one of the possibility that can be used as large scale predictor. Given that geopotential height is available at different pressure levels, multiple levels can also be considered (e.g. by considering difference of geopotential height obtained from two adjacent pressure levels) in downscaling methodology.

During quantile-quantile correction of RCM precipitation, Weibull distribution was used in this thesis. The parameters for which were estimated for each grid point and season (summer and winter). We were lucky in a sense that we had to deal with an area where the climatic conditions are not very different from each other. Assuming an area where available data are not on such a high resolution as we had the luxury to use, and climate which changes significantly due to topography of the area, it would not have been easy to find a distribution which fits all the climate conditions. An alternate way then to make use of quantile-quantile correction of RCM (or GCM) precipitation methodology is to use non-parametric distribution. One possibility of

fitting a non-parametric distribution to the data set is the so called Kernel density estimation. The advantage in comparison with the theoretical or empirical distribution are that Kernel distributions smoother and continuous. Additionally they cover the range of the values which exceeds the ones on which the Kernel densities were calculated. Hence practically one can deal with the values not simulated by RCM for which the quantile-quantile correction is intended.

Bibliography

Abaurrea, J. and Asín, J.: Forecasting local daily precipitation patterns in a climate change scenario, Climate Research, 28, 183–197, 2005.

Ahmed, S. and Marsily, G. D.: Comparison of Geostatistical Methods for Estimating Transmissivity Using Data on Transmissivity and Specific Capacity, Water resources research, 23, 1717–1737, 1987.

Anon: The 1975 Drought, Tech. rep., Welsh National Water Development Authority,Directorate of resource planning, 1977.

A.W.Wood, L.R.Leung, Sridhar, V., and Lettenmaier, D.: Hydrologic implications of dynamical and statistical approaches to downscaling climate model outputs, Climate change, 62, 189 – 216, 2004.

Bárdossy, A. and Filiz, F.: Identification of flood producing atmospheric circulation patterns, Journal of hydrology, 313, 48–57, 2005.

Bárdossy, A. and Plate, E. J.: Space time model for daily rainfall using atmospheric circulation patterns, Water resources research, 28, 1247–1259, 1992.

Bárdossy, A., Stehl/'ik, J., and Caspary, H.: Automated objective classification of daily circulation patterns for precipitation and temprature downscaling based on optimized fuzzy rules, Climate research, 23, 11–22, 2002.

Ben-Zvi, A.: Indices of hydrological drought in Israel, Journal of Hydrology, 92, 179–191, 1987.

Bergant, K. and Kajfez-Bogataj, L.: N-PLS regression as empirical downscaling tool in climate change studies, Theoretical and Applied Climatology, 81, 11–23, 2005.

Bergström, S.: Development and application of a conceptual runoff model for scandinavian catchments, Tech. Rep. RHO-7, Swedish Metereological and Hydrological Institute,Norrköping, Sweden, 1976.

Bergström, S.: "The HBV model" In Computer Models of Watershed Hydrology Edited by V.P.Singh, Water Resources Publications, Highlands Ranch, CO., 1995.

Biau, G., Zorita, E., von Storch, H., and Wackernagel, H.: Estimation of precipitation by kriging in the EOF space of the sea level pressure field, Journal of Climate, 12, 1070–1085, 1999.

Brandsma, T. and Buishand, T.: Statistical linkage of daily precipitation in Switzerland to atmospheric circulation and temperature, Journal of hydrology, 198, 98–123, 1997.

Breimann, L., Friedmann, J. H., Olsen, R. A., and Stone, J. C.: Classifications and Regression Trees, Wadsworth, Cambridge, 1984.

Brent, Y., Comrie, A. C., Frakes, B., and Brown, D. P.: Developments and prospects in synoptic climatology, International Journal of climatology, pp. 1923–1950, doi: 10.1002/joc.675, 2001.

Brinkmann, W.: Local versus remote grid points in climate downscaling, Climate Research, 21, 27–42, 2002.

Bronstert, A.: Encyclopedia of Hydrological Sciences, chap. 132, pp. 1–28, John Wiley and Sons, College Station, Texas, 2009.

Bürger, G.: Expanded downscaling for generating local weather scenarios, Climate Research, 7, 111–128, 1996.

Busuioc, A., Chen, D., and Hellström, C.: Performance of statistical downscaling models in GCM validation and regional climate change estimates: application for Swedish precipitation, International Journal of Climatology, 21, 557–578, 2001.

Calow, R., Robins, N., Macdonald, A., and Nicol, A.: Planning for ground water drought in Africa, in: Interdisciplinary international conference on integrated drought management, Pretoria, South-Africa, 1999.

Chebana, F. and Ouarda, T. B. M. J.: Depth and homogeneity in regional flood frequency analysis, Water resources research, 44, doi:10.1029/2007WR006 771, 2008.

Collins, M., Booth, B., Harris, G., Murphy, J., Sexton, D., and Webb, M.: Towards Quantifying Uncertainty in Transient Climate Change, Climate Dynamics, 27, 127–147, doi:10.1007/s00382-006-0121-0, 2005.

Cubasch, U., von Storch, H., Waszkewitz, J., and Zorita, E.: Estimates of climate changes in southern Europe using different downscaling techniques, Climate Research, 7, 129 – 149, 1996.

D., M.: The Europa-modell of the Deutscher wetterdienst, Tech. rep., ECMWF Seminar on Numerical Methods in Atmospheric Models, 2008.

D.C.Montgomery and Runger, G. C.: Applied statistics and probability for engineers, John Wiles and Sons, Inc., Arizona, 2002.

Dickinson, R., Errico, R. M., Giorgi, F., and Bates, G. T.: A regional climate model for western united states, climate change, 15, 383 – 422, 1989.

D.S.Wilks and R.L.Wilby: The weather generation game: a review of stochastic weather models, Progress in physical Geography, 23, 329–357, 1999.

E.L.Tate and Gustard, A.: Drought definition: A hydrological prespective, In Drought and Drought mitigation in Europe, chap. 2, pp. 23–48, Kluwer Academic Publishers, The Netherlands, 2000.

E.N.Lorenz: Atmospheric predictability as revealed by natural occurring analogues, Journal of atmospheric sciences, 26, 636 – 646, 1969.

Fieldhouse, D. and Palmer, W. C.: Meteorological and Agricultural drought, Tech. rep., University of Delaware, Agricultural Experiment Station,Delaware Bulletin 353, 1965.

Foufoula-Georgiou, E. and Lettenmaier, D.: A Markov renewal model for rainfall occurrences, Water Resources Research, 23, 875–884, 1987.

Fowler, H. J., Blenkinsop, S., and Tebaldi, C.: Linking climate change modelling to impact studies: recent advances in downscaling techniques for hydrological modelling, International journal of climatology, 27, 1547–1578, 2007.

Frei, C., Christensen, J. H., De´que´, M., Jacob, D., Jones, R. G., and Vidale, P. L.: Daily precipitation statistics in regional climate models:Evaluations and intercomparison for the European Alps, Jouranl of Geophysical research, 108(D3), doi:10.1029/2002JD002 287, 2003.

Frei, C., Schöll, R., Fukutome, S., Schmidli, J., and Vidale, P. L.: Future change of precipitation extremes in Europe:Intercomparison of scenarios from regional climate models, Jouranl of Geophysical research, 111, doi:10.1029/2005JD005 965, 2006.

Frére, M. and Popov, G.: Agrometerological crop monitoring and forecasting, FAO plant production and protection, pp. 1–64, 1979.

Giorgi, F. and Bates, G. T.: The climatological skill of a regional model over complex terrain, Monthly weather review, 117, 2325 – 2347, 1989.

Giorgi, F. and Mearns, L. O.: Introduction to special section:REgional climate modeling revisited, Journal of geophysical research, 104(D6), 6335 – 6352, 1999.

Grell, G., Schade, L., Knoche, R., Pfeiffer, A., and Egger, J.: Nonhydrostatic climate simulations of precipitation over complex terrain, Journal of Geophysical research, 105(D24), 29 595 – 29 608, 2000.

Grotch, S. and MacCracken, M.: The use of general circulation models to predict regional climatic change, Journal of climate, 4, 286 – 303, 1991.

Gumbel, E. J.: The Return Period of Flood Flows, The Annals of Mathematical Statistics, 12, 163–190, http://www.jstor.org/stable/2235766, 1941.

Haylock, M., Hofstra, N., Tank, A. K., Klok, E., and P.D. Jones, M. N.: A European daily high-resolution gridded dataset of surface temperature and precipitation, J. Geophys. Res (Atmospheres), 113, D20 119, doi:10.1029/2008JD10201, 2008.

Heyen, H., Zorita, E., and von Storch, H.: Statistical downscaling of monthly mean north Atlantic air-pressure to sea level anomalies in the Baltic Sea, Tellus Series A, Dynamic Meteorology and occeanography, 48, 312–323, 1996.

H.J.Fowler, Ekström, M., Kilsby, C. G., and Jones, P.: New estimates of future changes in extreme rainfall across the UK using regional climate model integrations 1.Assessment of control climate, Journal of Hydrology, 300, 212–233, 2005.

Houghton, J., Ding, Y., Griggs, D., Noguer, M., van der Linden, P., Dai, X., Maskell, K., and (eds.), C. J.: Climate Change 2001: The Scientific Basis. Contribution of Working Group I to the Third Assessment Report of the Intergovernmental Panel on Climate Change. Cambridge University Press, Cambridge, United Kingdom and New York, NY, USA , Tech. rep., Intergovernmental Panel on Climate Change, 2001.

Hulme, M.: climate change and south Africa an exploration of some potential impacts and implications for the SADCC region, Tech. rep., Climatic research unit, University of East Anglia,UK, 1996.

Hundecha, Y. and Bárdossy, A.: Modeling of the effect of land use changes on the runoff generation of a river basin through parameter regionalization of a watershed model, Journal of Hydrology, 292, 281–295, 2004.

Jacob, D.: A note to the simulation of the annual and inter-annual variability of the water budget over the Baltic Sea drainage basin, Meteorology and Atmospheric Physics, 77, 61 – 73, 2001.

Karl, T. R.: Climatological drought prediction, Proceedings of the Seminar and Workshop on Drought Management and Planning, pp. 9 – 16, Institute of agriculture and natural resources, University of Nebraska, 1991.

Katz, R. and Parlange, M.: Generalizations of chain dependent processes Application to hourly precipitation, Water resources research, 31, 1331 – 1341, 1995.

Katz, R., Parlange, M., and Naveau, P.: statistics of extremes in hydrology, Advances in water resources, 25, 1287 – 1304, 2002.

Lamb, H.: British Isles weather types and a register of daily sequences of circulation patterns 1861-1971, Geophysical Memoir, p. 85, 1972.

Laux, P.: Statistical modelling of precipitation for agriculutral planning in the Volta basin of West Africa, Ph.D. thesis, Universität Stuttgart, 2008.

Leung, R., L.O.Mearns, F.Giorgi, and R.L.Wilby: Regional Climate research:Needs and opportunities, Bulletin of the American Meteorological society, 84, 89 – 95, 2003.

Lindström, G.: A simple automatic calibration routine for the HBV model, Nordic Hydrology, 28, 153 – 168, 1997.

M. Noguer, R. J. and Murphy, J.: Sources of systematic errors in the climatology of a regional climate model over Europe, Climate Dynamics, 14, 691 – 712, doi: 10.1007/s003820050249, 1998.

McGregor, J.: Regional Climate modelling, Meteorology and Atmospheric Physics, 63, 105 – 117, 1997.

Mearns, L. O., Giorgi, F., Whetton, P., Pabon, D., Hulme, M., and M.Lal: Guidelines for use of Climate scenarios developed from Regional climate model experiments, Tech. rep., Intergovernmental Panel on Climate Change, 2003.

Meijgaard, E., van Ulft, L., van de Berg, W., Bosveld, F., van den Hurk, B., Lenderink, G., and Siebesma, A.: The KNMI regional atmospheric climate model RACMO, version 2.1, Tech. rep., KNMI, 2008.

Michel, D.: Frequency of precipitation and temperature extremes over France in an anthropogenic scenario: Model results and statistical correction according to observed values, Global and Planetary Change, 57, 16–26, 2007.

Nash, J. and Sutcliffe, J. V.: River flow forecasting through conceptual models part I-A discussion of principles, Journal of Hydrology, 10, 282–290, 1970.

Obled, C., Bontron, G., and Rémy, G.: Quantitative precipitation forecasts: a statistical adaptation of model outputs through an analogues sorting approach, Atmospheric research, 63, 303 – 324, 2002.

Petrasovits, I.: General review of drought strategies, Transactions of 14th congress on irrigation and drainage, 1, 1990.

Pfizenmayer, A. and Storch, H. V.: Anthropogenic climate change shown by local wave conditions in the north sea, Climate research, 19, 15 – 23, 2001.

Renard, B. and Lang, M.: Use of a Gaussian copula for multivariate extreme value analysis:Some case studies in hydrology, Advances in Water Resources, 30, 897 – 912, 2007.

R.G.Jones, J. and Noguer, M.: Simulation of climate change over Europe using a nested regional-climate model Part 1: Assessment of control climate, including sensitivity to locations of lateral boundaries, Quarterly journal of royal meteorological society, 121, 1413 – 1449, 1995.

R.L.Wilby: Statistical downscaling of daily precipitation using daily airflow and seasonal teleconnection indices, Climate research, 10, 163–178, 1998.

R.L.Wilby and T.M.L.Wigley: Precipitation predictors for downscaling: observed and general circulation model relationships, International Journal of Climatology, 20, 641–661, 2000.

R.L.Wilby, T.M.L.Wigley, D.Conway, P.D.Jones, B.C.Hewitson, J.Main, and D.S.Wilks: Statistical downscaling of general circulation model output: A comparison of methods, Water resources research, 34, 2995–3008, 1998.

Schubert, S.: Downscaling local extreme temperature changes in south-eastern Australia from the CSIRO Mark2 GCM., Journal of Climatology, 18, 1419 – 1438, 1998.

Schuepp, M.: Die Klassifikation der Wetterlagen im Alpengebiet, Geofis. Pura Appl., 44, 242 – 248, 1953.

Sen, Z.: Statistical analysis of hydrologic critical droughts, Journal of the Hydraulics Division, 106, 1980.

Storch, H. V.: Inconsistencies at the interface of climate impact studies and global climate research, Meteorol. Zeitschrift, 4 NF, 72 – 80, 1995.

Storch, H. V. and Zwiers, F.: Statistical analysis in climate research, Cambridge University Press, Cambridge, 1999.

T.A.McMahon and Diaz, A. A.: Methods of computation of low stream flow,Studies and reports in Hydrology, chap. 36, UNESCO press Paris, 1982.

Thornthwaite, C.: An approach towards a rational classification of climate, Geographical Review, 38, 55 – 94, 1948.

T.J.Chang and Stenson, J. R.: Is it realistic to define a 100-year drought for water management?, Water resources bulletin, 26, 823–829, 1990.

Tukey, J.: Mathematics and the picturing of data, Proceedings of the International Congress of Mathematicans, 2, 523 – 531, 1975.

van Lanen, H. and Peters, E.: Definitions, effects and assessment of groundwater droughts, Kulwer Academic Publishers, The Netherlands, 2000.

Watson, R., M.C.Zinyowera, and (Eds.), R. M.: Impacts, Adaptations and Mitigation of Climate Change: Scientific-Technical Analysis. Cambridge University Press,UK, Tech. rep., Intergovernmental panel on climate change, 1995.

W.C.Palmer: Meteorological Drought, Tech. rep., U.S. Weather Bureau, Washington D.C., 1965.

Wells, N., Goddard, S., and Hayes, M.: A self-calibrating Palmer drought severity index, Journal of Climate, 17, 2335–2351, 2004.

Widmann, M., Bretherton, C., and Jr., E. P. S.: Statistical Precipitation Downscaling over the Northwestern United States Using Numerically Simulated Precipitation as a Predictor, Journal of climate, 16, 799–816, 2003.

Wilks, D.: Multisite generalizations of a daily stochastic precipitation generation model, Journal of Hydrology, 210, 178–191, 1998.

Wilks, D.: Interannual variability and extreme value characteristics of several stochastic daily precipitation models, Agricultural and forest Meteorology, 93, 153–169, 1999.

Winkler, J., J.P.Palutikof, J.A.Andresen, and C.Goodess: The simulation of daily temperature time series from GCM output. Part II: Sensitivity analysis of an empirical transfer function methodology, Journal of Climate, 10, 2514–2532, 1997.

Woolhiser, D. and Pegram, G.: Maximum likelihood estimation of Fourier coefficients to describe seasonal variations of parameters in stochastic daily precipitation models, Journal of Applied Meteorology, 18, 34 – 42, 1979.

X.Cheng and Wallace, J. M.: Cluster analysis of the Northern Hemisphere wintertime 500-hPa height fields: Spatial patterns., Journal of atmospheric sciences, 50, 2647–2696, 1993.

Xu, C.-Y.: Climate Change and Hydrologic Models: A Review of Existing Gaps and Recent Research Developments, Water Resources Management, 13, 369 – 382, 1999.

Yang, W.: Discrete-continuous Downscaling Model for Generating Daily Precipitation Time Series, Ph.D. thesis, Universität Stuttgart, 2007.

Yang, W., Bárdossy, A., and Caspary, H.-J.: Downscaling daily precipitation time series using a combined circulation- and regression-based approach, Theoretical and Applied Climatology, pp. 1–16, http://dx.doi.org/10.1007/s00704-010-0272-0, 10.1007/s00704-010-0272-0, 2010.

Yi, H.: Application of a Non-Parametric Classification Scheme to Catchment Hydrology, Ph.D. thesis, Universität Stuttgart, 2008.

Zadeh, L.: Fuzzy sets, Information control, 8, 338 – 353, 1965.

Zhang, J.: Some extensions of Tukey's Depth Function, Journal of multivariate analysis, 82, 134 – 165, 2002.

Zorita, E. and Storch, H. V.: A survey of statistical downscaling techniques, Tech. Rep. GKSS 97/E/20, GKSS-Forschunszentrum Geesthacht GmbH, 1997.

Zorita, E. and von Storch, H.: The analog method as a simple statistical downscaling technique: Comparison with more complicated methods, 12, 2474–2489, 1999.

Zorita, E., Hughes, J., Lettenmaier, D., and von Storch, H.: Stochastic downscaling of regional circulation patterns for climate model diagnosis and estimation of local precipitation, Journal of climate, 8, 1023–1042, 1995.

A. German part of Rhine basin,Grid point locations

Table A.1.: Grid point location used for German part of Rhine basin

Grid No.	Easting[°]	Northing[°]	Grid No.	Easting[°]	Northing[°]
1	6.53	49.51	**32**	6.74	51.54
2	6.42	49.95	**33**	6.68	51.76
3	6.37	50.17	**34**	7.95	47.65
4	6.26	50.60	**35**	7.90	47.87
5	6.21	50.82	**36**	7.86	48.09
6	6.15	51.03	**37**	7.81	48.30
7	6.91	49.33	**38**	7.63	49.18
8	6.86	49.55	**39**	7.58	49.39
9	6.81	49.76	**40**	7.53	49.61
10	6.76	49.98	**41**	7.49	49.83
11	6.71	50.20	**42**	7.44	50.05
12	6.66	50.42	**43**	7.39	50.26
13	6.60	50.63	**44**	7.34	50.48
14	6.55	50.85	**45**	7.29	50.70
15	6.50	51.07	**46**	7.24	50.92
16	6.44	51.29	**47**	7.19	51.14
17	6.39	51.51	**48**	7.14	51.35
18	6.33	51.72	**49**	7.09	51.57
19	7.62	47.62	**50**	7.03	51.79
20	7.58	47.84	**51**	8.27	47.68
21	7.30	49.15	**52**	8.23	47.90
22	7.25	49.36	**53**	8.14	48.33
23	7.20	49.58	**54**	8.10	48.55
24	7.15	49.80	**55**	8.05	48.77
25	7.10	50.01	**56**	7.96	49.21
26	7.05	50.23	**57**	7.92	49.42
27	7.00	50.45	**58**	7.87	49.64
28	6.95	50.67	**59**	7.82	49.86
29	6.89	50.89	**60**	7.78	50.08
30	6.84	51.10	**61**	7.73	50.30
31	6.79	51.32	**62**	7.68	50.51
63	7.63	50.73	**104**	9.09	48.64

Continued on Next Page...

Table A.1 – Continued

Grid No.	Easting[°]	Northing[°]	Grid No.	Easting[°]	Northing[°]
64	7.59	50.95	**105**	9.05	48.85
65	7.54	51.17	**106**	9.01	49.07
66	7.49	51.38	**107**	8.97	49.29
67	7.44	51.60	**108**	8.92	49.51
68	8.51	48.15	**109**	8.88	49.73
69	8.47	48.36	**110**	8.84	49.95
70	8.43	48.58	**111**	8.80	50.16
71	8.38	48.80	**112**	8.76	50.38
72	8.34	49.02	**113**	8.71	50.60
73	8.30	49.24	**114**	8.67	50.82
74	8.25	49.45	**115**	8.58	51.26
75	8.21	49.67	**116**	8.53	51.47
76	8.16	49.89	**117**	8.49	51.69
77	8.12	50.11	**118**	9.60	47.57
78	8.07	50.33	**119**	9.57	47.79
79	8.02	50.54	**120**	9.45	48.44
80	7.98	50.76	**121**	9.42	48.66
81	7.93	50.98	**122**	9.38	48.88
82	7.88	51.20	**123**	9.34	49.10
83	7.84	51.42	**124**	9.30	49.32
84	7.79	51.63	**125**	9.26	49.54
85	8.92	47.74	**126**	9.22	49.75
86	8.88	47.95	**127**	9.18	49.97
87	8.80	48.39	**128**	9.14	50.19
88	8.76	48.61	**129**	9.10	50.41
89	8.71	48.83	**130**	9.06	50.63
90	8.67	49.04	**131**	9.01	50.85
91	8.63	49.26	**132**	8.97	51.06
92	8.59	49.48	**133**	8.84	51.72
93	8.54	49.70	**134**	9.93	47.59
94	8.50	49.92	**135**	9.89	47.81
95	8.46	50.14	**136**	9.75	48.69
96	8.41	50.35	**137**	9.71	48.90
97	8.37	50.57	**138**	9.67	49.12
98	8.32	50.79	**139**	9.64	49.34
99	8.23	51.23	**140**	9.60	49.56
100	8.19	51.44	**141**	9.56	49.78
101	8.14	51.66	**142**	9.52	50.00
102	9.24	47.76	**143**	9.48	50.22
103	9.13	48.42	**144**	9.44	50.44
145	9.93	49.58			

Continued on Next Page...

Table A.1 – Continued

Grid No.	Easting[°]	Northing[°]	Grid No.	Easting[°]	Northing[°]
146	9.90	49.80			
147	9.86	50.02			
148	9.82	50.24			
149	10.27	49.61			
150	10.24	49.83			
151	10.20	50.05			
152	10.16	50.26			
153	10.13	50.48			
154	10.61	49.63			
155	10.57	49.85			
156	10.54	50.07			
157	10.51	50.29			
158	11.01	49.22			
159	10.98	49.43			
160	10.95	49.65			
161	10.91	49.87			
162	10.88	50.09			
163	10.85	50.31			
164	11.32	49.45			
165	11.29	49.67			
166	11.26	49.89			
167	11.22	50.11			
168	11.19	50.33			
169	11.62	49.69			
170	11.60	49.91			
171	11.56	50.13			
172	11.53	50.35			

B. Spatial maps of wetness indices for all RCM control and SRES A1B scenario runs for each CP and season (Winter and Summer)

B.1. Spatial maps of wetness indices for all CPs for RACMO RCM

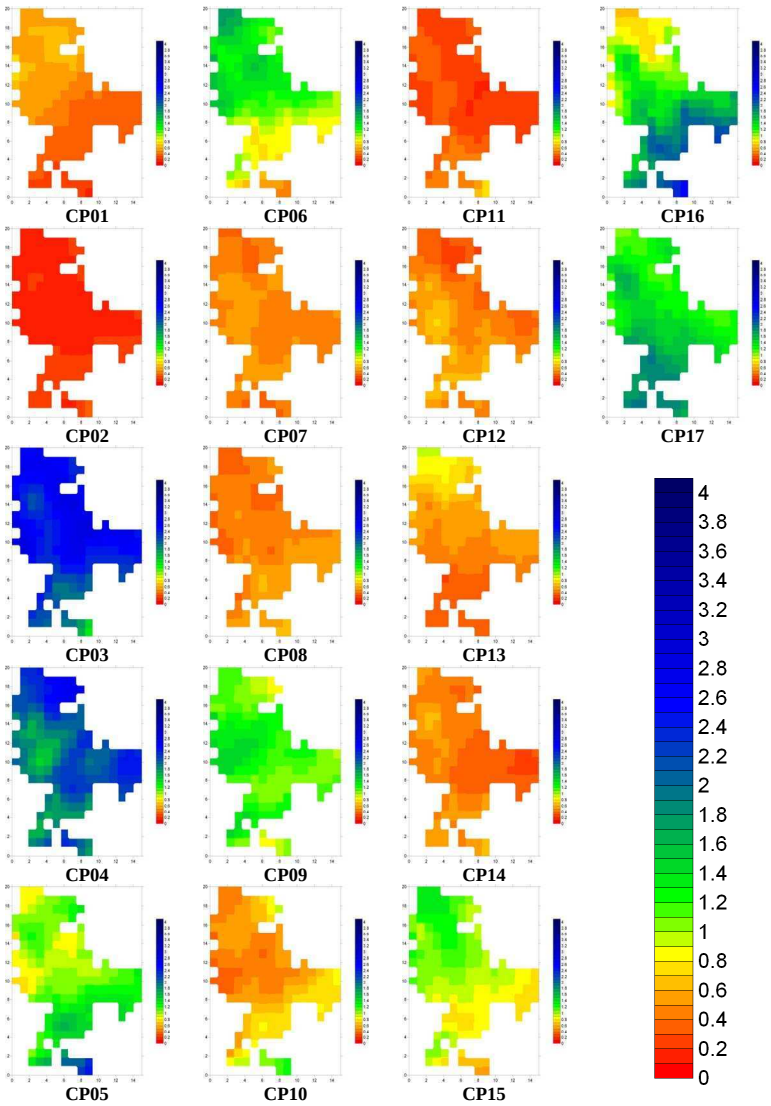

Figure B.1.: Spatial maps of wetness index for each CP of RACMO control run for winter

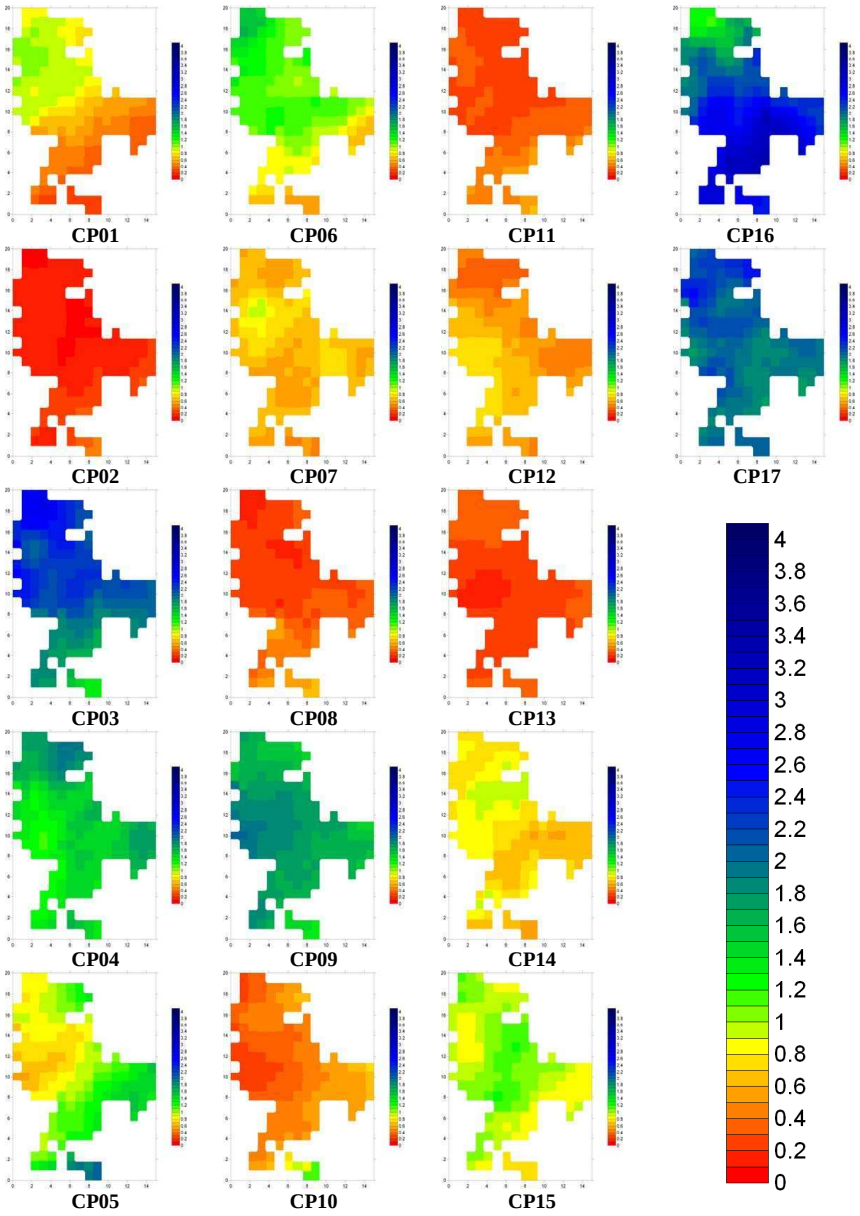

Figure B.2.: Spatial maps of wetness index for each CP of RACMO control run for summer

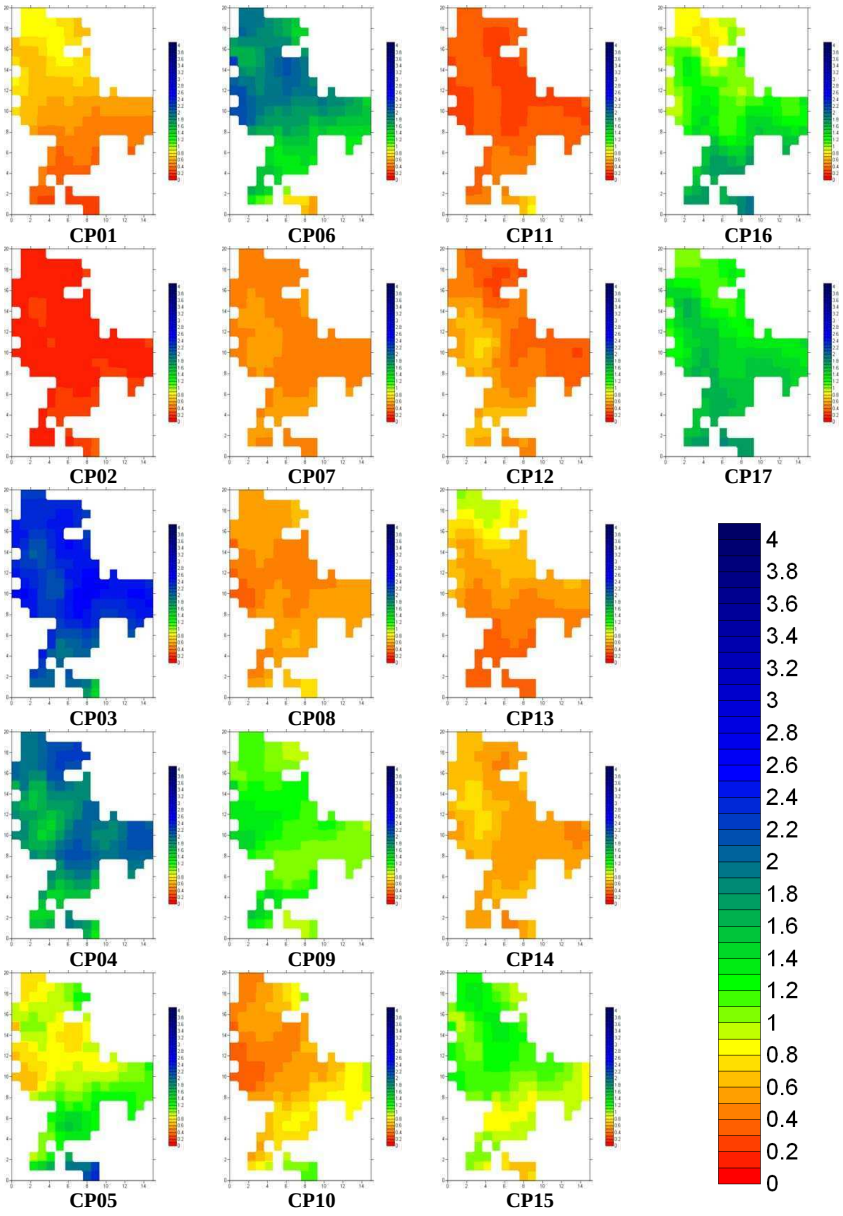

Figure B.3.: Spatial maps of wetness index for each CP of RACMO SRES A1B scenario run for winter

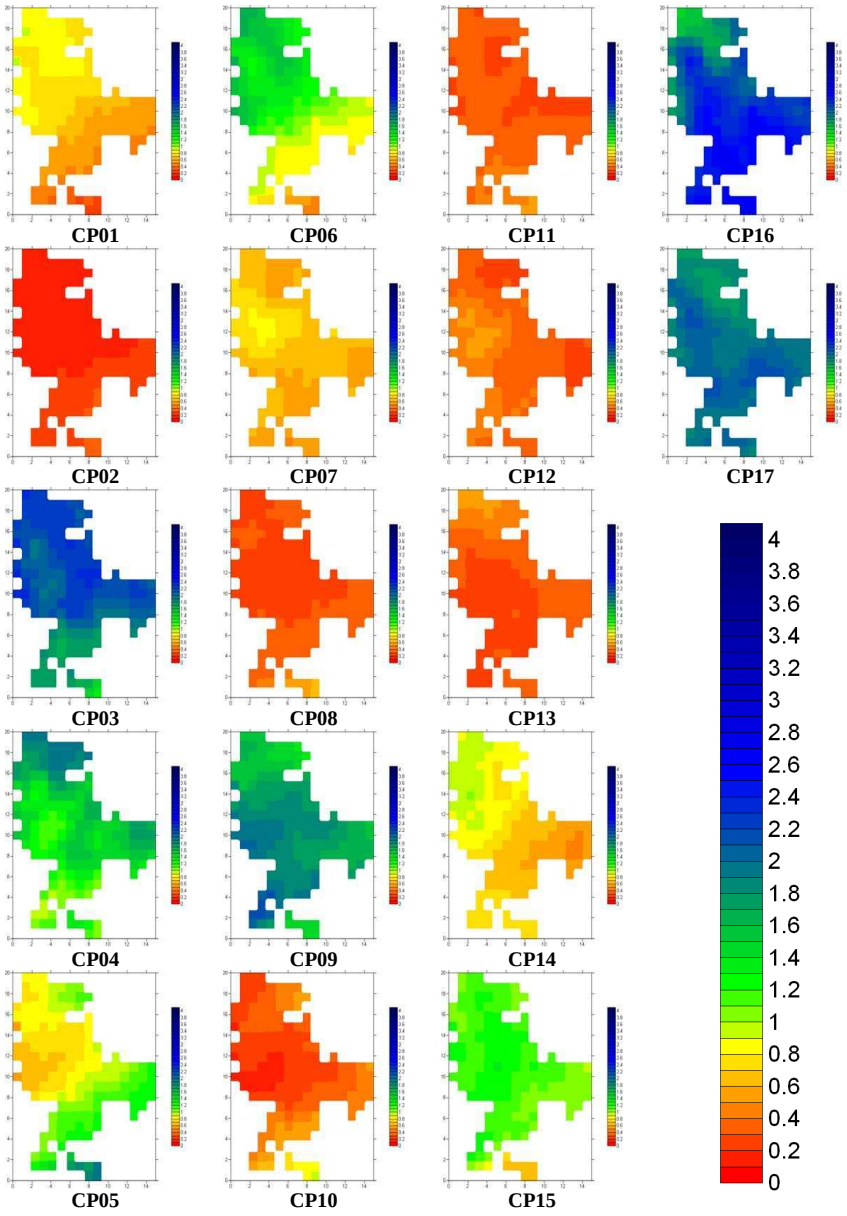

Figure B.4.: Spatial maps of wetness index for each CP for RACMO SRES A1B scenario run for summer

B.2. Spatial maps of wetness indices for all CPs for REMO RCM

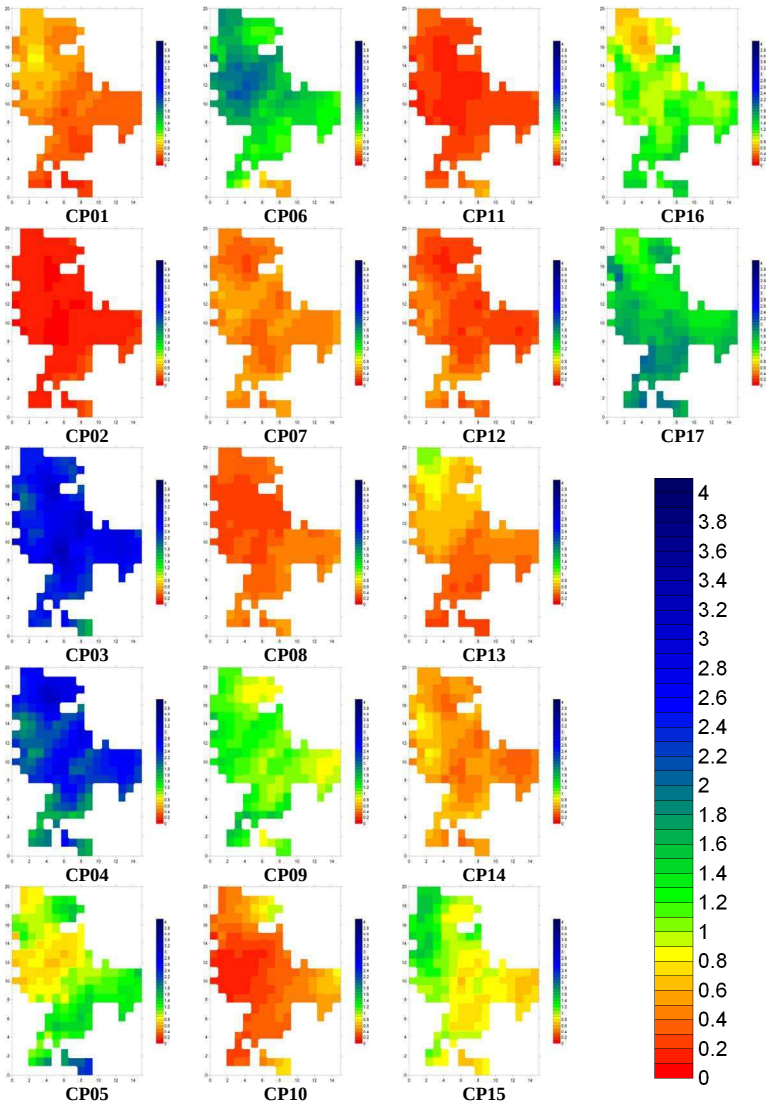

Figure B.5.: Spatial maps of wetness index for each CP for REMO control run for winter

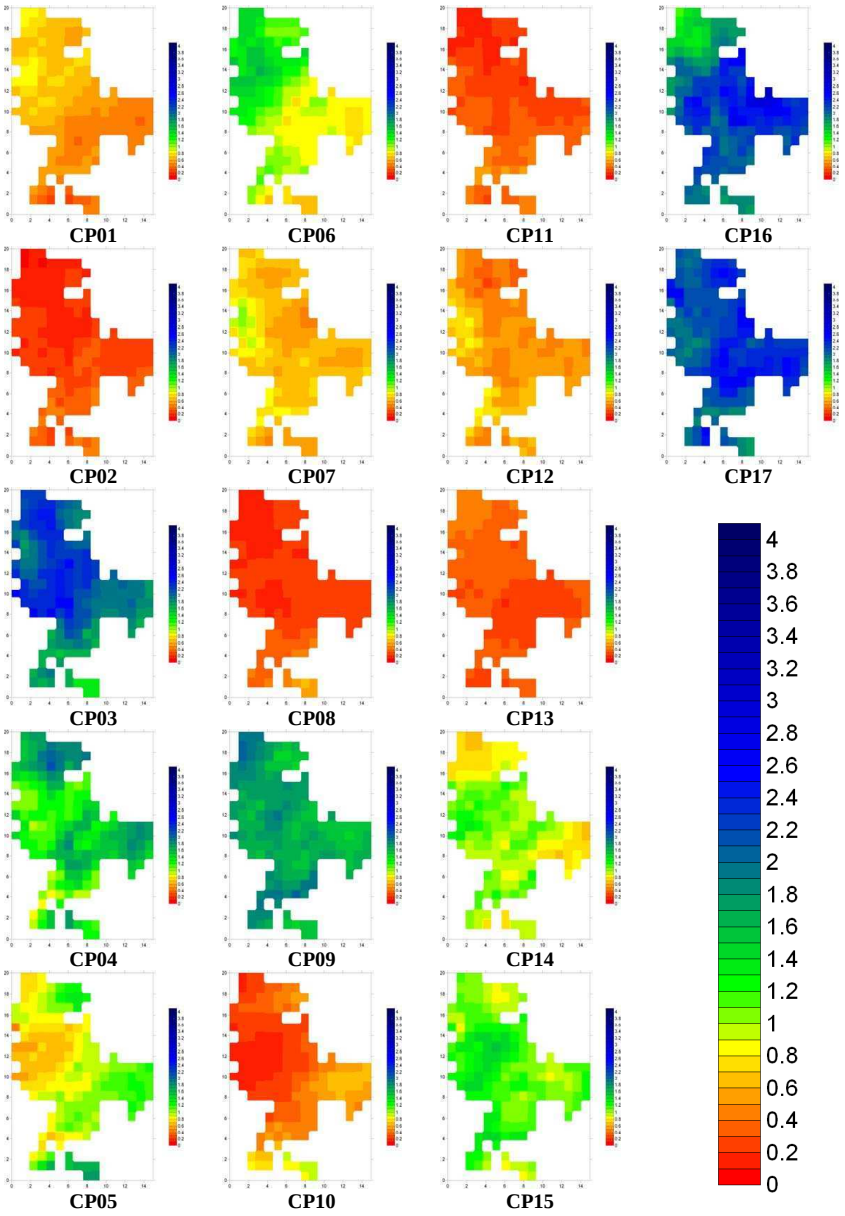

Figure B.6.: Spatial maps of wetness index for each CP for REMO control run for summer

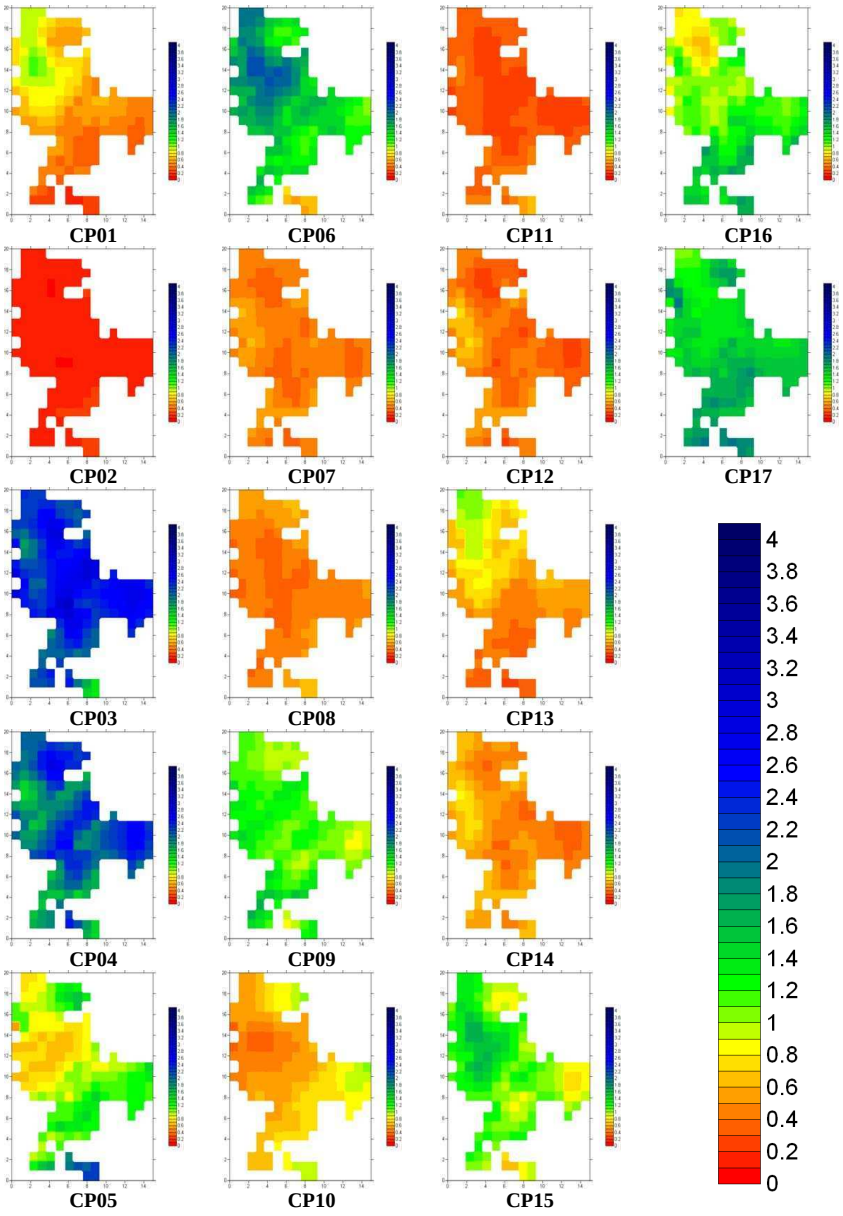

Figure B.7.: Spatial maps of wetness index for each CP for REMO SRES A1B scenario run for winter

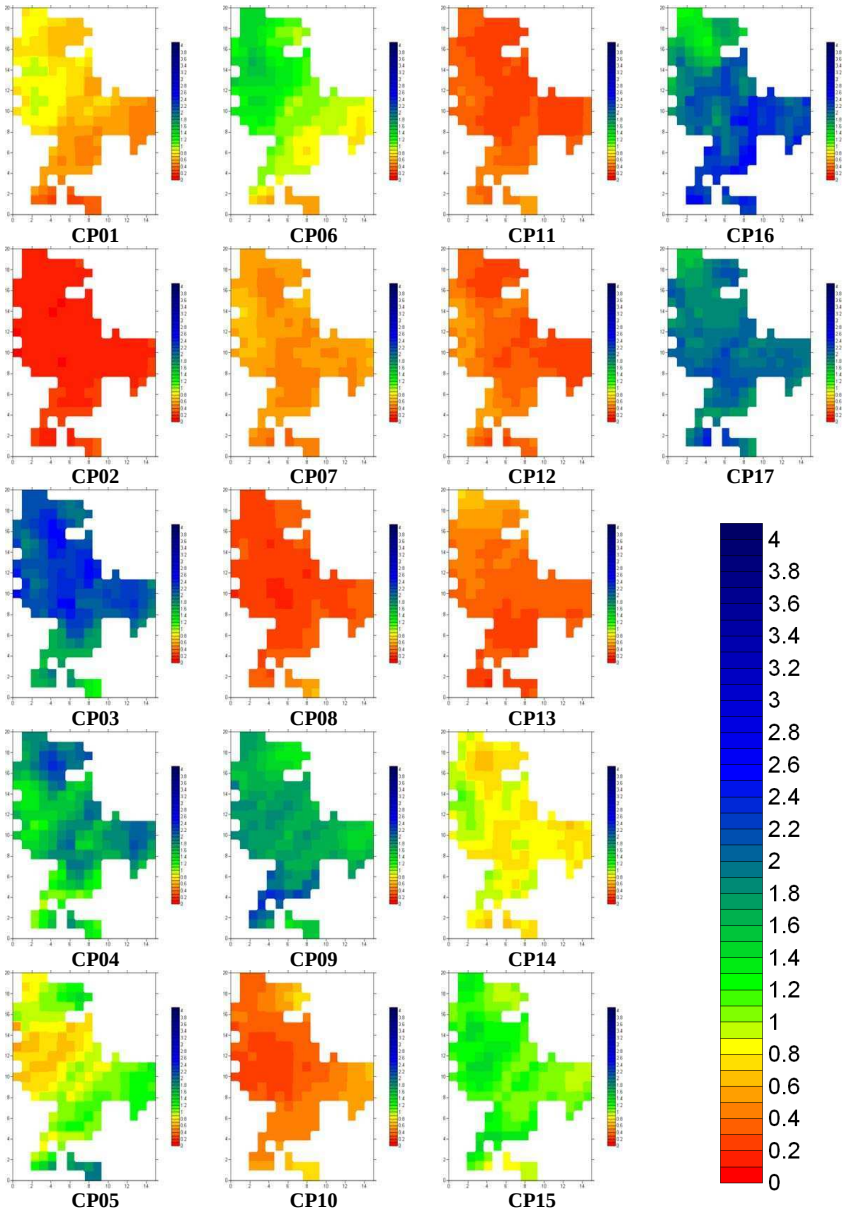

Figure B.8.: Spatial maps of wetness index for each CP for REMO SRES A1B scenario run for summer

B.3. Spatial maps of wetness indices for all CPs for HadRM RCM

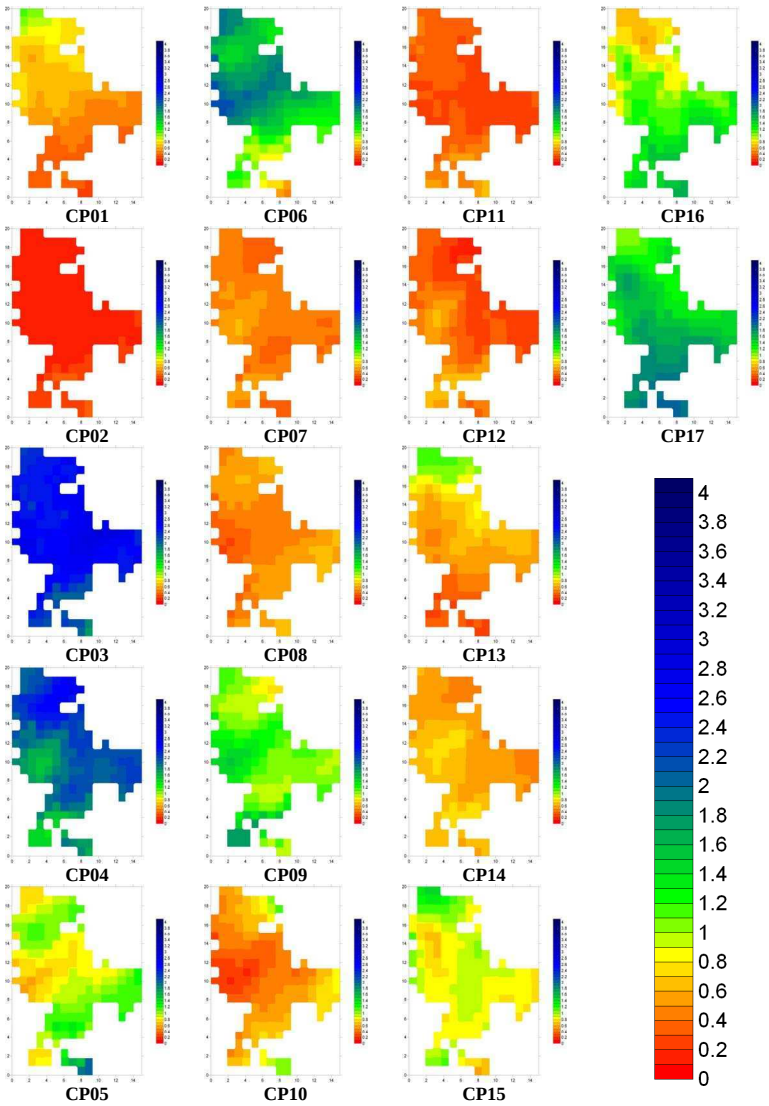

Figure B.9.: Spatial maps of wetness index for each CP for HadRM control run for winter

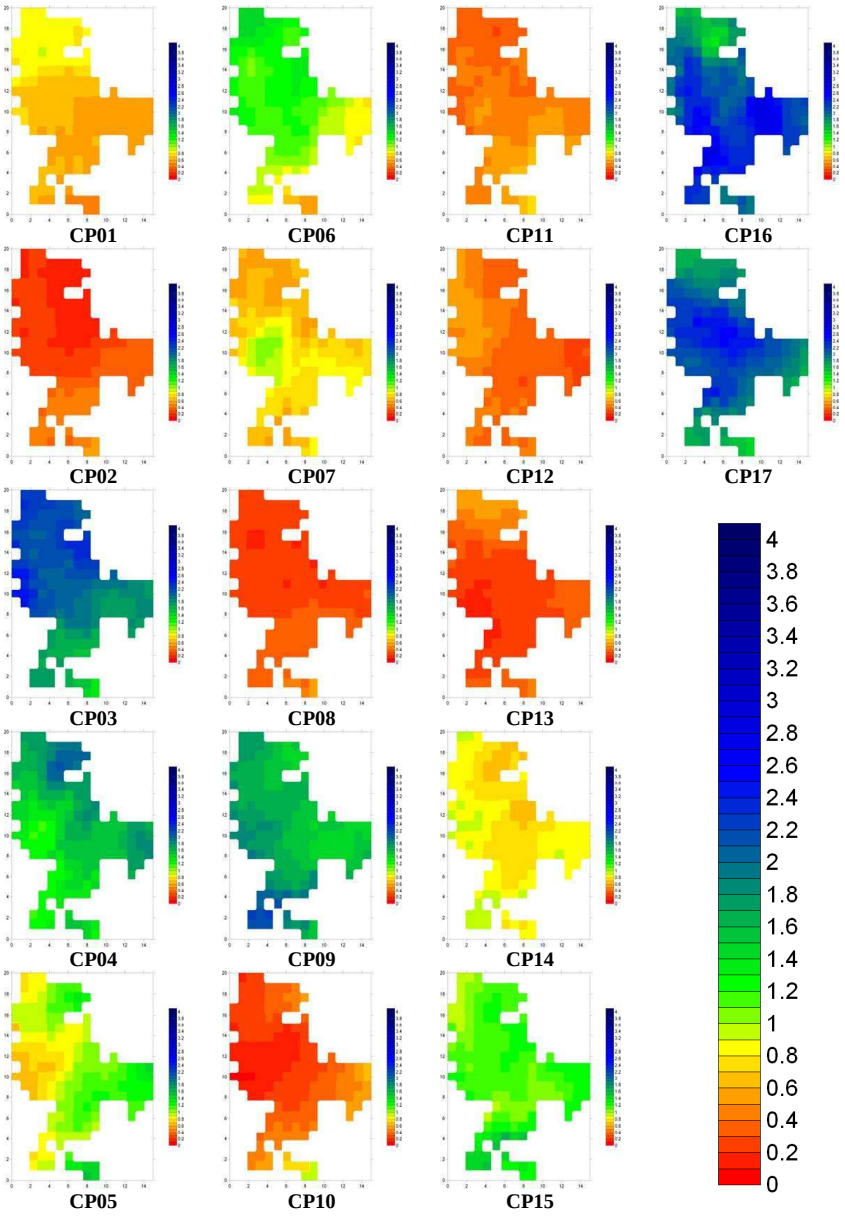

Figure B.10.: Spatial maps of wetness index for each CP for HadRM control run for summer

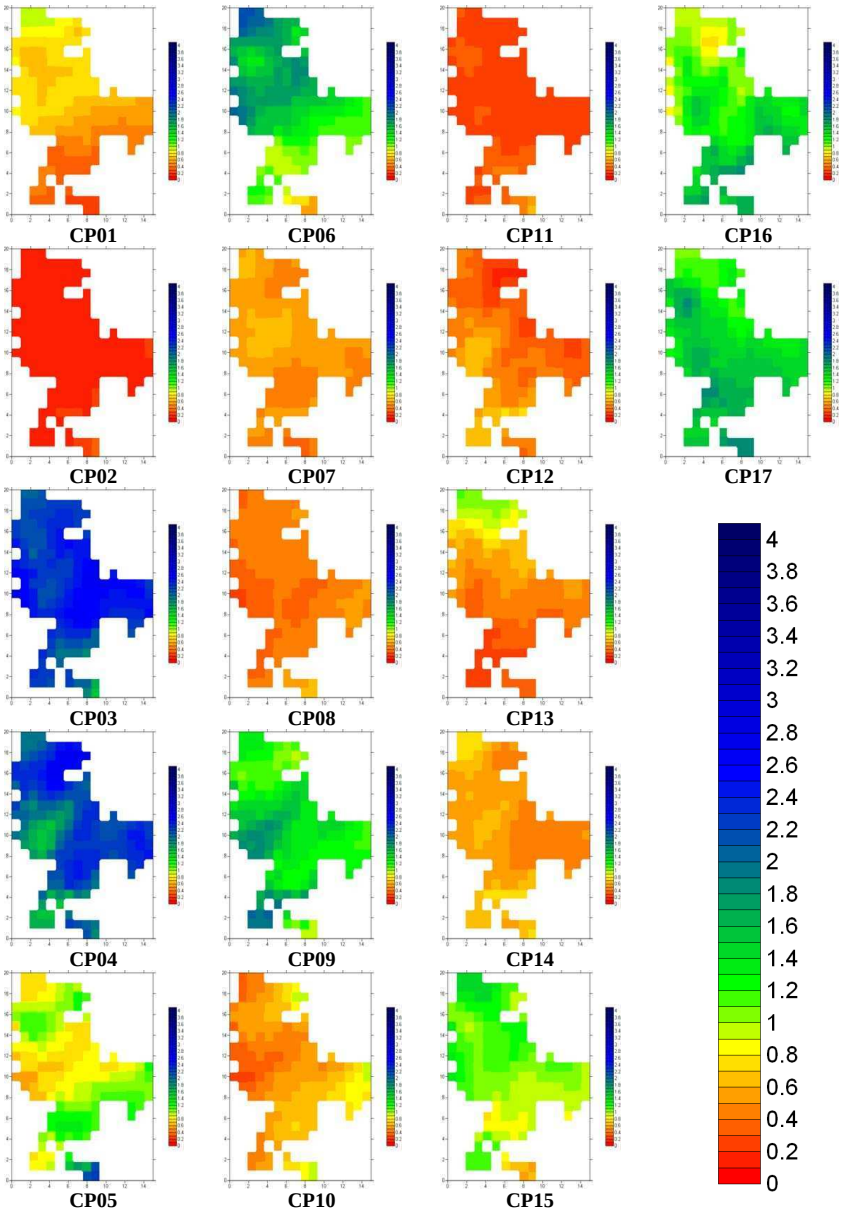

Figure B.11.: Spatial maps of wetness index for each CP for HadRM SRES A1B scenario run (low climate sensitivity) for winter

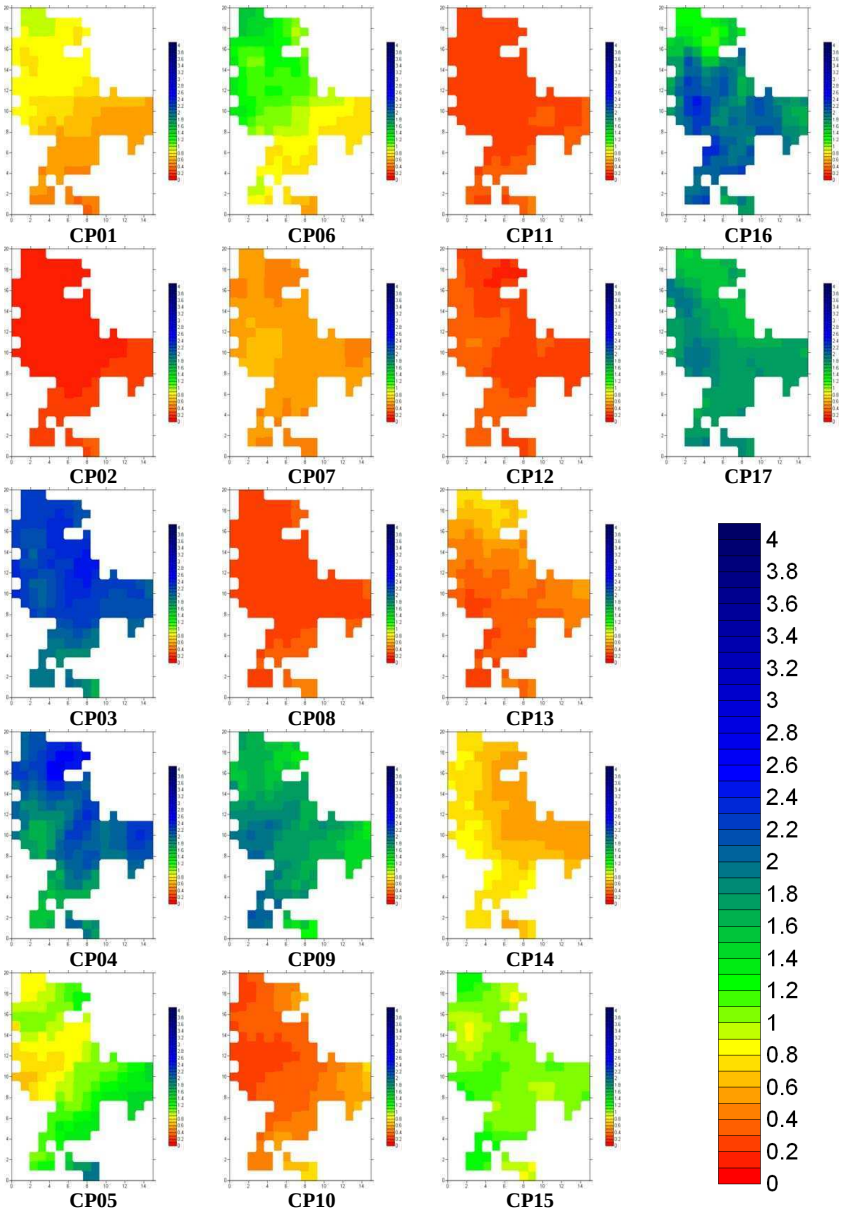

Figure B.12.: Spatial maps of wetness index for each CP for HadRM SRES A1B scenario run (low climate sensitivity) for summer

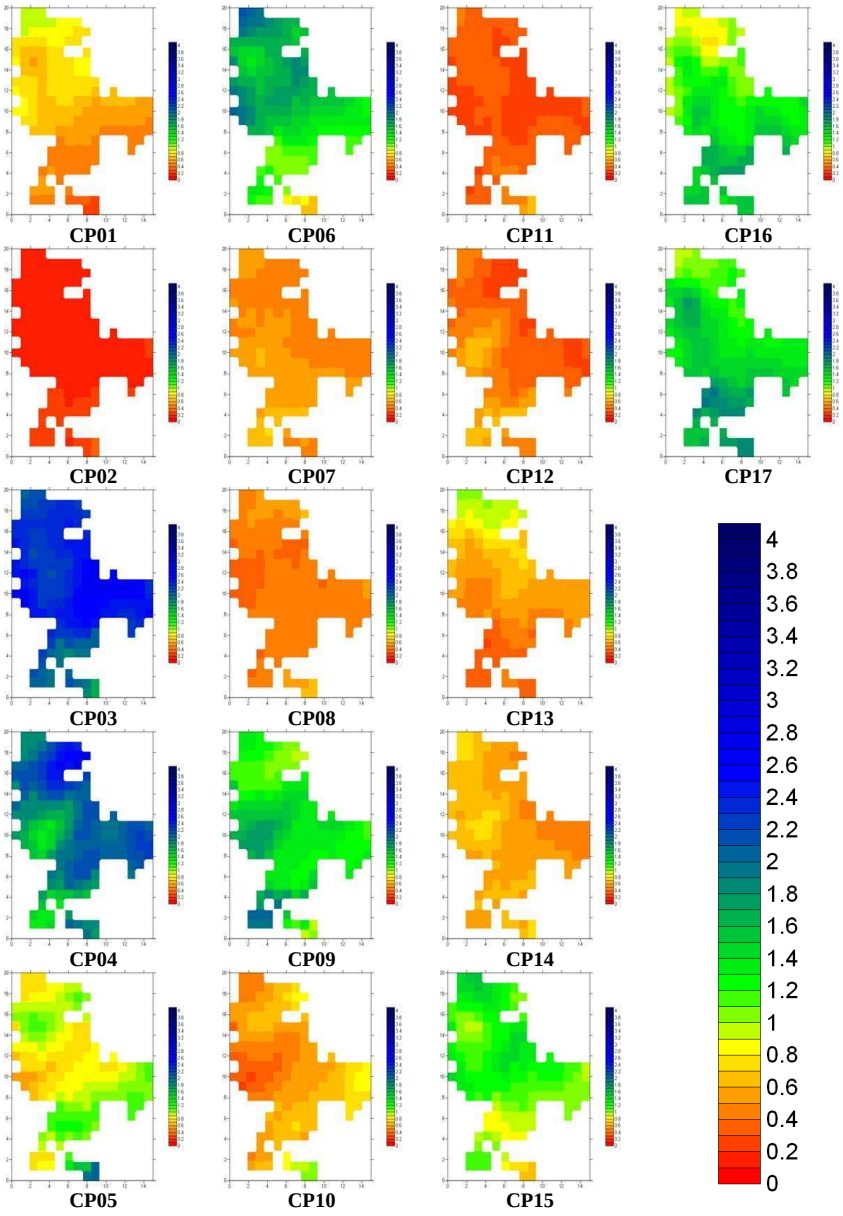

Figure B.13.: Spatial maps of wetness index for each CP for HadRM SRES A1B scenario run (normal climate sensitivity) for winter

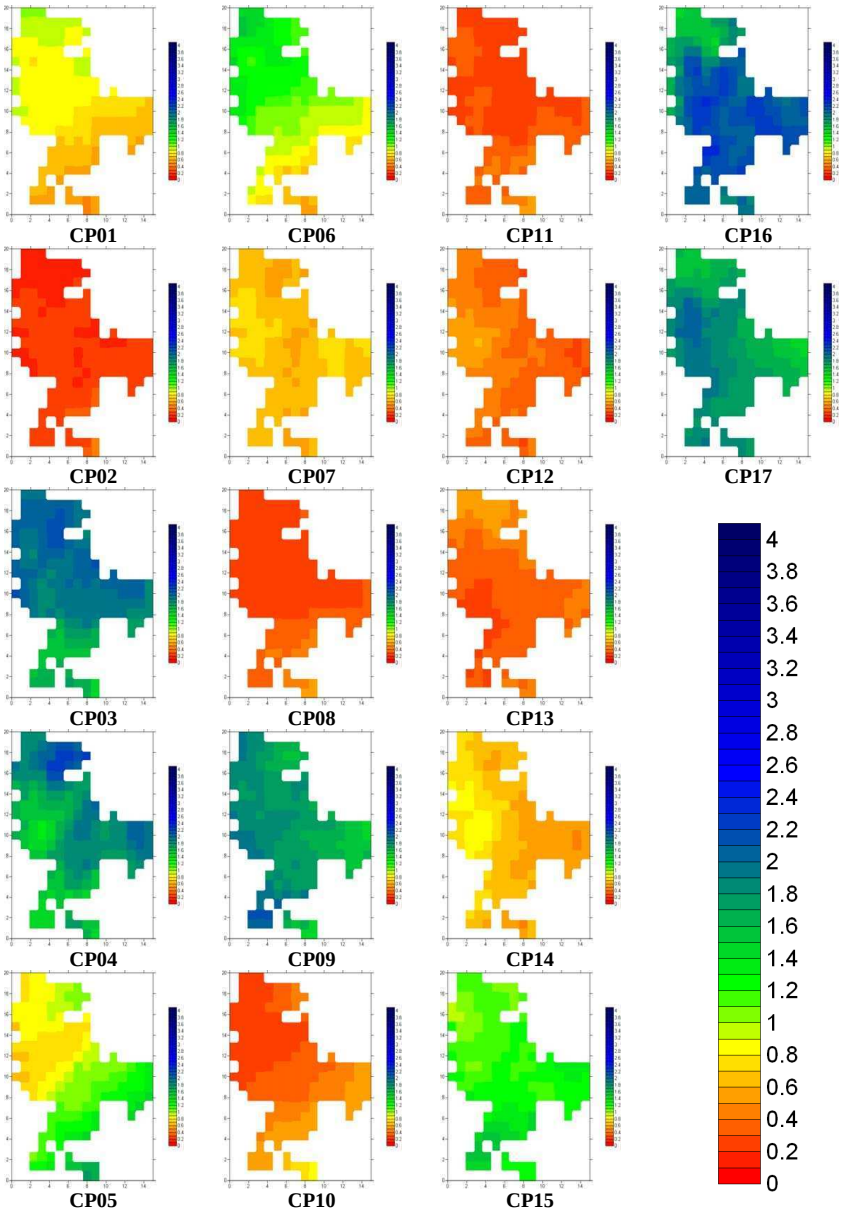

Figure B.14.: Spatial maps of wetness index for each CP for HadRM SRES A1B scenario run (normal climate sensitivity) for summer

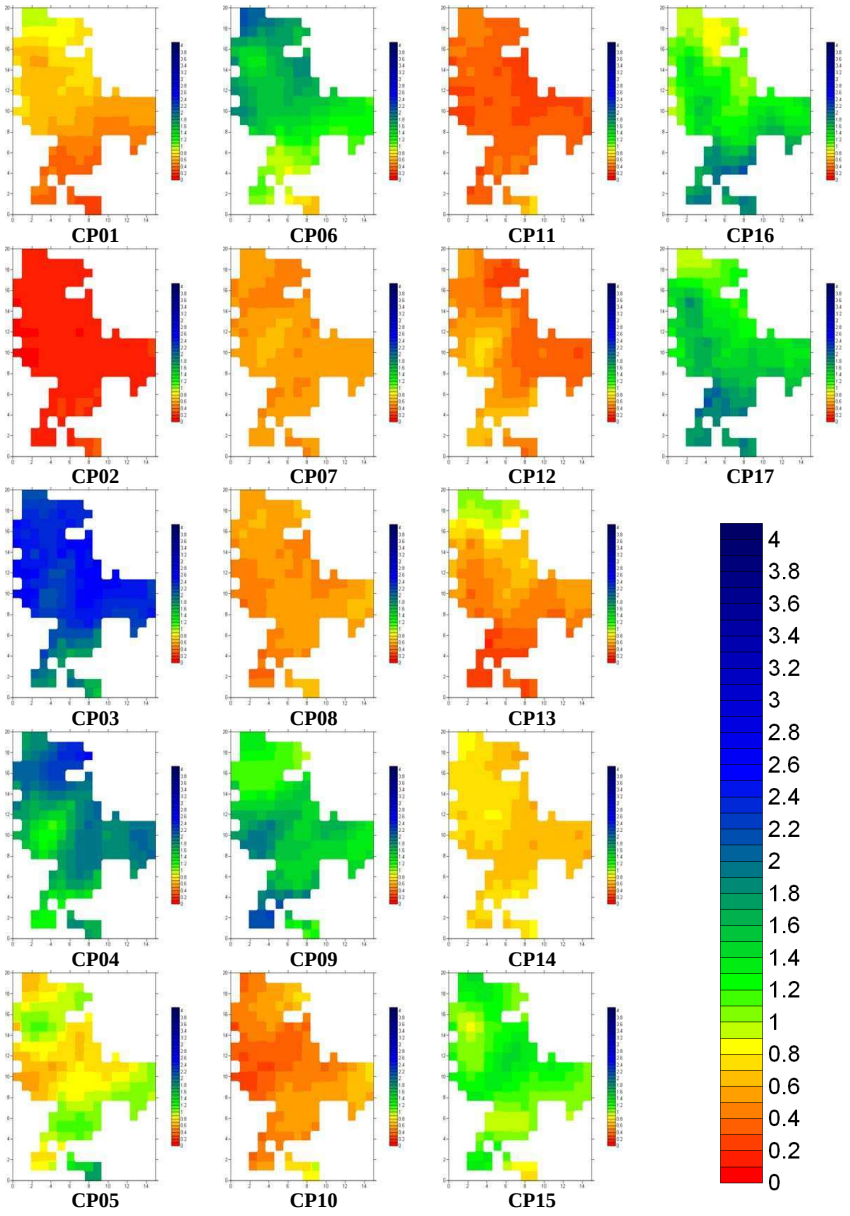

Figure B.15.: Spatial maps of wetness index for each CP for HadRM SRES A1B scenario run (high climate sensitivity) for winter

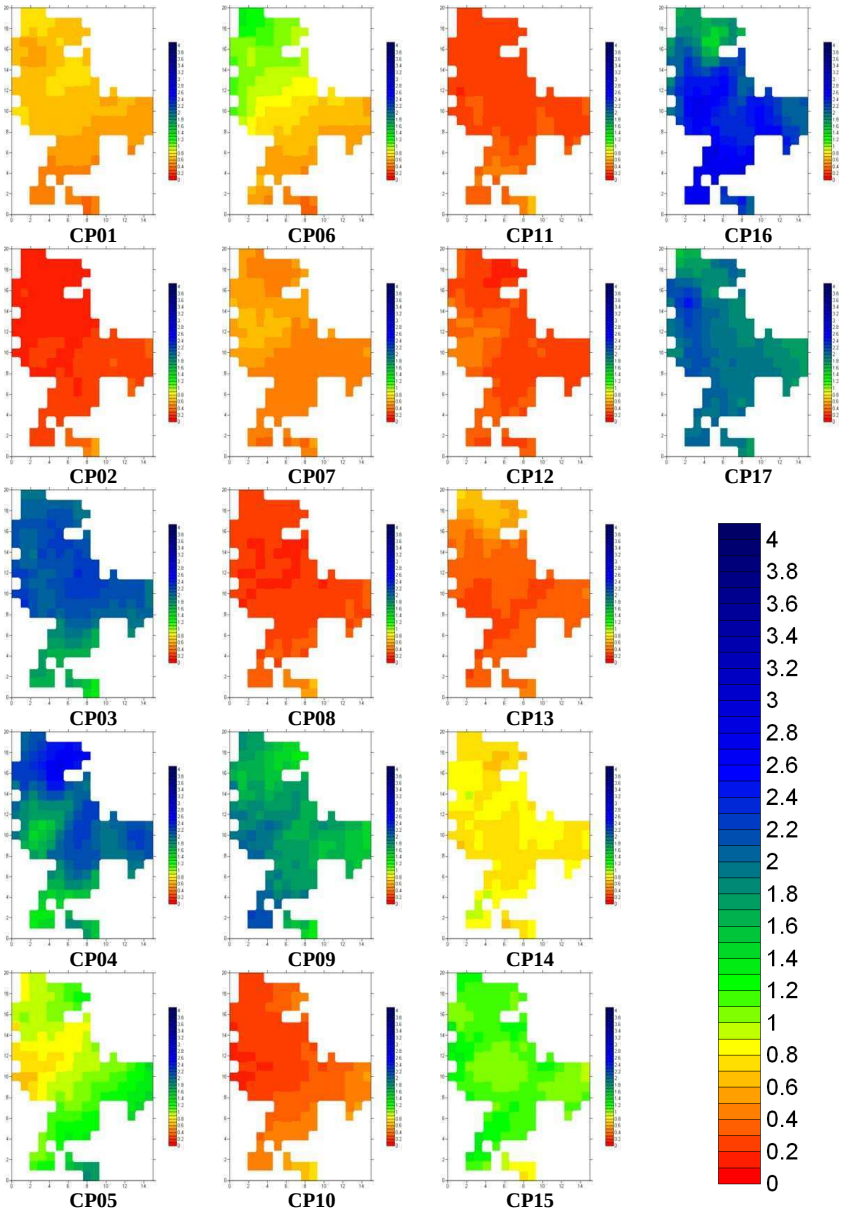

Figure B.16.: Spatial maps of wetness index for each CP for HadRM SRES A1B scenario run (high climate sensitivity) for summer

C. Contingency tables for all RCMs of ENSEMBLES data set

Table C.1.: Contingency Table for ERA40 and RACMO (control run) based classification of CPs

CP/CP	1	2	3	4	5	6	7	8	9	10	11	12	13	14	15	16	17	18
1	163	34	13	20	12	11	27	13	46	9	22	10	137	13	77	4	3	6
2	10	269	3	1	27	3	106	32	7	17	48	65	19	38	1	12	5	15
3	7	1	519	122	14	18	4	7	41	4	6	6	16	8	40	4	16	17
4	6	2	61	339	86	2	1	10	15	14	10	1	89	1	16	0	11	5
5	6	50	21	87	521	1	20	70	24	80	70	6	48	6	11	38	51	14
6	23	6	100	19	4	88	26	3	56	6	4	31	23	15	31	2	5	12
7	13	59	4	1	7	11	272	13	29	6	22	106	2	30	2	18	15	32
8	6	33	5	4	38	7	37	205	3	19	53	16	32	13	2	4	13	35
9	19	11	84	10	11	15	22	2	455	6	6	51	5	27	35	17	39	50
10	6	27	4	8	47	2	20	125	11	100	17	7	26	8	3	2	20	10
11	23	86	7	7	56	5	47	52	16	11	221	31	39	46	2	15	4	75
12	6	34	8	1	2	28	94	13	69	2	7	541	8	53	3	46	26	10
13	14	14	5	45	39	4	3	50	2	17	34	2	392	6	20	0	1	13
14	17	16	28	3	8	18	34	3	52	1	24	67	14	106	28	24	13	20
15	9	4	23	19	8	7	1	0	42	1	4	4	36	8	101	0	7	16
16	1	10	21	5	11	7	59	4	69	2	5	78	0	18	6	82	37	9
17	4	10	88	33	40	11	15	4	92	15	2	26	2	30	13	12	206	71
18	1	5	12	1	4	5	3	4	24	1	13	2	4	8	5	0	3	131
No. of classified days=11315, Cramer's V=0.393																		

Table C.2.: Contingency Table for ERA40 and REMO (control run) based classification of CPs

CP/CP	1	2	3	4	5	6	7	8	9	10	11	12	13	14	15	16	17	18
1	277	37	10	15	19	41	23	8	29	6	18	9	74	6	30	7	2	9
2	20	291	1	1	59	6	79	36	9	20	49	42	11	20	3	14	2	15
3	21	2	510	67	9	78	1	2	54	4	5	7	5	7	25	7	15	31
4	14	1	79	362	64	11	1	12	10	10	9	1	51	1	24	0	13	6
5	10	38	17	95	644	4	10	49	18	45	50	4	17	11	16	40	47	9
6	33	4	55	8	2	188	20	4	37	2	9	27	17	12	20	3	5	8
7	9	71	6	0	11	21	233	17	24	11	24	87	2	20	4	45	21	36
8	15	32	9	7	49	5	18	221	2	27	55	14	21	5	2	5	8	30
9	32	7	60	7	3	42	12	3	464	3	8	39	4	29	38	31	39	44
10	7	40	0	6	68	4	7	105	5	114	19	3	26	10	3	5	17	4
11	33	99	2	5	88	2	28	48	13	8	239	28	32	25	7	19	5	62
12	18	71	6	1	5	49	79	7	46	6	14	502	3	43	1	78	15	7
13	47	16	4	49	63	13	4	41	1	22	42	1	335	2	10	0	0	11
14	29	28	16	2	18	37	43	9	45	2	14	37	11	101	14	32	18	20
15	34	3	14	14	9	13	0	1	37	2	10	5	38	4	86	2	6	12
16	4	5	11	2	23	5	27	7	63	5	4	55	0	19	6	154	29	5
17	3	2	68	26	38	20	21	7	114	8	4	15	0	26	7	25	212	78
18	2	2	3	0	6	6	4	4	21	0	17	5	2	4	2	0	8	140
No. of classified days=11315, Cramer's V=0.422																		

Table C.3.: Contingency Table for ERA40 and HadRM (control run) based classification of CPs

CP/CP	1	2	3	4	5	6	7	8	9	10	11	12	13	14	15	16	17	18
1	216	33	31	26	20	36	30	8	44	10	11	17	70	6	36	5	2	19
2	31	243	3	1	69	9	82	26	13	13	41	51	23	24	4	13	4	28
3	29	2	418	80	20	71	4	7	49	7	7	11	13	24	31	14	19	44
4	7	3	120	280	81	11	1	20	27	11	8	1	53	2	18	5	12	9
5	11	45	49	106	551	3	14	69	17	45	49	8	36	14	7	31	40	29
6	41	7	48	4	6	144	28	7	38	4	1	41	15	9	18	12	10	21
7	24	75	3	0	19	13	224	18	30	9	17	73	6	20	7	46	23	35
8	10	39	5	6	49	9	31	207	4	37	41	22	19	6	0	3	4	33
9	42	19	46	12	20	31	23	5	393	6	6	43	7	33	40	58	26	55
10	5	36	7	22	80	6	15	80	10	95	13	12	22	6	4	2	14	14
11	41	89	10	11	91	3	28	53	14	15	175	39	53	14	4	22	9	72
12	25	76	14	3	9	49	94	16	58	6	22	416	2	47	9	64	27	14
13	60	16	23	81	58	11	7	40	4	12	19	7	284	4	14	2	2	17
14	26	28	16	5	11	29	31	6	42	4	21	51	11	88	20	44	21	22
15	27	3	35	12	8	12	6	2	43	3	8	5	22	5	72	6	5	16
16	3	21	22	3	35	1	40	7	43	2	6	62	1	22	3	124	22	7
17	9	11	62	34	60	11	17	10	93	15	5	19	5	24	17	39	172	71
18	3	6	8	3	7	5	9	6	22	1	20	3	3	3	1	0	8	118
No. of classified days=11315, Cramer's V=0.346																		

Curriculum vitae

30. Dec. 1977	born in Swat, Pakistan
1997 - 2001	B.Sc. Civil Engineering, N-W.F.P. University of Engineering and Technology,Peshawar,Pakistan.
2001 - 2003	Project Engineer, Al-Faylaka Ltd., Dubai, U.A.E.
2003 - 2006	Master of Science (M.Sc.) in Water Resources Engineering and Management (WAREM), Universität Stuttgart
since Sep. 2006	Research Assistant at the Institute for Hydraulic Engineering, Universität Stuttgart

Institut für Wasserbau
Universität Stuttgart

Pfaffenwaldring 61
70569 Stuttgart (Vaihingen)
Telefon (0711) 685 - 64717/64749/64752/64679
Telefax (0711) 685 - 67020 o. 64746 o. 64681
E-Mail: iws@iws.uni-stuttgart.de
http://www.iws.uni-stuttgart.de

Verzeichnis der Mitteilungshefte

1 Röhnisch, Arthur: *Die Bemühungen um eine Wasserbauliche Versuchsanstalt an der Technischen Hochschule Stuttgart*, und
Fattah Abouleid, Abdel: *Beitrag zur Berechnung einer in lockeren Sand gerammten, zweifach verankerten Spundwand*, 1963

2 Marotz, Günter: *Beitrag zur Frage der Standfestigkeit von dichten Asphaltbelägen im Großwasserbau*, 1964

3 Gurr, Siegfried: *Beitrag zur Berechnung zusammengesetzter ebener Flächentragwerke unter besonderer Berücksichtigung ebener Stauwände, mit Hilfe von Randwert- und Lastwertmatrizen*, 1965

4 Plica, Peter: *Ein Beitrag zur Anwendung von Schalenkonstruktionen im Stahlwasserbau*, und Petrikat, Kurt: *Möglichkeiten und Grenzen des wasserbaulichen Versuchswesens*, 1966

5 Plate, Erich: *Beitrag zur Bestimmung der Windgeschwindigkeitsverteilung in der durch eine Wand gestörten bodennahen Luftschicht*,
und
Röhnisch, Arthur; Marotz, Günter: *Neue Baustoffe und Bauausführungen für den Schutz der Böschungen und der Sohle von Kanälen, Flüssen und Häfen; Gestehungskosten und jeweilige Vorteile*, sowie Unny, T.E.: *Schwingungsuntersuchungen am Kegelstrahlschieber*, 1967

6 Seiler, Erich: *Die Ermittlung des Anlagenwertes der bundeseigenen Binnenschiffahrtsstraßen und Talsperren und des Anteils der Binnenschiffahrt an diesem Wert*, 1967

7 *Sonderheft anläßlich des 65. Geburtstages von Prof. Arthur Röhnisch mit Beiträgen von* Benk, Dieter; Breitling, J.; Gurr, Siegfried; Haberhauer, Robert; Honekamp, Hermann; Kuz, Klaus Dieter; Marotz, Günter; Mayer-Vorfelder, Hans-Jörg; Miller, Rudolf; Plate, Erich J.; Radomski, Helge; Schwarz, Helmut; Vollmer, Ernst; Wildenhahn, Eberhard; 1967

8 Jumikis, Alfred: *Beitrag zur experimentellen Untersuchung des Wassernachschubs in einem gefrierenden Boden und die Beurteilung der Ergebnisse*, 1968

9 Marotz, Günter: *Technische Grundlagen einer Wasserspeicherung im natürlichen Untergrund*, 1968

10 Radomski, Helge: *Untersuchungen über den Einfluß der Querschnittsform wellenförmiger Spundwände auf die statischen und rammtechnischen Eigenschaften*, 1968

11 Schwarz, Helmut: *Die Grenztragfähigkeit des Baugrundes bei Einwirkung vertikal gezogener Ankerplatten als zweidimensionales Bruchproblem*, 1969

12 Erbel, Klaus: *Ein Beitrag zur Untersuchung der Metamorphose von Mittelgebirgsschneedecken unter besonderer Berücksichtigung eines Verfahrens zur Bestimmung der thermischen Schneequalität*, 1969

13 Westhaus, Karl-Heinz: *Der Strukturwandel in der Binnenschiffahrt und sein Einfluß auf den Ausbau der Binnenschiffskanäle*, 1969

14 Mayer-Vorfelder, Hans-Jörg: *Ein Beitrag zur Berechnung des Erdwiderstandes unter Ansatz der logarithmischen Spirale als Gleitflächenfunktion*, 1970

15 Schulz, Manfred: *Berechnung des räumlichen Erddruckes auf die Wandung kreiszylindrischer Körper*, 1970

16 Mobasseri, Manoutschehr: *Die Rippenstützmauer. Konstruktion und Grenzen ihrer Standsicherheit*, 1970

17 Benk, Dieter: *Ein Beitrag zum Betrieb und zur Bemessung von Hochwasserrückhaltebecken*, 1970

18 Gàl, Attila: *Bestimmung der mitschwingenden Wassermasse bei überströmten Fischbauchklappen mit kreiszylindrischem Staublech*, 1971, vergriffen

19 Kuz, Klaus Dieter: *Ein Beitrag zur Frage des Einsetzens von Kavitationserscheinungen in einer Düsenströmung bei Berücksichtigung der im Wasser gelösten Gase*, 1971, vergriffen

20 Schaak, Hartmut: *Verteilleitungen von Wasserkraftanlagen*, 1971

21 *Sonderheft zur Eröffnung der neuen Versuchsanstalt des Instituts für Wasserbau der Universität Stuttgart mit Beiträgen von* Brombach, Hansjörg; Dirksen, Wolfram; Gàl, Attila; Gerlach, Reinhard; Giesecke, Jürgen; Holthoff, Franz-Josef; Kuz, Klaus Dieter; Marotz, Günter; Minor, Hans-Erwin; Petrikat, Kurt; Röhnisch, Arthur; Rueff, Helge; Schwarz, Helmut; Vollmer, Ernst; Wildenhahn, Eberhard; 1972

22 Wang, Chung-su: *Ein Beitrag zur Berechnung der Schwingungen an Kegelstrahlschiebern*, 1972

23 Mayer-Vorfelder, Hans-Jörg: *Erdwiderstandsbeiwerte nach dem Ohde-Variationsverfahren*, 1972

24 Minor, Hans-Erwin: *Beitrag zur Bestimmung der Schwingungsanfachungsfunktionen überströmter Stauklappen*, 1972, vergriffen

25 Brombach, Hansjörg: *Untersuchung strömungsmechanischer Elemente (Fluidik) und die Möglichkeit der Anwendung von Wirbelkammerelementen im Wasserbau*, 1972, vergriffen

26 Wildenhahn, Eberhard: *Beitrag zur Berechnung von Horizontalfilterbrunnen*, 1972

27 Steinlein, Helmut: *Die Eliminierung der Schwebstoffe aus Flußwasser zum Zweck der unterirdischen Wasserspeicherung, gezeigt am Beispiel der Iller*, 1972

28 Holthoff, Franz Josef: *Die Überwindung großer Hubhöhen in der Binnenschiffahrt durch Schwimmerhebewerke*, 1973

29 Röder, Karl: *Einwirkungen aus Baugrundbewegungen auf trog- und kastenförmige Konstruktionen des Wasser- und Tunnelbaues*, 1973

30 Kretschmer, Heinz: *Die Bemessung von Bogenstaumauern in Abhängigkeit von der Talform*, 1973

31 Honekamp, Hermann: *Beitrag zur Berechnung der Montage von Unterwasserpipelines*, 1973

32 Giesecke, Jürgen: *Die Wirbelkammertriode als neuartiges Steuerorgan im Wasserbau*, und Brombach, Hansjörg: *Entwicklung, Bauformen, Wirkungsweise und Steuereigenschaften von Wirbelkammerverstärkern*, 1974

33 Rueff, Helge: *Untersuchung der schwingungserregenden Kräfte an zwei hintereinander angeordneten Tiefschützen unter besonderer Berücksichtigung von Kavitation*, 1974

34 Röhnisch, Arthur: *Einpreßversuche mit Zementmörtel für Spannbeton - Vergleich der Ergebnisse von Modellversuchen mit Ausführungen in Hüllwellrohren*, 1975

35 *Sonderheft anläßlich des 65. Geburtstages von Prof. Dr.-Ing. Kurt Petrikat mit Beiträgen von*: Brombach, Hansjörg; Erbel, Klaus; Flinspach, Dieter; Fischer jr., Richard; Gàl, Attila; Gerlach, Reinhard; Giesecke, Jürgen; Haberhauer, Robert; Hafner Edzard; Hausenblas, Bernhard; Horlacher, Hans-Burkhard; Hutarew, Andreas; Knoll, Manfred; Krummet, Ralph; Marotz, Günter; Merkle, Theodor; Miller, Christoph; Minor, Hans-Erwin; Neumayer, Hans; Rao, Syamala; Rath, Paul; Rueff, Helge; Ruppert, Jürgen; Schwarz, Wolfgang; Topal-Gökceli, Mehmet; Vollmer, Ernst; Wang, Chung-su; Weber, Hans-Georg; 1975

36 Berger, Jochum: *Beitrag zur Berechnung des Spannungszustandes in rotationssymmetrisch belasteten Kugelschalen veränderlicher Wandstärke unter Gas- und Flüssigkeitsdruck durch Integration schwach singulärer Differentialgleichungen*, 1975

37 Dirksen, Wolfram: *Berechnung instationärer Abflußvorgänge in gestauten Gerinnen mittels Differenzenverfahren und die Anwendung auf Hochwasserrückhaltebecken*, 1976

38 Horlacher, Hans-Burkhard: *Berechnung instationärer Temperatur- und Wärmespannungsfelder in langen mehrschichtigen Hohlzylindern*, 1976

39 Hafner, Edzard: *Untersuchung der hydrodynamischen Kräfte auf Baukörper im Tiefwasserbereich des Meeres*, 1977, ISBN 3-921694-39-6

40 Ruppert, Jürgen: *Über den Axialwirbelkammerverstärker für den Einsatz im Wasserbau*, 1977, ISBN 3-921694-40-X

41 Hutarew, Andreas: *Beitrag zur Beeinflußbarkeit des Sauerstoffgehalts in Fließgewässern an Abstürzen und Wehren*, 1977, ISBN 3-921694-41-8, vergriffen

42 Miller, Christoph: *Ein Beitrag zur Bestimmung der schwingungserregenden Kräfte an unterströmten Wehren*, 1977, ISBN 3-921694-42-6

43 Schwarz, Wolfgang: *Druckstoßberechnung unter Berücksichtigung der Radial- und Längsverschiebungen der Rohrwandung*, 1978, ISBN 3-921694-43-4

44 Kinzelbach, Wolfgang: *Numerische Untersuchungen über den optimalen Einsatz variabler Kühlsysteme einer Kraftwerkskette am Beispiel Oberrhein*, 1978, ISBN 3-921694-44-2

45 Barczewski, Baldur: *Neue Meßmethoden für Wasser-Luftgemische und deren Anwendung auf zweiphasige Auftriebsstrahlen*, 1979, ISBN 3-921694-45-0

46 Neumayer, Hans: *Untersuchung der Strömungsvorgänge in radialen Wirbelkammerverstärkern*, 1979, ISBN 3-921694-46-9

47 Elalfy, Youssef-Elhassan: *Untersuchung der Strömungsvorgänge in Wirbelkammerdioden und -drosseln*, 1979, ISBN 3-921694-47-7

48 Brombach, Hansjörg: *Automatisierung der Bewirtschaftung von Wasserspeichern*, 1981, ISBN 3-921694-48-5

49 Geldner, Peter: *Deterministische und stochastische Methoden zur Bestimmung der Selbstdichtung von Gewässern*, 1981, ISBN 3-921694-49-3, vergriffen

50 Mehlhorn, Hans: *Temperaturveränderungen im Grundwasser durch Brauchwassereinleitungen*, 1982, ISBN 3-921694-50-7, vergriffen

51 Hafner, Edzard: *Rohrleitungen und Behälter im Meer*, 1983, ISBN 3-921694-51-5

52 Rinnert, Bernd: *Hydrodynamische Dispersion in porösen Medien: Einfluß von Dichteunterschieden auf die Vertikalvermischung in horizontaler Strömung*, 1983, ISBN 3-921694-52-3, vergriffen

53 Lindner, Wulf: *Steuerung von Grundwasserentnahmen unter Einhaltung ökologischer Kriterien*, 1983, ISBN 3-921694-53-1, vergriffen

54 Herr, Michael; Herzer, Jörg; Kinzelbach, Wolfgang; Kobus, Helmut; Rinnert, Bernd: *Methoden zur rechnerischen Erfassung und hydraulischen Sanierung von Grundwasserkontaminationen*, 1983, ISBN 3-921694-54-X

55 Schmitt, Paul: *Wege zur Automatisierung der Niederschlagsermittlung*, 1984, ISBN 3-921694-55-8, vergriffen

56 Müller, Peter: *Transport und selektive Sedimentation von Schwebstoffen bei gestautem Abfluß*, 1985, ISBN 3-921694-56-6

57 El-Qawasmeh, Fuad: *Möglichkeiten und Grenzen der Tropfbewässerung unter besonderer Berücksichtigung der Verstopfungsanfälligkeit der Tropfelemente*, 1985, ISBN 3-921694-57-4, vergriffen

58 Kirchenbaur, Klaus: *Mikroprozessorgesteuerte Erfassung instationärer Druckfelder am Beispiel seegangsbelasteter Baukörper*, 1985, ISBN 3-921694-58-2

59 Kobus, Helmut (Hrsg.): *Modellierung des großräumigen Wärme- und Schadstofftransports im Grundwasser*, Tätigkeitsbericht 1984/85 (DFG-Forschergruppe an den Universitäten Hohenheim, Karlsruhe und Stuttgart), 1985, ISBN 3-921694-59-0, vergriffen

60 Spitz, Karlheinz: *Dispersion in porösen Medien: Einfluß von Inhomogenitäten und Dichteunterschieden*, 1985, ISBN 3-921694-60-4, vergriffen

61 Kobus, Helmut: *An Introduction to Air-Water Flows in Hydraulics*, 1985, ISBN 3-921694-61-2

62 Kaleris, Vassilios: *Erfassung des Austausches von Oberflächen- und Grundwasser in horizontalebenen Grundwassermodellen*, 1986, ISBN 3-921694-62-0

63 Herr, Michael: *Grundlagen der hydraulischen Sanierung verunreinigter Porengrundwasserleiter*, 1987, ISBN 3-921694-63-9

64 Marx, Walter: *Berechnung von Temperatur und Spannung in Massenbeton infolge Hydratation*, 1987, ISBN 3-921694-64-7

65 Koschitzky, Hans-Peter: *Dimensionierungskonzept für Sohlbelüfter in Schußrinnen zur Vermeidung von Kavitationsschäden*, 1987, ISBN 3-921694-65-5

66 Kobus, Helmut (Hrsg.): *Modellierung des großräumigen Wärme- und Schadstofftransports im Grundwasser*, Tätigkeitsbericht 1986/87 (DFG-Forschergruppe an den Universitäten Hohenheim, Karlsruhe und Stuttgart) 1987, ISBN 3-921694-66-3

67 Söll, Thomas: *Berechnungsverfahren zur Abschätzung anthropogener Temperaturanomalien im Grundwasser*, 1988, ISBN 3-921694-67-1

68 Dittrich, Andreas; Westrich, Bernd: *Bodenseeufererosion, Bestandsaufnahme und Bewertung*, 1988, ISBN 3-921694-68-X, vergriffen

69 Huwe, Bernd; van der Ploeg, Rienk R.: *Modelle zur Simulation des Stickstoffhaushaltes von Standorten mit unterschiedlicher landwirtschaftlicher Nutzung*, 1988, ISBN 3-921694-69-8, vergriffen

70 Stephan, Karl: *Integration elliptischer Funktionen*, 1988, ISBN 3-921694-70-1

71 Kobus, Helmut; Zilliox, Lothaire (Hrsg.): *Nitratbelastung des Grundwassers, Auswirkungen der Landwirtschaft auf die Grundwasser- und Rohwasserbeschaffenheit und Maßnahmen zum Schutz des Grundwassers*. Vorträge des deutsch-französischen Kolloquiums am 6. Oktober 1988, Universitäten Stuttgart und Louis Pasteur Strasbourg (Vorträge in deutsch oder französisch, Kurzfassungen zweisprachig), 1988, ISBN 3-921694-71-X

72 Soyeaux, Renald: *Unterströmung von Stauanlagen auf klüftigem Untergrund unter Berücksichtigung laminarer und turbulenter Fließzustände*,1991, ISBN 3-921694-72-8

73 Kohane, Roberto: *Berechnungsmethoden für Hochwasserabfluß in Fließgewässern mit überströmten Vorländern*, 1991, ISBN 3-921694-73-6

74 Hassinger, Reinhard: *Beitrag zur Hydraulik und Bemessung von Blocksteinrampen in flexibler Bauweise*, 1991, ISBN 3-921694-74-4, vergriffen

75 Schäfer, Gerhard: *Einfluß von Schichtenstrukturen und lokalen Einlagerungen auf die Längsdispersion in Porengrundwasserleitern*, 1991, ISBN 3-921694-75-2

76 Giesecke, Jürgen: *Vorträge, Wasserwirtschaft in stark besiedelten Regionen; Umweltforschung mit Schwerpunkt Wasserwirtschaft*, 1991, ISBN 3-921694-76-0

77 Huwe, Bernd: *Deterministische und stochastische Ansätze zur Modellierung des Stickstoffhaushalts landwirtschaftlich genutzter Flächen auf unterschiedlichem Skalenniveau*, 1992, ISBN 3-921694-77-9, vergriffen

78 Rommel, Michael: *Verwendung von Kluftdaten zur realitätsnahen Generierung von Kluftnetzen mit anschließender laminar-turbulenter Strömungsberechnung*, 1993, ISBN 3-92 1694-78-7

79 Marschall, Paul: *Die Ermittlung lokaler Stofffrachten im Grundwasser mit Hilfe von Einbohrloch-Meßverfahren*, 1993, ISBN 3-921694-79-5, vergriffen

80 Ptak, Thomas: *Stofftransport in heterogenen Porenaquiferen: Felduntersuchungen und stochastische Modellierung*, 1993, ISBN 3-921694-80-9, vergriffen

81 Haakh, Frieder: *Transientes Strömungsverhalten in Wirbelkammern,* 1993, ISBN 3-921694-81-7

82 Kobus, Helmut; Cirpka, Olaf; Barczewski, Baldur; Koschitzky, Hans-Peter: *Versucheinrichtung zur Grundwasser und Altlastensanierung VEGAS, Konzeption und Programmrahmen*, 1993, ISBN 3-921694-82-5

83 Zang, Weidong: *Optimaler Echtzeit-Betrieb eines Speichers mit aktueller Abflußregenerierung*, 1994, ISBN 3-921694-83-3, vergriffen

84 Franke, Hans-Jörg: *Stochastische Modellierung eines flächenhaften Stoffeintrages und Transports in Grundwasser am Beispiel der Pflanzenschutzmittelproblematik*, 1995, ISBN 3-921694-84-1

85 Lang, Ulrich: *Simulation regionaler Strömungs- und Transportvorgänge in Karstaquiferen mit Hilfe des Doppelkontinuum-Ansatzes: Methodenentwicklung und Parameteridentifikation*, 1995, ISBN 3-921694-85-X, vergriffen

86 Helmig, Rainer: *Einführung in die Numerischen Methoden der Hydromechanik*, 1996, ISBN 3-921694-86-8, vergriffen

87 Cirpka, Olaf: *CONTRACT: A Numerical Tool for Contaminant Transport and Chemical Transformations - Theory and Program Documentation* -, 1996, ISBN 3-921694-87-6

88 Haberlandt, Uwe: *Stochastische Synthese und Regionalisierung des Niederschlages für Schmutzfrachtberechnungen*, 1996, ISBN 3-921694-88-4

89 Croisé, Jean: *Extraktion von flüchtigen Chemikalien aus natürlichen Lockergesteinen mittels erzwungener Luftströmung*, 1996, ISBN 3-921694-89-2, vergriffen

90 Jorde, Klaus: *Ökologisch begründete, dynamische Mindestwasserregelungen bei Ausleitungskraftwerken*, 1997, ISBN 3-921694-90-6, vergriffen

91 Helmig, Rainer: *Gekoppelte Strömungs- und Transportprozesse im Untergrund - Ein Beitrag zur Hydrosystemmodellierung*-, 1998, ISBN 3-921694-91-4, vergriffen

92 Emmert, Martin: *Numerische Modellierung nichtisothermer Gas-Wasser Systeme in porösen Medien,* 1997, ISBN 3-921694-92-2

93 Kern, Ulrich: *Transport von Schweb- und Schadstoffen in staugeregelten Fließgewässern am Beispiel des Neckars*, 1997, ISBN 3-921694-93-0, vergriffen

94 Förster, Georg: *Druckstoßdämpfung durch große Luftblasen in Hochpunkten von Rohrleitungen 1997*, ISBN 3-921694-94-9

95 Cirpka, Olaf: *Numerische Methoden zur Simulation des reaktiven Mehrkomponententransports im Grundwasser*, 1997, ISBN 3-921694-95-7, vergriffen

96 Färber, Arne: *Wärmetransport in der ungesättigten Bodenzone: Entwicklung einer thermischen In-situ-Sanierungstechnologie*, 1997, ISBN 3-921694-96-5

97 Betz, Christoph: *Wasserdampfdestillation von Schadstoffen im porösen Medium: Entwicklung einer thermischen In-situ-Sanierungstechnologie*, 1998, ISBN 3-921694-97-3

98 Xu, Yichun: *Numerical Modeling of Suspended Sediment Transport in Rivers*, 1998, ISBN 3-921694-98-1, vergriffen

99 Wüst, Wolfgang: *Geochemische Untersuchungen zur Sanierung CKW-kontaminierter Aquifere mit Fe(0)-Reaktionswänden,* 2000, ISBN 3-933761-02-2

100 Sheta, Hussam: *Simulation von Mehrphasenvorgängen in porösen Medien unter Einbeziehung von Hysterese-Effekten*, 2000, ISBN 3-933761-03-4

101 Ayros, Edwin: *Regionalisierung extremer Abflüsse auf der Grundlage statistischer Verfahren*, 2000, ISBN 3-933761-04-2, vergriffen

102 Huber, Ralf: *Compositional Multiphase Flow and Transport in Heterogeneous Porous Media*, 2000, ISBN 3-933761-05-0

103 Braun, Christopherus: *Ein Upscaling-Verfahren für Mehrphasenströmungen in porösen Medien*, 2000, ISBN 3-933761-06-9

104 Hofmann, Bernd: *Entwicklung eines rechnergestützten Managementsystems zur Beurteilung von Grundwasserschadensfällen*, 2000, ISBN 3-933761-07-7

105 Class, Holger: *Theorie und numerische Modellierung nichtisothermer Mehrphasenprozesse in NAPL-kontaminierten porösen Medien,* 2001, ISBN 3-933761-08-5

106 Schmidt, Reinhard: *Wasserdampf- und Heißluftinjektion zur thermischen Sanierung kontaminierter Standorte*, 2001, ISBN 3-933761-09-3

107 Josef, Reinhold:, *Schadstoffextraktion mit hydraulischen Sanierungsverfahren unter Anwendung von grenzflächenaktiven Stoffen*, 2001, ISBN 3-933761-10-7

108 Schneider, Matthias: *Habitat- und Abflussmodellierung für Fließgewässer mit unscharfen Berechnungsansätzen*, 2001, ISBN 3-933761-11-5

109 Rathgeb, Andreas: *Hydrodynamische Bemessungsgrundlagen für Lockerdeckwerke an überströmbaren Erddämmen*, 2001, ISBN 3-933761-12-3

110 Lang, Stefan: *Parallele numerische Simulation instätionärer Probleme mit adaptiven Methoden auf unstrukturierten Gittern*, 2001, ISBN 3-933761-13-1

111 Appt, Jochen; Stumpp Simone: *Die Bodensee-Messkampagne 2001, IWS/CWR Lake Constance Measurement Program 2001*, 2002, ISBN 3-933761-14-X

112 Heimerl, Stephan: *Systematische Beurteilung von Wasserkraftprojekten,* 2002, ISBN 3-933761-15-8

113 Iqbal, Amin: *On the Management and Salinity Control of Drip Irrigation,* 2002, ISBN 3-933761-16-6

114 Silberhorn-Hemminger, Annette: *Modellierung von Kluftaquifersystemen: Geostatistische Analyse und deterministisch-stochastische Kluftgenerierung,* 2002, ISBN 3-933761-17-4

115 Winkler, Angela: *Prozesse des Wärme- und Stofftransports bei der In-situ-Sanierung mit festen Wärmequellen,* 2003, ISBN 3-933761-18-2

116 Marx, Walter: *Wasserkraft, Bewässerung, Umwelt - Planungs- und Bewertungsschwerpunkte der Wasserbewirtschaftung,* 2003, ISBN 3-933761-19-0

117 Hinkelmann, Reinhard: *Efficient Numerical Methods and Information-Processing Techniques in Environment Water,* 2003, ISBN 3-933761-20-4

118 Samaniego-Eguiguren, Luis Eduardo: *Hydrological Consequences of Land Use / Land Cover and Climatic Changes in Mesoscale Catchments*, 2003, ISBN 3-933761-21-2

119 Neunhäuserer, Lina: *Diskretisierungsansätze zur Modellierung von Strömungs- und Transportprozessen in geklüftet-porösen Medien*, 2003, ISBN 3-933761-22-0

120 Paul, Maren: *Simulation of Two-Phase Flow in Heterogeneous Poros Media with Adaptive Methods*, 2003, ISBN 3-933761-23-9

121 Ehret, Uwe: *Rainfall and Flood Nowcasting in Small Catchments using Weather Radar*, 2003, ISBN 3-933761-24-7

122 Haag, Ingo: *Der Sauerstoffhaushalt staugeregelter Flüsse am Beispiel des Neckars - Analysen, Experimente, Simulationen -,* 2003, ISBN 3-933761-25-5

123 Appt, Jochen: *Analysis of Basin-Scale Internal Waves in Upper Lake Constance,* 2003, ISBN 3-933761-26-3

124 Hrsg.: Schrenk, Volker; Batereau, Katrin; Barczewski, Baldur; Weber, Karolin und Koschitzky, Hans-Peter: *Symposium Ressource Fläche und VEGAS - Statuskolloquium 2003, 30. September und 1. Oktober 2003,* 2003, ISBN 3-933761-27-1

125 Omar Khalil Ouda: *Optimisation of Agricultural Water Use: A Decision Support System for the Gaza Strip,* 2003, ISBN 3-933761-28-0

126 Batereau, Katrin: *Sensorbasierte Bodenluftmessung zur Vor-Ort-Erkundung von Schadensherden im Untergrund*, 2004, ISBN 3-933761-29-8

127 Witt, Oliver: *Erosionsstabilität von Gewässersedimenten mit Auswirkung auf den Stofftransport bei Hochwasser am Beispiel ausgewählter Stauhaltungen des Oberrheins*, 2004, ISBN 3-933761-30-1

128 Jakobs, Hartmut: *Simulation nicht-isothermer Gas-Wasser-Prozesse in komplexen Kluft-Matrix-Systemen*, 2004, ISBN 3-933761-31-X

129 Li, Chen-Chien: *Deterministisch-stochastisches Berechnungskonzept zur Beurteilung der Auswirkungen erosiver Hochwasserereignisse in Flussstauhaltungen,* 2004, ISBN 3-933761-32-8

130 Reichenberger, Volker; Helmig, Rainer; Jakobs, Hartmut; Bastian, Peter; Niessner, Jennifer: *Complex Gas-Water Processes in Discrete Fracture-Matrix Systems: Upscaling, Mass-Conservative Discretization and Efficient Multilevel Solution,* 2004, ISBN 3-933761-33-6

131 Hrsg.: Barczewski, Baldur; Koschitzky, Hans-Peter; Weber, Karolin; Wege, Ralf: *VEGAS - Statuskolloquium 2004,* Tagungsband zur Veranstaltung am 05. Oktober 2004 an der Universität Stuttgart, Campus Stuttgart-Vaihingen, 2004, ISBN 3-933761-34-4

132 Asie, Kemal Jabir: *Finite Volume Models for Multiphase Multicomponent Flow through Porous Media*. 2005, ISBN 3-933761-35-2

133 Jacoub, George: *Development of a 2-D Numerical Module for Particulate Contaminant Transport in Flood Retention Reservoirs and Impounded Rivers,* 2004, ISBN 3-933761-36-0

134 Nowak, Wolfgang: *Geostatistical Methods for the Identification of Flow and Transport Parameters in the Subsurface,* 2005, ISBN 3-933761-37-9

135 Süß, Mia: *Analysis of the influence of structures and boundaries on flow and transport processes in fractured porous media*, 2005, ISBN 3-933761-38-7

136 Jose, Surabhin Chackiath: *Experimental Investigations on Longitudinal Dispersive Mixing in Heterogeneous Aquifers,* 2005, ISBN: 3-933761-39-5

137 Filiz, Fulya: *Linking Large-Scale Meteorological Conditions to Floods in Mesoscale Catchments,* 2005, ISBN 3-933761-40-9

138 Qin, Minghao: *Wirklichkeitsnahe und recheneffiziente Ermittlung von Temperatur und Spannungen bei großen RCC-Staumauern*, 2005, ISBN 3-933761-41-7

139 Kobayashi, Kenichiro: *Optimization Methods for Multiphase Systems in the Subsurface - Application to Methane Migration in Coal Mining Areas*, 2005, ISBN 3-933761-42-5

140 Rahman, Md. Arifur: *Experimental Investigations on Transverse Dispersive Mixing in Heterogeneous Porous Media,* 2005, ISBN 3-933761-43-3

141 Schrenk, Volker: *Ökobilanzen zur Bewertung von Altlastensanierungsmaßnahmen,* 2005, ISBN 3-933761-44-1

142 Hundecha, Hirpa Yeshewatesfa: *Regionalization of Parameters of a Conceptual Rainfall-Runoff Model*, 2005, ISBN: 3-933761-45-X

143 Wege, Ralf: *Untersuchungs- und Überwachungsmethoden für die Beurteilung natürlicher Selbstreinigungsprozesse im Grundwasser,* 2005, ISBN 3-933761-46-8

144 Breiting, Thomas: *Techniken und Methoden der Hydroinformatik - Modellierung von komplexen Hydrosystemen im Untergrund*, 2006, 3-933761-47-6

145 Hrsg.: Braun, Jürgen; Koschitzky, Hans-Peter; Müller, Martin: *Ressource Untergrund: 10 Jahre VEGAS: Forschung und Technologieentwicklung zum Schutz von Grundwasser und Boden,* Tagungsband zur Veranstaltung am 28. und 29. September 2005 an der Universität Stuttgart, Campus Stuttgart-Vaihingen, 2005, ISBN 3-933761-48-4

146 Rojanschi, Vlad: *Abflusskonzentration in mesoskaligen Einzugsgebieten unter Berücksichtigung des Sickerraumes,* 2006, ISBN 3-933761-49-2

147 Winkler, Nina Simone: *Optimierung der Steuerung von Hochwasserrückhaltebecken-systemen,* 2006, ISBN 3-933761-50-6

148 Wolf, Jens: *Räumlich differenzierte Modellierung der Grundwasserströmung alluvialer Aquifere für mesoskalige Einzugsgebiete*, 2006, ISBN: 3-933761-51-4

149 Kohler, Beate: *Externe Effekte der Laufwasserkraftnutzung*, 2006, ISBN 3-933761-52-2

150 Hrsg.: Braun, Jürgen; Koschitzky, Hans-Peter; Stuhrmann, Matthias: *VEGAS-Statuskolloquium 2006,* Tagungsband zur Veranstaltung am 28. September 2006 an der Universität Stuttgart, Campus Stuttgart-Vaihingen, 2006, ISBN 3-933761-53-0

151 Niessner, Jennifer: *Multi-Scale Modeling of Multi-Phase - Multi-Component Processes in Heterogeneous Porous Media*, 2006, ISBN 3-933761-54-9

152 Fischer, Markus: *Beanspruchung eingeerdeter Rohrleitungen infolge Austrocknung bindiger Böden,* 2006, ISBN 3-933761-55-7

153 Schneck, Alexander: *Optimierung der Grundwasserbewirtschaftung unter Berücksichtigung der Belange der Wasserversorgung, der Landwirtschaft und des Naturschutzes*, 2006, ISBN 3-933761-56-5

154 Das, Tapash: *The Impact of Spatial Variability of Precipitation on the Predictive Uncertainty of Hydrological Models,* 2006, ISBN 3-933761-57-3

155 Bielinski, Andreas: *Numerical Simulation of CO_2 sequestration in geological formations*, 2007, ISBN 3-933761-58-1

156 Mödinger, Jens: *Entwicklung eines Bewertungs- und Entscheidungsunterstützungssystems für eine nachhaltige regionale Grundwasserbewirtschaftung*, 2006, ISBN 3-933761-60-3

157 Manthey, Sabine: *Two-phase flow processes with dynamic effects in porous media - parameter estimation and simulation,* 2007, ISBN 3-933761-61-1

158 Pozos Estrada, Oscar: *Investigation on the Effects of Entrained Air in Pipelines,* 2007, ISBN 3-933761-62-X

159 Ochs, Steffen Oliver: *Steam injection into saturated porous media – process analysis including experimental and numerical investigations*, 2007, ISBN 3-933761-63-8

160 Marx, Andreas: *Einsatz gekoppelter Modelle und Wetterradar zur Abschätzung von Niederschlagsintensitäten und zur Abflussvorhersage, 2007,* ISBN 3-933761-64-6

161 Hartmann, Gabriele Maria: *Investigation of Evapotranspiration Concepts in Hydrological Modelling for Climate Change Impact Assessment*, 2007, ISBN 3-933761-65-4

162 Kebede Gurmessa, Tesfaye: *Numerical Investigation on Flow and Transport Characteristics to Improve Long-Term Simulation of Reservoir Sedimentation*, 2007, ISBN 3-933761-66-2

163 Trifković, Aleksandar: *Multi-objective and Risk-based Modelling Methodology for Planning, Design and Operation of Water Supply Systems*, 2007, ISBN 3-933761-67-0

164 Götzinger, Jens: *Distributed Conceptual Hydrological Modelling - Simulation of Climate, Land Use Change Impact and Uncertainty Analysis*, 2007, ISBN 3-933761-68-9

165 Hrsg.: Braun, Jürgen; Koschitzky, Hans-Peter; Stuhrmann, Matthias: *VEGAS – Kolloquium 2007,* Tagungsband zur Veranstaltung am 26. September 2007 an der Universität Stuttgart, Campus Stuttgart-Vaihingen, 2007, ISBN 3-933761-69-7

166 Freeman, Beau: *Modernization Criteria Assessment for Water Resources Planning; Klamath Irrigation Project, U.S.*, 2008, ISBN 3-933761-70-0

167 Dreher, Thomas: *Selektive Sedimentation von Feinstschwebstoffen in Wechselwirkung mit wandnahen turbulenten Strömungsbedingungen*, 2008, ISBN 3-933761-71-9

168 Yang, Wei: *Discrete-Continuous Downscaling Model for Generating Daily Precipitation Time Series*, 2008, ISBN 3-933761-72-7

169 Kopecki, Ianina: *Calculational Approach to FST-Hemispheres for Multiparametrical Benthos Habitat Modelling,* 2008*,* ISBN 3-933761-73-5

170 Brommundt, Jürgen: *Stochastische Generierung räumlich zusammenhängender Niederschlagszeitreihen*, 2008, ISBN 3-933761-74-3

171 Papafotiou, *Alexandros: Numerical Investigations of the Role of Hysteresis in Heterogeneous Two-Phase Flow Systems*, 2008, ISBN 3-933761-75-1

172 He, Yi: *Application of a Non-Parametric Classification Scheme to Catchment Hydrology*, 2008, ISBN 978-3-933761-76-7

173 Wagner, Sven: *Water Balance in a Poorly Gauged Basin in West Africa Using Atmospheric Modelling and Remote Sensing Information*, 2008, ISBN 978-3-933761-77-4

174 Hrsg.: Braun, Jürgen; Koschitzky, Hans-Peter; Stuhrmann, Matthias; Schrenk, Volker: *VEGAS-Kolloquium 2008 Ressource Fläche III*, Tagungsband zur Veranstaltung am 01. Oktober 2008 an der Universität Stuttgart, Campus Stuttgart-Vaihingen, 2008, ISBN 978-3-933761-78-1

175 Patil, Sachin: *Regionalization of an Event Based Nash Cascade Model for Flood Predictions in Ungauged Basins*, 2008, ISBN 978-3-933761-79-8

176 Assteerawatt, Anongnart: *Flow and Transport Modelling of Fractured Aquifers based on a Geostatistical Approach,* 2008, ISBN 978-3-933761-80-4

177 Karnahl, Joachim Alexander: *2D numerische Modellierung von multifraktionalem Schwebstoff- und Schadstofftransport in Flüssen*, 2008, ISBN 978-3-933761-81-1

178 Hiester, Uwe: *Technologieentwicklung zur In-situ-Sanierung der ungesättigten Bodenzone mit festen Wärmequellen,* 2009, ISBN 978-3-933761-82-8

179 Laux, Patrick: *Statistical Modeling of Precipitation for Agricultural Planning in the Volta Basin of West Africa,* 2009, ISBN 978-3-933761-83-5

180 Ehsan, Saqib: *Evaluation of Life Safety Risks Related to Severe Flooding,* 2009, ISBN 978-3-933761-84-2

181 Prohaska, Sandra: *Development and Application of a 1D Multi-Strip Fine Sediment Transport Model for Regulated Rivers,* 2009, ISBN 978-3-933761-85-9

182 Kopp, Andreas: *Evaluation of CO_2 Injection Processes in Geological Formations for Site Screening,* 2009, ISBN 978-3-933761-86-6

183 Ebigbo, Anozie: *Modelling of biofilm growth and its influence on CO_2 and water (two-phase) flow in porous media,* 2009, ISBN 978-3-933761-87-3

184 Freiboth, Sandra: *A phenomenological model for the numerical simulation of multiphase multicomponent processes considering structural alterations of porous media*, 2009, ISBN 978-3-933761-88-0

185 Zöllner, Frank: *Implementierung und Anwendung netzfreier Methoden im Konstruktiven Wasserbau und in der Hydromechanik*, 2009, ISBN 978-3-933761-89-7

186 Vasin, Milos: *Influence of the soil structure and property contrast on flow and transport in the unsaturated zone*, 2010, ISBN 978-3-933761-90-3

187 Li, Jing: *Application of Copulas as a New Geostatistical Tool*, 2010, ISBN 978-3-933761-91-0

188 AghaKouchak, Amir: *Simulation of Remotely Sensed Rainfall Fields Using Copulas*, 2010, ISBN 978-3-933761-92-7

189 Thapa, Pawan Kumar: *Physically-based spatially distributed rainfall runoff modelling for soil erosion estimation*, 2010, ISBN 978-3-933761-93-4

190 Wurms, Sven: *Numerische Modellierung der Sedimentationsprozesse in Retentionsanlagen zur Steuerung von Stoffströmen bei extremen Hochwasserabflussereignissen*, 2011, ISBN 978-3-933761-94-1

191 Merkel, Uwe: *Unsicherheitsanalyse hydraulischer Einwirkungen auf Hochwasserschutzdeiche und Steigerung der Leistungsfähigkeit durch adaptive Strömungsmodellierung*, 2011, ISBN 978-3-933761-95-8

192 Fritz, Jochen: *A Decoupled Model for Compositional Non-Isothermal Multiphase Flow in Porous Media and Multiphysics Approaches for Two-Phase Flow*, 2010, ISBN 978-3-933761-96-5

193 Weber, Karolin (Hrsg.): *12. Treffen junger WissenschaftlerInnen an Wasserbauinstituten*, 2010, ISBN 978-3-933761-97-2

194 Bliefernicht, Jan-Geert: *Probability Forecasts of Daily Areal Precipitation for Small River Basins,* 2011, ISBN 978-3-933761-98-9

195 Hrsg.: Koschitzky, Hans-Peter; Braun, Jürgen: *VEGAS-Kolloquium 2010 In-situ-Sanierung - Stand und Entwicklung Nano und ISCO -,* Tagungsband zur Veranstaltung am 07. Oktober 2010 an der Universität Stuttgart, Campus Stuttgart-Vaihingen*,* 2010*,* ISBN 978-3-933761-99-6

196 Gafurov, Abror: *Water Balance Modeling Using Remote Sensing Information - Focus on Central Asia,* 2010, ISBN 978-3-942036-00-9

197 Mackenberg, Sylvia: *Die Quellstärke in der Sickerwasserprognose: Möglichkeiten und Grenzen von Labor- und Freilanduntersuchungen,* 2010, ISBN 978-3-942036-01-6

198 Singh, Shailesh Kumar: *Robust Parameter Estimation in Gauged and Ungauged Basins,* 2010, ISBN 978-3-942036-02-3

199 Doğan, Mehmet Onur: *Coupling of porous media flow with pipe flow,* 2011, ISBN 978-3-942036-03-0

200 Liu, Min: *Study of Topographic Effects on Hydrological Patterns and the Implication on Hydrological Modeling and Data Interpolation,* 2011, ISBN 978-3-942036-04-7

201 Geleta, Habtamu Itefa: *Watershed Sediment Yield Modeling for Data Scarce Areas,* 2011, ISBN 978-3-942036-05-4

202 Franke, Jörg: *Einfluss der Überwachung auf die Versagenswahrscheinlichkeit von Staustufen,* 2011, ISBN 978-3-942036-06-1

203 Bakimchandra, Oinam: *Integrated Fuzzy-GIS approach for assessing regional soil erosion risks,* 2011, ISBN 978-3-942036-07-8

204 Alam, Muhammad Mahboob: *Statistical Downscaling of Extremes of Precipitation in Mesoscale Catchments from Different RCMs and Their Effects on Local Hydrology,* 2011, ISBN 978-3-942036-08-5

Die Mitteilungshefte ab der Nr. 134 (Jg. 2005) stehen als pdf-Datei über die Homepage des Instituts: www.iws.uni-stuttgart.de zur Verfügung.